UNIVERSIDADE DO VALE DO RIO DOS SINOS

UNIDADE ACADÊMICA DE PÓS-GRADUAÇÃO

PROGRAMA DE PÓS-GRADUAÇÃO EM GEOLOGIA

PRÉ-CARACTERIZAÇÃO MICROESTRUTURAL DE MICROFÓSSEIS CALCÁRIOS APLICADOS COMO *PROXIES* PALEOAMBIENTAIS E PALEOECOLÓGICAS NO INÍCIO DO DANIANO

Marlone Heliara Hünnig Bom

Orientador: Prof. Dr. Gerson Fauth

Coorientador: Prof. Dr. Karlos Guilherme Diemer Kochhann

São Leopoldo, Setembro de 2023

PRÉ-CARACTERIZAÇÃO MICROESTRUTURAL DE MICROFÓSSEIS CALCÁRIOS APLICADOS COMO *PROXIES* PALEOAMBIENTAIS E PALEOECOLÓGICAS NO INÍCIO DO DANIANO

Marlone Heliara Hünnig Bom

Tese de Doutorado apresentado como parte
das exigências para obtenção do título de doutora, pelo
Programa de Pós-Graduação em Geologia da UNISINOS
Área de Concentração: Geologia Sedimentar
Linha de Pesquisa: Paleontologia Aplicada

Banca

Profa. Dra Ana Luiza Spadano Albuquerque

Prof. Dr. Cristianini Trescastro Bergue

Prof. Dr. Rodrigo Scalise Horodyski

São Leopoldo, Setembro de 2023

B695p Bom, Marlone Heliara Hünnig.
Pré-caracterização microestrutural de microfósseis calcários aplicados como proxies paleoambientais e paleoecológicas no início do Daniano / Marlone Heliara Hünnig Bom. – 2023.
259 f. : il. ; 30 cm.

Tese (doutorado) – Universidade do Vale do Rio dos Sinos, Programa de Pós-Graduação em Geologia, 2023.
"Orientador: Prof. Dr. Gerson Fauth
Coorientador: Prof. Dr. Karlos Guilherme Diemer Kochhann."

1. Microfósseis calcários – Daniano. 2. Proxies paleoambientais. 3. Proxies paleoecológicas. I. Título.

CDU 56

(Bibliotecária: Amanda Schuster – CRB 10/2517)

AGRADECIMENTOS

Esta tese contou com o apoio e a colaboração de muitas pessoas e instituições, às quais eu gostaria muito de agradecer.

À Coordenação de Aperfeiçoamento de Pessoal de Nível Superior, pela modalidade de bolsa PROSUC - AIU, concedida durante o período de Doutorado;

À Universidade do Vale do Rio dos Sinos, em especial ao Programa de Pós- Graduação em Geologia da UNISINOS pelo apoio institucional e de infraestrutura durante todo o processo de doutoramento;

Ao itt OCEANEON pelo apoio institucional e de infraestrutura durante todo o processo de doutoramento;

À secretaria do Programa de Pós-Graduação em Geologia da UNISINOS, por meio das secretárias Bruna Severo e Patricia Pescke por todo apoio nos trâmites institucionais burocráticos;

À Universidade de Buenos Aires e ao CONICET pela coleta das amostras referidas à Seção Cerro Azul, Bacia de Neuquén, Argentina.

Ao Laboratório de Astrobiologia, do Instituto de Química da USP (Universidade Estadual de São Paulo) pela Infraestrutura e as análises de Micro Raman. Ao Técnico responsável do laboratório, Evandro Pereira da Silva e ao Prof. Fabio Rodrigues meus profundos agradecimentos;

Ao Laboratório de Geoquímica Orgânica da Universidade de Kiel na Alemanha, que por meio do Professor Lorenz Schwarck e o PhD. Thorsten Bauersacks foi possível a realização das análises de TEX_{86};

Ao Laboratório Nacional de Luz Síncrotron, que por meio da Linha CARNAÚBA, foi possível realizar as análises de micro Fluorescência. Meus agradecimentos aos pesquisadores Douglas Galant e Itamar Tomio Neckel, o Neto, por todo apoio instrumental e nos mapeamentos gerados;

Ao meu orientador, Prof. Dr. Gerson Fauth, por acreditar na multidisciplinaridade desta pesquisa, pela orientação e todo o suporte necessário para a realização desta tese;

Ao meu co-orientador Prof. Karlos G.D. Kochhann, por todo apoio crítico das ideias, textos e orientação durante este período;

Á banca examinadora, que é composta por professores mais que especiais: Prof. Dra. Ana Luiza, que em esteve presente na minha qualificação. É muito bom tê-la novamente avaliando e contribuindo para esta pesquisa. Ao Prof. Dr. Cristianini, que me apresentou a micropaleontologia e que sempre admirei como pesquisador e ao Prof. Dr. Rodrigo, que um dia comentou sobre o Raman e o Sírius e acabou me incentivando a conhecer e aplicar esse caminho tão legal que é a Paleometria. Muito obrigada!

Aos pesquisadores, Rodrigo Guerra, Guilherme Krahl, Daiane Ceolin e Karlos Kochhann, meus profundos agradecimentos. Genuinamente, vocês são os irmãos que eu tenho no meu ambiente de trabalho. Obrigada por serem colaboradores desta tese e por estarem presentes em todos os momentos desta caminhada.

À Prof. Andrea Concheyro, da Universidad de Buenos Aires, pela amizade, carinho, torcida e, principalmente por confiar em nosso trabalho cedendo as amostras da Bacia de Neuquén para este estudo.

Aos colegas da área técnica do itt OCEANEON: Lucas, Luciana, Jordana, Andressa e Valeska. Obrigada por aceitarem este desafio comigo. Sem a competência de vocês, não teríamos resultados tão expressivos;

À Prof. Mirian L.F. Pacheco, da UFSCAR Campus Sorocaba, por todo aprendizado e companheirismo nas medidas e interpretações de Micro Raman e no Síncrotron.;

Aos demais coautores dos manuscritos que compõem esta tese, muito obrigada;

Aos meus pais e meus irmãos por todo carinho, amor e apoio de sempre, e neste período de doutoramento não foi diferente;

A minha família linda, meu combustível diário para seguir sempre adiante: Marcelo, Alice, Mariana e Nico, obrigada pelo apoio, amor, cumplicidade e carinho. Dedico esta tese a vocês.

RESUMO

Esta tese aborda a importância da pré-caracterização geoquímica, baseada na análise microestrutural de microfósseis calcários do Daniano, para garantir a fidedignidade de indicadores paleoceanográficos. Partindo da hipótese de que estimativas de paleotemperatura mais assertivas possam ser construídas por meio da análise microestrutural de fósseis, a presente tese permitiu realizar novas contribuições paleoambientais e paleoclimáticas para o Daniano no Oceano Atlântico Sul. O estudo realizado com amostras do *Ocean Drilling Program* (ODP) Site 1262, Walvis Ridge revelou que os registros de isótopos de oxigênio ($\delta^{18}O$) de foraminíferos bentônicos foram diageneticamente alterados pela formação de carbonatos autigênicos. Esse processo foi observado em níveis estratigráficos que registraram condições de reduzida oxigenação de fundo oceânico, como nos eventos Dan-C2 e Chron C29n. A superfície do oceano, neste local também foi afetada, como observado nas estruturas internas dos foraminíferos planctônicos. As mudanças no ecossistema, associadas a elevações de temperatura, parecem ter formado um ambiente favorável para os dinocistos calcários. Tais esferas calcárias que, por meio das suas medidas isotópicas, demonstraram ter preservado suas assinaturas ambientais originais. Em um contexto marinho epicontinental raso, na Bacia de Neuquén, Argentina, o limite Cretáceo-Paleogene (K-Pg) é muito bem delimitado e caracterizado. Para o Daniano inferior, a excelente preservação da assembleia de ostracodes foi confirmada por diferentes técnicas de pré-caracterização geoquímica, como MEV-EDS (microscopia eletrônica de varredura acoplado a espectroscopia de energia dispersiva), μXRD (micro difração de raios x) e μRAMAN (micro espectroscopia por Raman). Registros de matéria orgânica, tais como querogênio, foram identificados nos ostracodes, sugerindo excelente preservação dos fósseis. Os excelentes resultados permitiram inferir preferências paleocológicas de quatro espécies de ostracodes do Daniano, contribuindo para o escasso banco de dados

isotópicos disponível para este grupo fóssil nesse intervalo de tempo. Sinais claros de dispersão dos registros de carbono $\delta^{13}C$ e oxigênio revelaram evidentes diferenças intra-específicas entre espécies ornamentadas e lisas.

ABSTRACT

This thesis addresses the importance of geochemical pre-characterization, based on microstructural analysis of Danian calcareous microfossils. Based on the hypothesis that more assertive paleotemperature estimates can be reconstructed with microstructural analysis of fossils, this thesis allowed to make new paleoenvironmental and paleoclimatic contributions for the Danian in the South Atlantic Ocean. The study carried out with samples from Ocean Drilling Program (ODP) Site 1262, Walvis Ridge, revealed that stable oxygen isotope ($\delta^{18}O$) records from benthic foraminifera were diagenetically altered by growth of authigenic carbonates. This process was observed at stratigraphic levels that recorded reduced bottom water oxygenation, such as during the Dan-C2 and Chron C29n events. The ocean surface at this location was also affected, as observed in the internal structures of planktonic foraminifera. Changes in the ecosystem, associated with increases in temperature, appear to have been environment for calcareous dinocysts. Isotopic measurements of these calcareous spheres reflect original environmental signatures. In a shallow marine context, in the Neuquén Basin, Argentina, the Cretaceous (K-Pg) boundary is very well delimited and characterized. The excellent preservation of early Danian ostracod assemblage was confirmed by different geochemical pre-characterization techniques, such as SEM-EDS (scanning electron microscopy coupled energy dispersive spectroscopy), µXRD (micro x-ray diffraction) and µRAMAN (Raman spectroscopy). Records of organic matter, such as kerogen, were identified in ostracod valves, suggesting excelent preservation. The excellent results allowed us to infer paleecological preferences of four Danian species, contributing to the scarce isotopic database recorded for this Fossil Group over this time interval. Clear disperion patterns of carbon ($\delta^{13}C$) and

oxygen isotope values revealed evident intraspecific differences between ornate and smooth species.

SUMÁRIO

APRESENTAÇÃO

Nos últimos anos, com os avanços analíticos, uma nova gama de parâmetros geoquímicos vem surgindo, contribuindo com alta precisão, os estudos paleoclimáticos, paleoceanográficos e paleoambientais. As técnicas espectrométricas apresentam características favoráveis para este tipo de aplicação. Sua capacidade de análise multielementar, alta sensibilidade e medidas de razão isotópicas, estão entre as suas grandes vantagens (Yu et al., 2005; Harding et al., 2006; Thomas, 2013).

Os microfósseis calcários podem ser uma excelente matriz para tais análises geoquímicas. A aplicação de foraminíferos, por exemplo, como ferramenta em análises isotópicas e de elementos traços, tem mostrado grande importância em estudos paeloceanográficos e paleoclimáticos. A utilização destes micro-organismos protistas cria a possibilidade de se obter dados das características oceânicas de várias profundidades, tendo em vista que diferentes espécies habitam diferentes profundidades na coluna d'água. O material secretado pelos foraminíferos apresenta cerca de 99% em massa de carbonato de cálcio puro ($CaCO_3$) e, cerca de 1%, correspondem a elementos-traço, como Mg, Sr, Ba e Cd (Lea et al., 1999). Os ostracodes são pequenos crustáceos que estão disseminados em ambientes aquáticos marinhos e continentais (Horne et al., 2012). Suas carapaças constituem de duas valvas de calcita com baixo Mg (Decrouy et al., 2011a). O conteúdo de oligoelementos presentes nessas valvas também provou ser útil para reconstruções ambientais tanto em ambientes marinhos, como salobros e de água doce (e.g., Börner et al., 2013; Pint et al., 2017; Roberts et al., 2018). A espécie *Cyprideis torosa*, por exemplo, é amplamente utilizada para reconstruções paleoambientais. Biogeograficamente difundida, esta espécie eurialina é tolerante a uma ampla gama de condições ecológicas, sendo encontrada em águas quase doces a hipersalinas (De Decker & Lord, 2017; Scharf et al.,

2017). O gênero *Krithe*, também é onipresente em diferentes profundidades oceânicas (Elmore et al., 2012). As carapaças são lisas e apresentam poucos poros, minimizando o potencial de contaminação por detritos, tornando o gênero favorável para reconstruções paleoceanográficas.

As potencialidades desses estudos se tornam limitadas à medida que se recua no tempo geológico (Bice et al., 2005; Bice et al., 2006). Fatores como a abundância dos espécimes e, principalmente, a aumento da intensidade da diagênese, são conhecidos como fonte de erros nas análises químicas. Além disso, a dissolução parcial dos microfósseis calcários pode resultar no enviesamento de resultados analíticos e, consequentemente, levar a imprecisões em estimativas de parâmetros oceanográficos pretéritos (e.g., Regemberg et al., 2014).

Poderosas ferramentas, com excelentes resoluções espaciais, permitem mapear essas alterações em microfósseis carbonáticos. Técnicas como espectroscopia por Raman e microdifração de raio-x permitem analisar mineralogicamente a composição das testas, carapaças e/ou valvas. A ablação a laser permite mapear a área desejada em termos quantitativos dos elementos traços. Tais mapeamentos possibilitam verificar o estado de preservação, para o uso desses espécimes em análises isotópicas e de razões elementares.

Portanto, para se ter um resultado confiável e mais fidedigno possível quanto às condições ambientais do passado, é fundamental a realização de um estudo aprofundado das possíveis fases contaminantes existentes em espécimes que serão utilizados para análises geoquímicas. Esta tese aborda a importância da pré-caracterização geoquímica através da análise microestrutural de microfósseis calcários aplicados como *proxies* paleoambientais. Diferentes técnicas são aplicadas em microfósseis calcários do Daniano em dois diferentes contextos do Oceano Atlântico Sul: (i) ambiente marinho profundo da Walvis Ridge, no *Ocean Drilling Program* (ODP) *Site* 1262; e (ii) ambiente marinho

epicontinental raso da Seção Cerro Azul, Bacia de Neuquén, Argentina. A Bacia de Neuquén é uma bacia sedimentar, localizada no oeste da Argentina e possui depósitos que variam em idade do Triássico superior ao Paleógeno. As amostras utilizadas neste estudo compreendem o superciclo sedimentar Riográndico, que inclui a Formação Jagüel.

ORGANIZAÇÃO DA TESE

O ***Capítulo 1*** apresenta a motivação, para o desenvolvimento da tese, assim como a hipótese, além dos objetivos gerais e específicos que compõe a tese. Na sequência, os capítulos 2 a 6 irão, individualmente, apresentar as aplicações dos objetivos. Ainda neste capítulo será dissertado sobre o contexto geográfico e oceanográfico dos locais avaliados para este estudo, além do conhecimento da evolução climática no início do Paleoceno. Por fim, será apresentado um resumo das técnicas analíticas aplicadas na tese.

O ***Capítulo 2*** apresenta o primeiro estudo microestrutural na calcita de foraminíferos bentônicos para início do Daniano. Foram avaliados os sinais ambientais e vieses pós-deposicionais na calcita bentônica, além de novos registros de isótopos de carbono ($\delta^{13}C$) e oxigênio ($\delta^{18}O$) de foraminíferos planctônicos e dinocistos calcários no *Ocean Drilling Program* (ODP) Site 1262 (Oceano Atlântico Sul). O capítulo é intitulado "*Disentangling environmental and diagenetic $\delta^{18}O$ and $\delta^{13}C$ signals from marine carbonates deposited under warm climate conditions during the early Danian*" e foi publicado no periódico *Palaeogeography, Palaeoclimatology, Palaeoecology*.

As mudanças paleoambientais ocorridas no início do Paleoceno também são expressivas em contexto marinho epicontinental raso e registradas no ***Capítulo 3***. A Seção Cerro Azul, localizada na Bacia de Neuquén, Argentina, possui um registro contínuo da transição Cretáceo-Paleógeno. Neste estudo, foi realizada a pré-caracterização geoquímica em ostracodes do início do Daniano e posterior análise de isótopos de $\delta^{13}C$ e $\delta^{18}O$ em suas valvas. Tais registros foram comparados com os parâmetros associados a variação de salinidade, oxigenação e distribuição de nutrientes, sugerindo diferenças entre as preferências ecológicas das espécies avaliadas. O capítulo intitulado "*Paleoecology of*

selected Danian marine ostracods suggested by stable carbon ($\delta^{13}C$) and oxygen ($\delta^{18}O$) isotopes" foi submetido ao periódico *Marine Micropaleontology.*

Os intervalos estratigráficos avaliados nesta tese são oriundos de locais explorados previamente pela equipe de pesquisa do Instituto Tecnológico de Paleoceanografia e Mudanças Climáticas (itt OCEANEON—UNISINOS). Nos capítulos 4 e 5 serão apresentados dois artigos publicados com a mesma amostragem, no qual a proponente da tese participou como coautora, e que são relevantes para a compreensão dos contextos estratigráficos das seções analisadas.

O ***Capítulo 4*** apresenta os impactos de eventos hipertermais do Daniano nas assembleias de foraminíferos planctônicos no ODP Site 1262. O artigo "*Impact of early Danian environmental perturbations on mid-latitude planktic foraminiferal assemblages from the ODP Site 1262 (South Atlantic Ocean)*", de G. Krahl, I. Arenillas, V. Gilabert, K. G. D. Kochhann, M. H. H. Bom, G. Fauth e J. A. Arz , foi publicado no periódico *Newsletter on Stratigraphy*.

O ***Capítulo 5*** apresenta o resultado da investigação de nanofósseis calcários e ostracodes associados a mudanças paleoambientais registradas na Bacia de Neuquén ao longo da transição Cretáceo-Paleogeno (K-Pg). O artigo "Calcareous microfossils and paleoenvironmental changes across the Cretaceous-Paleogene (K-Pg) boundary at the Cerro Azul Section, Neuquén Basin, Argentina", de R. M. Guerra, Andrea Concheyro, K. G. D. Kochhann, M. H.H. Bom, D. Ceolin, T. Musso, J. F. Savian, G. Fauth, foi publicado no periódico *Palaeogeography, Palaeoclimatology, Palaeoecology*.

Por fim, uma síntese integradora dos resultados da tese é apresentada no ***Capítulo 6***.

CAPÍTULO 1 – INTRODUÇÃO

Capítulo 1

Introdução

INTRODUÇÃO

1.1 MOTIVAÇÃO

O limite Cretáceo–Paleogeno (K-Pg) compreende um dos eventos geológicos mais devastadores que ocorreram na Terra (Alvarez et al., 1980). O impacto do asteroide em Chicxulub, causou uma série de efeitos catastróficos, impactando fortemente o clima no planeta. Outras consequências como flutuações no nível do mar, acidificação dos oceanos, poluição por metais pesados, também são relatadas (Vellekoop et al., 2014; 2016; Gibbs et al., 2020). As fases eruptivas do vulcanismo Deccan Trap, localizado na Índia, também vêm sendo associadas a essa grande fase de transformação biótica (Schoene et al., 2015; Renne et al., 2015). Recentes pesquisas com datação radiométrica demonstram que a diferença de idades entre esses dois eventos se restringe a um período de apenas algumas centenas de milhares de anos, durante o magnetocron C29r (Chenet et al., 2007; Schoene et al., 2015). As distinções desses dois momentos permanecem ainda em pleno debate (Archibald et al., 2010; Keller et al., 2010). Datações Ar^{40}/Ar^{39} das lavas do Deccan Traps sugerem que erupções mais volumosas do vulcanismo ocorreram durante o início do Daniano (Sprain et al., 2019), enquanto datações U/Pb sugerem que maior volume eruptivo ocorreu no final do Maastrichtiano (Schoene et al., 2019).

Outras assinaturas geoquímicas como excursões de Os^{187}/Os^{188} e enriquecimentos de Hg, também ilustram evidências de vulcanismo antecedendo o limite K-Pg (Zhao et al., 2021; Font et al.,2022). Os avanços geoquímicos, associados aos modelos de taxas de emissão de CO_2, sugerem que as grandes emissões começaram e terminaram distintamente antes do impacto (Hull et al., 2020).

De fato, o Paleoceno (65-55Ma) representa uma época na qual o sistema climático e o ciclo do carbono estavam passando por mudanças críticas em função dos elevados

níveis de gases com efeito estufa (Westerhold et al., 2011). Após a extinção em massa no limite K-Pg, os ecossistemas se recuperaram de forma hesitante sob condições instáveis (e.g., Coxall et al., 2005; D'Hont, 2005; Birch et al., 2021), caracterizando uma das maiores extinções em massa da história da Terra (Gradstein et al., 2012).

Nesta passagem, os foraminíferos planctônicos e os nanoplâncton calcários, foram caracterizados por baixa diversidade, existindo espécies oportunistas que poderiam prosperar sob condições eutróficas e instáveis (Bown et al., 2004; Gibbs et al., 2020). No entanto, dúvidas ainda permanecem sobre a taxa e a magnitude dessas mudanças ambientais e, exatamente, como ela se relaciona com a recuperação biótica na superfície e no oceano profundo. Camadas ricas em micrita, de origem microbiana, foram encontradas em nível global, no limite K-Pg (Bralower et al., 2020). Esta comunidade microbiana se adaptou de forma única para prosperar sob os efeitos do impacto Chicxulub e dominou determinados ambientes oceânicos até milhares de anos após o evento de extinção (Bralower et al., 2020).

Os conjuntos de foraminíferos bentônicos documentados, mostram que esses micro-organismos não foram severamente afetados pelo evento de extinção (e.g., Thomas, 1990; Alegret et al., 2003; Alegret & Thomas, 2007; Krahl et al., 2021; Arreguin-Rodriguez et al., 2021). Os registros isotópicos com base em foraminíferos bentônicos revelam uma história bastante complexa de resfriamento inicial de longo prazo, seguido de aquecimento, com vários e rápidos eventos de transição de curto prazo (Barnet et al., 2018). Essas mudanças teriam sido impulsionadas principalmente por grandes variações da pressão parcial de dióxido de carbono (pCO_2) na atmosfera, inferidas pelos dados isotópicos de carbono (Zachos et al., 2001, Barnet et al., 2019). Quando houve mudanças temporárias significativas nas estruturas das faunas dos foraminíferos bentônicos, essas estiveram possivelmente relacionadas ao colapso na cadeia alimentar pelágica e uma posterior

queda de nutrientes para os organismos bentônicos (Alegret et al., 2002; 2003). Entretanto, determinadas áreas geográficas, como em Seções da Espanha e do México apresentaram características contrárias, com maior disponibilidade de nutrientes e em condições de baixa oxigenação (Alegret & Thomas, 2005).

As mudanças nas assembleias de ostracodes do Paleoceno, são pouco documentadas e compreendidas (Yamaguchi et al., 2017). Em locais de águas profundas, as amostras que possuem ostracodes são raras e os trabalhos existentes apontam que estes organismos bentônicos registram altas taxas de extinção no limite K-Pg (e.g., Benson, 1990, Guernet &Bellier, 2000; Guernet & Danelian, 2006; Hewaidy et al., 2021; Du et al., 2021). Pesquisas que identificaram o surgimento e a extinção de ostracodes no Oceano Atlântico Sul também são raros (Fauth, 2000; Ceolin et al., 2011; Ceolin et al., 2015, Barros et al., 2018). Dados isotópicos para o Daniano com base em ostracodes estão limitados a dois estudos de Rodrigues et al. (2014; para o Atlântico Sul) e Bornemann et al. (2012; Tunísia). Nenhum estudo de paleotemperatura com base em ostracodes para este período geológico foi documentado.

Os eventos transitórios de aquecimento global (hipertermais) são conhecidos como eventos transientes de curta duração. A descoberta do “Máximo termal do Paleoceno/Eoceno (PETM; ~55Ma), evento impulsionado pelos gases do efeito estufa, gerou uma busca por eventos análogos em outras partes do Paleógeno (Quillévéré et al., 2008). Ainda, os hipertermais do Paleoceno incluem o LowerC29n (Coccioni et al., 2010), o Latest Danian event (também chamado de Top C27n event, Westerhold et al., 2008) e o evento biótico tardio do Paleoceno inicial (Petrizzo, 2005; Bralower, 2006). O evento chamado de Dan-C2 é o evento climático mais antigo causado por gases do efeito estufa no Paleogeno e possui uma duração de ~100 mil anos (Arreguín-Rodrigues et al., 2021).

Este é caracterizado por notáveis excursões negativas de $\delta^{13}C$ e $\delta^{18}O$, associadas à diminuição no teor de carbonato de cálcio no oceano profundo (e.g., Quilléveré et al., 2008; Barnet et al., 2018;2019; Krahl et al.,2020; 2023).

Trabalhos recentes mostram que o Dan-C2 não se caracteriza claramente como um evento hipertermal e sim como uma perturbação no ciclo do carbono associado a aquecimento de águas superficiais com eminente dissolução de carbonato de cálcio (e.g., Barnet et al., 2019; Arreguín-Rodriguez et al., 2020). Essas afirmações foram feitas com base na observação de que nenhum registro bentônico existente de $\delta^{18}O$ exibe uma forte resposta de temperatura (Figura 1-C; Barnet et al., 2019), sugerindo que não houve aquecimento das águas oceânicas profundas. Quanto ao evento hipertermal Dan-C2 do Daniano (Quillévéré et al., 2008), os mecanismos paracem estar associados a variações orbitais (e.g. Gilabert et al. 2020). Adicionalmente, estudos recentes sugerem que este sucedeu a maior fase eruptiva do Deccan traps no Daniano (Krahl et al., 2023; Krahl et al., 2023a; Nauter-Alves et al., 2023).

Pearson et al. (2001) questionaram a validade dos dados de paleotermometria baseados em $\delta^{18}O$ em função da má preservação e alteração diagenética. De fato, o grau de alteração pós-deposicional de um fóssil, está fortemente relacionado com os aspectos gerais da zona tafonomicamente ativa em sofrer alterações (Golreihan et al., 2018). Logo, avaliar o estado de preservação dos espécimes e os processos diagenéticos que podem ocorrer nas paredes dos microfósseis a serem analisados vão muito além do critério visual.

A extensão de alteração diagenética pode ser avaliada pelos aspectos microestruturais da calcita de foraminífero. Existem pelo menos três processos diagenéticos principais que podem ocorrer na parede de um foraminífero: a dissolução parcial, o crescimento excessivo e a recristalização. Todos os processos podem afetar a geoquímica original do foraminífero num momento de zona tafonomicamente ativa (TAZ), tanto na coluna

d'água, quanto no fundo do oceano (Edgar et al., 2015). A ausência da aparência vítrea na testa é uma consequência da alteração diagenética em microescala (Pearson et al., 2001).

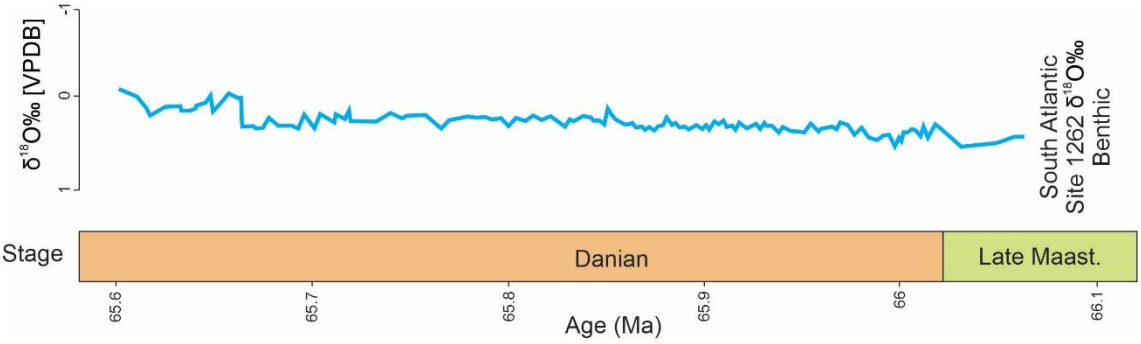

Figura 1: Compilação de dados de isótopos estáveis de $\delta^{18}O$ em foraminíferos bentônicos do *Site* ODP 1262 Atlântico Sul (Barnet et al., 201º, modificado).

No registro geológico, locais que contenham microfósseis calcários amplamente amostrados e com uma preservação vítrea (*sensu* Sexton et al., 2006) são relativamente raros. A grande maioria dos locais profundos disponíveis para reconstruções paleoceanográficas são ricos em carbonato onde predomina calcita recristalizada. Uma solução, na medida do possível, está em escolher espécimes preservados em estratos ricos em argila. A natureza relativamente impermeável desses sedimentos ricos em argila, pode impedir a interação significativa de calcita do foraminífero com fluidos de poros circundantes, levando a excelente preservação do carbonato.

Apesar do óbvio impacto diagenético em vários parâmetros geoquímicos, algum componente original da calcita é frequentemente retido. Portanto, a identificação e a quantificação da alteração diagenética e seu impacto sobre a composição química da calcita do foraminífero continua sendo um grande desafio para as reconstruções paleoambientais.

Raros são os registros paleoclimáticos e paleoecológicos sobre as seções Danianas e/ou K-Pg do hemisfério sul (e.g., Vellekoop et al., 2017; Woelders et al., 2017). Porém, tão importante quanto ter esses dados é se ter a segurança dos dados adquiridos. A geoquímica em escala fina das estruturas carbonáticas pode clarificar processos de biomineralização na química das valvas e ou câmaras, além de caracterizar possíveis fontes de tais vieses. Diante de todas essas problemáticas citadas, sejam elas, metodológicas, paleoceanográficas e paleoambientais, uma série de questionamentos foram levantados para esta pesquisa, surgindo a hipótese, além dos objetivos gerais e específicos da tese.

1.2 HIPÓTESE

Estudos geoquímicos metodológicos expressam a necessidade aprimorar paleotermômetros em intervalos profundos no tempo geológico. A hipótese da tese é de que a pré-caracterização dos microfósseis carbonáticos, considerando fases contaminantes, para posterior ajuste de protocolo e análise instrumental, possa contribuir para estimativas de paleotemperatura mais assertivas.

1.3 QUESTIONAMENTOS DA PESQUISA E OBJETIVOS

Alguns questionamentos sobre os assuntos abordados na motivação, geraram os principais objetivos da tese:

(1) Os eventos de aquecimento rápido, ocorrido no início do Paleoceno, afetaram o processo de biomineralização dos foraminíferos bentônicos?

(2) A resposta silenciosa do fundo do oceano com base nos dados de $\delta^{18}O$ em foraminíferos bentônicos significa que não houve variação de temperatura da água de fundo ao longo do Paleoceno no oceano Atlântico Sul?

(3) Seriam as calcisferas uma ferramenta para reconstituições paleoceanográficas?

(4) É possível inferir preferências ecológicas de diferentes espécies de ostracodes com *proxies* geoquímicos?

Baseados nesses questionamentos, foi formado o objetivo o objetivo geral da tese.

1.3.1 Objetivo

Aprimorar protocolos de pré-caracterização geoquímica para identificar amostras adequadas para investigações isotópicas do início do Daniano.

Com o objetivo e os questionamentos da pesquisa definidos, foi possível traçar alguns objetivos específicos.

1.3.2 Objetivos específicos

(1) Realizar um estudo na microestrutura dos microfósseis utilizados nas análises geoquímicas, visando avaliar a qualidade da calcita identificando a ausência/ocorrência de possíveis fases contaminantes;

(2) Avaliar os sinais isotópicos de $\delta^{13}C$ e $\delta^{18}O$ em diferentes matrizes carbonáticas, tais como foraminíferos bentônicos, ostracodes e dinocistos calcários;

1.4 LOCALIZAÇÃO E ÁREA DE ESTUDO

Nesta pesquisa foram utilizadas amostras oriundas de duas distintas localidades do Oceano Atlântico Sul: (i) Walvis Ridge - ODP Leg 208, Site 1262 e (ii) a Seção Cerro Azul (38°50’48’’S, 67°52’20’’), que está localizada na Bacia de Neuquén, na Argentina (Figura 2). No ODP Site 1262, foi possível testemunhar a transição K-Pg. O Site, está localizado na porção leste do Oceano Atlântico Sul (27°11.15’S, 1°34.62’W, Zachos et al., 2004). O intervalo estratigráfico selecionado, é constituído de argilas e lodos ricos em carbonatos, atribuídos a unidade litológica III (Zachos et al., 2004). Os resultados oriundos deste material serão apresentados nos capítulos 2 e 5.

A Seção Cerro Azul, Bacia de Neuquén, está inserida na Formação Jaguel (Andreis et al., 1974) e é caracterizada por uma sucessão sedimentar homognênea de granulação fina, com fósseis que indicam idade Maastrichtiana a Daniana (Uliana e Dellapé, 1981). O intervalo estratigráfico selecionado para os estudos referentes aos capítulos 3 e 4, compreende o início do Paleoceno, enquanto o material explorado no capítulo 6, compreende ao K-Pg.

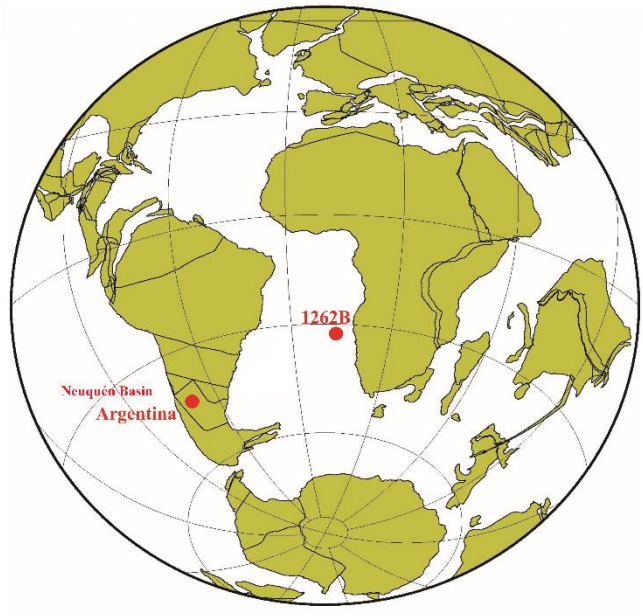

Figura 2: Reconstituição paleogeográfica do início do Paleógeno com a localização dos pontos investigados nesta tese. (modificado de www.odsn.de).

1.5 TÉCNICAS INSTRUMENTAIS UTILIZADAS NA TESE

A importância da avaliação do estado de preservação dos espécimes utilizados nas análises geoquímicas é crucial para a fidedignidade dos estudos paleoceanográficos e paleoclimáticos. Alterações diagenéticas podem comprometer a interpretação de registros de isótopos estáveis e de análises de elementos-traço (Golreihan et al., 2018). Sendo assim, a presente tese, envolveu uma série de metodologias, abrangendo diferentes técnicas de análise instrumental, em variados níveis de resolução. A Tabela 1, apresenta as instrumentações utilizadas e a principal finalidade da análise.

Técnica/Instrumentação	**Localização**	**Finalidade**
Microscopia Eletrônica de Varredura / EVO MA15Zeiss	Itt OCEANEON	Imageamento e análise microestrutural por meio de análise qualitativa de espectroscopia por energia dispersiva (EDS). Medição da espessura das valvas.
Isótopos estáveis de $\delta^{13}C$ e $\delta^{18}O$ em microfósseis calcários/ Kiel IV carbonate device	Itt OCEANEON	Determinação de isótopos estáveis de carbono e oxigênio em foraminíferos bentônicos, planctônicos, ostracodes e dinocistos calcários.
Isótopos estáveis de $\delta^{13}C$ e $\delta^{18}O$ em sedimentos /Carbo Kiel Device	Leibniz Laboratory, Kiel	Determinação de isótopos estáveis de carbono e oxigênio em sedimentos.
Microdifração de raios x /Empyrean PanAlytical	Itt OCEANEON	Identificação de fases carbonáticas autigênicas em microfósseis calcários
Espectroscopia por MicroRaman/ Renishaw	Laboratório de Astrobiologia USP	Identificação de fases minerais e /ou orgânicas via teoria do orbital molecular
LA-ICP-MS/ iCAPQc-laser Analyte Excite 193nm	Itt OCEANEON	Determinação pontual das razões El/Ca (cálcio) em testas de foraminíferos e para identificação de fases autigênicas.
FRX/Epsilon 1 PAnAlytical	Itt OCEANEON	Razões elementares de sedimentos como *proxies* de reconstituição paleoambiental e paleoclimática.

1.6 REFERÊNCIAS

Alegret, L., Arenillas, I., Arz, J. A., Liesa, C., Meléndez, A., Molina, E., Soria, A.R., Thomas, E., 2002. The Cretaceous/Tertiary boundary: sedimentology and micropalaeontology at El Mulato section, NE Mexico. Terra Nova, 14(5), 330-336.

Alegret, L., Molina, E., Thomas, E., 2003. Benthic foraminiferal turnover across the Cretaceous/Paleogene boundary at Agost (southeastern Spain): paleoenvironmental inferences. Marine Micropaleontology, 48(3-4), 251-279.

Alegret, L., Thomas, E., 2005. Cretaceous/Paleogene boundary bathyal paleo-environments in the central North Pacific (DSDP Site 465), the Northwestern Atlantic (ODP Site 1049), the Gulf of Mexico and the Tethys: The benthic foraminiferal record. Palaeogeography, Palaeoclimatology, Palaeoecology, 224(1-3), 53-82.

Alegret, L., Thomas, E., 2007. Deep-sea environments across the Cretaceous/Paleogene boundary in the eastern South Atlantic Ocean (ODP leg 208, Walvis Ridge). Marine Micropaleontology, 64(1-2), 1-17.

Alvarez, L. W., Alvarez, W., Asaro, F., Michel, H. V., 1980. Extraterrestrial cause for the Cretaceous-Tertiary extinction. Science, 208(4448), 1095-1108.

Archibald, J. D., Clemens, W. A., Padian, K., Rowe, T., Macleod, N., Barrett, P. M., Gale, A., Holroyd, P., Sues, H.D., Arens, N.C., Horner, J.R., Wilson, G.P., Goodwin, M.B.,Brochu, C.A., Lofgren, D.L., Hulbert, S.H., Hartman, J.H., Eberth, D.A., Wignall, P.B., Currie, P.J., Weil, A., Prasad, G.V.R., Dingus, L., Courtillot, V., Milner, A., Milner, A., Baijpai, S., Ward, D.J., Sahni, A., 2010. Cretaceous extinctions: multiple causes. Science, 328(5981), 973-973.

Arreguín-Rodríguez, G. J., Barnet, J. S., Leng, M. J., Littler, K., Kroon, D., Schmidt, D. N., Thomas, E., Alegret, L., 2021. Benthic foraminiferal turnover across the Dan-C2 event in the

eastern South Atlantic Ocean (ODP Site 1262). Palaeogeography, Palaeoclimatology, Palaeoecology, 572, 110410.

Barnet, J. S., Littler, K., Kroon, D., Leng, M. J., Westerhold, T., Röhl, U., Zachos, J. C., 2018. A new high-resolution chronology for the late Maastrichtian warming event: Establishing robust temporal links with the onset of Deccan volcanism. Geology, 46(2), 147-150.

Barnet, J. S., Littler, K., Westerhold, T., Kroon, D., Leng, M. J., Bailey, I., Röhl, U., Zachos, J. C., 2019. A high-Fidelity benthic stable isotope record of late Cretaceous–early Eocene climate change and carbon-cycling. Paleoceanography and Paleoclimatology, 34(4), 672-691.

Benson, R. H., 1990. Ostracoda and the discovery of global Cainozoic palaeoceanographical events. In Ostracoda and global events (pp. 41-58).

Bice, K. L., Layne, G. D., Dahl, K., 2005. Application of secondary ion mass spectrometry to the determination of Mg/Ca in rare, delicate, or altered planktonic foraminifera: Examples from the Holocene, Paleogene, and Cretaceous. Geochemistry, Geophysics, Geosystems, 6(12).

Bice, K. L., Birgel, D., Meyers, P. A., Dahl, K. A., Hinrichs, K. U., Norris, R. D., 2006. A multiple proxy and model study of Cretaceous upper ocean temperatures and atmospheric CO2 concentrations. Paleoceanography, 21(2).

Birch, H., Schmidt, D. N., Coxall, H. K., Kroon, D., Ridgwell, A., 2021. Ecosystem function after the K/Pg extinction: Decoupling of marine carbon pump and diversity. Proceedings of the Royal Society B, 288(1953), 20210863.

Bornemann, A., Pirkenseer, C. M., Steurbaut, E., Speijer, R. P., 2012. Early paleogene δ 13 c and δ 18 o records based on marine ostracodes: implications for the upper Danian succession at Sidi Nasseur (Tunisia) and their application value in paleoceanography. Austrian Journal of Earth Sciences, 105(1).

Börner, N., De Baere, B., Yang, Q., Jochum, K. P., Frenzel, P., Andreae, M. O., Schwalb, A., 2013. Ostracod shell chemistry as proxy for paleoenvironmental change. Quaternary International, 313, 17-37.

Bown, P. R., Lees, J. A., Young, J. R., 2004. Calcareous nannoplankton evolution and diversity through time. Coccolithophores: from molecular processes to global impact, 481-508.

Bralower, T. J., 2006. Proceedings of the Ocean Drilling Program, Scientific Results. Vol. 198. Extreme Warmth in the Cretaceous and Paleogene: a Depth Transect on Shatsky Rise, Central Pacific: Covering Leg 198 of the Cruises of the Drilling Vessel" Joides Resolution", Yokohama, Japan, to Honolulu, Hawaii, Sites 1207-1214, 27 August-23 October 2001. Texas A & M University Ocean Drilling Program.

Bralower, T.J., Cosmidis, J., Heaney, P.J., Kump, L.,R., Morgan, J.V., Harper, D.T., Lyons, S.L., Freeman, K.H., Grice, K., Wendler, J.E., Zachos, J.C., Artemieva, N., Chen, S.A., Gulick, S.P.S., Schaefer, B., Thomas, E., Vajda, V., 2020. Origin of a global carbonate layer deposited in the aftermath of the Cretaceous-Paleogene boundary impact. Earth and Planetary Science Letters, 548, 116476.

Ceolin, D., Fauth, G., Coimbra, J. C., 2011. Cretaceous–Lower Paleogene ostracods from the Pelotas Basin, Brazil. Palaeobiodiversity and Palaeoenvironments, 91, 111-128.

Ceolin, D., Whatley, R., Fauth, G., Concheyro, A., 2015. New genera and species of Ostracoda from the Maastrichtian and Danian of the Neuquén Basin, Argentina. Papers in Palaeontology, 1(4), 425-495.

Chenet, A. L., Quidelleur, X., Fluteau, F., Courtillot, V., Bajpai, S., 2007. ^{40}K–^{40}Ar dating of the Main Deccan large igneous province: Further evidence of KTB age and short duration. Earth and Planetary Science Letters, 263(1-2), 1-15.

Chivas, A. R., P. De Deckker, J. M. G. Shelley, 1983. Magnesium, strontium, and barium partitioning in nonmarine ostracode shells and their use in paleoenvironmental reconstructions – a preliminary study. In R. F. Maddocks (ed.), Applications of Ostracoda, Univ. Houston, Geosci., Houston: 238–249.

Coccioni, R., Frontalini, F., Bancalà, G., Fornaciari, E., Jovane, L., Sprovieri, M., 2010. The Dan-C2 hyperthermal event at Gubbio (Italy): Global implications, environmental effects, and cause (s). Earth and Planetary Science Letters, 297(1-2), 298-305.

Coxall, H. K., D'Hondt, S., Zachos, J. C., 2006. Pelagic evolution and environmental recovery after the Cretaceous-Paleogene mass extinction. Geology, 34(4), 297-300.

Decrouy, L., Vennemann, T. W., Ariztegui, D., 2011. Controls on ostracod valve geochemistry, Part 1: Variations of environmental parameters in ostracod (micro-) habitats. Geochimica et Cosmochimica Acta, 75(22), 7364-7379.

De Deckker, P., & Lord, A., 2017. Cyprideis torosa: a model organism for the Ostracoda?. Journal of Micropalaeontology, 36(1), 3-6.

De Lima Barros, C., Piovesan, E. K., Agostinho, S. M. O., 2018. Cretaceous-Paleogene ostracods from the Paraíba Basin, northeastern Brazil. Journal of South American Earth Sciences, 83, 117-136.

D'Hondt, S., 2005. Consequences of the Cretaceous/Paleogene mass extinction for marine ecosystems. Annu. Rev. Ecol. Evol. Syst., 36, 295-317.

Du, S. X., Wang, H., Liu, F. C., Lu, H. N., Song, X. S., Li, S., Zhang, H. C., 2021. Ostracods from the Upper Cretaceous–Paleocene Jiaozhou Formation of Jiaozhou, Shandong, China and their biostratigraphic significance. Palaeoworld, 30(2), 323-336.

Dwyer, G. S., Cronin, T. M., Baker, P. A. 2002. Trace elements in marine ostracods. Geophysical Monograph-American Geophysical Union, 131, 205-226.

Edgar, K.M., Anagnostou, E., Pearson, P.N., Foster, G.L., 2015. Assessing the impact of diagenesis on δ11B, δ 13C, δ 18O, Sr/Ca and B/Ca values in fossil planktic foraminiferal calcite. Geochimica et Cosmochimica Acta, 1661 189-209.

Elmore, A. C., Sosdian, S., Rosenthal, Y., Wright, J.D., 2012. A global evaluation of temperature and carbonate ion control on Mg/Ca ratios of ostracoda genus Krithe. Geochemistry, Geophysics, Geosystems, 13(9).

Fauth, G. 2000. Cretaceous–Tertiary (K–T) boundary ostracodes from the Poty quarry, Pernambuco-Paraíba Basin, northeastern Brazil: systematics, biostratigraphy, palaeoecology and palaeobiogeography. University of Heidelberg, (Ruprecht-Karls), R.K.U.H., Heidelberg, pp 158

Font, E., Chen, J., Regelous, M., Regelous, A., Adatte, T., 2022. Volcanic origin of the mercury anomalies at the Cretaceous-Paleogene transition of Bidart, France. Geology, 50(2), 142-146.

Gibbs, S. J., Bown, P. R., Ward, B. A., Alvarez, S. A., Kim, H., Archontikis, O. A., Sauterey, B., Poulton, A.J., Wilson, J., Ridgwell, A., 2020. Algal plankton turn to hunting to survive and recover from end-Cretaceous impact darkness. Science Advances, 6(44), eabc9123.

Golreihan, A., Steuwe, C., Woelders, L., Deprez, A., Fujita, Y., Vellekoop, J., Swennen, R., Roeffaers, M. B., 2018. Improving preservation state assessment of carbonate microfossils in paleontological research using label-free stimulated Raman imaging. PLoS One, 13(7), e0199695.

Gradstein, F. M., Ogg, J. G., Schmitz, M. D., Ogg, G. M. (Eds.). , 2012. The geologic time scale 2012. Elsevier.

Guernet, C., Bellier, J. P., 2000. Ostracodes paléoccnes et éoccnes du blake nose (Leg ODP 171B) et évolution des environnements bathyaux au large de la Floride. Revue de Micropaléontologie 43(4), 249-279.

Guernet, C., Danelian, T., 2006. Ostracodes bathyaux du Crétacé terminal–Éocène moyen en Atlantique tropical (Plateau de Demerara, Leg 207). Revue de micropaléontologie 49(4), 215-225.

Harding, D. J., Arden, J. W., Rickaby, R. E. M., 2006. A method for precise analysis of trace element/calcium ratios in carbonate samples using quadrupole inductively coupled plasma mass spectrometry. Geochemistry, Geophysics, Geosystems 7(6).

Hewaidy, A. G. A., Morsi, A. M. M., Samir, A., 2021. Maastrichtian-Paleocene Ostracoda from Teneida section, Dakhla Oasis, Western Desert, Egypt: Systematics, biostratigraphy, paleobathymetry and paleobiogeography. Journal of African Earth Sciences 174, 104072.

Horne, D. J., Holmes, J. A., Rodriguez-Lazaro, J., Viehberg, F.A., 2012. Ostracoda as proxies for Quaternary climate change: overview and future prospects. Developments in Quaternary Sciences 17, 305-315.

Hull, P.M., Bornemann, A., Penman, D.E., Henehan, M.J., Norris, R.D., Wilson, P.A., Blum, P., Alegret, L., Batenburg, S.J., Bown, P.R., Bralower, T.j., Cournede, C., Deutsch, A., Donner, B., Friedrich, O., Jehle, S., Kim, H., Kroon, D., Lippert, P.C., Loroch, D., Moebius, I., Moriya, K Peppe, D.J., Ravizza, G.E., Röhl, U., Schueth, J.D., Sepúlveda, J.,Sexton, P.F., Sibert, E.C., S´liwin´ska, K.K., Summons, R.E., Thomas, E., Westerhold, T., Whiteside, J.H., Yamaguchi, T Zachos, J.C., 2020. On impact and volcanism across the Cretaceous-Paleogene boundary. Science, 367, 266-272. 10.1126/science.aay5055

Keller, G., Adatte, T., Pardo, A., Bajpai, S., Khosla, A., Samant, B., 2010. Cretaceous extinctions: evidence overlooked. Science, 328(5981), 974-975.

Krahl, G., Bom, M. H., Kochhann, K. G., Souza, L. V., Savian, J. F., Fauth, G., 2020. Environmental changes occurred during the early Danian at the Rio Grande rise, South Atlantic Ocean. Global and Planetary Change, 191, 103197.

Krahl, G., Kochhann, K. G., Fauth, G., Sial, A. N., de Lacerda, L. D., 2021. Evaluation of deep-water environmental conditions during the latest Maastrichtian-early Danian: Insights from the western South Atlantic ocean. Journal of South American Earth Sciences, 112, 103630.

Krahl, G., Arenillas, I., Gilabert, V., Kochhann, K. G., Bom, M. H., Fauth, G., Arz, J. A., 2023. Impact of early Danian environmental perturbations on mid-latitude planktic foraminiferal assemblages from the ODP Site 1262 (South Atlantic Ocean). Newsletters on Stratigraphy.

Krahl, G., Kochhann, K. G. D., Bom, M. H. H., Fauth, G., 2023. Mercury stratigraphy of early Danian sediments from the Rio Grande Rise and the timing of Deccan volcanism. Journal of South American Earth Sciences, 128, 104488.

Lea, D. W., Mashiotta, T. A., Spero, H. J., 1999. Controls on magnesium and strontium uptake in planktonic foraminifera determined by live culturing. Geochimica et Cosmochimica Acta, 63(16), 2369-2379.

Nauter-Alves, A., Dunkley-Jones, T., Bruno, M. D. R., Mota, M. A. D. L., Cachão, M., Krahl, G., Fauth, G., 2023. Biotic turnover and carbon cycle dynamics in the early Danian event (Dan-C2): New insights from Blake Nose, North Atlantic. Global and Planetary Change, 221, 104046.

Pearson, P. N., Ditchfield, P. W., Singano, J., Harcourt-Brown, K. G., Nicholas, C. J., Olsson, R. K., Shackleton, N.J., Hall, M. A., 2001. Warm tropical sea surface temperatures in the Late Cretaceous and Eocene epochs. Nature, 413(6855), 481-487.

Petrizzo, M. R., 2005. An early late Paleocene event on Shatsky Rise, northwest Pacific Ocean (ODP Leg 198): Evidence from planktonic foraminiferal assemblages. In Proceedings of the Ocean Drilling Program. Scientific Results (Vol. 198). Ocean Drilling Program.

Pint, A., & Frenzel, P., 2017. Ostracod fauna associated with Cyprideis torosa–an overview. Journal of Micropalaeontology, 36(1), 113-119.

Quillévéré, F., Norris, R. D., Kroon, D., Wilson, P. A., 2008. Transient ocean warming and shifts in carbon reservoirs during the early Danian. Earth and Planetary Science Letters, 265(3-4), 600-615.

Regenberg, M., Regenberg, A., Garbe-Schönberg, D., Lea, D. W., 2014. Global dissolution effects on planktonic foraminiferal Mg/Ca ratios controlled by the calcite-saturation state of bottom waters. Paleoceanography, 29(3), 127-142.

Renne, P. R., Sprain, C. J., Richards, M. A., Self, S., Vanderkluysen, L., Pande, K., 2015. State shift in Deccan volcanism at the Cretaceous-Paleogene boundary, possibly induced by impact. Science, 350(6256), 76-78.

Roberts, L.R., Holmes, J. A., Leng, M.J., Sloane, H.J., Horne, D. J., 2018. Effects of cleaning methods upon preservation of stable isotopes and trace elements in shells of Cyprideis torosa (Crustacea, Ostracoda): Implications for palaeoenvironmental reconstruction. Quaternary Science Reviews 189, 197-209.

Rodrigues, G. B., Fauth, G., Santos, R. V., Koutsoukos, E. A., Colin, J. P. (2014). Tracking paleoecological and isotopic changes through the K-Pg boundary from marine ostracodes: the Poty quarry section, northeastern Brazil. Cretaceous Research, 47, 105-116.

Scharf, B., Herzog, M., & Pint, A., 2017. New occurrences of Cyprideis torosa (Crustacea, ostracoda) in Germany. Journal of Micropalaeontology, 36(1), 120-126.

Schoene, B., Samperton, K. M., Eddy, M. P., Keller, G., Adatte, T., Bowring, S. A., Khadri, S.F.R., Gertsch, B., 2015. U-Pb geochronology of the Deccan Traps and relation to the end-Cretaceous mass extinction. Science, 347(6218), 182-184.

Sprain, C. J., Renne, P. R., Vanderkluysen, L., Pande, K., Self, S., Mittal, T., 2019. The eruptive tempo of Deccan volcanism in relation to the Cretaceous-Paleogene boundary. Science, 363(6429), 866-870.

Thomas, E., 1990. Late Cretaceous–early Eocene mass extinctions in the deep sea. Geol. Soc. Am. Spec. Publ, 247, 481-495.

Thomas, R., 2013. Practical Guide to ICP-MS: A Tutorial for Beginners, Third Edition (3rd ed.). CRC Press. https://doi.org/10.1201/b14923

Westerhold, T., Röhl, U., Donner, B., McCarren, H. K., Zachos, J. C., 2011. A complete high-resolution Paleocene benthic stable isotope record for the central Pacific (ODP Site 1209). Paleoceanography, 26(2).

Vellekoop, J., Sluijs, A., Smit, J., Schouten, S., Weijers, J. W., Sinninghe Damsté, J. S., Brinkhuis, H., 2014. Rapid short-term cooling following the Chicxulub impact at the Cretaceous–Paleogene boundary. Proceedings of the National Academy of Sciences, 111(21), 7537-7541.

Vellekoop, J., Esmeray-Senlet, S., Miller, K. G., Browning, J. V., Sluijs, A., van de Schootbrugge, B., Sinninghe, J.S., Brinkhuis, H., 2016. Evidence for Cretaceous-Paleogene boundary bolide "impact winter" conditions from New Jersey, USA. Geology, 44(8), 619-622.

Yamaguchi, T., Bornemann, A., Matsui, H., Nishi, H., 2017. Latest Cretaceous/Paleocene deep-sea ostracode fauna at IODP Site U1407 (western North Atlantic) with special reference to the Cretaceous/Paleogene boundary and the Latest Danian Event. Marine Micropaleontology, 135, 32-44.

Yu, J., Day, J., Greaves, M., Elderfield, H., 2005. Determination of multiple element/calcium ratios in foraminiferal calcite by quadrupole ICP-MS. Geochemistry, Geophysics, Geosystems, 6(8).

Zachos, J.C., Kroon, D., Blum, P., et al. 2004. Proceedings of the Ocean Drilling 1003 Program Initial Reports, volume 208, Texas A&M University, College Station TX 1004 77845-9547, USA. [CD-ROM]. Available from: Ocean Drilling Program.

Zhao, M., Ma, M., He, M., Qiu, Y., Liu, X., 2021. Evaluation of the four potential Cretaceous-Paleogene (K-Pg) boundaries in the Nanxiong Basin based on evidences from volcanic activity and paleoclimatic evolution. Science China Earth Sciences, 64, 631-641.

CAPÍTULO 2 – SEPARANDO OS SINAIS AMBIENTAIS E DIAGENÉTICOS DE CARBONATOS MARINHOS DO INÍCIO DO DANIANO

Capítulo 2:

Disentangling environmental and diagenetic $\delta^{18}O$ and $\delta^{13}C$ signals from marine carbonates deposited under warm climate conditions during the early Danian

Marlone H.H. Bom, Karlos G.D. Kochhann, Guilherme Krahl, Nils Andersen,Lucas V. Oliveira, Valeska Meirelles, Mírian L.A.F. Pacheco, Andressa Esswein, Bruna C. Schneider, Gerson Fauth

Publicado em: *Palaeogeography, Palaeoclimatology, Palaeoecology*, 622(2023)111576 doi: 10.1016/j.palaeo.2023.111576

Disentangling environmental and diagenetic $\delta^{18}O$ and $\delta^{13}C$ signals from marine carbonates deposited under warm climate conditions during early Danian

Marlone H.H.Bom[a,b], Karlos G.D. Kochhann[a,b], Guilherme Krahl[a,b], Nils Andersen[c], Lucas V. Oliveira[a], Valeska Meirelles[a], Mírian L.A.F. Pacheco[d], Andressa Esswein[a], Bruna C. Schneider[b], Gerson Fauth[a,b]

[a] itt OCEANEON, Technological Institute for Paleoceanography and Climate Changes, Universidade do Vale do Rio dos Sinos, Av. Unisinos, 950, Cristo Rei, São Leopoldo, RS, Brazil.

[b] Geology Graduate Program, Universidade do Vale do Rio dos Sinos, São Leopoldo 93.022-750, Brazil

[c] Leibniz Laboratory for Radiometric Dating and Stable Isotope Research, Christian Albrechts University, Kiel, Germany

[d] São Carlos Federal University, Departamento de Biologial, Rodovia João Leme dos Santos,18052780 Sorocaba, SP, Brazil

Corresponding author: Marlone H. H. Bom (marloneb@unisinos.br)

Highlights

- Authigenic carbonate phases were identified in Danian benthic foraminifera.
- Crystallization of these phases affected environmental $\delta^{18}O$ signals.
- After the Dan-C2 event, foraminiferal calcite preservation improved.
- Bulk $\delta^{18}O$ records, dominated by micrite/dinocysts, recorded environmental signals.

Keywords: diagenesis, Danian, microstructural analysis, foraminifera, oxygen and carbon isotopes, Dan-C2 event

Abstract

Paleoceanographic reconstructions are usually based on the chemical composition of foraminiferal tests, and pristine calcite preservation is crucial to support reliable interpretations. Therefore, prior knowledge about the structure and chemical composition of microfossils calcite is important to assess whether geochemical results reflect environmental and/or post-burial signals. Here, we present the first microstructural study of early Danian benthic foraminiferal calcite, and evaluate environmental signals and post depositional biases in benthic and planktonic foraminiferal and bulk carbon ($\delta^{13}C$) and oxygen ($\delta^{18}O$) isotope records at Ocean Drilling Program (ODP) Site 1262 (South Atlantic Ocean). We focused our study on the first ~350 kyr that followed the Cretaceous-Paleogene (K-Pg) boundary, encompassing the Dan-C2 carbon cycle perturbation. Benthic and planktonic $\delta^{13}C$ records show the expected surface-to-bottom gradient, suggesting the preservation of original environmental signals. However, benthic and planktonic $\delta^{18}O$ records show strongly overlapping and scatterred values, suggesting diagenetic alteration of isotopic signals. We identified the occurrence of authigenic carbonates, such as girvasite and siderite, in benthic foraminiferal tests, which increased Mg, Mn, Ba and Fe contents of tests calcite. Our results support that thermodynamic changes occurred in tandem with the decrease in bottom and pore water oxygenation to favor the precipitation of authigenic carbonate phases, which altered the isotopic fractionation of $\delta^{18}O$. Nevertheless, bulk sediments clearly depict the negative $\delta^{13}C$ and $\delta^{18}O$ excursions characteristic of the Dan-C2, with remarkably low values, characterizing the record of a surface ocean environmental signal. This low $\delta^{13}C$ and $\delta^{18}O$ were mostly recorded by highly-abundant

calcispheres (calcareous dinocysts), suggesting that this microfossils group has a high potential for surface ocean paleoceanographic reconstructions.

2.1 INTRODUCTION

Oxygen isotope thermometry is the most widely used geochemical proxy for paleotemperature reconstruction (e.g., Lear et al., 2000; Katz et al., 2010; Daëron et al., 2019), specially during the Paleogene when ice volume effects on $\delta^{18}O$ were likely minor. The theoretical foundation for the use of $\delta^{18}O$ as a paleothermometer is based on the premise that $^{18}O/^{16}O$ partitioning among water and carbonate minerals primarily reflects thermodynamic equilibrium (Daëron et al., 2019). Different inorganic substances and biogenic carbonates appear to follow distinct fractionation laws, requiring specific calibrations (Daëron et al., 2019).

For deep time studies, the $\delta^{18}O$ proxy is usually measured on foraminiferal shells found in deep-sea sediments, which can record conditions at different depths in the water column. Foraminiferal shells are preserved in marine sediments as calcite, a stable polymorph of calcium carbonate (Jacob et al., 2017). Usually, the geochemistry of foraminiferal shells diverges significantly from inorganic calcite, since the former is affected by biomineralization processes, in approximate equilibrium with seawater (e.g., Spero et al., 1997; Zeebe, 2001; Pearson et al., 2012; de Nooijer et al., 2014). Some parameters, such as temperature, salinity and pH, in addition to the concentration of certain ions, will influence the formation and quality of the calcite (Nürnberg et al., 1996). Furhtermore, kinetic effects can also cause chemical changes in the carbonate ion composition and consequently in the isotopic fractionation.

The Paleocene was punctuated by a series of warming events linked to perturbations of the carbon cycle (e.g, Westerhold et al., 2011; 2020; Dinarès-Turrel et al., 2014). These events

were associated with carbonate content drops in deep ocean sediments, caused by ocean acidification as a consequence of increased greenhouse gases levels (Zachos et al., 2010). For the Danian time interval, the Dan-C2 (e.g., Quillévéré et al., 2008, Coccioni et al., 2010, Krahl et al., 2020, Gilabert et al., 2021) and the lower Chron C29n events (e.g., Coccioni et al., 2010 and Krahl et al., 2020) were considered the first warming events of the Cenozoic Era, being recorded in the Atlantic and Tethys oceans. These events occurred under warm background climate states, since the surface ocean warmed by approximately 4 °C after the Cretaceous-Paleogene (K-Pg) mass extinction (e.g., Quillévéré et al., 2008; Woelders, et al., 2018). Nevertheless, the lack of deep water warming, suggested by benthic foraminiferal oxygen isotope ($\delta^{18}O$) values, raises questions on whether the Dan-C2 was in fact a global warming event (Barnet et al., 2019).

Calcareous microfossils are susceptible to diagenesis, which can impair calcite preservation (e.g., Erez, 2003; Sexton et al., 2006; Pearson and Burguess, 2008; Huber et al., 2011, O'Brien et al., 2017, Golreihan et al., 2018). Therefore, examining microstructural aspects and the geochemical nature of diagenetic alterations of foraminiferal calcite helps to put forward robust paleoceanographic hypotheses. Here we evaluated possible diagenetic alterations of the calcite, and their effects on $\delta^{18}O$ and $\delta^{13}C$ records, of *Nuttallides truempyi*, one of the benthic foraminiferal species most used for paleotemperature reconstructions. We also compared our benthic $\delta^{18}O$ and $\delta^{13}C$ series with recently planktonic and bulk $\delta^{18}O$ and $\delta^{13}C$ records (Krahl et al., 2023) spanning the first ~350 kyr of the Danian at Ocean Drilling Program (ODP) Site 1262, located in the South Atlantic Ocean. This time interval spanned the Dan-C2 and lower Chron C29n carbon cycle perturbations, and we used different analythical

techniques to evaluate microstructural and geochemical characteristics of benthic foraminiferal tests, as well as (paleo) bottom and pore water redox conditions.

2.2 MATERIAL AND METHODS

2.2.1 Study area and age models

During ODP Leg 208, Site 1262 cored the K-Pg transition at the Walvis Ridge, eastern South Atlantic Ocean (27°11.15′S, 1°34.62′W; Zachos et al., 2004) (Figure 1). We studied 40 samples collected between 216.83 and 214.70 meters below seafloor (mbsf) at Hole 1262B, over the interval spanning the latest Maastrichtian and the first ~400 kyr of the Danian. Sediments of this stratigraphic interval are clays and carbonate-rich oozes, assigned to lithologic unit III (Zachos et al., 2004). For this study, we followed the Site 1262 astronomically-tuned chronology of Dinarès-Turell et al. (2014), which resulted in a ~15 kyr sampling resolution for our data sets. We followed the identification of the Dan-C2 event at Site 1262 of Barnet et al. (2019), which was based on a double negative $\delta^{13}C_{bulk}$ negative excursion. During the latest Maastrichtian-earliest Danian, Site 1262 was located at a paleolatitude of ~40°S (Van Hinsbergen et al., 2015).

2.2.2 Stable oxygen ($\delta^{18}O$) and carbon ($\delta^{13}C$) isotopes

For stable isotope analysis, we picked six to ten specimens of *Nuttallides truempyi* and 20-30 specimens of *Subbotina trivialis* from sediment size fraction >250 μm. Benthic foraminiferal specimens were broken and cleaned in ethanol in an ultrasonic bath, and oven dried at 40°C. They were measured with a Finnigan MAT 253 mass spectrometer coupled to a Carbo-Kiel Device (Type IV) system at the Leibniz Laboratory, at University of Kiel. We tested reaction times of four and 18 minutes to ensure reaction of all carbonate phases. Since both

runs do not result in significantly different results, we only report $\delta^{13}C$ and $\delta^{18}O$ measurements performed with four minutes reaction time. Results were calibrated using the international standards NBS 19 and IAEA-603, as well as the internal standards Hela1, HB1 and SHK.

We additionally measured $\delta^{13}C$ and $\delta^{18}O$ on calcispheres from selected samples (n=9). For each sample, we picked the first 70 calcisphere specimens, which were not broken and cleaned due to their small dimentions of calcispheres (38µm). Samples were analyzed in a Finnigan MAT 253 mass spectrometer coupled to a Carbo-Kiel Device (Type IV) system at the Technological Institute for Paleoceanography and Climate Change (itt OCEANEON; UNISINOS University). For ~70 calcispheres, reaction with phosphoric acid resulted in ~400 µbar of CO_2, enabling measurements that were calibrated against the IAEA-603, CO-8, and SHP2L as internal standard (Crivellari et al., 2021).

All $\delta^{13}C$ and $\delta^{18}O$ values are reported in the Vienna PeeDee Belemnite (VPDB) scale. Water temperatures were estimated from $\delta^{18}O$ values following the equations by Erez and Luz (1983), and assuming no continental ice sheets during the Danian.

2.2.3 Identifying foraminiferal tests mineralogy

We used micro X-Ray diffraction (XRD) on nine individual specimens of *Nuttalides truempyi* to identify mineral phases composing the benthic tests and authigenic coatings. Due the dimensions of the specimens, it was possible to mount them with stick glue directly on the zero-background silicon sample holder. Mineral phases were also identified with XRD for ground bulk sediments at two stratigraphic levels: (i) 216.35 mbsf (after the K-Pg boundary),

and (ii) 215.55 mbsf (within Dan-C2 event). The equipment used was an Empyrean Panalytical x-ray diffractometer (CuKα radiation) set at 40kV and 40 mA.

Raman spectral analysis was also applied to identify minerals present in the benthic foraminiferal tests from the same nine levels analysed with XRD. We collected Raman spectra with a Renishaw inVia Reflex, coupled to a Leica DM2500 M microscope available at the Laboratory of Astrobiology, University of São Paulo (USP). Samples were excited with 632.8 nm (He-Ne, Renishaw) and 785 nm (diode laser-Renishaw) beams, at 17 mW total power (attenuated to 0.1%, 0.5%, 1%, 5% and 10%), and with variable exposures and accumulation times. Spectra were processed using the WiRE 4.1 software. We used the auto-correction mode for background corrections and compared the collected Raman spectra with references spectra from the RUFF database (http://rruff.info./) to identify mineral phases.

2.2.4 Test microstructure

Selected specimens of planktonic and benthic foraminifera (n=20) were imaged in an EVO MA15 Zeiss scanning electron microscope (SEM) at itt OCEANEON. Specimens were analyzed for test microstructure, and we used energy dispersive X-Ray spectrometry (EDS) to evaluate the chemical composition of *Nuttalides truempyi* tests (n=4). For these EDS analyses, we selected specimens assigned to frosty and pseudo-glassy preservations under stereomicroscope.

2.2.5 Elemental composition of benthic foraminiferal tests

For elemental analysis of individual *Nuttalides truempyi* tests, specimens with pseudo-glassy to frosty preservations, picked from the 63-125 µm sediment fractions, were selected. We chose nine specimens, from the same stratigraphic levels analysed with XRD, and

measured element concentrations of, preferentially, on the penultime (f-1 measurements) and antepenultime (f-2 measurements) chambers of each specimen (named as f and f-1 positions). Data were acquired using a Analyte Excite+ 193 nm excimer laser ablation system (Teledyne CETAC Technologies) coupled to an ICP-MS iCAP Qc (Thermo Scientific) and performed at itt OCEANEON. We followed the methodology of Ni et al. (2020), which consisted in ablation from the test's outer surface towards the inside of chambers, and then separated the laser signal of each foraminiferal wall into the outer surface layer (coatings) and the middle layer (primarily foraminiferal calcite) using changes in the element signal in the LA profiles. We measured Ca, Mg, Sr, Fe, Al concentrations, and calculated the element/calcium (El/Ca) ratios. Data were processed with the Glitter-GEMOC 4.4.2 software. Experimental parameters are summarized in Table 1.

Table 1: Experimental parameters for elemental analysis (El/Ca ratios) of *Nuttalides truempyi*.

ICP-MS	iCAP Qc
RF Power	1550 W
Argon auxiliary gas flow	0.8 L min^{-1}
Argon coolant gas flow	14 L min^{-1}
Argon (carrier) gas flow	0.66 L min^{-1}
Dwell time per mass	0.01 s
Scan mode	Peak hopping
Isotopes	^{24}Mg, ^{27}Al, ^{28}Si, ^{29}Si, ^{43}Ca, ^{44}Ca, ^{54}Fe, ^{55}Mn, ^{57}Fe, ^{85}Rb, ^{87}Rb, ^{88}Sr, ^{137}Ba, ^{232}Th, ^{238}U, $^{232}Th.^{16}O$
Laser ablation system	UV excimer laser
Wavelength	193 nm
Sample Cell	HelEx II
Energy density (fluence)	1.04 J cm^{-1}
Energy	5.00 mJ
Pulse length	< 5 ns
Laser repetition rate	10 Hz
Power	30%
Laser spot size	20 □m
He gas flow	1: 0.65 L min^{-1} 2: 0.3 L min^{-1}
ThO^+/Th^+	<0.5%
U^+/Th^+	~1

2.2.6 Bulk sediments elemental ratios

X-ray fluorescence (XRF) analyses were performed on 5 to 10 g of bulk sediment samples (n = 40), with elemental concentrations reported as raw counts per second (cps) and interpreted as elemental ratios. Samples were measured at 10 kV (150 µA, no filter) for Al, Mg, Si intensities; 12 kV (400 µA, Al-50 filter) for Ca, K, Ti and V intensities; 20 kV (250 µA, Al – 200 filter) for Co, Cr, Fe and Mn intensities; and 50 kV (100 µA, Ti filter) for Ba and Rb intensities. Analyses were performed in a PanAlytical Epsilon 1 XRF spectrometer at itt OCEANEON. In this work we used V/(V+Ni) and Mn/Al to evaluate changes in bottom water oxygenation (Croudace and Rothwell, 2015).

2.3 RESULTS

2.3.1 Oxygen and carbon isotope records

Nuttalides truempyi $\delta^{13}C$ values throughout the studied interval (66.03 to 65.62 Ma) oscillate between 1.28 and 2.25‰ (Figure 2A, blue squares), while for *Subbotina trivialis* $\delta^{13}C$ values vary between 1.62 and 2.43‰ (Figure 2A, red crosses). At the K-Pg transition, a noticeable $\delta^{13}C$ drop occurred in both benthic (from 2.25 to 2.19‰) and planktic (from 2.38 to 2.13‰) foraminiferal records. At the onset of the Dan-C2 event (65.87 Ma), remarkable $\delta^{13}C$ minima occurred in the *Nuttalides truempyi* (1.41‰) and for *Subbotina trivialis* (1.68‰) records. After the Dan-C2, drops in *Nuttalides truempyi* and *Subbotina trivialis* $\delta^{13}C$ values occurred during the Chron C29n event centered at 65.63 Ma (Figure 2A). Bulk sediments $\delta^{13}C$ measurements revealed overall similar trends, with the lowest values occurring within the Dan-C2 and Chron C29n events (Figure 2A). One remarkable feature of the $\delta^{13}C_{bulk}$ record, however, is that values crossed those of the *Nuttalides truempyi* and *Subbotina trivialis* $\delta^{13}C$ records within the first 30 kyr of the Danian and remain unusually low throughout the younger part of the studied interval (Figure 2A, light blue circles). Calcisphere $\delta^{13}C$ measurements

depict even lower values, varying from -1.53 to -0.87‰ between 65.77 and 65.98 Ma (Figure 2A, green squares).

Nuttalides truempyi $\delta^{18}O$ values varied between -0.21 and 0.46‰ (Figure 2B, blue squares), while *Subbotina trivialis* oscillated between -0.26 and 0.62‰ (Figure 2B, red crosses) within the studied interval (66.03 to 65.62 Ma). Within the Danian interval of Hole 1262B, our results did not depict any significant trend, with no clear difference in the range of absolute values for the *Nuttalides truempyi* and *Subbotina trivialis* $\delta^{18}O$ records (Figure 2B). However, $\delta^{18}O$ measurements of bulk sediments depicted an increasing trend across the K-Pg interval and within the first 30 kyr of the Danian, as well as marked negative excursions during the Dan-C2 and Chron C29n events (Figure 2A, light blue circles). Remarkably low $\delta^{18}O$ values, from -1.73 to -0.93‰ were recorded by calcispheres between 65.77 and 65.98 Ma (Figure 2A, green squares).

2.3.2 Evaluating benthic foraminiferal preservation

We analysed *Nuttallides truempyi* tests from selected stratigraphic levels with SEM, micro-Raman spectroscopy and X-ray diffraction. Based on SEM and stereomiscroscope analyses, these levels yielded well-preserved specimens with a pseudo-glassy preservation (sensu Poirier et al., 2021; at 215.45 (65.85 Ma- during Dan-C2) and 215.25 mbsf (65.79 Ma- after Dan-C2)), as well as poorly-preserved specimens, with a frosty preservation (sensu Sexton et al., 2006 and Poirier et al., 2021; occurring at 214.80 mbsf (65.65 Ma – during lower C29n), 214.95 mbsf (65.68 Ma – during lower C29n) and 215.65 mbsf (65.89 Ma – during Dan C2) (Figure 3). Furthermore, SEM images of both external and internal areas of *Nuttalides truempyi* tests indicated that the cracked texture of the frosty tests occurs troughout the tests' walls (Figure 3- 214.8, 214.95, 215.65 mbsf). We also identified elements characteristic of

contaminating phases, such as iron, via SEM-EDS analysis - (Additional Supporting information Figure S1).

For X-ray diffraction analysis, we chose nine stratigraphic levels, being eight with frosty preservation, for instance at the onset of the Dan-C2 (215.55 m – 65.87 Ma), and one level with pseudo-glassy preservation, such as just after the K-Pg boundary (216.35 m- 66.00 Ma). During the Dan-C2 interval, diffratograms of *Nuttalides truempyi* tests present a high amorphism halo from around 10-25 (°2Θ) which suggest the presence of amorphous phases. This amorphism is also present after cleaning the specimen in an ultrasonic bath, but with less intensity. Most *Nutallides truempyi* tests analized show a mineralogical prominence of calcite and high-Mg calcite, besides accessory minerals such as siderite (e.g., 216.45 m – 66.01 Ma) (Table 2; details in additional Supporting information Figure S3).

Table 2: Main mineralogical composition of *Nuttalides truempyi* specimens over the studied interval.

Core	Section	Depht (mbsf)		Age (Ma)	Minerals		
22	3	214.8	193.79	65.65	high- Mg- calcite	Barytocalcite (?)	Girvasite
22	3	214.95	193.94	65.69	high- Mg- calcite		
22	4	215.25	194.24	65.80	high- Mg- calcite		Girvasite
22	4	215.45	194.44	65.85	calcite		
22	4	215.55	194.54	65.87	calcite	Kuthnohorite (?)	Barytocalcite(?)
22	4	216.00	194.99	65.97	calcite		
22	4	216.35	195.34	66.00	calcite	Boggsite (?)	Girvasite/siderite
22	4	216.45	195.44	66.01	calcite	Kuthnohorite (?)	Girvasite/siderite
22	4	216.5	195.49	66.02	calcite	Kuthnohorite (?)	Boggsite (?)

We used micro - Raman analyses to identify calcite on single *Nuttalides truempyi* tests from nine stratigraphic levels (Additional Supporting information Figure S2), based on characteristic Raman shifts: 1088 cm^{-1}; 713 cm^{-1}; 283 cm^{-1} and 156 cm^{-1} (e.g., du Châtelet et

al., 2013; DeCarlo et al., 2019; Cuny–Guirriec et al., 2019). From those nine samples, only one (at 216.35 mbsf; 66.00 Ma) presented a clear calcite signal in Raman spectroscopy in raw data (Additional Supporting information Figure S2A), which was also identified as having a pseudo-glassy preservation (Figure 4). The sample representative of the Dan-C2 interval presented a silent Raman spectrum throughout the mapping area. However, when we normalized and subtracted the baseline from all spectra (WR 07, WR14, WR23 and WR 40) we did not observe significant variation on peak intensities: all Raman peaks are characteristic of calcite (Additional Supporting information Figure S2 B - C). We averaged all spectra obtained from each sample in order to refine comparison, and still all peaks and bands characteristic of calcite are detected in same intensities with no significant dislocations on Raman shift (maybe 156 cm^{-1} shift seems dislocated to the right due to a luminescent effect) (Additional Supporting information Figure S2 C).

The comparison with Raman bands characteristic of calcite (from all measured samples) shows that the FWHM values and mean values from 282, 712 and 1087 cm^{-1} (Additional Supporting information Figure S2 D - G), tend to be higher in spectra obtained from WR23 and WR40 (post K-Pg samples) than those from WR07 and WR14 (pre-K-Pg samples).

Elemental analysis of Mg, Ca, Fe, Ba and Mn, directly on *Nuttalides truempyi* specimens, was measured on the penultimate (f-1 measurements) and antepenultimate (f-2 measurements) chambers of specimens selected from the same nine stratigraphic levels. We did not consider the last chamber of each test (f), since they were usually infilled with sediments. We express our results as calculated the El/Ca ratios; Mg/Ca values were in range of 1.908 to 52.10 $mmol.mol^{-1}$, Mn/Ca varied between 0.049 and 5.145 $mmol.mol^{-1}$, Ba/Ca values were in the range of 0.003 to 0.195 $mmol.mol^{-1}$, and Fe/Ca oscillated between 0.796 and 153.512 $mmol.mol^{-1}$ (see Table 3). We identified evidence for diagenetic alteration and/or

the presence of contaminating phases, such as the anomalously elevated Mg/Ca, Fe/Ca and Mn/Ca at 66.03 Ma, anomalously high Mg/Ca within the Dan-C2 and the Chron C29n event, and high Mg/Ca and Mn/Ca at 65.68 (Figure 5). Despite the lack of comparative data in the literature for the El/Ca ratios in *Nuttalides truempyi* in the Danian, traditional cleaning protocols for removing contaminating phases from clays in silicates, it is recommended to reject data in which Mn/Ca is greater than 0.1 mmol.mol^{-1} (e.g., Martin and Lea, 2002; Barker et al., 2003). Higher Mn/Ca values are attributed to the presence of contaminant Mn phases, including oxides and mixed authigenic Mn-Ca-Mg coatings (Boyle, 1983).

Table 3: El/Ca ratios of f-1 and f-2 chambers in nine specimens of *Nuttalides truempyi*

Depth (mbsf)		Mg/Ca (mmol.mol^{-1})		Mn/Ca (mmol.mol^{-1})		Ba/Ca (mmol.mol^{-1})		Fe/Ca (mmol.mol^{-1})	
		f-1	f-2	f-1	f-2	f-1	f-2	f-1	f-2
214.8	193.79	5.315	27.057	0.177	0.832	0.005	0.049	4.348	65.223
214.95	193.94	9.624	16.707	5.145	1.307	0.178	0.087	6.616	9.648
215.25	194.24	52.210	43.730	1.136	0.931	0.158	0.040	24.647	37.016
215.45	194.44	11.342	8.064	0.381	0.265	0.041	0.009	51.561	4.015
215.55	194.54	10.051	10.783	0.199	0.149	0.013	0.030	8.328	7.029
216.00	194.99	22.834	7.590	2.135	0.604	0.195	0.053	12.571	1.956
216.35	195.34	34.342	2.601	4.299	0.149	0.121	0.005	153.512	0.839
216.45	195.44	2.300	1.908	0.049	0.053	0.003	0.003	1.235	0.796
216.5	195.49	2.764	2.237	0.143	0.097	0.004	0.011	1.015	5.439

2.3.3 Changes in bottom water oxygenation and sediments carbonate content

Our interpretation for bottom water oxygenation is based on two proxies: the Mn/Al ratio and the V/(V+Ni) ratio. Mn/Al is interpreted as recording changes in bottom water oxygenation, with high Mn/Al suggesting periodic oxygenation, resulting in the precipitation of Mn-rich oxi-hydroxides (Croudace and Rothwell, 2015). Vanadium and nickel are considered as indicators of redox conditions (Rivera et al., 2018). According to He et al. (2016), V/(V+Ni) ratios above 0.84 indicate euxinic conditions, ratios between 0.54 and 0.82 indicate anoxic conditions, and ratios between 0.46 and 0.60 indicate dysoxic conditions. In the studied

interval, Mn/Al ratio varies between 0.99 and 11.05 (averaging 4.91) while V/(V+Ni) varies between 0.73 and 3.59 (averaging 1.67) (Figure 6). V/(V+Ni) increased during the Dan-C2 and Chron C29n events, whereas Mn/Al values decreased over these intervals (Figure 6).

2.4 DISCUSSION

2.4.1 Disentangling environmental and diagenetic signals in the $\delta^{18}O$ and $\delta^{13}C$ records

Foraminifera and other organisms that precipitate carbonates near to equilibrium with seawater can potentially preserve an environmental isotopic signal for millions of years, in case diagenetic processes do not overwrite the primary signal (e.g., Killingley, 1983; Pearson et al., 2001; Huber et al., 2011; Edgar et al., 2015; Jehle et al., 2015). At Site 1262, benthic and planktonic $\delta^{13}C$ records display the expected offset between deep and surface waters, with higher ratios recorded by planktonic foraminifera and lower ratios depicted by epibenthic foraminifera (Figure 2). This offset occurs mainly because photosynthetic activity at surface water preferentially captures light carbon (^{12}C), leaving the surface ocean dissolved inorganic carbon (DIC) pool relatively enriched in heavy carbon (^{13}C) (e.g., Katz et al., 2010; Tipple et al., 2010). Even though foraminiferal $\delta^{13}C$ signatures can additionally vary due to specific vital effects and/or seasonal calcification (e.g., Fraass and Lowery, 2017; Pracht et al., 2018), the differentiation between planktonic and benthic $\delta^{13}C$ records at Site 1262 is robust throughout the studied interval. Besides, our new *Nuttalides truempyi* $\delta^{13}C$ measurements present values in the same range as those reported for Site 1262 by, Barnet et al. (2019), and Hull et al. (2020) for the same species (Figure 7).

Pristine bulk $\delta^{18}O$ and $\delta^{13}C$ records generally reflect surface ocean conditions, since most of their volume is usually composed of calcareous nannofossils and planktonic foraminifera (e.g., Barnet et al., 2019; Arreguín-Rodriguez, 2021). Therefore, it is expected that bulk $\delta^{13}C$ values would be higher than those of benthic foraminifera, and within a range

comparable to that of planktonic foraminiferal values. However, over most of the studied interval of Site 1262, $\delta^{13}C_{bulk}$ is remarkably lower than both the planktonic and benthic foraminferal $\delta^{13}C$ records (Figure 2), even though all records present similar general trends of drops within the Dan-C2 and lower Chron C29n events. Birch et al. (2012) suggested that, immediately after Dan-C2, reduced ocean productivity and proliferation of opportunistic planktonic foraminifera, characterized by extreme vital effects, could account for significant drops in $\delta^{13}C$ records. However, we consider that this explanation is not likely for the studied interval of Site 1262, because the magnitudes of the decreasing trends in the bulk $\delta^{13}C$ record are much higher than those of the decreasing trends in the *Subbotina trivialis* $\delta^{13}C$ record (Figure 2). Similarly, massive methane release in the water column could account for remarkably low $\delta^{13}C$ values, but we assume that such a mechanism would result is much higher magnitudes that those observed for the negative bulk $\delta^{13}C$ excursions, due to the extremely low signatures of methane. At most, moderate methane release (e.g., Garidel-Thoron et al., 2004), limited to surface sediments (not spreading through the water column), could be agreed for explaining the increased gradient between bulk and planktonic $\delta^{13}C$ within the Dan-C2 at Site 1262 (Figure 2).

One alternate explanation considers the micrite layer, deposited immediately above the K-Pg transition at Site 1262, which Bralower et al. (2020) interpreted as the possible result of the activity of carbonate-producing cyanobacteria ("cyanobacteria whitening"). A gradual seasonal decoupling of cyanobacteria from planktonic foraminifera, and reducing paleoproductivity towards the Dan-C2, may explain anomalously low $\delta^{13}C$ of bulk sediments, if they are mainly composed of bacterial-produced micrite. This hypothesis also accounts for

the likely environmental signal depicted by the bulk $\delta^{13}C$ drops at the Dan-C2 and lower C29n events.

Calcispheres are also observed in abundance during the first ~2.5 Ma following the K-Pg extinction event in several locations (Gibbs et al., 2020), including at Site 1262. Isotope measurements of vegetative cysts of *Thoracosphaera heimii* are used for reconstructing environmental conditions in the intermediate photic zone, since these microfossils are highly resistant against dissolution (Minoletti et al., 2014). Modern *Thoracosphaera heimii* species present remarkably low $\delta^{18}O$ and $\delta^{13}C$ values, supporting that the negative $\delta^{18}O$ and $\delta^{13}C$ values recorded by Danian calcispheres at Site 1262 in fact depict environmental signals, and may account for the observed negative excursions depicted by the bulk $\delta^{18}O$ and $\delta^{13}C$ records. Additionally, $\delta^{13}C$ records of single-species of dinoflagellate cyst from Bass River, across the Paleoce-Eocene Thermal Maximum (PETM), indicated that the $\delta^{13}C$ of dissolved inorganic carbon exerts a major control on dinocyst $\delta^{13}C$ (Sluijs et al., 2018).

Benthic and planktonic foraminiferal $\delta^{18}O$, however, show scattered values that strongly overlap throughout most of the studied interval (Figure 2). We interpret that this overlapping benthic and planktonic $\delta^{18}O$ records, which do not depict any clear trend, are most likely the result of diagenetic changes that strongly affected the $\delta^{18}O$, since, if this pattern was an environmental signal, it would imply a complete lack of temperature and/or salinity stratification in the water column (e.g., Katz et al., 2010; Huber et al., 2011). After the Dan-C2 event, benthic $\delta^{18}O$ became slightly higher than planktonic values, suggesting improved preservation of foraminiferal calcite. Overall, our *Nuttalides truempyi* $\delta^{18}O$ record, when converted to paleotemperatures, compares well with data from Site 1049 (Hull et al., 2020). It should be noted that these sites presented different paleobathymetries and were influenced by different water masses (see Supporting Information Figure S6). Our *Nuttalides truempyi* $\delta^{13}C$

measurements, are also similar to those reported by Barnet et al. (2019) and Hull et al. (2020) for Site 1262 (Figure 7).

Conversely, the Site 1262 bulk $\delta^{18}O$ record depicts gradual trends and varied overall in phase with the bulk $\delta^{13}C$ record. Particularly, low bulk $\delta^{18}O$ values occurred within the Dan-C2 and the lower Chron C29n events. Therefore, we suggest that the bulk $\delta^{18}O$ series depicts original environmental trends recorded in a more resistant calcite phase, such as micrite and/or calcispheres despite their small sizes and large reactive surface (e.g., Bralower et al., 2020; Gibbs et al., 2020).

2.4.2 Evaluation of authigenic carbonate phases of foraminiferal tests

Foraminifera tests can be altered by dissolution, recrystallization and/or overgrowth of carbonates. All these factors have the potential to compromise isotopic signals (O'Brien et al., 2017). In our results we confirm that even apparently glassy foraminiferal calcite may have been altered by micro-recrystallization, impacting mostly $\delta^{18}O$ values. Our SEM observations of *Nuttalides truempyi* tests revealed secondary calcites (Figure 3 and Additional Supporting information Figure S4) and micrites (see details in Figure 5). Authigenic carbonates formed on the surface of and/or inside foraminiferal tests can significantly interfere with the application of foraminiferal geochemical proxies (e.g. Edgar et al., 2013; Hasenfratz et al., 2017). For trace elements analyses, traditional methods used to clean foraminiferal samples aim to remove clay particles, Mn-Fe-coatings and organic matter, using oxidative and reductive cleaning steps (e.g. Barker et al., 2003). Authigenic overgrowths are usually difficult to be removed, unless the overgrown layers are very thin and fragile, being removable with weak acid leaches, or if oxides are present between the foraminiferal test and authigenic carbonate layers. However,

for $\delta^{18}O$ and $\delta^{13}C$ measurements, benthic foraminiferal tests are usually only cleaned with an ultrasonic bath, which apparently cannot remove authigenic phases according to our results.

In our case study, we found different authigenic carbonate phases in *Nuttalides truempyi* specimens (see Table 4). These minerals also have standard free energies (Table 5), depending on bivalent cations (Svarjensky, 1984), being these: Ca^{2+}, Mg^{2+}, Mn^{2+}, Zn2+ and Fe^{2+} in decreasing order of standard free energies. Therefore, precipitation of pure calcite takes much more energy than precipitation of Mg-rich, Mn-rich, Fe-rich carbonates. In fact, our LA-ICP-MS elemental analyses and XRD data support the presence of authigenic carbonate phases rich in Mg, Mn, Ba and Fe (Figure 5), at stratigraphic levels characterized by frosty foraminiferal preservation, as previously observed by Ni et al. (2020) in the deepest part of the Landsort Deep. Conversely, at 65.85 Ma (215.45 mbsf), we observed lower values of El/Ca ratios in specimens characterized by pseudo-glassy preservation (Figure 5).

Despite the discussion on whether the Dan-C2 was an hyperthermal event (e.g., Barnet et al., 2019; Krahl et al., 2020), our redox proxy records suggest that poorly oxygenated bottom waters occurred at Site 1262 during the event (Figure 6). A comparable pattern was also observed in the western South Atlantic Ocean at Site 516 (Krahl et al., 2020). In modern marine sediments, poorly oxygenated bottom and pore waters may lead to precipitation of Mn-rich carbonate phases, such as kuthnohorite and rhodocrosite (e.g., van Dijk et al., 2019; Ni et al., 2020). Therefore, the thermodynamic changes described above would have acted in tandem with decreased bottom and pore water oxygenation to favor precipitation of authigenic carbonate phases, which could alter isotopic fractionation. Although we have specifically

evaluated tests of *Nuttalides truempyi*, signs of secondary calcite were also observed in other planktonic foraminiferal assemblages (see additional Supporting information Figure S5).

Table 4: Chemical compositions of the main minerals found in *Nuttalides truempyi* along the studied interval of Site 1262.

Mineral	Chemical Formula
Magnesium calcite	$(CaMg)CO_3$
Calcite	$CaCO_3$
Siderite	$FeCO_3$
Boggsite	$Ca_8Na_3(Si,Al)_{96}O_{192}.70H_2O$
Kuthnohorite	$Ca(Mn,Mg,Fe)(CO_3)_2$
Girvasite	$NaCa_2Mg_3(PO_4)_3(CO_3)(H_2O)_6$

Table 5: Standard formation free energies of bivalent aqueous ions for calcite-type carbonates at 25°C and 1 bar (Svarjensky, 1984).

Metal	$\Delta G°_{f.M^{+2}}$ cal.mol-1
Ca	-132.155
Mg	-108.700
Mn	-54.500
Zn	-35.331
Fe	-21.830

2.5 CONCLUSIONS

Our study case of the earliest Danian interval at Site 1262 revealed that benthic and planktonic $\delta^{18}O$ records were diagenetically altered by crystallization of authigenic carbonates. In fact, we identified trace carbonate phases such as kuthnohorite, siderite and girvasite in *Nuttalides truempyi* tests, which modified $\delta^{18}O$ values at times of reduced bottom and pore water oxygenation, such as during the Dan-C2 and the lower Chron C29n events. Benthic and

planktonic $\delta^{13}C$ records were apparently less affected by the crystallization of these authigenic phases, and bulk $\delta^{13}C$ and $\delta^{18}O$ values, which are apparently dominated by a signal of bacterial micrite and/or dinocysts, likely preserved original environmental signatures. In summary, our study highlights the need for comprehensive characterizations of foraminiferal calcites, mainly for paleoceanographic reconstructions of intervals characterized by warm climate states and a less ventilated deep ocean.

Data availability

New benthic, planktonic stable isotopes, LA-ICP-MS, DRX and XRF-derived elemental data will are available at the Zenodo data publisher. https://doi.org/10.5281/zenodo.6798734

Acknowledgments, Samples, and Data

The authors thank the International Ocean Discovery Program (IODP) for providing the studied material; CAPES (Coordenação de Aperfeiçoamento de Pessoal de Nível Superior) for financial support to Project IODP/Capes #88887.091703/2014-1. We thank the technical staff at itt OCEANEON for assistance with XRD (Michele Goulart), XRF analyses, LA-ICP-MS (Valeska Meirelles) and the Laboratory of Astrobiology at USP University for Raman Spectroscopy analysis. The authors M.H.H. Bom and G. Krahl are CAPES fellows.

2.6 REFERENCES

Alegret, L. and Thomas, E., 2013. Benthic foraminifera across the Cretaceous/Paleogene boundary in the Southern Ocean (ODP Site 690): Diversity, food and carbonate saturation. Marine Micropaleontology, 105, 40-51.

Arreguín-Rodriguez, G.J., Barnet, J.S.K., Leng, M.J., Litter, K., Kroon, D., Schmidt, D.N., Tomas, E., Alegret, L., 2021. Benthic foraminiferal turnover across the Dan-C2 event in the

eastern South Atlantic Ocean (ODP Site 1262). Palaeogeography, Palaeoclimatology, Palaeoecology, 572, 110410. https://doi.org/10.1016/j.palaeo.2021.110410

Barker, S., Greaves, M., Elderfield, H., 2003. A study of cleaning procedures used for foraminiferal Mg/Ca paleothermometry. Geochemistry, Geophysics, Geosystems, 4(9), doi: 10.1029/2003GC000559.

Barnet, J. S., Littler, K., Kroon, D., Leng, M. J., Westerhold, T., Röhl, U., Zachos, J. C., 2018. A new high-resolution chronology for the late Maastrichtian warming event: Establishing robust temporal links with the onset of Deccan volcanism. Geology, 46(2), 147-150.

Barnet, J.S.K., Litter, K., Westerhold, T., Kroon, D., Leng, M.J., Bailey, I., Röhl, U., Zachos, J.C., 2019. A High-Fidelity Benthic Stable Isotope Record of Late Cretaceous–Early Eocene Climate Change and Carbon-Cycling. Paleoceanography and Paleoclimatology, 34. https://doi.org/10.1029/2019PA003556

Birch, H.S., Coxall, H.K., Pearson, P.N., 2012. Evolutionary ecology of Early Paleocene planktonic foraminifera: size, depth habitat and symbiosis. Paleobiology, 38, 374-390.

Boyle, E.A., 1983. Manganese carbonate overgrowths on foraminifera tests. Geochimica et Cosmochimica Acta, 47, 1815-1819.

Bralower, T.J., Cosmidis, J., Heaney, P.J., Kump, L.,R., Morgan, J.V., Harper, D.T., Lyons, S.L., Freeman, K.H., Grice, K., Wendler, J.E., Zachos, J.C., Artemieva, N., Chen, S.A., Gulick, S.P.S., Schaefer, B., Thomas, E., Vajda, V., 2020. Origin of a global carbonate layer deposited in the aftermath of the Cretaceous-Paleogene boundary impact. Earth and Planetary Science Letters, 548, 116476.

Coccioni, R., Frontalini, F., Bancalà, G., Fornaciari, E., Jovane, L., Sprovieri, M., 2010. The Dan-C2 hyperthermal event at Gubbio (Italy): Global implications, environmental effects, and

cause(s). Earth and Planetary Science Letters, 297,0298-305. http://dx.doi.org/10.1016/j.epsl.2010.06.031

Crivellari, S., Viana, P.J., Campos, M.C., Kuhnert, H., Lopes, A.B.M., Da Cruz Jr, F.W., Chiessi, C.M., 2021. Development and characterization of a new in-house reference material for satbel carbon and oxygen isotopes analyses. Journal of Analytical Atomic Spectrometry, 36, 1125-1134.

Croudace, I.W., and Rothwell, R.G., 2015. Micro-XRF studies of sediment cores. Applications of a non-destructive tool for the environmental sciences. In, Croudace, I,W. and Rothwell, R.G, (eds.) Micro-XRF Studies of Sediment Cores: Applications of a non-destructive tool for the environmental sciences. (Developments in Paleoenvironmental Research, 17) Dordrecht, NL. Springer, pp. 1-21.

Cuny-Guirriec, K., Douville, E., Reynaud, S., Allemand, D., Bordier, L., Canesi, M., Mazzoli, C., Taviani, M., Canese, S., McCulloch, M., trotter, J., Rico-Esenaro, S.D., Sanchez-Cabeza,

.A., Ruiz-Fernandez, A.C., Carricart-Ganivet, J.P., Scott, P.M., Sadekiv, A., Montagna, P., 2019. Coral Li/Mg thermometry: Caveats and constraints. Chemical Geology, 523, 162-178.

Daëron, M., Drysdale, R.N., Peral, M., Huyghe, D., Blamart, D., Coplen, T.B., Lartaud, F., Zanchetta, G., 2019. Most Earth-surface calcites precipitate out of isotopic equilibrium. Nature Communications, 10:429. doi.org/10.1038/s41467-019-08336-5

DeCarlo, T, M., Comeau, S., Cornwall, C.E., Gajdzik, L., Guagliardo, P., Sadekov, A., Thillainath, E.C., Trotter, J., McCulloch, T.M., 2019. Investigating marine bio-calcification mechanisms in a changing ocean with in vivo and high-resolution ex vivo Raman spectroscopy. Global Change Biology, 25, 1877-1888.

De Nooijer, L.J., Spero, H.J., Erez, J., Bijma, J. &Reichart, G.J., 2014. Biomineralization in perforate foraminifera. Earth-Science Reviews, 135, 48–58. doi.org/10.1016/j.earscirev.2014.03.013

Dinarès-Turell, J., Westerhold, T., Pujalte, V., Röhl, U. & Kroon, D., 2014. Astronomical calibration of the Danian stage (Early Paleocene) revisited settling chronologies of sedimentary

records across the Atlantic and Pacific Oceans. Earth and Planetary Science Letters. 405, 119–131. https://doi.org/10.1016/j.epsl.2014.08.027

Du Châtelet, E.A., Frontalini, F., Guillot, F., Recourt, P., & Ventalon, S., 2013. Surface analysis of agglutinated benthic foraminifera through SEM-EDS and Raman analyses: An expeditious approach for tracing mineral diversity. Marine Micropaleontology, 105, 18-29. http://dx.doi.org/10.1016/j.marmicro.2013.10.001

Edgar, K.M., Pälike, H., Wilson, P.A., 2013. Testing the impact of diagenesis on the $\delta^{18}O$ and $\delta^{13}C$ of benthic foraminiferal calcite from a sediment burial depth transect in the equatorial Pacific. Paleoceanography, 28, 468-480.

Edgar, K.M., Anagnostou, E., Pearson, P.N., Foster, G.L., 2015. Assessing the impact of diagenesis on $\delta^{11}B$, $\delta^{13}C$, $\delta^{18}O$, Sr/Ca and B/Ca values in fossil planctik foraminiferal calcite. Geochimica et Cosmochimica Acta, 1661 189-209.

Erez, J., Luz, B. 1983. Experimental paleotemperature equation for planktonic foraminifera. Geochimica et Cosmochimica Acta, 47,6. 1025-1031.

Erez, J., 2003. The source of ions for biomineralization in foraminifera and their implications for paleoceanographic proxies, in Biomineralization, edited by P. M. Dove, J. J. De Yoreo, & S. Weiner, pp. 115–149, Mineralogical Society of America., Washington, D. C.

Fraass, A.J., Lowery, C.M., 2017. Defining uncertainty and error in planctik foraminiferal oxygen isotope measurements. Paleoceanography, 32, 104-102.

Garidel-Thoron, T., Beaufort, L., Bassinot, F., Henry, P., 2004. Evidence for large methane realeases to the atmosphere from deep-sea gas-hydrate dissociation during the last glacial episode. PNAS, 25, 9187-9192.

Gibbs, S.J., Bown, P.R., Ward, B.A., Alvarez, S.A., Kim, H., Archontikis, O.A., Sauterey, B., Poulton, A.J., Wilson, J., Ridgwell, A., 2020. Algal plankton turn to hunting to survive and recover from end-Cretaceous impact darkness. Science Advances, 6, eabc9123. 10.1126/sciadv.abc9123

Gilabert, V., Arenillas, I., Arz, J.A., Batenburg, S.J., Robinson, S.A., 2021. Multiproxy analysis of paleoenvironmental, paleoclimatic and paleoceanographic changes during the early Danian in the Caravaca section (Spain). Palaeogeography, Palaeoclimatology, Palaeoecology, 576, 110513. https://doi.org/10.1016/j.palaeo.2021.110513

Golreihan A, Steuwe C, Woelders L, Deprez A, Fujita Y, & Vellekoop J., 2018. Improving preservation state assessment of carbonate microfossils in paleontological research using label-free stimulated Raman imaging. PLOS ONE 13(7): e0199695. doi:10.1371/journal.pone.0199695

Hasenfratz, A.P., Martínez-Garcia, A., Jaccard, S.L., Vance, D., Wälle, M., Greaves, M., Haug, G.H., 2017. Determination of the Mg/Mn ratio in foraminiferal coatings: Anapproach to correct Mg/Ca temperatures for Mn-rich contaminant phases. Earth and Planetary Science Letters, 457, 335-347.

He, C., Ji, L., Wu, Y, Su, A., Zhang, M., 2016. Characteristics of hydrothermal sedimentation process in the Yanchang Formation, south Ordos Basin, China: Evidence from element geochemistry. Sedimetary Geology, 345, 33-41.

Huber, B.T., MacLeod, K.G., Gröcke, D.R., Kucera, M., 2011. Paleotemperature and paleosalinity inferences. and chemostratigraphy across the Aptian/Albian boundary in the subtropical North Atlantic. Paleoceanography, 26, PA4221, doi:10.1029/2011PA002178.

Hull, P.M., Bornemann, A., Penman, D.E., Henehan, M.J., Norris, R.D., Wilson, P.A., Blum, P., Alegret, L., Batenburg, S.J., Bown, P.R., Bralower, T.j., Cournede, C., Deutsch, A., Donner, B., Friedrich, O., Jehle, S., Kim, H., Kroon, D., Lippert, P.C., Loroch, D., Moebius, I., Moriya, K Peppe, D.J., Ravizza, G.E., Röhl, U., Schueth, J.D., Sepúlveda, J.,Sexton, P.F., Sibert, E.C., S´liwin´ska, K.K., Summons, R.E., Thomas, E., Westerhold, T., Whiteside, J.H., Yamaguchi, T Zachos, J.C., 2020. On impact and volcanism across the Cretaceous-Paleogene boundary. Science, 367, 266-272. 10.1126/science.aay5055

Jacob, D. E., Wirth, R., Agbaje, O.B.A., Branson, O. & Eggins, S.M., 2017. Planktic foraminifera form their shells via metastable carbonate phases. Nature Communications, 8(1), 1–8. doi.org/10.1038/s41467-017-00955-0

Jehle, S., Bornemann, A., Deprez, A., Speijer, R.O., 2015. The Impact of the Latest Danian Event on Planktic Foraminiferal Faunas at ODP Site 1210 (Shatsky Rise, Pacific Ocean). PLOS ONE, 10, 11, e0141644. doi:10.1371/journal.pone.0141644.

Katz, M.E., Cramer, B.S., Franzese, A., Hönisch, B., Miller, K.G., Rosenthal, Y., Wright, J.D., 2010. Traditional and emerging geochemical proxies in foraminifera. Journal of Foraminiferal Research, 40(2). doi:10.2113/gsjfr.40.2.165

Killingley, J.S., 1983. Effects of diagenetic recrystallization on $^{18}O/^{16}O$ values of deep-sea sediments. Nature, 301,594-597. https://doi.org/10.1038/301594a0

Krahl, G., Bom, M.H.H., Kochhann, K.G.D., Souza, L.V., Savian, J.F., Fauth, G., 2020. Environmental changes occurred during the Early Danian at the Rio Grande Rise, South Atlantic Ocean. Global and Planetary Change, 191, 103197.

Krahl, G., Arenillas, I., Gilabert, V., Kochhann, K.G.D., Bom, M.H.H., Fauth, G., Arz, J.A., 2023. Impact of early Danian environmental perturbations on mid-latitude planktic foraminiferal assemblages from the ODP Site 1262 (South Atlantic Ocean). Newsletter on Stratigraphy, Early-Acess-Article. DOI: 10.1127/nos/2023/0744

Krahl G., Kochhann, K.G.D., Bom, M.H.H., Geshev, J., Nicolodi, S., Bianchi, L.L., Gambeta, J.H., Savian, J.F., Fauth, G., 2021. Multiproxy stratigraphy evidence of paleoenvironmental shift and organization at the early Danian from Walvis Ridge: a link on global signature (In Press).

Lear, C.H., Elderfield, H., Wilson, P.A., 2000. Cenozoic Deep-Sea temperatures and Global Ice Volumes from Mg/Ca in Benthic Foraminiferal Calcite. Science, 287,269-272, doi: 10.1126/science.287.5451.269.

Martin, P. A., and Lea, D.W., 2002. A simple evaluation of cleaning procedures on fossil benthic foraminiferal Mg/Ca. Geochemistry Geophysics Geosystems, 3(10), 8401.

Minoletti, F., Hermoso, M., Candelier, Y., Probert, I., 2014. Calibration of stable isotope composition of Thoracosphaera heimii (dinoflagellate) calcite for reconstructing paleotemperatures in the intermediate photic zone. Paleoceanography and Paleoclimatology, 29, 1111-1126. https://doi.org/10.1002/2014PA002694

Ni, S., Krupinski, Q.N.B., Groeneveld, J., Persson, P., Somogyi, A., Brinkmann, I., Knudsen, K.L., Seidenkratz, M.S., Filipsson, H.L., 2020. Early diagenesis of foraminiferal calcite under anoxic conditions: A case study from the Landsort Deep, Baltic Sea (IODP Site M0063). Chemical Geology, 558, 119871.

Nürnberg, D., J. Bijma, and C. Hemleben, 1996. Assessing the reliability of magnesium in foraminiferal calcite as a proxy for water mass temperatures. Geochimica et Cosmochimica Acta, 60, 803–814. doi:10.1016/0016-7037(95)00446-7

O'Brien, C.L., Robinson, S.A., Pancost, R.D., Damnsté, J.S.S., Schouten, S., Lunt, D.J., Alsenz, H., Bornemann, A., Bottini, C., Brassel, S.C., Farnsworth, A., Fosrter, A., Huber, B.T., Inglis, G.N., Jenkyns, H.C., Linnert, C., Littler, K., Markwick, P., McAnena, A., Mutterlose, J., Naafs, B.D.A., Püttmann, W., Sluijs, A., van Helmond, N.A.G.M., Vallekoop, J., Wagner, T., Wrobel, N.E., 2017. Cretaceous sea-surface temperature evolution: Constraints from TEX86 and planktonic foraminiferal oxygen isotopes. Earth-Science Reviews, 172, 224-247.

Pearson, P.N., Ditchfield, P.W., Singano, J., Horcourt-Brown, K.G., Nicholas, C.J., Olsson, R.K, Shacklenton, N.J., Hall, M.A., 2001. Warm tropical sea surface temperatures in the Late Cretaceous and Eocene epochs. Nature, 413, 481-487. https://doi.org/10.1038/35097000

Pearson, P.N. and Burgess, C.E., 2008. Foraminifer test preservation and diagenesis: comparison of high latitude Eocene sites. From: Austin, W. E. N. & James, R. H. (eds) Biogeochemical Controls on Palaeoceanographic Environmental Proxies. Geological Society, London, Special Publications, 303, 59–72. doi:10.1144/SP303.5

Pearson, P.N., 2012. Oxygen isotopes in foraminifera: overview and historical review. In Reconstructing Earth's Deep-Time Climate—The State of the Art in 2012, Paleontological

Society Short Course, November 3, 2012. The Paleontological Society Papers, Volume 18, Linda C. Ivany and Brian T. Huber (eds.), pp. 1–38.

Poirier, R.K., Gaetano, M.Q., Acevedo, K., Schaller, M.F., Raymo, M.E., Kozdon, R., 2021. Quantifying Diagenesis, Contributing Factors, and Resulting Isotopic Bias in Benthic

Foraminifera Using the Foraminiferal Preservation Index: Implications for Geochemical Proxy Records. Paleoceanography and Paleoclimatology, 36, https://doi.org/10.1029/2020PA004110

Pracht, H., Metcalfe, B., Peeters, F.J.C., 2018. Oxygen isotope composition of final chamber of planktick foraminifera provides evidence for vertical migration and depth integrated growth. Biogeosciences Discussions, https://doi.org/10.5194/bg-2018-146

Quillévéré, F., Norris, R.D., Kroon, D., Wilson, P.A., 2008. Transient ocean warming and shifts in carbon reservoirs during the early Danian. Earth and Planetary Science Letters, 265, 600-615.

Rivera, H.A., Le Roux, J.P., Sánchez, L.K., Mariño-Martínez, J.E., Salazar, C., Barragán, J.C., 2018. Palaeoredox conditions and sequence stratigraphy of the Cretaceous storm-dominated,

mixed siliciclastic-carbonate ramp in the Eastern Cordillera Basin (Colombia): Evidence from sedimentary geochemical proxies and facies analysis. Sedimentary Geology, 372, 1-24.

Sexton, P.F.; Wilson, P. A. & Pearson, P. N., 2006. Microstructural and geochemical perspectives on planktic foraminiferal preservation: “Glassy” versus “Frosty”. Geochemistry Geophysics Geosystems, 7,(12), 1-29. doi:10.1029/2006GC001291

Sluijs, A., vanRoij, L., Frieling, J., Laks, J., Reichart, G.J., 2018. Single-species dinoflagellate cyst carbon isotope ecology across the Paleocene-Eocene Thermal Maximum. Geology, 46, 79-82. https://doi.org/10.1130/G39598.1

Spero, H., Bijma, J., Lea, D., Bemis, B.E., 1997. Effect of seawater carbonate concentration on foraminiferal carbon and oxygen isotopes. Nature, 390, 497–500. doi.org/10.1038/37333

Sverjensky, D.A., 1984. Prediction of Gibbs free energies of calcite – type carbonates and the equilibrium distribution of trace elements between carbonates and aqueous solutions. Geochimica et Cosmochimica Acta, 48, 1127-1134.

Tipple, B.J., Meyers, S.R., Pagani, M., 2010. Carbon isotope ratio of Cenozoic CO_2: A comparative evaluation of available geochemical proxies. Paleoceanography, 25, PA 3202. doi:10.1029/2009PA001851

Van Dijk, I., Mouret, A., Cotte, M., Le Houedec, S., Oron, S., Reichart, G.J., Reyes-Herrera, J., Fillipsson, H.L., Barras, C., 2019. Chemical heterogeneity of Mg, Mn, Na, S and Sr in benthic foraminiferal calcite. Frontiers in Earth Science,7, 281. doi: 10.3389/feart.2019.00281

Van Hinsbergen, D.J.J., Groot, L.V., Van Schaik, J.S., Spakman, W., Bijl, P.K., Sluijs, A., Langereis, C.G. & Brinkhuis, H., 2015. A Paleolatitude Calculator for Paleoclimate Studies. PLOS ONE, 10(6), e0126946. doi: 10.1371/journal.pone.0126946

Westerhold, T., Röhl, U., Donner, B., McCarren, H.K., Zachos, J.C., 2011. A complete high-resolution Paleocene benthic stable isotope record for the central Pacific (ODP Site 1209). Paleoceanography, 26, PA2216. http://dx.doi.org/10.1029/2010PA002092

Westerhold, T., Marwan, N., Drury, A.J., Liebrand, D., Agnini, C., Anagnostou, E., Barnet, J.S.K., Bohaty, S.M., De Vleeschouwer, D., Florindo, F., Frederichs, T., Hodell, D.A., Holbourn, A.E., Kroon, D., Lauretano, V., Littler, K., Lourens, L.J., Lyle, M., Pälike, H., Röhl, U., Tian, J.,Wilkens20, Wilson, P.A., Zachos, J.C., 2020. An astronomically dated record of Earth's climate and its predictability over the last 66 million years. Science, 11, 369, 1383-1387. 10.1126/science.aba6853

Woelders, L., Vellekoop, J., Weltje, G.J., de Nooijer, L., Reichart, G.J., Peterso, F., Claeys, P., Speijer, R.P., 2018. Robust multi-proxy data integration, using late Cretaceous paleotemperature records as a case study. Earth and Planetary Science Letters, 500, 215-224. https://doi.org/10.1016/j.epsl.2018.08.010

Zachos, J.C., Kroon, D., Blum, P., et al. 2004. Proceedings of the Ocean Drilling 1003 Program Initial Reports, volume 208, Texas A&M University, College Station TX 1004 77845-9547, USA. [CD-ROM]. Available from: Ocean Drilling Program.

Zachos, J.C., McCarren, H., Murphy, B., Röhl, U., Westerhold, T., Tempo and scale of late Paleocene and early Eocene carbon isotope cycles: Implications for the origin of hyperthermals. Earth and Planetary Science Letters, 299, 242-249. http://dx.doi.org/10.1016/j.epsl.2010.09.004

Zeebe, R.E., 2001. Seawater pH and isotopic paelotemperatures of Cretaceous oceans. Palaeogeography, Paleeoclimatology, Palaeoecology, 170, 49-57. doi.org/10.1016/S0031-0182(01)00226-7

Figure 1: Paleogeographic reconstruction for the K-Pg Boundary (~66 Ma), with the location of ODP Site 1262. Map generated with the ODSN system: http://www.odsn.de/odsn/services/paleomap/paleomap.html.

Figure 2: Carbon (A) and oxygen (B) isotope records measured on benthic foraminifera (blue squares), planktonic foraminifera (red crosses) and bulk sediments (light blue circles - Krahl et al., 2023), and calcispheres (green squares) at Site 1262.

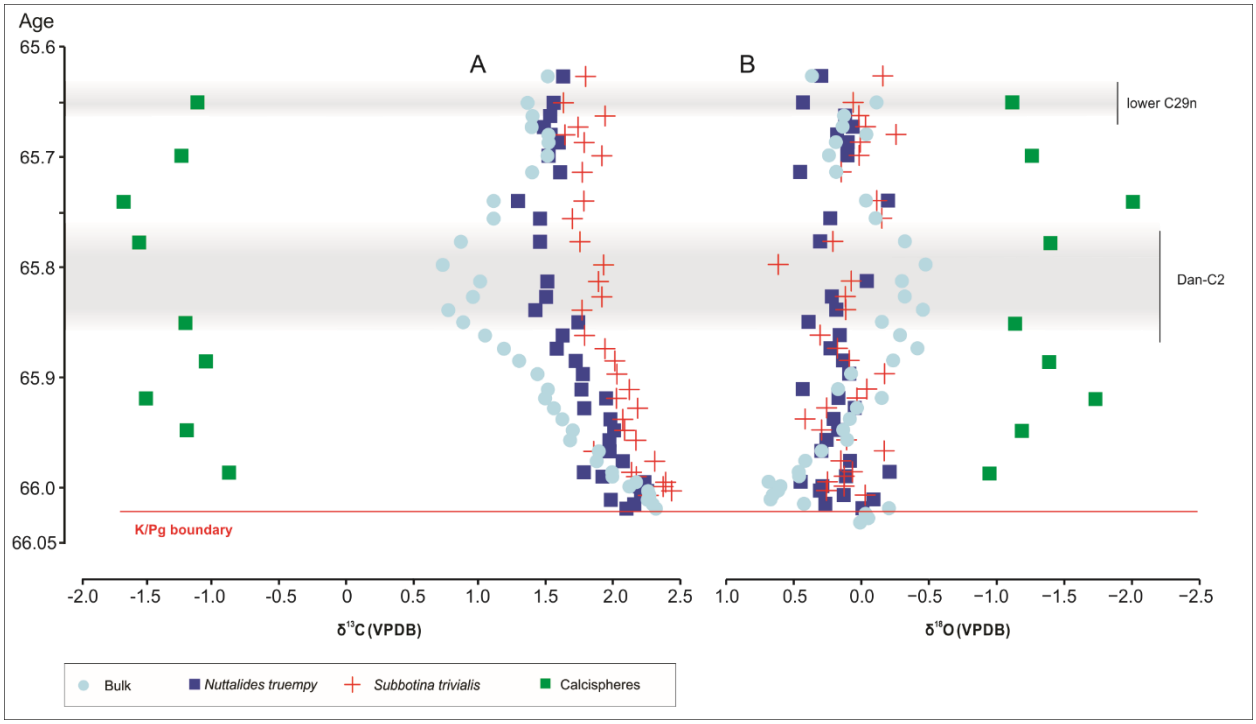

Figure 3: Scaning Electron Microscope images for assessing calcite preservation of *Nuttalides truempyi* tests. Good preservation (pseudo-glassy; *sensu* Poirier et al., 2021) occurs at 215.25 mbsf; Poor preservation (frosty; sensu Sexton and Pearson, 2006 and Poirier et al., 2021) occurs at 215.45 mbsf, 214.95 mbsf and 215.65 mbsf. Despite an external glassy appearance of the specimen retrieved at 214.8 mbsf, externally the tests appear to be a glassy calcite, but internally the growth of secondary carbonates is evident.

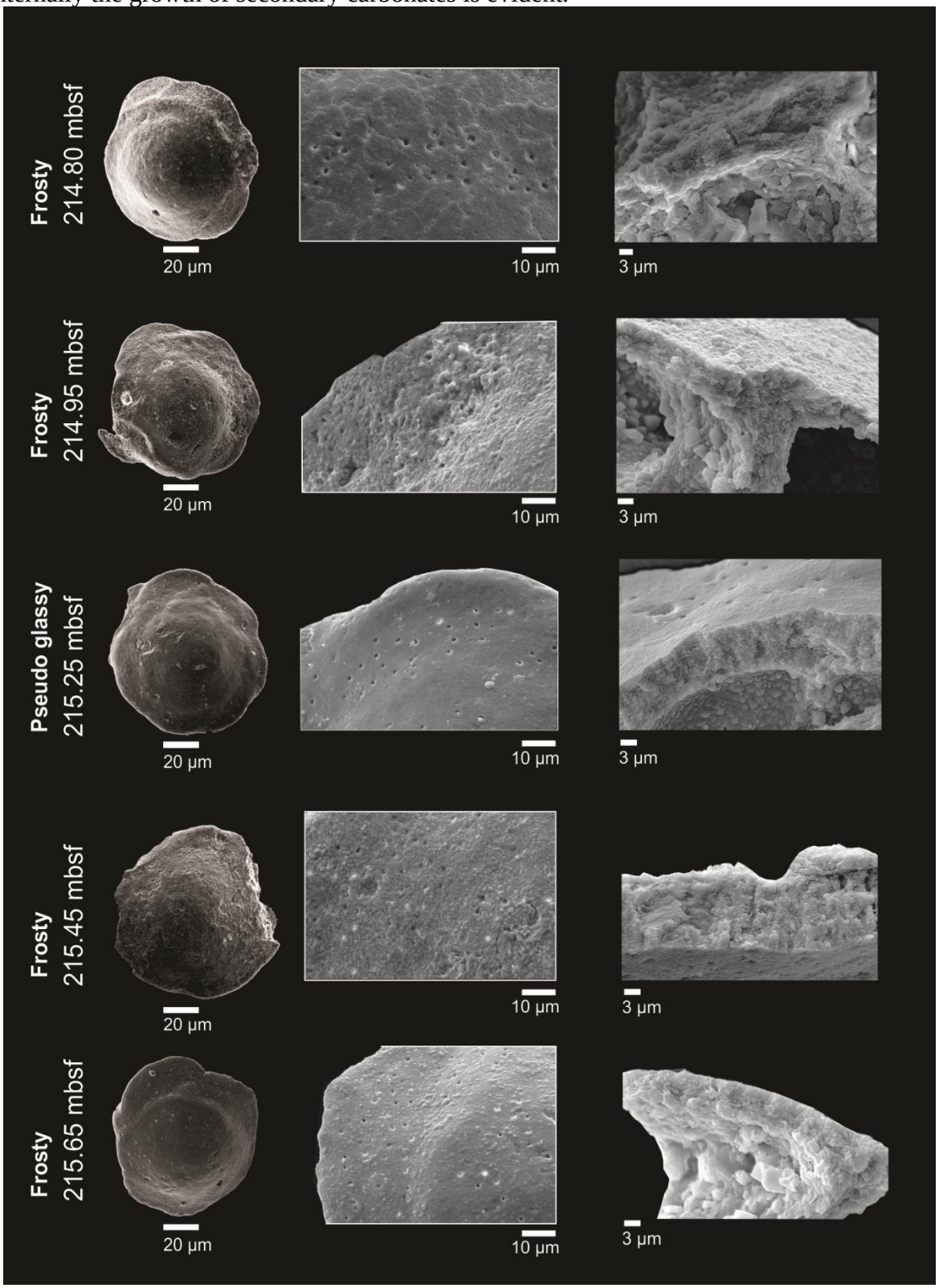

Figure 4: Raman shift by spectra of frosty (A) and a pseudo-glassy (B) *Nuttalides truempyi* specimens. Four characteristic peaks of calcite are identified in B, whereas the spectrum in A is “silent”. SEM and stereomicroscope images are provided to illustrate calcite preservations.

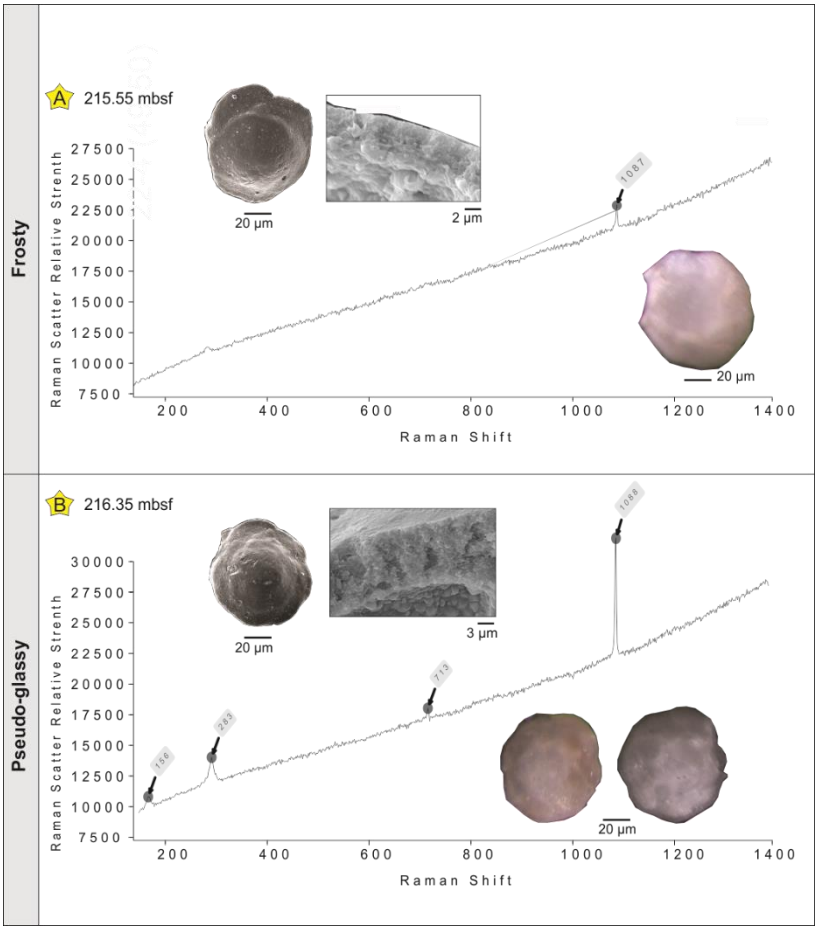

Figure 5: Variability of element/Ca ratios of *Nuttalides truempyi* tests over the studied interval at ODP Site 1262. Note that lower El/Ca ratio are observed in pseudo-glassy specimens, whereas high El/Ca ratios occur in frosty specimens. Orange curves refers to (f-1) and green curves refers to (f-2) position. Yellow stars indicate the samples evaluated. Lower panel details ablation spots. (For interpretation of the references to colour in this figure legend, the reader is referred to the web version of this article.)

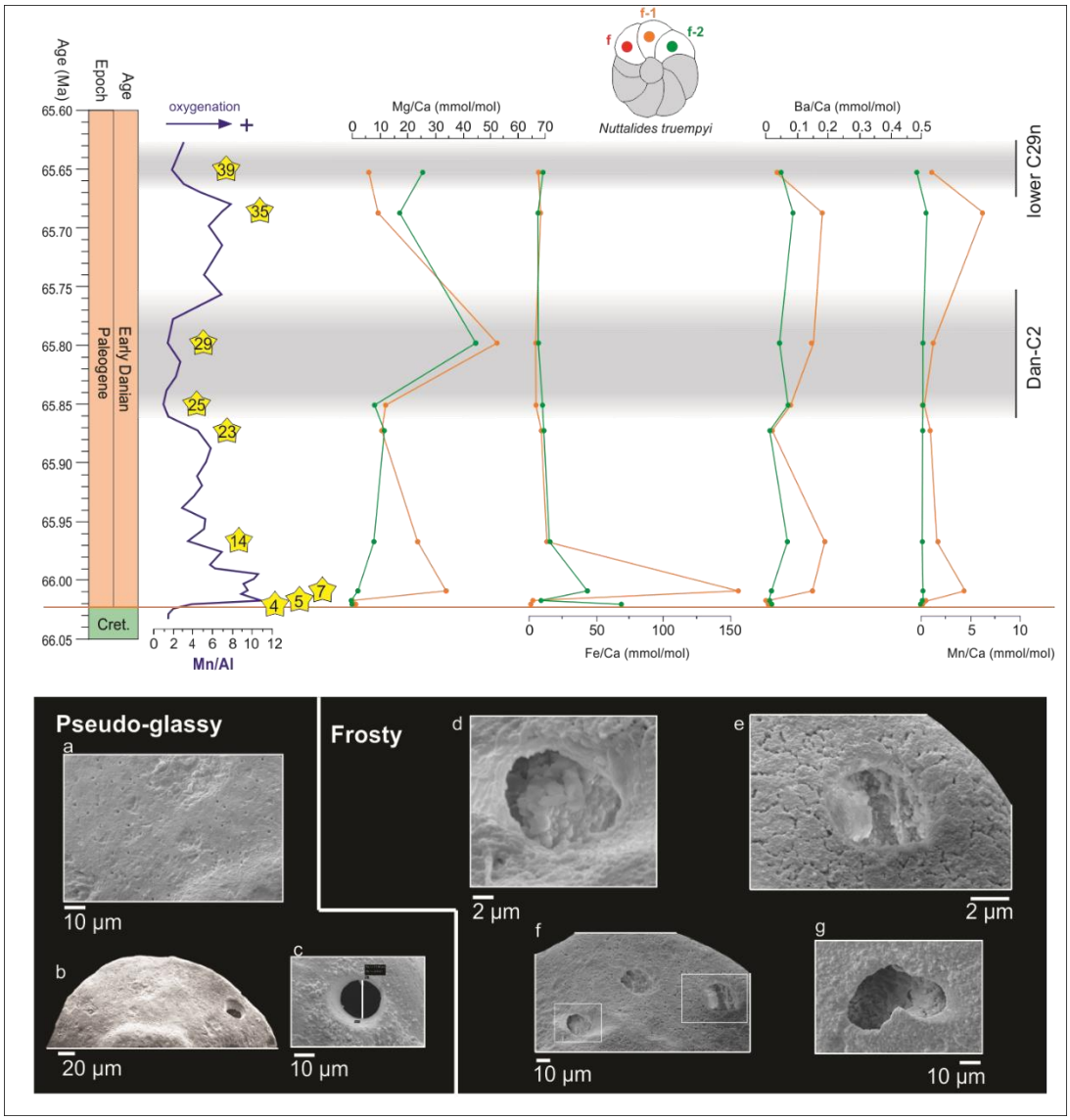

Figure 6: Bottom and pore water oxygenation proxies and carbonate content at Site 1262. Note that reduced bottom water oxygenation (evidenced by high Mn/Ca and V/(V+Ni)) occurred in tandem with calcium carbonate content drops during the Dan-C2 and the lower C29n events.

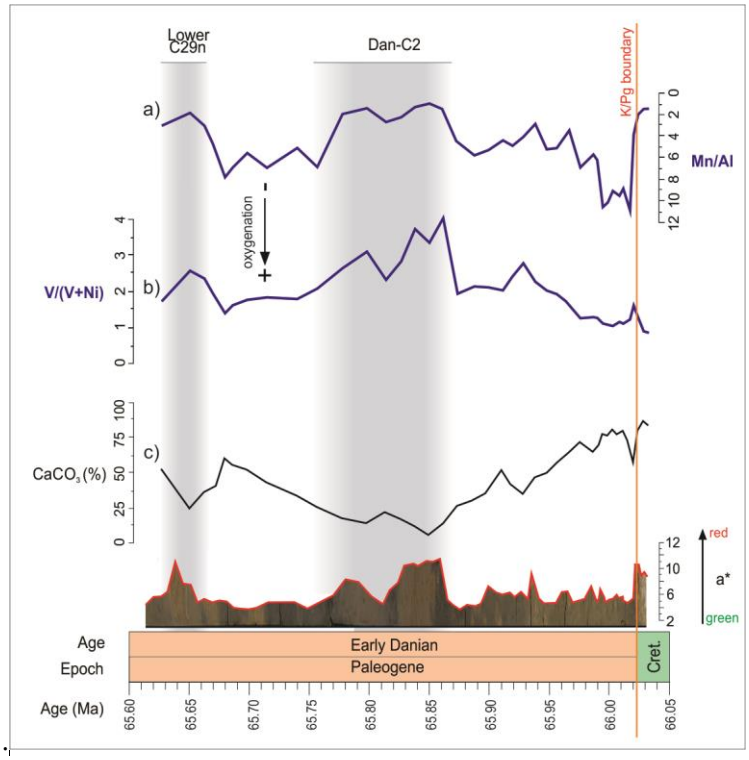

Figure 7: Comparison of our new benthic foraminiferal $\delta^{13}C$ and $\delta^{18}O$ (black squares) records at Site 1262 with the benthic foraminiferal records of Barnet et al. (2018, 2019; red circles), Alegret et al. (2012; green circles) and Hull et al. (2020; blue circles).

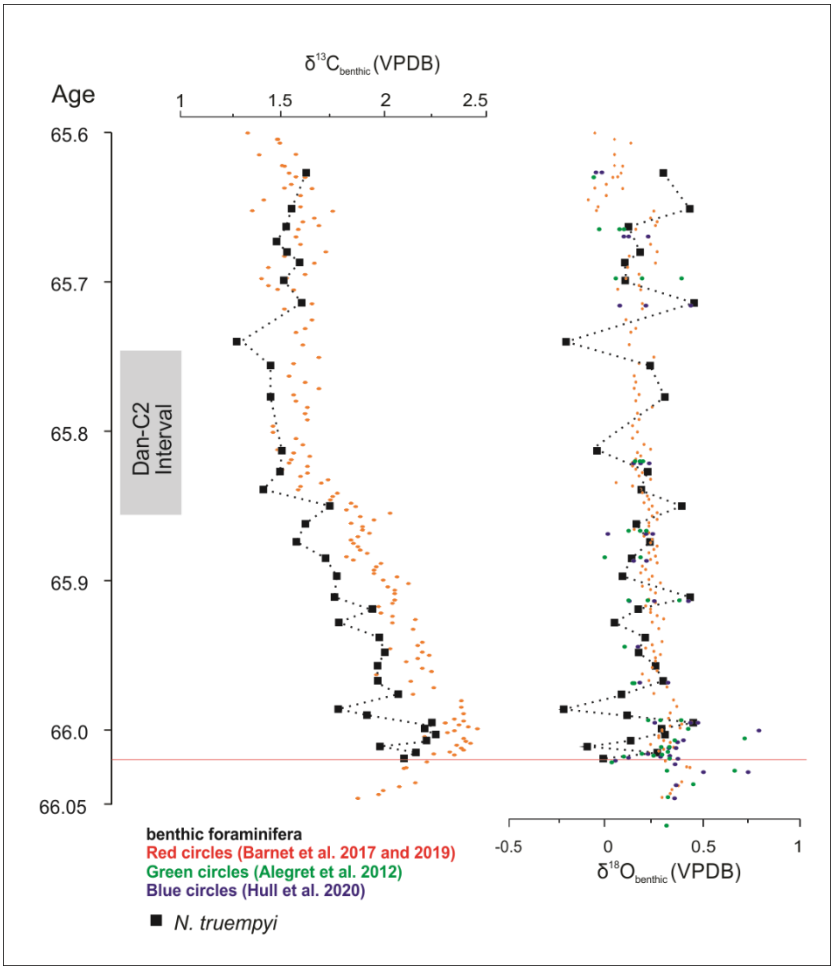

Palaeogeography, Palaeoclimatology, Palaeoecology

Supporting Information for:

Disentangling environmental and diagenetic $\delta^{18}O$ and $\delta^{13}C$ signals from marine carbonates deposited under warm climate conditions during early Danian

Marlone H.H.Bom[a,b] , Karlos G.D. Kochhann[a,b], Guilherme Krahl[a,b], Nils Andersen[c] ,Lucas V. Oliveira[a], Valeska Meirelles[a], Andressa Esswein[a], Mírian L.A.F. Pacheco[d], Bruna C. Schneider[b], Gerson Fauth[a,b]

[a] itt OCEANEON , Technological Institute for Paleoceanography and Climate Changes, Universidade do Vale do Rio dos Sinos, Av. Unisinos, 950, Cristo Rei, São Leopoldo, RS, Brazil.

[b] Geology Graduate program, UNISINOS University, São Leopoldo, RS, Brazil

[c] Leibniz Laboratory for Radiometric Dating and Stable Isotope Research, Christian Albrechts University, Kiel, Germany

[d] Universidade Federal de São Carlos, Departamento de Biologia, Rodovia João Leme dos Santos,18052780 Sorocaba, SP, Brazil

*Corresponding author: Marlone Bom (marloneb@unisinos.br)

Contents of this file

Introduction

This supporting information file provides additional information for methods and results of this study case.

Supporting information Figure S1. EDS (Energy Dispersive Spectroscopy) analyses of *Nuttallides truempyi* from Site 1262. Analyzed samples are from 215.55 mbsf (65.87 Ma) and 216.35 mbsf (66.00 Ma).

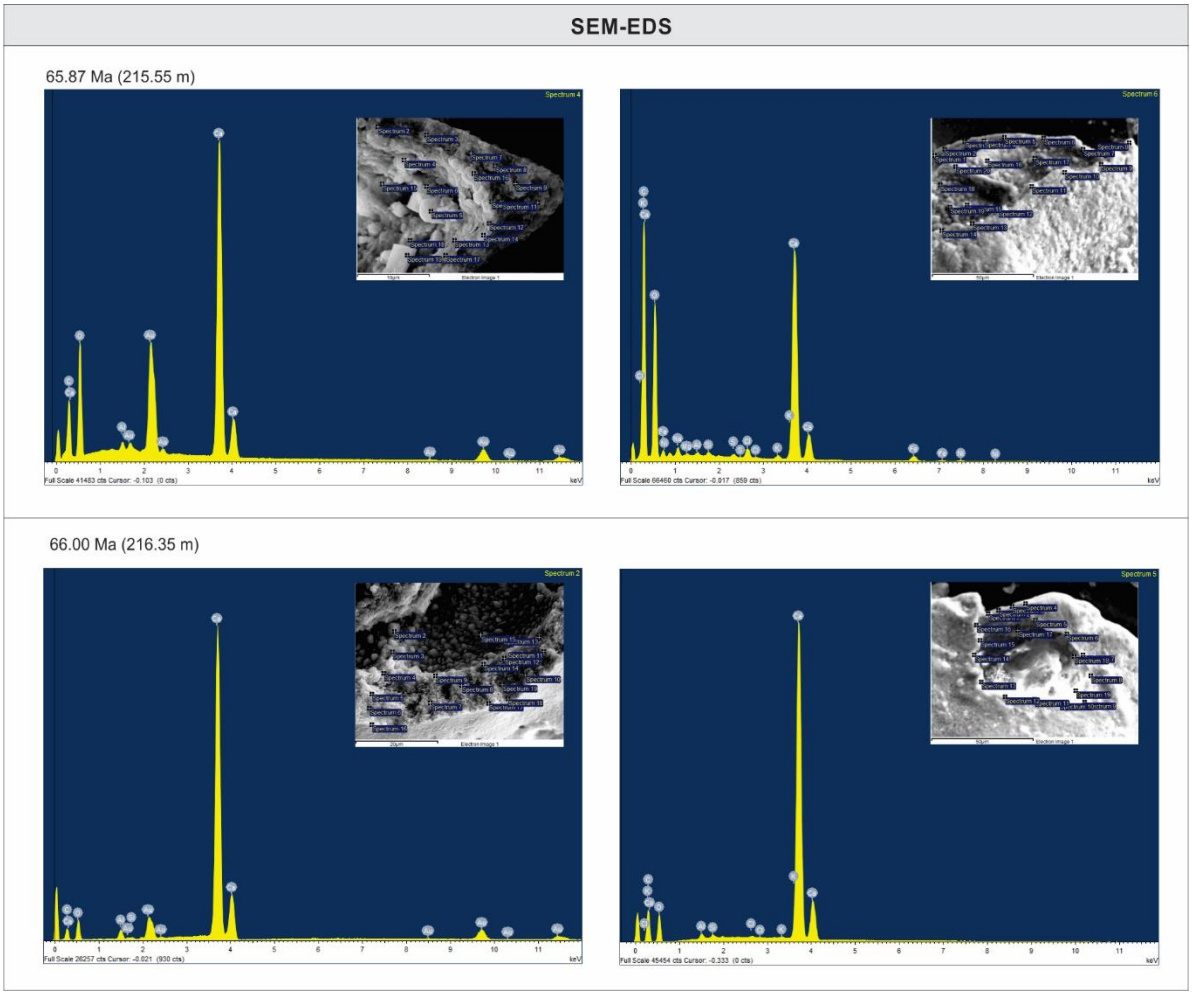

Supporting information Figure S2.

(A) Raman Spectroscopy mapping and raw data spectra of *Nuttallides truempyi* from Site 1262, sample 216.35 – 195.34 mbsf (66.00 Ma). Yellow grades represent the intensity of the calcite Raman shift identified (1088 cm^{-1}; 713 cm^{-1}; 283 cm^{-1} and 156 cm^{-1}).

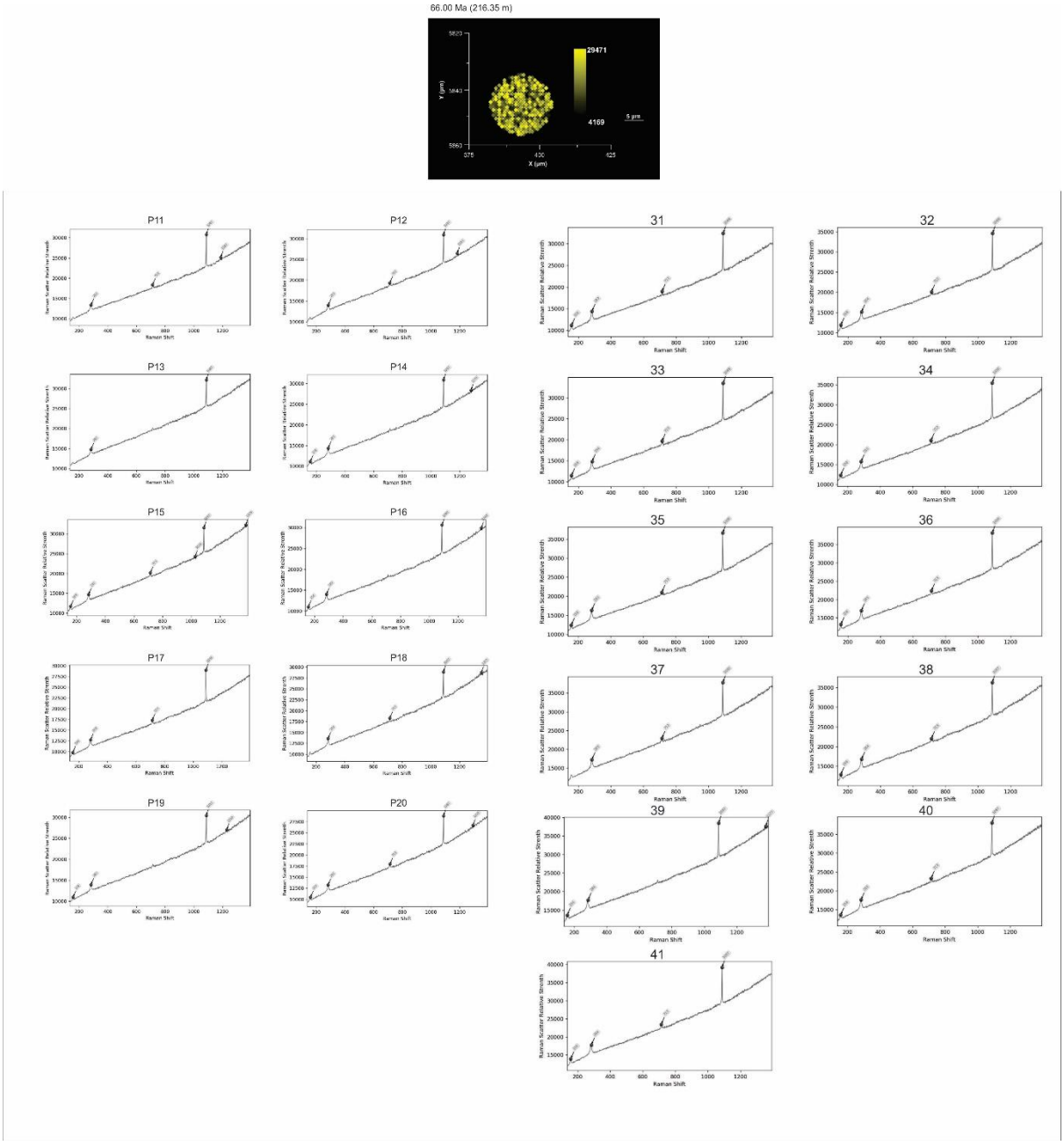

(B) Characteristic Raman peaks for each sample

Sample number	**Raman shift (1/cm)**		
	282.43	712.6	1087.1
wr_07	283.49	712.88	1087.2
	282.13	713.35	1087.2
wr_14	282.14	712.02	1086.3
	282.41	712.35	1086.3
	282.65	716.22	1086.3
wr_23	282.94	711.91	1086.2
	281.49		1086.2
	281.94	712.69	1086.9
wr_40	281.65	712.54	1086.8
	282.28	712.64	1087

(C) Characteristic Raman peaks for each sample. Normalized and averaged spectra

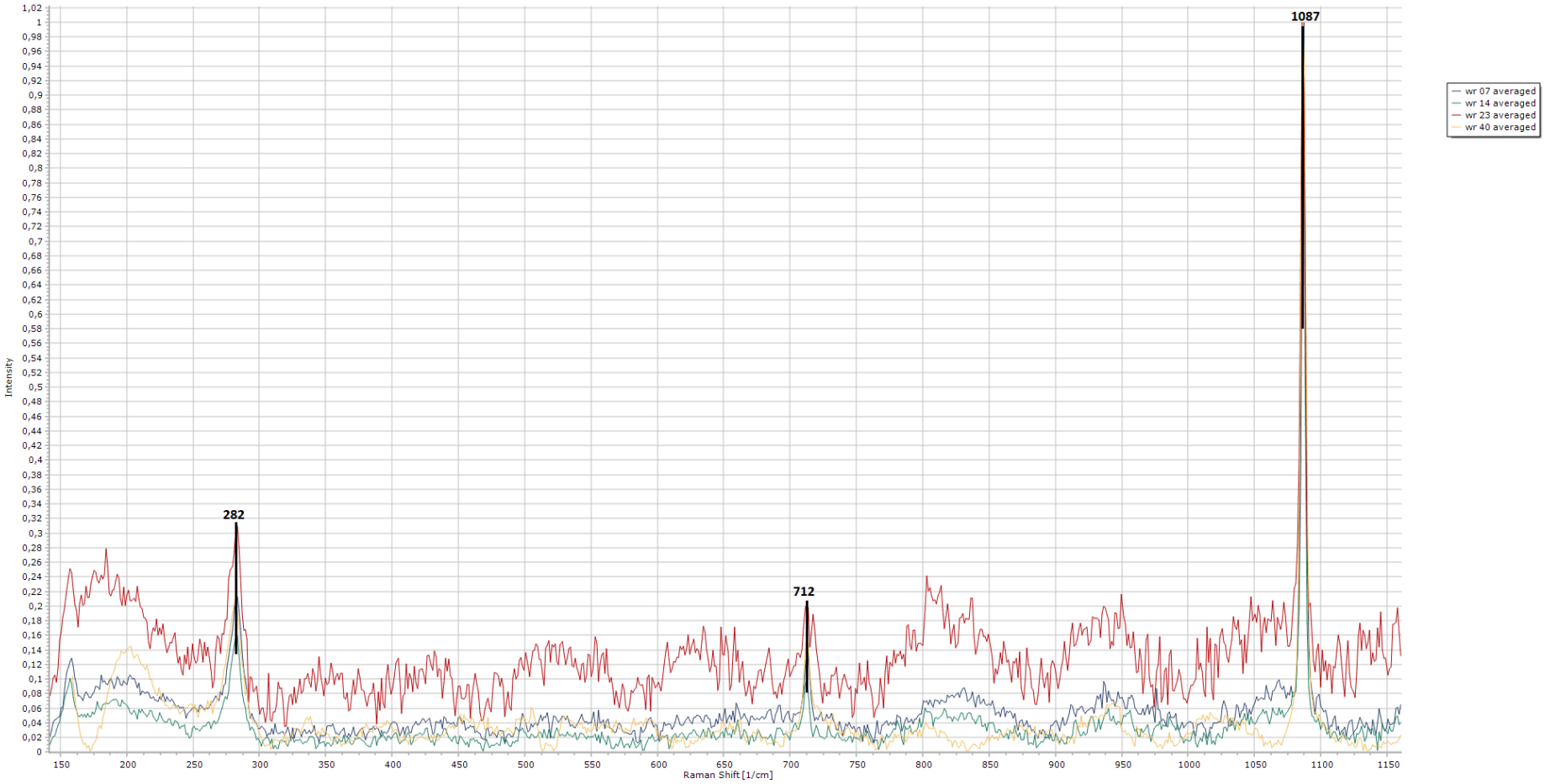

(D) FWHM values x Raman shift

Sample number	**FWHM values x Raman shift**		
	282 1/cm	*712 1/cm*	*1087 1/cm*
	13.722	8.6643	3.9595
wr_07	11.198	7.7701	4.0544
	13.787	6.5632	3.9787
wr_14	9.959	8.2628	3.716
	10.266	4.7625	3.9344
	22.89	17.326	4.5069
wr_23	17.712	16.859	4.3641
	11.666		4.6266
	15.502	7.485	4.6164
wr_40	15.095	7.3174	4.6797
	17.384	7.2469	4.6604

(E) FWHM values versus Raman shift

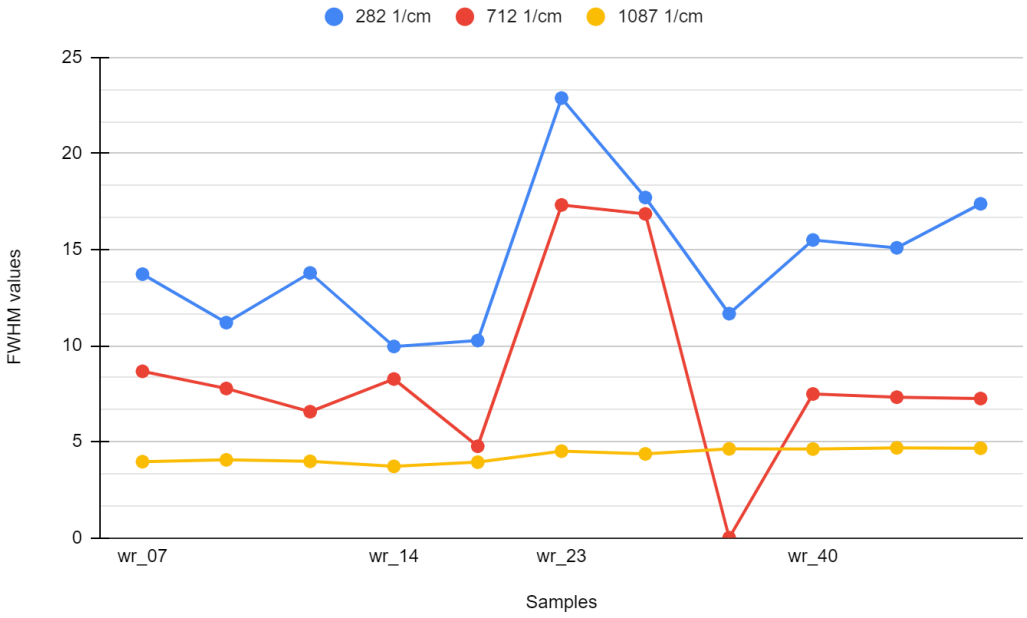

(F) FWHM mean values versus Raman shift

Sample number	FWHM mean values x Raman shift (1/cm)		
	282	712	1087
wr_07	11.79	7.67	4
wr_14	10	6.51	3.83
wr_23	17.42	17.1	4.5
wr_40	15	7.35	6.65

(G) FWHM mean values versus Raman shift

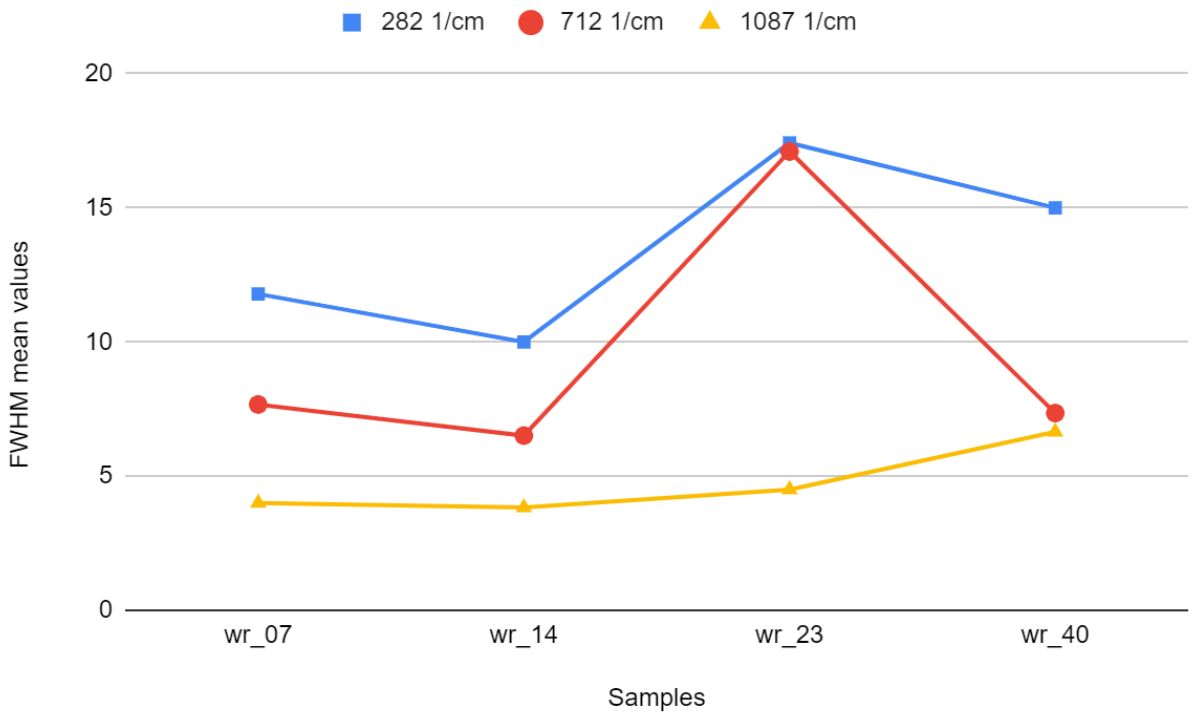

Supporting information Figure S3. Minerals authigenic phases observed with XRD in benthic foraminiferal specimens from Site 1262. Identification of samples: 4 (66.02 Ma); 5 (66.01 Ma), 7 (66.00 Ma), 14 (65.97 Ma), 23 (65.87 Ma), 25 (65.85 Ma), 29 (65.90 Ma), 35 (65.69 Ma) and 39 (65.65 Ma).

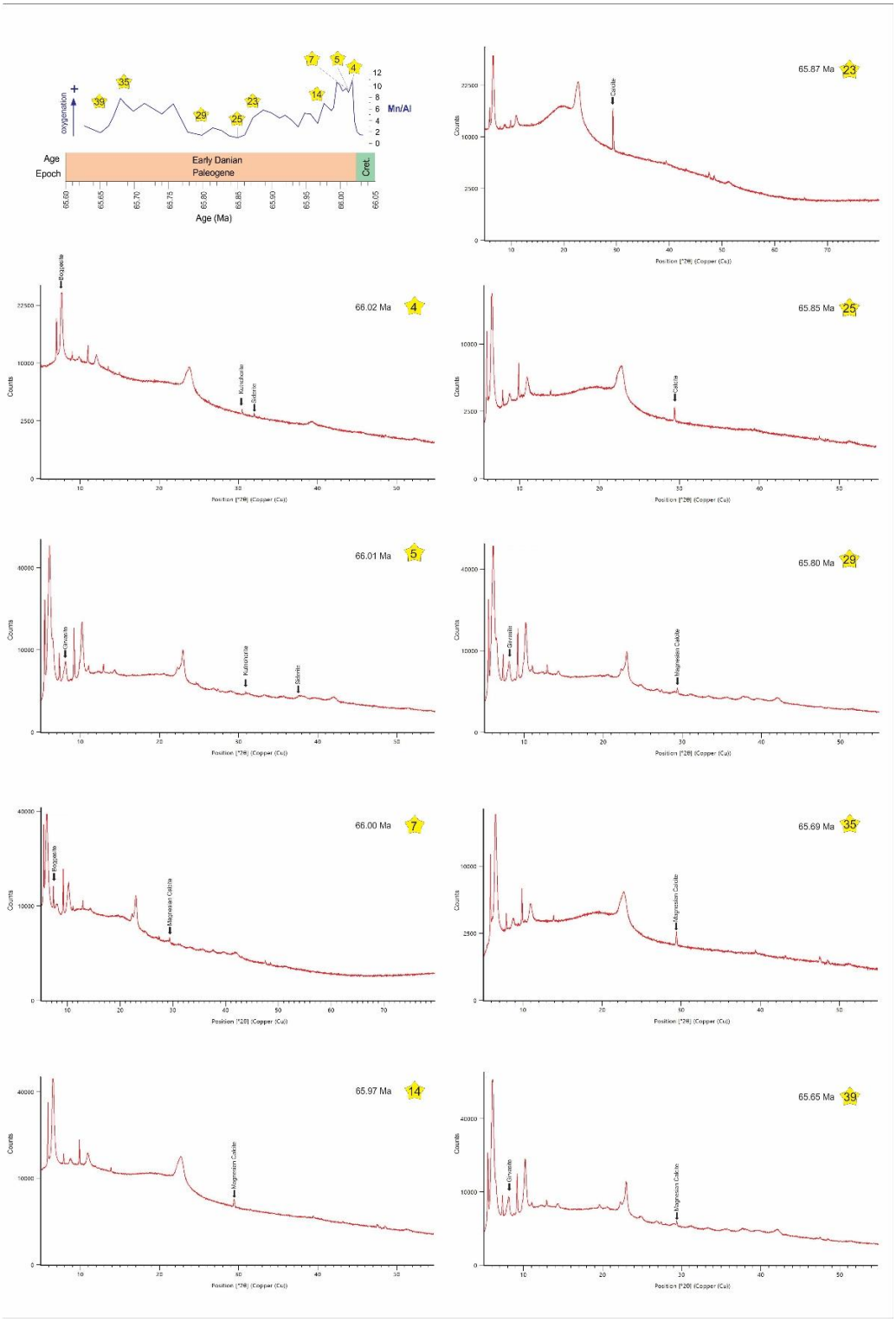
oxygenation
Mn/Al
Age
Epoch
Early Danian
Paleogene
Cret.
Age (Ma)
65.87 Ma
66.02 Ma
65.85 Ma
66.01 Ma
65.80 Ma
66.00 Ma
65.69 Ma
65.97 Ma
65.65 Ma
Counts
Position [°2θ] (Copper (Cu))

Supporting information Figure S4. Benthic foraminifera SEM images with ablated details. For each sample, we present an overview of the specimens and details of the wall texture. Identification of samples: 4 (66.02 Ma); 5 (66.01 Ma), 7 (66.00 Ma), 14 (65.97 Ma), 23 (65.87 Ma), 25 (65.85 Ma), 29 (65.90 Ma), 35 (65.69 Ma) and 39 (65.65 Ma). All scale bars represent 10 µm.

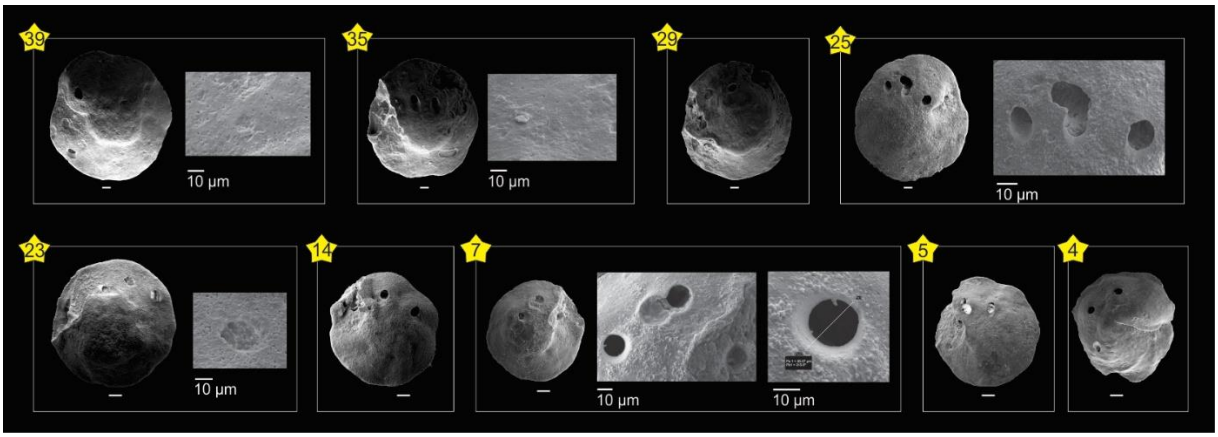

Supporting information Figure S5. Planktonic foraminiferal SEM micrographs showing different degrees of preservation, similar to those described for benthic foraminifera, at Site 1262. We present images of *Subbotina* spp., *Praemurica nikolasi* and *Guembelitria cretacea*. All scale bars represent 10 µm.

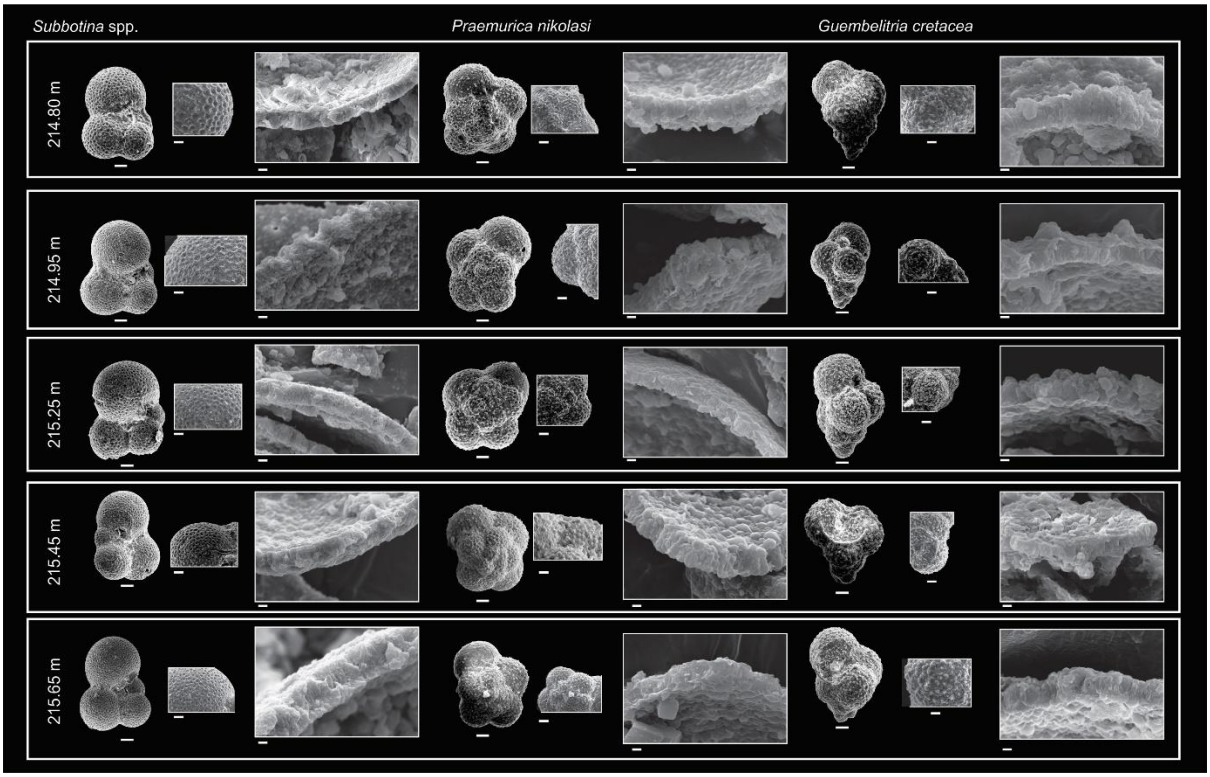

Supporting information Figure S6: Reconstructed bottom water temperatures at sites 1262 (this study) and site 1049 (Hull et al., 2020).

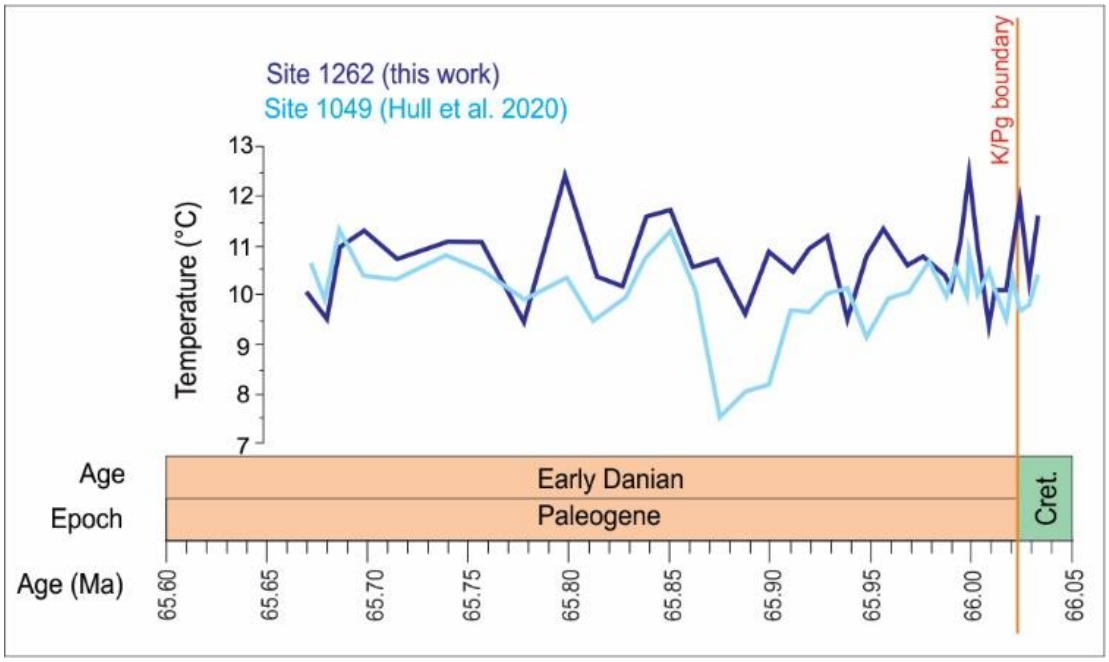

CAPÍTULO 3 – PALEOECOLOGIA DE OSTRACODES DO DANIANO COM BASE EM SEUS SINAIS DE $\delta^{13}C$ E $\delta^{18}O$

Capítulo 3

Paleoecology of selected Danian marine ostracods suggested by stable carbon ($\delta^{13}C$) and oxygen ($\delta^{18}O$) isotopes

Marlone H.H. Bom; Daiane Ceolin, Karlos G.D. Kochhann, Rodrigo do Monte Guerra, Guilherme Krahl, German Patarroyo, Mírian L.F.A Pacheco, Lucas V. Oliveira, Telma Musso, Andrea Concheyro, Gerson Fauth

Manuscrito a submetido ao periódico *Marine Micropaleontology*

MARMIC-D-23-00075 - Confirming your submission to Marine Micropaleontology

MM em.marmic.0.860a2f.02aa439a@editorialmanager.com em nome de Marine Micropaleontology <em@editorialmanager.com>
Para: Marlone Heliara Hunnig Bom
Qui, 14/09/2023 17:41

This is an automated message.

Paleoecology of selected Danian marine ostracods suggested by stable carbon (δ13C) and oxygen (δ18O) isotopes

Dear Mrs Bom,

We have received the above referenced manuscript you submitted to Marine Micropaleontology. It has been assigned the following manuscript number: MARMIC-D-23-00075.

To track the status of your manuscript, please log in as an author at https://www.editorialmanager.com/marmic/, and navigate to the "Submissions Being Processed" folder.

Thank you for submitting your work to this journal.

Kind regards,
Marine Micropaleontology

More information and support

You will find information relevant for you as an author on Elsevier's Author Hub: https://www.elsevier.com/authors

FAQ: How can I reset a forgotten password?
https://service.elsevier.com/app/answers/detail/a_id/28452/supporthub/publishing/kw/editorial+manager/

For further assistance, please visit our customer service site: https://service.elsevier.com/app/home/supporthub/publishing/. Here you can search for solutions on a range of topics, find answers to frequently asked questions, and learn more about Editorial Manager via interactive tutorials. You can also talk 24/7 to our customer support team by phone and 24/7 by live chat and email.

This journal uses the Elsevier Article Transfer Service. This means that if an editor feels your manuscript is more suitable for an alternative journal, then you might be asked to consider transferring the manuscript to such a journal. The recommendation might be provided by a Journal Editor, a dedicated Scientific Managing Editor, a tool assisted recommendation, or a combination. For more details see the journal guide for authors.

#AU_MARMIC#

To ensure this email reaches the intended recipient, please do not delete the above code

Paleoecology of selected Danian marine ostracods suggested by stable carbon ($\delta^{13}C$) and oxygen ($\delta^{18}O$) isotopes

Marlone H.H. Bom[1,2]; Daiane Ceolin[2], Karlos G.D. Kochhann[1,2], Rodrigo do Monte Guerra[1], Guilherme Krahl[1], German Patarroyo[1,2], Mírian L.F.A Pacheco[3], Lucas V. Oliveira[1], Telma Musso[4], Andrea Concheyro[4], Gerson Fauth[1,2]

(1) itt OCEANEON, Instituto Tecnológico de Paleoceanografia e Mudanças Climáticas, Universidade do Vale do Rio dos Sinos, UNISINOS, São Leopoldo, RS.

(2) Programa de Pós-Graduação em Geologia, Universidade do Vale do Rio dos Sinos, UNISINOS, São Leopoldo, RS.

(3) Universidade Federal de São Carlos, Departamento de Biologia, Sorocaba, SP.

(4) IDEAN-CONICET, Departamento de Ciências Geológicas, Universidade de Buenos Aires, Buenos Aires, Argentina.

Keywords: Paleogene, Paleonutrients, Paleosalinity, *Henryhowella*

Abstract: The Cerro Azul Section provides a continuous record of the Cretaceous-Paleogene (K-Pg) transition in a shallow marine context of the South Atlantic Ocean in the Neuquén Basin. Ostracod assemblages were severely affected by environmental changes across the event. Excellent ostracod preservation at the Cerro Azul Section allows to infer paleoecological preferences of four Danian species based on carbon and oxygen stable isotopes. The studied species were *Paracypris bertelsae* Ceolin and Whatley, 2015, *Cytherella* spp., *Togoina argentinensis* and *Henryhowella (Wichmannela) meridionalis* (Bertels, 1974). To assess the reliability of ostracod $\delta^{13}C$ and $\delta^{18}O$ values as paleoenvironmental proxies, we pre-characterized valves with micro x-ray mi-

crodiffraction (μXRD) and microRaman (μRaman spectroscopy). *Togoina argentinensis* and *Henryhowella (Wichmannela) meridionalis* present in their entireties calcitic compositions, with small differences of crystallinity within intervals of environmental stress, but no authigenic phases formed during diagenesis. $\delta^{13}C$ and $\delta^{18}O$ values depict clear interspecific differences between smooth specimens and ornamented specimens. These differences in stable isotope values were likely controlled by microhabitat preferences, which would be comparable with patterns described for benthic foraminifera.

3.1 INTRODUCTION

The Cretaceous-Paleogene (K-Pg) boundary (~66Ma) is the most recent mass extinction, and possibly the most studied event in Phanerozoic (Sepúlveda et al., 2019). The main cause of this mass extinction was the Chicxulub bolide impact (e.g., Alvarez et al., 1980; 1987; Hull et al., 2010; Hull et al., 2020), and additional effects of Deccan Traps volcanism are also debated (e.g., Keller et al., 2008; 2020; Font et al., 2011; 2016; 2018). The early Paleogene time interval, specifically, was a time of environmental recovery in the aftermath of the K-Pg event, and recorded a series of perturbations of the global carbon cycle that were associated with global warming, known as hyperthermal events (e.g., Thomas and Zachos, 2000; Cramer et al., 2003, Littler et al., 2014; Barnet et al., 2019).

These global events affected marine calcareous fossil groups in different ways. During the earliest Danian, planktic foraminiferal and calcareous nannoplankton assemblages were characterized by low diversity, high species dominance, rapid evolutionary turnovers, and blooms of smaller generalist or opportunist taxa that could thrive under eutrophic and unstable conditions (e.g.,

Guerra et al., 2021; Krahl et al., 2023, Elbra et al., 2023). Selective elimination of organisms directly dependent upon the flux of organic matter from the surface occurred (Arthur et al., 1987). Benthic foraminifera did not suffer significant extinction across the K-Pg (Alegret et al., 2001). Temporary changes in the structures of benthic foraminiferal faunas have been identified, likely due to the collapse of the pelagic food web and a subsequent drop in food availability for benthic organisms (e.g., Alegret et al., 2002; Alegret et al., 2003). However, the opposite behavior occurred in areas such as the North Pacific (DSDP Site 465) and the Northwestern Atlantic (ODP Site 1049), with greater nutrients availability, and low bottom water oxygenation following the K-Pg (e.g., Alegret and Thomas, 2005). In fact, geographic heterogeneity must be considered when comparing Danian abundance, diversity, and nutrient availability trends (Hull and Norris, 2011).

Ostracods are the second most common microfauna in the deep sea after benthic foraminifera, and their fossilized calcareous shells can provide environmental information to reconstruct past ecosystem (e.g., Cronin et al., 1999; Didie and Bauch, 2000). Ostracods distribution in the ocean floor is controlled by the flux of organic matter from surface waters, temperature, salinity, and the sediments composition (Corrège, 1993; Didie and Bauch, 2000). In contrast to benthic foraminifera, the K-Pg mass extinction event led to the disappearance of numerous bathyal ostracod species, followed by a very slow diversity recovery during the Paleocene (e.g., Boomer, 1999, Bergue and Dias Nicolaidis, 2012, Ceolin et al., 2015). Evidence from the equatorial Atlantic Ocean suggest that the extinction event was more damaging for detritus-eating ostracods than for filter-feeding or silt-eating groups, the latter appearing to have crossed the K-Pg boundary without experiencing a major turnover (Guernet e Danelian, 2006).

In this paper, we present new carbon and oxygen isotope data for four ostracod species over the lower Danian interval at the Cerro Azul Section, Neuquén Basin, Argentina. Parameters such

as paleoxygenation, paleosalinity and nutrients distribution were evaluated and compared with species-specific carbon isotope values, allowing us to draw paleoecologic inferences for *Paracypris bertelsae* Ceolin and Whatley, 2015, *Cytherella* spp., *Togoina argentinensis* and *Henryhowella* (*Wichmannela*) *meridionalis* (Bertels, 1974).

3.2 MATERIAL AND METHODS

3.2.1 Study area and sampling strategy

The Cerro Azul Section (38° 50'48'' S, 67° 52'20'') is located in the Neuquén Basin, where the Jagüel Formation crops out (see Fig.1). This sedimentary basin in western Argentina encompasses deposits ranging in age from Upper Triassic to Paleogene. One of the supercycles representing the infilling of the basin (Riograndico cycle) comprises the Malargüe Group, which contains the Jagüel, Roca and Carrizo formations. The Jagüel Formation is characterized by a homogenous fine-grainded sedimentary succession, with fossils that indicate a Late Maastrichtian to Danian age (Uliana and Dellapé, 1981). Previous analyzes revealed that lithofacies of the Jaguel Formation are mostly composed of clays, calcite, quartz, feldspar, zeolite and cristobalite, with clay minerals being interstratified illite/smectite (Musso et al., 2012).

Here we used the sampling of the Cerro Azul Section described by Guerra et al. (2021), with 17 samples spanning the yellow greenish calcareous mudstone (upper Maastrichtian), followed by an olive calcareous mudstone at the base of Paleocene (Figure 1). Samples designated as CA1 to CA 17 comprise the Maastrichian-Danian interval, with the K-Pg boundary occurring between samples CA8 and CA9 (16.50-16.60) (see Guerra et al., 2021). For stable isotope studies of ostracods (*Paracypris bertealse; Cytherella spp.; Togoina argentinensis ans Henryhowella*

(Wichmanella) meridionalis) and benthic foraminifera (genera *Gavelinella* and *Lenticulina*), we strategically worked with the beginning of the Danian, due to the stratigraphic distribution of these fossils, with sampling every 10 cm (n =8). This interval occurs within biozone NP1 (*sensu* Watkins et al., 1996) as described by (Guerra et al., 2021).

3.2.2 Stable Carbon ($\delta^{13}C$) and Oxygen ($\delta^{18}O$) Isotopes

The carbon ($\delta^{13}C$) and oxygen ($\delta^{18}O$) isotopic compositions of benthic foraminifera (n=13) and ostracods (n=26) were analyzed with a Finnigan MAT 253 mass spectrometer coupled to a Carbo-Kiel Device (Type IV) system at Technological Institute for Paleoceanography and Climate Change (itt OCEANEON- UNISINOS University). Isotope analyses were performed in well-preserved ostracods and benthic foraminifera of >180 μm sieved grain-size residues. For ostracods, we used only valves of adult specimens and for foraminifera we used whole tests. All valves and tests were ultrasonically cleaned in ethanol. Measurements were calibrated in reference to the IAEA-603, CO-8 and SHP2L (Crivellari et al., 2021) international standards. All $\delta^{13}C$ and $\delta^{18}O$ values are reported as deviations from the Vienna Pee Dee Belemnite (VPDB) scale. Results of all measurements are documented in Table1.

3.2.3 Valve microstructure analysis by SEM, Raman Spectroscopy and X-Ray Diffraction

Selected valves of *Henryhowella* (*Wichmanella*) *meridionalis* (Bertels, 1969) (n=8) and *Togoina argentinensis* Bertels, 1975 (n=8) were imaged in an EVO MA15 Zeiss scanning electron microscope (SEM) at itt OCEANEON-UNISINOS. We also measured valve thickness of each specimen with the SEM set at EHT = 15 kV.

We performed micro-Raman spectroscopy to check for the occurrence of Mg-enriched carbonates (according to Borromeo et al., 2016), as well as calcite/dolomite carbonates and organic matter (OM) at valves edges, using a Renishaw InVia micro-Raman spectrometer with 785 nm laser. Analyses were performed on static mode in order to investigate a broad range of mineral phases and OM in the center and at the edges of valves. We collected 3 to 5-point measurements in each valve region (center ant edge). Different powers were tested to obtain more informative spectra. We adjusted parameters to 25 mW, using a LW 50x objective, with 30 accumulations of 2 seconds each. We treated recognized Raman peaks and bands of the most informative spectra (supplementary material 1) using the software SpectraGryph 1.2. We normalized (0-1 variability) and subtracted the baseline of all spectra. All spectra were smoothed for the calculations and comparison of FWHM. Then, we consulted the ruff database and specialized literature for comparison with the peaks of the spectra obtained in our studies.

We also used X-Ray diffraction (XRD) in the same valves (n=18) to identify mineral phase composing valves and authigenic coatings. Due the dimensions of the specimens, it was possible to mount them with stick glue directly on the zero background silicon sample holder. The equipament used was an Empyrean Panalytical x-ray diffractometer (CuKα radiation) at itt OCEANEON, set at 40 kV and 40 mA.

3.2.4 Bulk sediments trace elements analyses

For trace metals analysis, ~180 mg of sediment aliquots (n=19) were placed in Teflon tubes for microwave (Ethos Up, Milestone) digestion with 5 mL of 65% HNO_3 (m/v) + 2 mL of 40% HF (m/v). After addition of the acid mixture, samples were digested with 30 minutes ramp-heating to 230 °C, and the same time at the plateau temperature (230 °C). After digestion, solutions were

transferred to polypropylene tubes and placed to evaporate on a hot plate (DigiBlock EDS36S, LabTech) at 105°C, until almost complete evaporation.

Elements such as P, Ti, Ba, B, Ga, V and Cr were analyzed by inductivity coupled plasma – optical emission spectrometry (ICP OES) and inductivity coupled plasma mass spectrometry (ICP-MS) at itt OCEANEON. For quality control, we used the standard reference materials BHVO, BCR-2, GSP-2, SARM40, SARM42, SARM52, Nist 1646a and Till-3. Detection limits range from 0.026 ppm for ICP OES and 0.000271 ppm from ICP-MS measurements. We monitored analytical reproducibility by triplicate measurements of standard reference materials, with standard deviation smaller than 5%.

Paleonutrients/paleoproductivity ratios were used in this study: P/Ti (phosphorous/aluminium); Ba/Ti (barium/titanium) (e.g., Hou et al., 2022). Phosphorous (P) is one of major nutrients, and plays a key role in sustaining biological productivity of the world's oceans (Montagna et al., 2006). Due to its control on primary productivity, P availability can affect organic carbon burial (Papadomanolaki et al., 2022). Barite ($BaSO_4$) is a marine mineral and is the primary form of biogenic barium (Ba) .Barium has a strong relationship with the export of organic carbon to the sea in oxic to suboxic conditions , in open ocean sedimentary environments (Hull and Norris, 2011).

The B/Ga (boron-galium) ratio was used as a paleosalinity proxy (e.g., Zhang et al., 2017; Wei and Algeo, 2020). Boron and gallium have different chemical properties. Boron concentrations are much higher in seawater than in freshwater, while Ga is generally depleted in seawater (Remírez and Algeo, 2020).

For assessing bottom water paleoxygenation, we used the V/Cr ratio. We followed the standard classification systems for paleoredox conditions (Tyson and Pearson, 1991), and previously reported V/Cr threshold values (Rivera et al., 2018) as follows: <2.0 – oxic conditions; 2.0-4.25 – dysoxic conditions; >4.25 – suboxic-anoxic conditions.

3.3 RESULTS

3.3.1 Valves microstructure and thickness

Evaluating the state of preservation of calcite in ostracod valves is crucial to obtain effective and reliable results. The initial goal of our study was to compare ostracod $\delta^{13}C$ and $\delta^{18}O$ values with benthic foraminiferal genera usually used for the same purposes: *Lenticulina* and *Ganvelinella*. However, low benthic foraminiferal abundances prevented such comparison. Furthermore, the quality of calcite preservation in ostracods is much better than that of the recovered foraminiferal tests (Fig. S1). All four ostracod species evaluated here showed excellent preservation. The two most abundant Danian ostracod species the Cerro Azul Section were used to evaluate valves microstructure. In general, they are perfectly preserved, showing primary morphological features such as ornamentation and pores without any signs of recrystallization.

We analyzed *H.* (*Wichmanella*) *meridionalis* (n=9) in selected stratigraphic levels with SEM and X-Ray diffraction. Based on SEM and steromicroscope analyses, we observed very good preservation with *glassy* preservation (*sensu* Sexton et al., 2006) (Fig. 2; CA-14 to CA17). Specimens from the lowermost Danian (Fig. 2; CA10 to CA13) had pseudo-glassy preservation (*sensu* Poirier et al., 2021), with some clay minerals observed in this ornamented species, and gypsum crystals at 17 m (sample CA13; Fig. S2). X-ray diffraction analysis reveals that all nine evaluated

stratigraphic levels present calcite phases with low amorphism. By SEM analysis, we could also measure the thickness of each valve (Fig. 2 see tables S1 and S2). Henryhowella valves thicknesses measurements varied between 11.3 and 38.4 µm (mean 24.9 µm).

For *Togoina argentinensis* (n=9) we also observe very good preservation, varying from pseudo-glassy (CA13 - 17 m and CA10 - 16.7 m) to glassy (CA17 - 17.45 m; CA16 - 17.30 m; CA 15 - 17.20 m; CA14 - 17.10 m; CA12 -16.9 m; CA11 - 16.8 m). X-ray diffraction evidenced more ordered crystal structure, which may be related to its less ornamented surface (Fig. 3). *Togoina* valves thickness measurements varied between 10.9 and 23.9 µm (mean 18.6 µm).

Selected *H.* (*Wichmanella*) *meridionalis* were evaluated by micro Raman spectroscopy. We found peaks compatible with carbon D (~1326-1344 cm^{-1} shift) and G (~1585-1619 cm^{-1} shift) positions, which are characteristic of kerogen (Fig. S3) in sample CA10, at 16.70 m. We also found characteristic calcite peaks, mostly blue-shifted (~285; ~715; ~1087 cm^{-1}), indicating Mg enrichment in samples CA10 (16.70 m) and CA17 (17.45 m; Fig. S4). We did not find Raman shift differences between the central and edge areas of valves. We compared possible FWHM (full width at half maximum) differences, but we did not find them.

3.3.2 $\delta^{13}C$ and $\delta^{18}O$ measured on ostracods

Some specimens of benthic foraminifera of the genera *Lenticulina* and *Gavelinella* were analyzed, aiming a comparison with ostracods isotopic records. All data are reported in Table 1 and Figure 4. Benthic foraminifera $\delta^{13}C$ values ranged from -1.65‰ (CA16 - 17.30 m) to 1.02‰ (CA10 - 16.70m) for *Lenticulina*, and from -1.33‰ (CA16 - 17.30 m) to 1.40‰ (CA10 - 16.70 m) for *Gavelinella* records. Benthic foraminiferal $\delta^{18}O$ values ranged from -8.05‰ (CA13 - 17.00 m)

to -3.37‰ (CA15 – 17.2m) for *Lenticulina*, and from -8.17‰ (CA16 - 17.30 m) to -3.77‰ (CA13 – 17.00 m) for *Gavelinella* records.

Ostracod $\delta^{13}C$ values are generally lower, except for *Cytherella* spp., than those of benthic foraminifera at the Cerro Azul Section, with values between -4.67‰ and 1.71‰ (Fig. 4). *Togoina argentinensis* and *H.*(*Wichmanella*) *meridionalis* cover the entire studied interval, whereas *P. bertelse* and *Cytherella spp* depict a partial coverage. The highest $\delta^{13}C$ values were recorded for *Cytherella* spp. (-0.78‰ - CA12 to 1.73‰ - CA14), and *P. bertelse* (-1.07‰ CA13 to -0.27‰ CA15). *Togoina argentinensis* varied between -3.59‰ (CA17) and -0.91‰ (CA11), while *H.*(*Wichmanella*) *meridionalis* varied from -4.67‰ (CA17) to -1.01‰ (CA10). The majority of the studied ostracod species depicted low $\delta^{13}C$ values at 16.8 m (CA11) and 17.2 m (CA15).

Regarding $\delta^{18}O$ values, *P. bertelse* values ranged from -2.44‰ (CA16) to -1.99‰ (CA17); *Cytherella* spp. values ranged from -5.48‰ (CA13) to -1.64‰ (CA17); *T. argentinensis* values ranged from -7.45‰ (CA11) to -1.61‰ (CA17); and *H.(Wichmanella) meridionalis* values ranged from -11.04‰ (CA15) to -1.71‰ (CA11) (Fig. 4). As with ostracod $\delta^{13}C$ records, most studied species depicted low $\delta^{18}O$ values at 16.8 m (CA11) and 17.2 m (CA15).

3.3.3 Paleoenvironmental proxies

To evaluate the variability of paleonutrients availability, we selected two elemental ratios: P/Ti and Ba/Ti. The P/Ti ratio presented values between 0.128 (CA09 - 16.6 m) and 0.308 (CA13 – 17 m) (average: 0.203). High P/Ti values coincide with dysoxic intervals depicted by the V/Cr ratio. V/Cr values varied between 1.75 (CA15 - 17.2 m) and 2.45 (CA14 – 17.1 m) (average: 2.04), with trends that are similar to those depicted by P/Ti (Fig. 5). The Ba/Ti ratio presented values

between 0.0324 (CA09 - 16.6 m) and 0.0482 (CA13 – 17 m) (average: 0.041). Also high Ba/Ti values coincide with dysoxic intervals depicted by the V/Cr ratio (see Fig.5). At the Cerro Azul Section, B/Ga ratios varied between 3.17 (CA11 - 16.7 m) and 5.29 (CA16 - 17.3 m) (average: 0.041).

3.4 DISCUSSIONS

3.4.1 Ostracod preservation, valves thickness, calcification and vital effects

The calcification process of ostracods carapaces occurs differently than that of foraminifera. With foraminifera, calcification occurs continuously, and the measured isotopic data represent an average of the complete ontogeny (de Nooijer et al., 2009). For ostracods, the isotopic compositions may only reflect a specific moment of life, bounded to specific paleoceanographic conditions. After all, the formation and calcification of ostracod carapaces occurs extremely quickly, which is carried out in days, or even hours (e.g., Chivas et al., 1983). Mineralogically, carapaces consist of a complex arrangement of low-Mg calcite and organic components such as fibrils, chitins and proteins (Keyser and Walter, 2004; Holmes et al., 2012). In carapaces of adult specimens, most of the time and regardless of species, amorphous material will have crystallized, whereas in the early juvenile stages, crystallization is sometimes incomplete, and amorphous material is left (Bornemann et al., 2012). Therefore, it is recommended to use adult specimens for geochemical analysis, to ensure that the entire calcification process has occurred throughout and uniformly.

We detected kerogen in well-preserved *Henryhowella* specimens in the lowermost Danian (CA10- 16.6m) at the Cerro Azul Section (Fig.S3) (detected by micro Raman spectroscopy). Increased preservation of biomarkers of kerogen plants and macerals is reported just after the K-Pg

event (e.g., Arinobu et al., 2005; Kaiho, 1999, Mizukami et al., 2013; Lyons et al., 2020), as for instance in bulk sediments across K-Pg boundary at Caravaca Section (Kaiho et al., 1999; Sepulveda et al., 2019); Red Sea, Egypt (Khozyen et al., 2019). However, this is the first time that it was found in calcareous microfossils. Kerogen refers to the solid, insoluble, fraction of organic material that survives diagenetic processes and becomes stored in sedimentary rocks (Duran, 1980), and likely played an important role in marine productivity and carbon cycling across the K-Pg boundary (Sepúlveda et al., 2019). Because of its resistance, kerogen represents an inestimable archive of past microbial life that can be investigated using various molecular analytical approaches (e.g., Loron et al., 2022). Previous records of fossil ostracods (subfamily *Cypridinae*, family *Cyprididae*) suggest a mineral replacement of the mineral chitin (Bate, 1971).

Our thickness measurements of adult valves show that *Henryhowella* individuals present greater thickness variability along the studied interval, than those of *Togoina Argentinensis* (Fig.5). *Henryhowela* $\delta^{18}O$ isotopic values appear to be positively correlate with valve thicknesses: more positive isotopic values are associated with greater valve thicknesses, and more negative $\delta^{18}O$ isotopic signals appear to be associated with thinner thicknesses. In the case of *Togoina argentinensis*, in which thicknesses variability was lower, such pattern is not observed. Still regarding valve thicknesses, Berndt et al. (2019) evaluated valve thicknesses of adult *Cypideis torosa* (Jones) specimens from the Middle Holocene, and found a good correlation with salinity ($R^2 = 0.56$). Carapaces were significantly thicker in relatively stable saline conditions, but thinner in highly variable, low-salinity deltaic lakes. Overall, thicknesses measured in this study for *Henrihowella* and *Togoina argentinensis*, when compared with paleosalinity variations, depicted by the B/Ga ratio, present a pattern comparable to that described by Berndt et al. (2019) (see Fig. 5). Additionally, freshwater

input would also have significantly lowered $\delta^{18}O$ values, which would explain the positive correlation between *Henryhowela* $\delta^{18}O$ values and valves thicknesses.

Metabolic processes can lead to a wide intraspecific dispersion in the stable compositions of biomineralized tissues. These processes are referred to as vital effects, and can influence the isotopic composition of analyzed biogenic calcite (Alvim et al., 2021). Vital effects occur in different fossil groups and are mainly visualized in $\delta^{18}O$ values (e.g., Holmes et al., 2012; Bornemann et al., 2012; Alvim et al., 2021). Ostracods show positive oxygen isotopic balance offsets, and their shifts are apparently constant across genera, families and/or subfamilies (Holmes et al., 2012). Therefore, small deviations between foraminifera and ostracods in their isotopic signals can be explained by their vital effects, not forgetting interspecific variances. Another relevant aspect in relation to vital effects is geographic heterogeneity and differences in diet. Ostracod measurements in the lower Danian of the Cerro Azul Section, presented very similar $\delta^{13}C$ values for the ornamented species *Henryhowela* and *Togoina Argentinensis*, which are consistently more negative than those of *Cytherella* spp., *Gavelinella* spp. and *Lenticulina* spp. These deviations between signals are interspecific, and probably caused by vital effects.

Diagenesis is also a factor that can influence the original chemical and isotopic composition, not only of microfossils, but also of sediments (Allan and Matthews, 1990). In the case of calcareous microfossils, diagenesis may favor the formation of authigenic carbonate phases, which, consequently, will have the dissociation of ions during measurements from these secondary phases and not from calcite, as expected (Bom et al., 2023). Another aspect that can modify depositional isotopic values of microfossils is the interaction with pore filling by clays and accumulation of organic matter in valves (e.g., Alvim et al., 2021). Organic matter would yield very negative $\delta^{13}C$ values, while clays can affect Sr isotopic compositions (Alvim et al., 2021). Bennett al. (2011)

proposed a protocol and established six stages of diagenesis for ostracod carapaces that must be observed for geochemical analysis. These authors clearly showed that the lowest $\delta^{18}O$ values reflect those stages most affected by diagenesis, while the most positive $\delta^{18}O$ values would be related to pristine calcites. In fact, in our results, the more negative $\delta^{18}O$ value is related to the pseudo-glassy preservation of *Togoina argeninensis* at CA11-16.8 m (-7.45‰), whereas for *Henryhowella* CA15-17.2 m, the -11.04‰ signal does not seem to be related with the state of preservation.

3.4.2 Paleocological inferences for Danian ostracods based on $\delta^{13}C$ and $\delta^{18}O$ values

Stable carbon and oxygen isotope compositions of calcareous microfossils are powerful tools for estimating paleoenvironmental and paleoclimatic conditions. The $\delta^{13}C$ values represent the inorganic carbon dissolved in the solution as a function of the formed phase (calcite or aragonite) (Wendler et al., 2013).

There are few carbon isotope records of Danian ostracods (e.g., Bornemann et al., 2012; Rodrigues et al., 2014). At the Cerro Azul Section, average $\delta^{13}C$ values were -0.72‰ for *Paracypris bertelse*, 0.93 ‰ for *Cytherella* spp., -2.56 ‰ for *Togoina argentinensis*, and -2.83 ‰ for *Henryhowella* (*Wichmanella*) *merdionalis*. Note that the larger isotopic offsets are of taxa with smoother carapaces (*Paracypris bertelse; Cytherella* spp.). Maximum $\delta^{13}C$ variabililty in the studied interval was ~0.8 ‰ among smooth species, and ~2.40 ‰ among ornamented species, suggesting oscillating environmental conditions (Fig.4). Comparable $\delta^{13}C$ amplitude ranges were observed for the Danian species *Soudanella laciniosa* (-1.7‰ to 1.48‰) and *Cytherella piacabucuensis* (0.02‰ to 1.57‰) (Rodrigues et al., 2014) and in the genus *Bairdia* (-1.6‰ to 0.5‰) (Bornemann et al., 2012). The Cerro Azul Section represents subtropical deposits, which likely underwent remarkable seasonal changes in productivity and precipitation/evaporation. This could

also account for the observed geographic heterogeneity, besides intra-specific changes. We additionally argue that these isotopic variability may be related to the availability of nutrients existing at different depths in the water column in which these specimens inhabited and fed, in addition to changes in salinity and changes in temperature of the water column (see section 4.3). For benthic foraminifera, *Gavelinella* $\delta^{13}C$ ranged from -1.33‰ to 1.4, while *Lenticulina* $\delta^{13}C$ ranged from -1.65‰ to 1.01‰, which are comparable to values recorded at the Brazos River Section, Texas (Ashckenazi-Polivoda et al., 2014).

For Danian ostracod $\delta^{18}O$ values at the Cerro Azul Section, there is a variability of -2.44‰ to -1.99‰ for *Paracypris bertelsae*, from -5.48‰ to -1.64‰ for *Cytherella* spp., -7.45‰ to -1.69‰ for *Togoina argentinensis*, and from -11.04‰ to -1.71‰ for *Henryhowella* (*Wichmanella*) *merdionalis*. Although ornamented species have similar $\delta^{13}C$ values along the studied interval, $\delta^{18}O$ values of *Henryhowella* (*Wichmanella*) *meridionalis* are more negative, especially at CA15-17.2m when compare with those of *Togoina argentinensis*. For benthic foraminifera, *Gavelinella* $\delta^{18}O$ ranged from -8.2‰ to -3.8‰, while *Lenticulina* $\delta^{18}O$ ranged from -8.05‰ to -3.37‰, which are comparable to values recorded at the Brazos River Section, Texas (Ashckenazi-Polivoda et al., 2014).

Cross plots of ostracods $\delta^{13}C$ and $\delta^{18}O$ values evaluated here depict wide difference associated with the morphologies of taxa (Fig.4). Smoother carapace ostracods have relatively high $\delta^{13}C$ and $\delta^{18}O$ values than ornamented ones. These findings were also observed by other authors, both for the Danian (e.g., Bornemann et al., 2012a; Borneman et al., 2012b; Rodrigues et al., 2014), and for other time intervals, such as the Eocene (e.g., Didié and Bauch, 2002). Changes in isotopic values may be related to diet, metabolism and processes that control the calcification of taxa (van

Hardenbroek et al., 2018). Another factor that may explain these differences is that different carapace structures have specific calcification mechanisms, with higher calcification rates for ornamented taxa, possibly causing a kinetic fractionation effect with depletion of heavier isotopes (Bornemann et al., 2012).

Ornamented ostracods of the genus *Henryhowella* from the Iceland Plateau are are assigned to an epibenthic micro-habitat habit, and considered as indicators of well-ventilated bottom waters (Didiè and Bauch, 2000; Zarikian et al., 2009; 2015). Their distribution in relation to water depths varies from bathyal to abyssal depths (e.g. Whatley et al., 1984; Yasuhara et al., 2008). *Henryhowella* is also an indicator of high food supply. At the Cerro Azul Section, *Henryhowella* (*Wichmanella*) *meridionalis* exhibited a carbon isotope signal that could indicate in infaunal microhabitat with high food supply (more negative $\delta^{13}C$). This observation is supported by less ventilated bottom waters waters (highV/Cr) and greater nutrients availability (high Ba/Ti and P/Ti).

The differences in ecological preferences of the ostracods evaluated are probably responsible for contrasts observed in isotope valve chemistry. *Henryhowella* (*Wichmanella*) *meridionalis* and *Togoina argentinenses* probably had similar ecologicals preferences, whereas *Cytherella* spp. seems have had the preferences similar to *Gavelinela*, and *Paracypris bertealse* seems had preference for high nutrient supply (Fig.7).

3.4.3 Paleoenvironmental inferences

The fauna reorganization in the ocean across the K-Pg boundary has been linked to a drop in surface water productivity and the collapse of the pelagic food web, which provides food for benthics (eg, Thomas, 1990, Kuhnt and Kaminski, 1993, D'Hondt et al., 1998, Culver, 2003).

The sparse Danian ostracod assemblage recovered from Site U1370 supports earlier findings of post-K-Pg low-diversity faunas. Evidence from Demerara Rise, in the Atlantic Ocean, suggests that the extinction event was more detrimental for detritus-feeding ostracods than for filter-feeders or silt-eater groups, which appear to have crossed the K-Pg boundary without any or little taxonomic change (Guernet and Danelian, 2006). The K-Pg boundary at the Cerro Azul Section was marked by the extinction of 22 ostracod species, suggesting that, at least in shallow marine environments, these organisms were severely affected by the event (Guerra et al., 2021). The succession after the event represents a recovery phase, in which we could continuously recover *Cytherella* spp.; *Henryhowella (Wichmanella) meridionalis*; *Togoina argentinensis* and *Paracypris bertelsae*. Abundance and diversity considerably decreased in the lowermost and uppermost studied samples (Fig. 6). It is also observed that species richness is the highest at CA13 – 17 m (95 specimens) and CA15 - 17.2 m (117 specimens) (Fig.5). The CA13-17m level corresponds to the highest ratios of paleonutrient proxies (Fig.6). From this range up to CA16-17.3, $\delta^{13}C$ values of *Henryhowella* (*Wichmanella*) *meridionalis* and *Togoina argentinensis* seem to be in synchronicity and with considerable nutrient availability. However, at the top of the Section (CA-17-17.45m), $\delta^{13}C$ values fall sharply (-3.59 for *Togoina argentinensis* and -4.67 for *Henryhowella* (*Wichmanella*) *meridionalis*, lower ratios of paleonutrient proxies (Fig.6).

The early Danian is also characterized by major carbon cycle perturbations, such as a series of short-term warming events known as hyperthermals (e.g., Zachos et al., 2001, 2008; Quillévéré et al., 2008; Coccioni et al., 2012; Gilmour et al., 2014; Krahl et al., 2020; 2023). The magnitude of the $\delta^{13}C$ negative excursion associated with the first Danian hyperthermal (Dan-C2) measured on benthic foramifera and bulk sediments changes with respect to paleogeography, but is relatively constant regarding depositional settings. In deep marine contexts the $\delta^{13}C$ negative excursion had

a mean of ~1-2‰ (e.g., Westerhold et al., 2011; Dinarès -Turrel et al., 2014; Barnet et al., 2018; Gilabert et al., 2021), whereas in shallow marine sequences it had a mean of ~-1.04‰–0.5‰ (e.g., Keller et al., 1989; Keller et al., 2008; Ezampanah et al., 2018).

According to Guerra et al. (2020), the base of Danian in Cerro Azul Section was recognized by the occurrence of *B. sparsus* (Biozone NP1: GTS-2020). This biozone has a stratigraphic range restricted to the C29r and base of C29n magnetic polarities. Despite being characterized by single points, the reported negative $\delta^{13}C$ excursions measured on ostracods, associated in dysoxic conditions, suggest that hyperthermal events, such as the Dan-C2, may be recorded at the Cerro Azul Section and should be explored in higher-resolution by future studies.

3.5 CONCLUSIONS

This study provides isotopic records based on marine ostracods in the early stages of the Paleogene, at the Cerro Azul Section, Neuquén Basin. The section consists of a shallow marine sedimentary system, with low rates of organic carbon flux and high concentration of clay minerals. Our results showed that ostracod specimens have an excellent degree of preservation, especially when compared to recovered benthic foraminifera. Ostracod $\delta^{13}C$ and $\delta^{18}O$ values depict clear differences between smooth and ornamented species, which suggest different in ecological preferences. The processes that showed the highest values from $\delta^{13}C$ were the smooth carapaces of *Cytherella* spp followed *Paracypris bertealse* and the lowest signals for the ornamented species *Togoina argentinensis* and *Henryhowella* (*Wichmanella*) *merdionalis*.

Acknowledgements

We would like to thank to Instituto de Estudios Andinos “Don Pablo Groeber” (UBA-CONICET) for providing the studied samples, as well as to the support of technicians at itt OCEANEON (UNISINOS) during SEM, XRD and ICP OES analysis. We also thank the Laboratory of Astrobiology at USP University for micro-Raman Spectroscopy analysis and the Technician Evandro P.Silva for all the support and assistance in using the equipment. M.H.H.B. would also thank the Coordination for Improvement of Higher Education Personal (CAPES) for the scholar ship and G.F is a research fellow of CNPq (grant: 308087/2019-4)

3.6 REFERENCES

Alegret, L., Molina, E., Thomas, E., 2001. Benthic foraminifera at the Cretaceous-Tertiary boundary around the Gulf of Mexico. Geology, 29(10), 891-894.

Alegret, L., Arenillas, I., Arz, J. A., Molina, E., 2002. Environmental changes triggered by the K/T impact event at Coxquihui (Mexico) based on foraminifera. NEUES JAHRBUCH FUR GEOLOGIE UND PALAONTOLOGIE MONATSHEFTE, (5), 295-309.

Alegret, L., Molina, E., Thomas, E., 2003. Benthic foraminiferal turnover across the Cretaceous/Paleogene boundary at Agost (southeastern Spain): paleoenvironmental inferences. Marine Micropaleontology, 48(3-4), 251-279.

Alegret, L., Thomas, E., 2005. Cretaceous/Paleogene boundary bathyal paleo-environments in the central North Pacific (DSDP Site 465), the Northwestern Atlantic (ODP Site 1049), the Gulf of Mexico and the Tethys: The benthic foraminiferal record. Paleogeography, Paleoclimatology, Paleoecology, 224(1-3), 53-82.

Allan, J. R., Matthews, R. K., 1990. Isotope signatures associated with early meteoric diagenesis. Carbonate diagenesis, 197-217.

Alvarez, L.W., Alvarez, W., Asaro, F., Michel, H.V., 1980. Extraterrestrial cause for the Cretaceous-Tertiary extinction. Science 208, 1095–1108.

Alvarez, L.W., 1987. Mass extinctions caused by large bolide impacts. Phys. Today 87, 25–33.

Alvim, A. M. V., Santos, R. V., Roddaz, M., Antoine, P. O., Ramos, M. I. F., Do Carmo, D. A., Linhares, A.P., Negri, F. R., 2021. Fossil isotopic constraints (C, O and $^{87}Sr/^{86}Sr$) on Miocene shallow-marine incursions in Amazonia. Palaeogeography, Palaeoclimatology, Palaeoecology, 573, 110422.

Arp, G., & Mennerich, C., 2008. Ostracod assemblages, palaeoenvironment and cyclicity of Purbeck-type sediments of the Münder Formation (Lower Cretaceous, Hils Syncline, N-Germany). Palaeogeography, Palaeoclimatology, Palaeoecology, 264(3-4), 230-249.

Arthur, M. A., Zachos, J. C., Jones, D. S., 1987. Primary productivity and the Cretaceous/Tertiary boundary event in the oceans. Cretaceous Research, 8(1), 43-54.

Barnet, J. S., Littler, K., Kroon, D., Leng, M. J., Westerhold, T., Röhl, U., Zachos, J. C., 2018. A new high-resolution chronology for the late Maastrichtian warming event: Establishing robust temporal links with the onset of Deccan volcanism. Geology, 46(2), 147-150.

Barnet, J. S., Littler, K., Westerhold, T., Kroon, D., Leng, M. J., Bailey, I., Röhl, U., Zachos, J. C., 2019. A high-Fidelity benthic stable isotope record of late Cretaceous–early Eocene climate change and carbon-cycling. Paleoceanography and Paleoclimatology, 34(4), 672-691.

Bennett, C. E., Williams, M., Leng, M. J., Siveter, D. J., Davies, S. J., Sloane, H. J., Wilkinson, I. P., 2011. Diagenesis of fossil ostracods: Implications for stable isotope based palaeoenvironmental reconstruction. Palaeogeography, Palaeoclimatology, Palaeoecology, 305(1-4), 150-161.

Bergue, C. T., Nicolaidis, D. D., 2012. The Paleocene-Oligocene ostracodes from DSDP Site 329 (Falkland Plateau): taxonomy and paleozoogeographical remarks. Paleontological Research, 16(1), 47-58.

Bom, M. H., Ceolin, D., Kochhann, K. G., Krahl, G., Fauth, G., Bergue, C. T., Savian, J.F., Strohschoen Junir, O., Simões, M.G., Assine, M. L., 2021. Paleoenvironmental evolution of the Aptian Romualdo Formation, Araripe Basin, Northeastern Brazil. Global and Planetary Change, 203, 103528.

Bom, M. H., Kochhann, K. G., Krahl, G., Andersen, N., Oliveira, L. V., Meirelles, V., Pacheco, M.L.A.F., Esswein, A., Schneider, B.C., Fauth, G., 2023. Disentangling environmental and diagenetic $\delta^{18}O$ and $\delta^{13}C$ signals from marine carbonates deposited under warm climate conditions during the early Danian. Palaeogeography, Palaeoclimatology, Palaeoecology 622, 111576.

Bornemann, A., Pirkenseer, C. M., De Deckker, P., Speijer, R. P., 2012a. Oxygen and carbon isotope fractionation of marine ostracod calcite from the eastern Mediterranean Sea. Chemical Geology 310, 114-125.

Bornemann, A., Pirkenseer, C. M., Steurbaut, E., Speijer, R. P., 2012b. Early Paleogene $\delta^{13}C$ and $\delta^{18}O$ records based on marine ostracods: implications for the upper Danian succession at Sidi Nasseur (Tunisia) and their application value in paleoceanography. Austrian Journal of Earth Sciences 105(1).

Boomer, I., 1999. Late Cretaceous and Cainozoic bathyal Ostracoda from the central Pacific (DSDP site 463). Marine Micropaleontology 37(2), 131-147.

Ceolin, D., Whatley, R., Fauth, G., Concheyro, A., 2015. New genera and species of Ostracoda from the Maastrichtian and Danian of the Neuquén Basin, Argentina. Papers in Palaeontology 1(4), 425-495.

Chivas, A. R., De Deckker, P., Shelley, J. M. G., 1983. Magnesium, strontium, and barium partitioning in nonmarine ostracode shells and their use in paleoenvironmental reconstructions–a preliminary study. Applications of ostracoda 238, e249.

Coccioni, R., Bancalà, G., Catanzarit, R., Fornaciari, E., Frontalini, F., Giusberti, L., Jovane, L., Giusberti, L., Luciani, V., Sprovieri, M., 2012. An integrated stratigraphic record of the Palaeocene–lower Eocene at Gubbio (Italy): new insights into the early Palaeogene hyperthermals and carbon isotope excursions. Terra Nova 24(5), 380-386.

Corrège, T., 1993. The relationship between water masses and benthic ostracod assemblages in the western Coral Sea, Southwest Pacific. Palaeogeography, Palaeoclimatology, Palaeoecology 105(3-4), 245-266.

Cramer, B. S., Wright, J. D., Kent, D. V., and Aubry, M.-P., 2003. Orbital climate forcing of δ13C excursions in the late Paleocene–early Eocene (chrons C24n–C25n), Paleoceanography 18, 1097, doi:10.1029/2003PA000909, 4.

Crivellari, S., Viana, P. J., de Carvalho Campos, M., Kuhnert, H., Lopes, A. B. M., da Cruz, F. W., Chiessi, C. M., 2021. Development and characterization of a new in-house reference material for stable carbon and oxygen isotopes analyses. Journal of Analytical Atomic Spectrometry 36(6), 1125-1134.

Cronin, T. M., DeMartino, D. M., Dwyer, G. S., & Rodriguez-Lazaro, J., 1999. Deep-sea ostracode species diversity: response to late Quaternary climate change. Marine Micropaleontology 37(3-4), 231-249.

Culver, S. J., 2003. Benthic foraminifera across the Cretaceous–Tertiary (K–T) boundary: a review. Marine Micropaleontology 47(3-4), 177-226.

Decrouy, L., Vennemann, T. W., Ariztegui, D., 2011. Controls on ostracod valve geochemistry: Part 2. Carbon and oxygen isotope compositions. Geochimica et Cosmochimica Acta 75(22), 7380-7399.

de Nooijer, L. J., Toyofuku, T., & Kitazato, H., 2009. Foraminifera promote calcification by elevating their intracellular pH. Proceedings of the National Academy of Sciences 106(36), 15374-15378.

Didie, C., Bauch, H. A., 2000. Species composition and glacial–interglacial variations in the ostracode fauna of the northeast Atlantic during the past 200,000 years. Marine Micropaleontology 40(1-2), 105-129.

Didié, C., Bauch, H. A., 2002. Implications of upper Quaternary stable isotope records of marine ostracodes and benthic foraminifers for paleoecological and paleoceanographical investigations. Geophysical Monograph-American Geophysical Union 131, 279-300.

Dinarès-Turell, J., Westerhold, T., Pujalte, V., Röhl, U., & Kroon, D., 2014. Astronomical calibration of the Danian stage (Early Paleocene) revisited: Settling chronologies of sedimentary records across the Atlantic and Pacific Oceans. Earth and Planetary Science Letters 405, 119-131.

D'Hondt, S., Donaghay, P., Zachos, J. C., Luttenberg, D., & Lindinger, M., 1998. Organic carbon fluxes and ecological recovery from the Cretaceous-Tertiary mass extinction. Science 282(5387), 276-279.

Durand, B., 1980. Ed. Kerogen: Insoluble organic matter from sedimentary rocks. Editions technip.

Elbra, T., Soták, J., Kdýr, Š., Kohout, T., Schnabl, P., Skála, R., Pruner, P., 2023. Cretaceous to Palaeogene boundary events and palaeoenvironmental responses across pelagic sequences of the Žilina core section, Slovakia: Rock magnetic, biotic, and geochemical characterization. Palaeogeography, Palaeoclimatology, Palaeoecology 111682.

Erez, J., Luz, B., 1983. Experimental paleotemperature equation for planktonic foraminifera. Geochimica et Cosmochimica Acta, 47(6), 1025-1031.

Font, E., Nedelec, A., Ellwood, B.B., Mirao, J., Silva, P.F., 2011. A new sedimentary benchmark for the Deccan Traps volcanism? Geophyiscal Research Letters 38, L24309.

Font, E., Adatte, T., Sial, A. N., de Lacerda, L. D., Keller, G., Punekar, J., 2016. Mercury anomaly, Deccan volcanism, and the end-Cretaceous mass extinction. Geology 44(2), 171-174.

Font, E., Adatte, T., Andrade, M., Keller, G., Bitchong, A.M., Carvalho, C., Ferreira, J.,Diogo, Z., Mir˜ao, J., 2018. Deccan volcanism induced high-stress environment during the Cretaceous-Paleogene transition at Zumaia, Spain: evidence from magnetic, mineralogical and biostratigraphic records. Earth and Planetary Science Letters 484, 53–66.

Gilabert, V., Arenillas, I., Arz, J. A., Batenburg, S. J., Robinson, S. A., 2021. Multiproxy analysis of paleoenvironmental, paleoclimatic and paleoceanographic changes during the early Danian in the Caravaca section (Spain). Palaeogeography, Palaeoclimatology, Palaeoecology 576, 110513.

Gilmour, I., Jolley, D., Kemp, D., Kelley, S., Gilmour, M., Daly, R., Widdowson, M., Kerr, A. C., 2014. The early Danian hyperthermal event at Boltysh (Ukraine): Relation to Cretaceous-Paleogene boundary events. Volcanism, Impacts, and Mass Extinctions: Causes and Effects: Geological Society of America, Special Paper (505), 133-146.

Guernet, C., Danelian, T., 2006. Ostracodes bathyaux du Crétacé terminal–Éocène moyen en Atlantique tropical (Plateau de Demerara, Leg 207). Revue de micropaléontologie 49(4), 215-225.

Guerra, R. M., Concheyro, A., Kochhann, K. G., Bom, M. H., Ceolin, D., Musso, T., Savian, J.F., Fauth, G., 2021. Calcareous microfossils and paleoenvironmental changes across the Cretaceous-Paleogene (K-Pg) boundary at the Cerro Azul section, Neuquén Basin, Argentina. Palaeogeography, Palaeoclimatology, Palaeoecology 567, 110217.

Holmes, J. A., De Deckker, P., 2012. The chemical composition of ostracod shells: applications in Quaternary palaeoclimatology. In Developments in Quaternary Sciences (Vol. 17, pp. 131-143). Elsevier.

Hou, H., Shao, L., Li, Y., Liu, L., Liang, G., Zhang, W., Whang,X., Wang, W., 2022. Effect of paleoclimate and paleoenvironment on organic matter accumulation in lacustrine shale: Constraints from lithofacies and element geochemistry in the northern Qaidam Basin, NW China. Journal of Petroleum Science and Engineering 208, 109350.

Hull, P. M., 2010. Macroevolutionary patterns in planktonic foraminifera and the recovery of pelagic ecosystems from the Cretaceous-Paleogene mass extinction. University of California, San Diego.

Hull, P. M., Bornemann, A., Penman, D. E., Henehan, M. J., Norris, R. D., Wilson, P. A., Blum, P., Alegret, L., Batenburg, S.J., Bown, P.R., Bralower, T.j., Cournede, C., Deutsch, A., Donner,

B., Friedrich, O., Jehle, S., Kim, H., Kroon, D., Lippert, P.C., Loroch, D., Moebius, I., Moriya, K Peppe, D.J., Ravizza, G.E., Röhl, U., Schueth, J.D., Sepúlveda, J.,Sexton, P.F., Sibert, E.C., S´liwin´ska, K.K., Summons, R.E., Thomas, E., Westerhold, T., Whiteside, J.H., Yamaguchi, T., Zachos, J. C., 2020. On impact and volcanism across the Cretaceous-Paleogene boundary. Science 367(6475), 266-272.

Jones, B., and Manning, D. A., 1994. Comparison of geochemical indices used for the interpretation of palaeoredox conditions in ancient mudstones. Chemical Geology 111(1-4), 111-129.

Kaiho, K., Kajiwara, Y., Tazaki, K., Ueshima, M., Takeda, N., Kawahata, H., Lamolda, M. A., 1999. Oceanic primary productivity and dissolved oxygen levels at the Cretaceous/Tertiary boundary: their decrease, subsequent warming, and recovery. Paleoceanography 14(4), 511-524.

Keatings, K. W., Holmes, J. A., Heaton, T. H., 2006. Effects of pre-treatment on ostracod valve chemistry. Chemical Geology 235(3-4), 250-261.

Keller, G., Lindinger, M., 1989. Stable isotope, TOC and $CaCO_3$ record across the Cretaceous/Tertiary boundary at El Kef, Tunisia. Palaeogeography, Palaeoclimatology, Palaeoecology 73(3-4), 243-265.

Keller, G., Adatte, T., Gardin, S., Bartolini, A., Bajpai, S., 2008. Main Deccan volcanism phase ends near the K-T boundary: evidence from the Krishna-Godavari Basin, SE India. Earth and Planetary Science Letters 268, 293–311

Keller, G., Mateo, P., Monkenbusch, J., Thibault, N., Punekar, J., Spangenberg, J. E., Abramovich, S., Ashckenazi-Polivoda, S., Schoene, B., Eddy, M.P., Samperton, K.M., Khadri, S.F.R., Adatte, T., 2020. Mercury linked to Deccan Traps volcanism, climate change and the end-Cretaceous mass extinction. Global and Planetary Change 194, 103312.

Keyser, D., Walter, R., 2004. Calcification in ostracodes. Revista Española de Micropaleontología, 36, 1-11.

Khozyem, H., Tantawy, A. A., Mahmoud, A., Emam, A., Adatte, T., 2019. Biostratigraphy and geochemistry of the Cretaceous-Paleogene (K/Pg) and early danian event (Dan-C2), a possible link to deccan volcanism: New insights from Red Sea, Egypt. Journal of African Earth Sciences, 160, 103645.

Krahl, G., Bom, M. H., Kochhann, K. G., Souza, L. V., Savian, J. F., Fauth, G., 2020. Environmental changes occurred during the early Danian at the Rio Grande rise, South Atlantic Ocean. Global and Planetary Change 191, 103197.

Krahl, G., Koutsoukos, E. A., Kochhann, K. G., Bom, M. H., Fauth, G., Esswein, A., Meirelles, V., 2023. Paleoecological Inferences for Turborotalita Nikolasi (Koutsoukos, 2014) Based on Stable Carbon and Oxygen Isotopes. Journal of Foraminiferal Research 53(2), 136-142.

Kuhnt, W., Kaminski, M. A., 1993. Changes in the Community Structure of Deep Water Agglutinated Foraminifers across the K/T Boundary in the Basques Basin (Northern Spain). Revista Española de Micropaleontología 25(1), 57-92.

Lyons, S. L., Karp, A. T., Bralower, T. J., Grice, K., Schaefer, B., Gulick, S. P., Morgan, J.V., Freeman, K. H., 2020. Organic matter from the Chicxulub crater exacerbated the K–Pg impact winter. Proceedings of the National Academy of Sciences 117(41), 25327-25334.

Littler, K., Röhl, U., Westerhold, T., Zachos, J. C., 2014. A high-resolution benthic stable-isotope record for the South Atlantic: Implications for orbital-scale changes in Late Paleocene–Early Eocene climate and carbon cycling. Earth and Planetary Science Letters 401, 18-30.

Loron, C. C., Sforna, M. C., Borondics, F., Sandt, C., Javaux, E. J., 2022. Synchrotron FTIR investigations of kerogen from Proterozoic organic-walled eukaryotic microfossils. Vibrational Spectroscopy 123, 103476.

Marquillas, R., Sabino, I., Sial, A. N., del Papa, C., Ferreira, V., Matthews, S., 2007. Carbon and oxygen isotopes of Maastrichtian–Danian shallow marine carbonates: Yacoraite Formation, northwestern Argentina. Journal of South American Earth Sciences 23(4), 304-320.

Meixnerová, J., Blum, J. D., Johnson, M. W., Stüeken, E. E., Kipp, M. A., Anbar, A. D., Buick, R., 2021. Mercury abundance and isotopic composition indicate subaerial volcanism prior to the end-Archean "whiff" of oxygen. Proceedings of the National Academy of Sciences 118(33), e2107511118.

Meyer, K. W., Petersen, S. V., Lohmann, K. C., Blum, J. D., Washburn, S. J., Johnson, M. W., Winkelstern, I. Z., 2019. Biogenic carbonate mercury and marine temperature records reveal global influence of Late Cretaceous Deccan Traps. Nature communications 10(1), 5356.

Mizukami, T., Kaiho, K., Oba, M., 2013. Significant changes in land vegetation and oceanic redox across the Cretaceous/Paleogene boundary. Palaeogeography, Palaeoclimatology, Palaeoecology 369, 41-47.

Montagna, P., McCulloch, M., Taviani, M., Mazzoli, C., Vendrell, B., 2006. Phosphorus in cold-water corals as a proxy for seawater nutrient chemistry. Science, 312(5781), 1788-1791.

Musso, T., Concheyro, A., Pettinari, G.,2012. Mineralogía de arcillas y nanofósiles calcáreos de las formaciones Jagüel y Roca en el sector oriental del lago Pellegrini, Cuenca Neuquina, República Argentina. Andean geology 39(3), 511-540.

Nauter-Alves, A., Dunkley-Jones, T., Bruno, M. D. R., Mota, M. A. D. L., Cachão, M., Krahl, G., Fauth, G., 2023. Biotic turnover and carbon cycle dynamics in the early Danian event (Dan-C2): New insights from Blake Nose, North Atlantic. Global and Planetary Change 221, 104046.

Papadomanolaki, N. M., Lenstra, W. K., Wolthers, M., Slomp, C. P., 2022. Enhanced phosphorus recycling during past oceanic anoxia amplified by low rates of apatite authigenesis. Science advances 8(26), eabn2370.

Poirier, R. K., Gaetano, M. Q., Acevedo, K., Schaller, M. F., Raymo, M. E., Kozdon, R., 2021. Quantifying diagenesis, contributing factors, and resulting isotopic bias in benthic foraminifera using the foraminiferal preservation index: Implications for geochemical proxy records. Paleoceanography and Paleoclimatology 36(5), e2020PA004110.

Quillévéré, F., Norris, R. D., Kroon, D., Wilson, P. A., 2008. Transient ocean warming and shifts in carbon reservoirs during the early Danian. Earth and Planetary Science Letters 265(3-4), 600-615.

Qiu, Z., Wei, H., Tian, L., Corso, J. D., Zhang, J., & Zou, C., 2022. Different controls on the Hg spikes linked the two pulses of the Late Ordovician mass extinction in South China. Scientific Reports 12(1), 5195.

Rodrigues, G. B., Fauth, G., Santos, R. V., Koutsoukos, E. A., Colin, J. P., 2014. Tracking paleoecological and isotopic changes through the K-Pg boundary from marine ostracodes: the Poty quarry section, northeastern Brazil. Cretaceous Research 47, 105-116.

Remírez, M. N., and Algeo, T. J., 2020. Paleosalinity determination in ancient epicontinental seas: A case study of the T-OAE in the Cleveland Basin (UK). Earth-Science Reviews 201, 103072.

Rivera, H. A., Le Roux, J. P., Sánchez, L. K., Mariño-Martínez, J. E., Salazar, C., Barragán, J. C., 2018. Palaeoredox conditions and sequence stratigraphy of the Cretaceous storm-dominated, mixed siliciclastic-carbonate ramp in the Eastern Cordillera Basin (Colombia): Evidence from sedimentary geochemical proxies and facies analysis. Sedimentary Geology 372, 1-24.

Sepúlveda, J., Alegret, L., Thomas, E., Haddad, E., Cao, C., & Summons, R. E., 2019. Stable isotope constraints on marine productivity across the Cretaceous-Paleogene mass extinction. Paleoceanography and Paleoclimatology 34(7), 1195-1217.

Sexton, P. F., Wilson, P. A., Pearson, P. N., 2006. Microstructural and geochemical perspectives on planktic foraminiferal preservation: “Glassy” versus “Frosty”. Geochemistry, Geophysics, Geosystems 7(12).

Shen, J., Feng, Q., Algeo, T. J., Liu, J., Zhou, C., Wei, W., Liu, J., Them II, T.R., Gill, B.C., Chen, J., 2020. Sedimentary host phases of mercury (Hg) and implications for use of Hg as a volcanic proxy. Earth and Planetary Science Letters 543, 116333.

Smolarek-Lach, J., Marynowski, L., Trela, W., & Wignall, P. B., 2019. Mercury spikes indicate a volcanic trigger for the Late Ordovician mass extinction event: An example from a deep shelf of the peri-Baltic region. Scientific Reports 9(1), 3139.

Thomas, E., 1990. Late Cretaceous–early Eocene mass extinctions in the deep sea. Geol. Soc. Am. Spec. Publ. 247, 481-495.

Thomas, E., Zachos, J. C., 2000. Was the late Paleocene thermal maximum a unique event? Gff, 122(1), 169-170.

Tyson, R. V., Pearson, T. H., 1991. Modern and ancient continental shelf anoxia: an overview. Geological Society, London, Special Publications, 58(1), 1-24.

Uliana, M. A., Dellapé, D. A., 1981, September. Estratigrafía y evolución paleoambiental de la sucesión maastrichtiana-eoterciaria del engolfamiento neuquino (Patagonia Septentrional). In Congreso Geológico Argentino (Vol. 8, pp. 673-711). Surquillo, Peru: La Asociación.

Van Hardenbroek, M., Chakraborty, A., Davies, K. L., Harding, P., Heiri, O., Henderson, A. C. G., .Holmes, J.A., Lasher, G.E., Leng, M.J., Panizzo, V.N., Roberts, L.,Schilder, J., Treuman, C.N., Wooller, M. J., 2018. The stable isotope composition of organic and inorganic fossils in lake sediment records: Current understanding, challenges, and future directions. Quaternary Science Reviews 196, 154-176.

Watkins, D. K., Wise Jr, S. W., Popsichal, J. J., Crux, J., 1996. Upper Cretaceous calcareous nannofossil biostratigraphy and paleoceanography of the Southern Ocean.

Wei, W., Algeo, T. J., 2020. Elemental proxies for paleosalinity analysis of ancient shales and mudrocks. Geochimica et Cosmochimica Acta 287, 341-366.

Wendler, I., Huber, B. T., MacLeod, K. G., Wendler, J. E., 2013. Stable oxygen and carbon isotope systematics of exquisitely preserved Turonian foraminifera from Tanzania—Understanding isotopic signatures in fossils. Marine Micropaleontology 102, 1-33.

Westerhold, T., Röhl, U., Donner, B., McCarren, H. K., & Zachos, J. C., 2011. A complete high-resolution Paleocene benthic stable isotope record for the central Pacific (ODP Site 1209). Paleoceanography 26(2).

Zachos, J., Pagani, M., Sloan, L., Thomas, E., Billups, K., 2001. Trends, rhythms, and aberrations in global climate 65 Ma to present. Science 292(5517), 686-693.

Zachos, J. C., Dickens, G. R., & Zeebe, R. E., 2008. An early Cenozoic perspective on greenhouse warming and carbon-cycle dynamics. Nature 451(7176), 279-283.

Zarikian, C. A. A., Stepanova, A. Y., & Grützner, J., 2009. Glacial–interglacial variability in deep sea ostracod assemblage composition at IODP Site U1314 in the subpolar North Atlantic. Marine Geology 258(1-4), 69-87.

Zarikian, C. A. A., 2015. Cenozoic bathyal and abyssal ostracods beneath the oligotrophic South Pacific Gyre (IODP Expedition 329 Sites U1367, U1368 and U1370). Palaeogeography, Palaeo-climatology, Palaeoecology 419, 115-142.

Zhang, X., Lin, C., Zahid, M. A., Jia, X., & Zhang, T., 2017. Paleosalinity and water body type of eocene Pinghu formation, Xihu depression, East China Sea Basin. Journal of Petroleum Science and Engineering 158, 469-478.

Table 1: Summary of all data from stable Carbon and oxygen isotopes in Danian from Cerro Azul. Abbreviation: O: ostracods; BF: benthic foraminifera

Sample	**Genera/Specie**		**N°valves(O) specimens (BF)**	**$\delta^{13}C$ [‰]VPDB**	**$\delta^{18}O$ [‰]VPDB**
CA17 – 17.45 m	*Paracypris bertelse*	O	2	-0.53	-1.99
CA16 – 17.30 m	*Paracypris bertelse*	O	2	-0.98	-2.44
CA15 – 17.20 m	*Paracypris bertelse*	O	2	-0.27	-2.02
CA14 – 17.10 m	*Paracypris bertelse*	O	2	-0.74	-2.41
CA13 – 17.00 m	*Paracypris bertelse*	O	2	-1.07	-2.39
CA17 – 17.45 m	*Cytherella spp*	O	2	1.05	-1,64
CA16 – 17.30 m	*Cytherella spp*	O	2	1.71	-2.01
CA15 – 17.20 m	*Cytherella spp*	O	2	0.97	-5.06
CA14 – 17.10 m	*Cytherella spp*	O		1.73	-2.37
CA13 – 17.00 m	*Cytherella spp*	O	2	0.93	-5.48
CA12 – 16.90 m	*Cytherella spp*	O		-0.78	-1.82

CA17 – 17.45 m	*Togoina argentinensis*	O	1	-3.59	-1.61
CA15 – 17.20 m	*Togoina argentinensis*	O	1	-3.10	-2.17
CA14 – 17.10 m	*Togoina argentinensis*	O	1	-2.98	-1.88
CA13 – 17.00 m	*Togoina argentinensis*	O	1	-2.25	-2.32
CA12 – 16.90 m	*Togoina argentinensis*	O	1	-3.28	-2.66
CA11 – 16.80 m	*Togoina argentinensis*	O	1 carapace	-0.91	-7.45
CA10 – 16.70 m	*Togoina argentinensis*	O	1	-3.17	-3.60
CA17 – 17.45 m	*H.(Wichmanella) meridionalis*	O	1	-4.67	-1.99
CA16 – 17.30 m	*H.(Wichmanella) meridionalis*	O	1	-2.21	-6.99
CA15 – 17.20 m	*H.(Wichmanella) meridionalis*	O	1	-3.16	-11.04
CA14 – 17.10 m	*H.(Wichmanella) meridionalis*	O	1	-3.18	-2.87

CA13 – 17.00 m	*H.(Wichma-nella) meridio-nalis*	O	1	-2.50	-2.43
CA12 – 16.90 m	*H.(Wichma-nella) meridio-nalis*	O	1	-3.14	-1.93
CA11 – 16.80 m	*H.(Wichma-nella) meridio-nalis*	O	1	-2.72	-1.71
CA10 – 16.70 m	*H.(Wichma-nella) meridio-nalis*	O	1	-1.01	-1.75
CA16 – 17.30 m	*Lenticulina spp*	BF	2	-1.65	-7.93
CA15 – 17.20 m	*Lenticulina spp*	BF	6	-1.12	-3.37
CA13 – 17.00 m	*Lenticulina spp*	BF	2	-0.65	-8.06
CA12 – 16.90 m	*Lenticulina spp*	BF	5	0.49	-7.29
CA11 – 16.80 m	*Lenticulina spp*	BF	14	0.95	-5.13
CA10 – 16.70 m	*Lenticulina spp*	BF	15	1.02	-3.59
CA17 – 17.45 m	*Gavelinella spp*	BF	16	0.82	-4.35
CA16 – 17.30 m	*Gavelinella spp*	BF	9	-1.33	-8.17

CA15 – 17.20 m	*Gavelinella spp*	BF	9	1.23	-4.91
CA13 – 17.00 m	*Gavelinella spp*	BF	17	1.28	-3.77
CA12 – 16.90 m	*Gavelinella spp*	BF	9	1.22	-5.08
CA11 – 16.80 m	*Gavelinella spp*	BF	15	1.34	-4.84
CA10 – 16.70 m	*Gavelinella spp*	BF	9	1.40	-4.19

Figures captions

Figure 1: (a) Paleogeographic reconstruction for the Cretaceous-Paleogene (~66Ma) with the location of Cerro Azul section red circle; (b) Stratigraphic succession at the Cerro Azul Section with stratigraphic ranges of selected samples for this work (in red circles); (c) Local Cerro Azul Section; (d) K-Pg Boundary

Figure 2: SEM *Henryhowella (wichmanella)meridionalis* images with its respective diffratogram and its thickness (in µm) at the early Daian in Cerro Azul Section.

Figure 3: SEM *Togoina argentinensis* images with its respective diffratogram and its thickness (in µm) at the early Daian in Cerro Azul Section.

Figure 4: $\delta^{13}C$ and $\delta^{18}O$ records of ostracods from early Danian of the Cerro Azul Section, Neuquen Basin, Argentina. $\delta^{13}C$ and $\delta^{18}O$ cross plots of ostracods species and *Lenticulina* and *Gavelinella* dispersions.

Figure 5: Geochemical proxies from evaluate: Paleosalinity (B/Ga) and valve thickness: *Togoina argentinensis*(in red) and *Henryhowella (Wichmanella) meridionalis* (in orange); Paleoxygenation (V/Cr) paleonutrients (Ba/Ti (in orange) and P/Ti (in green)); Species richness of the ostracods: *Paracypris bertealsae* (in grey); *Togoina argentinensis* (in red); *Henryhowella (Wichmanella) meridionalis* (in orange) and *Cytherella spp* (in blue).

Figure 6: Ostracods genera abundances and geochemical proxies values and paleonutrients (P/Ti, Ba/Ti). Results comparing with $\delta^{13}C$ records from *Togoina argentinensis*(in red) and *Henryhowella (Wichmanella) meridionalis* (in orange).

Figure 7: Palecological preferences of the ostracods evaluated according $\delta^{13}C$ and $\delta^{18}O$ records. Note that *Cytherella spp* values are similar to benthic foraminifera records.

Figures

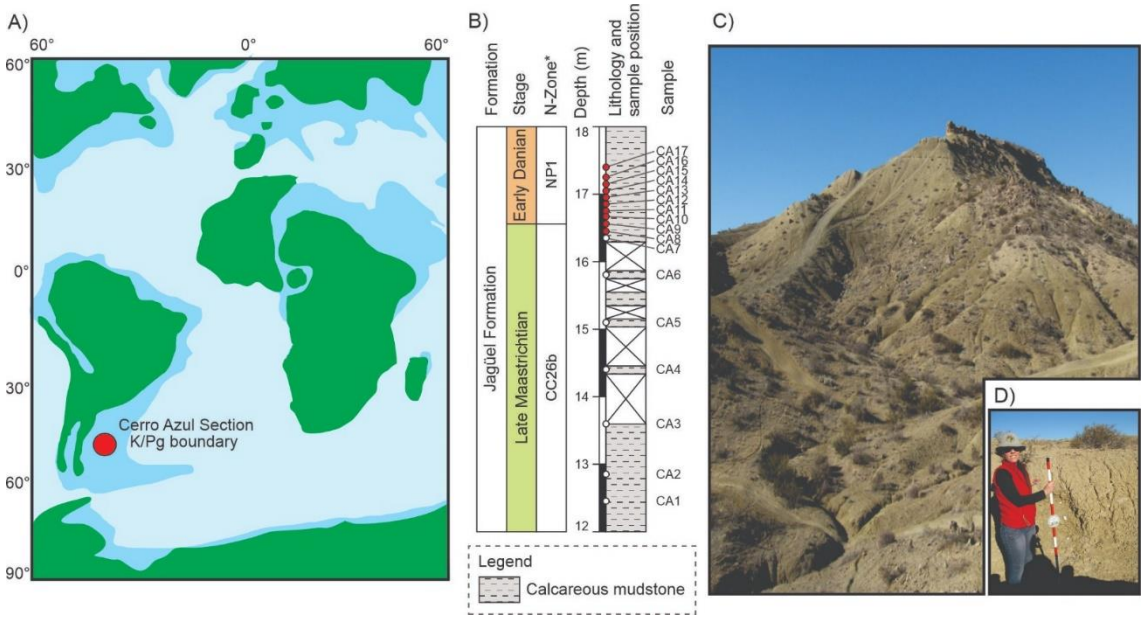

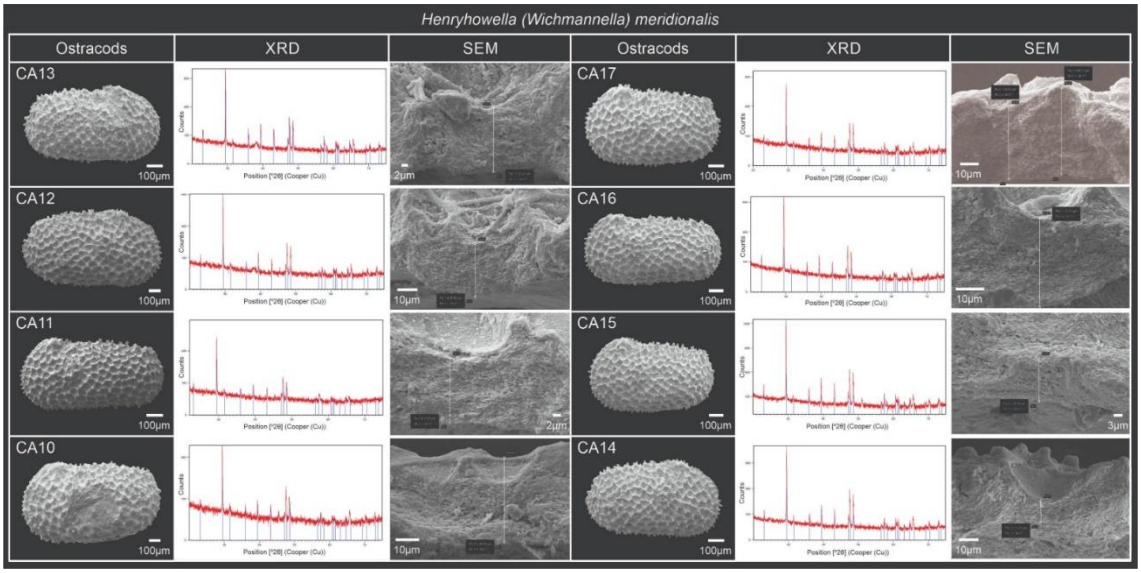
Henryhowella (Wichmannella) meridionalis
Ostracods
XRD
SEM
Ostracods
XRD
SEM
CA13
CA17
CA12
CA16
CA11
CA15
CA10
CA14
100µm
2µm
10µm
3µm

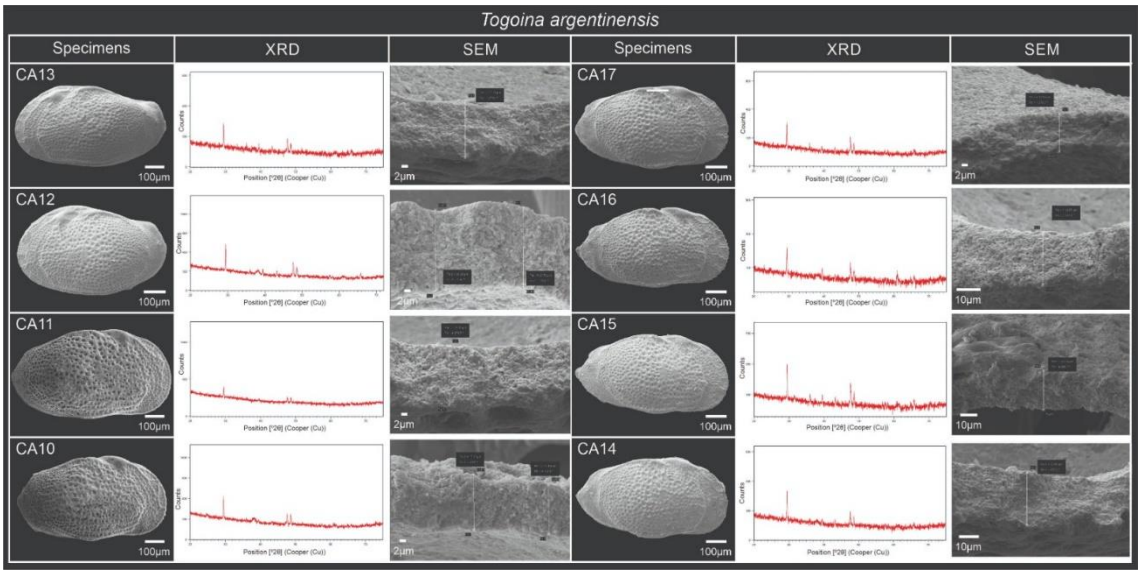
Togoina argentinensis
Specimens
XRD
SEM
Specimens
XRD
SEM
CA13
CA17
CA12
CA16
CA11
CA15
CA10
CA14
100µm
2µm
10µm

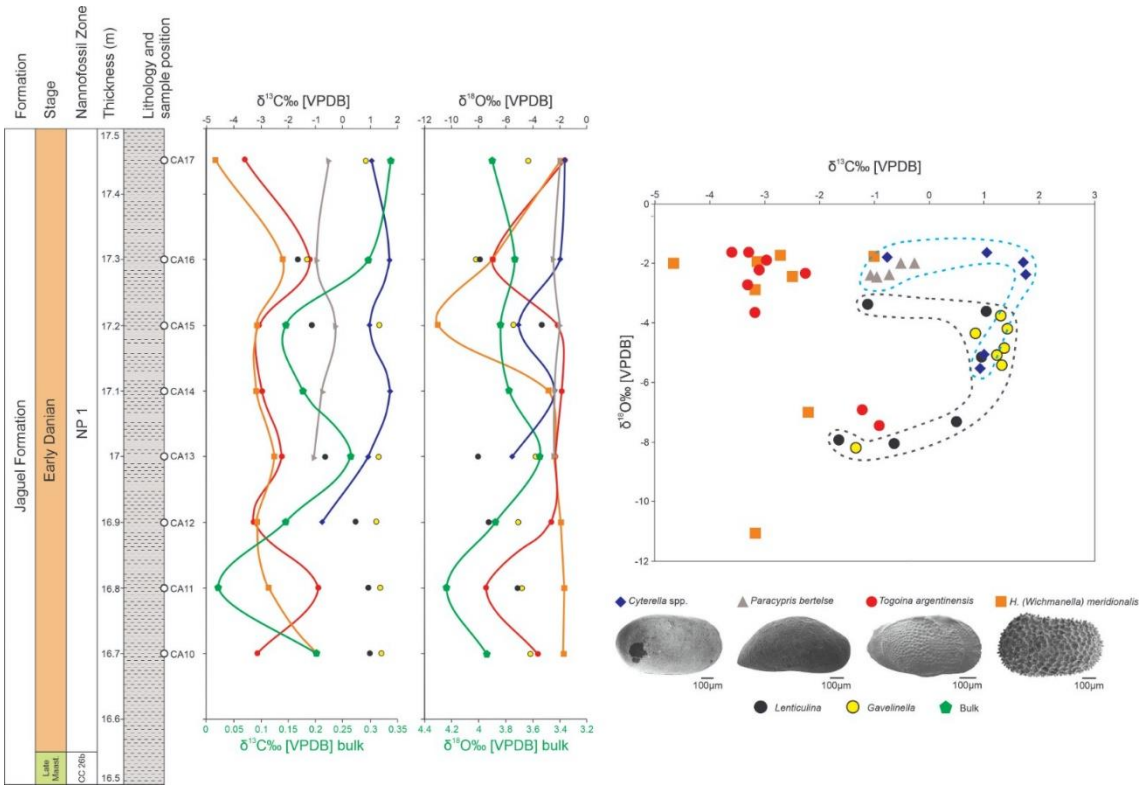
Formation
Stage
Nannofossil Zone
Thickness (m)
Lithology and sample position
Jaguel Formation
Early Danian
NP 1
Late Maast.
CC 26b
δ13C‰ [VPDB]
δ18O‰ [VPDB]
CA17
CA16
CA15
CA14
CA13
CA12
CA11
CA10
δ13C‰ [VPDB] bulk
δ18O‰ [VPDB] bulk
Cyterella spp.
Paracypris bertelse
Togoina argentinensis
H. (Wichmannella) meridionalis
Lenticulina
Gavelinella
Bulk
100µm

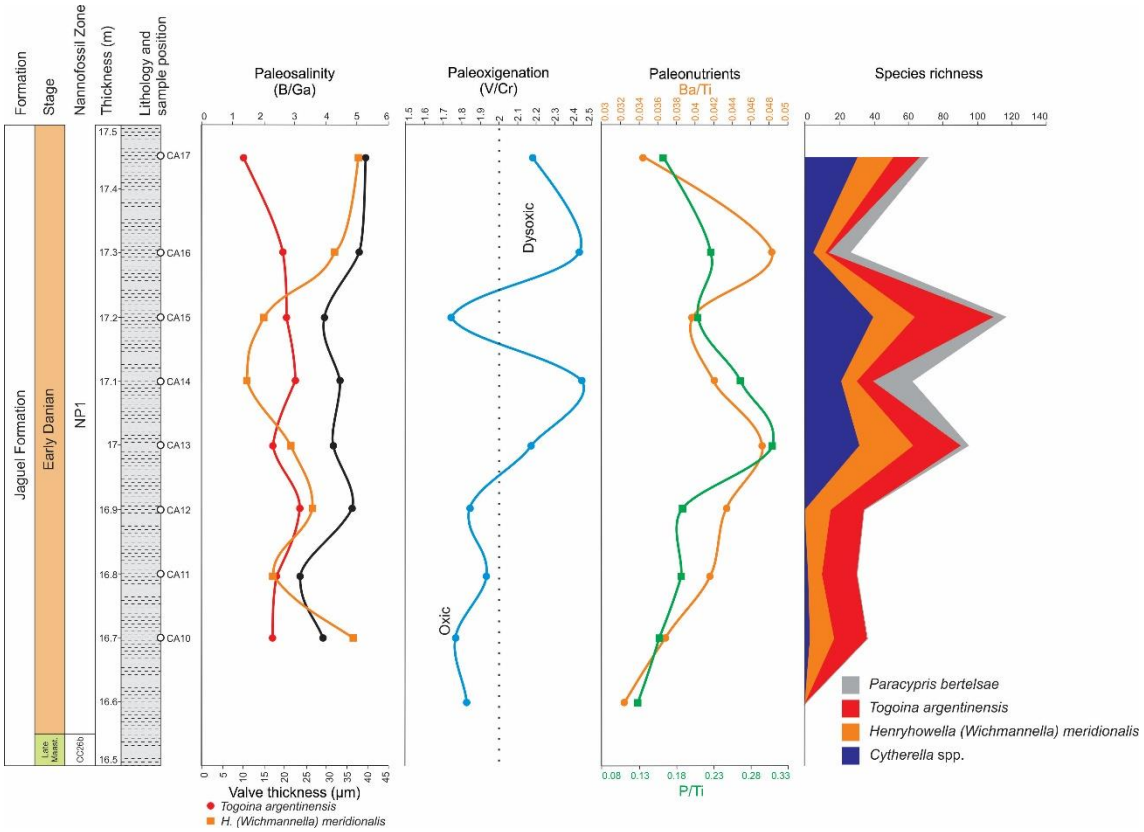
Formation
Stage
Nannofossil Zone
Thickness (m)
Lithology and sample position
Jaguel Formation
Early Danian
NP1
Paleosalinity (B/Ga)
Paleoxigenation (V/Cr)
Paleonutrients Ba/Ti
Species richness
Dysoxic
Oxic
P/Ti
Valve thickness (µm)
Togoina argentinensis
H. (Wichmannella) meridionalis
Paracypris bertelsae
Togoina argentinensis
Henryhowella (Wichmannella) meridionalis
Cytherella spp.

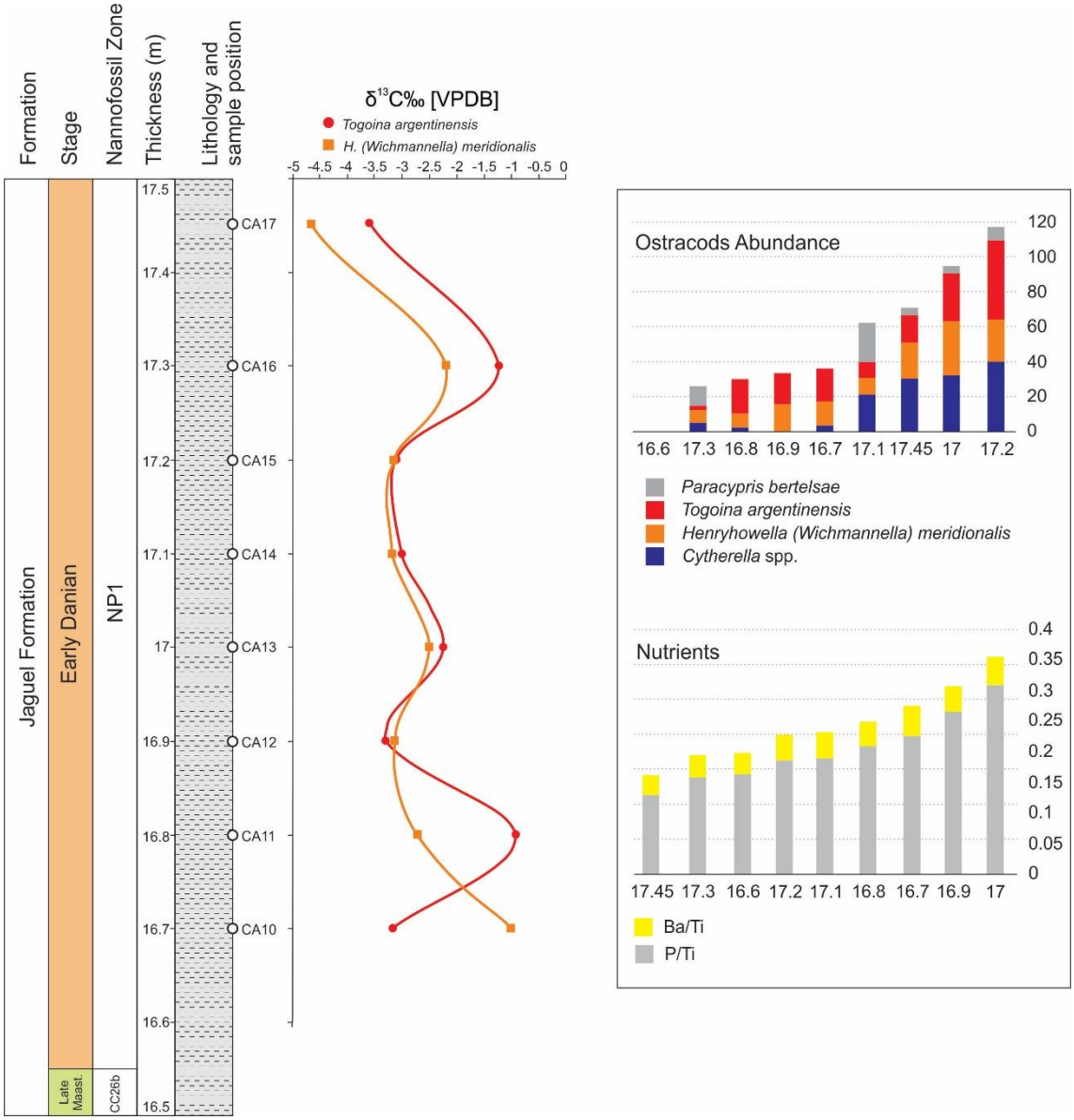
Formation
Stage
Nannofossil Zone
Thickness (m)
Lithology and sample position
Jaguel Formation
Early Danian
Late Maast.
NP1
CC26b
17.5
17.4
17.3
17.2
17.1
17
16.9
16.8
16.7
16.6
16.5
CA17
CA16
CA15
CA14
CA13
CA12
CA11
CA10
δ13C‰ [VPDB]
Togoina argentinensis
H. (Wichmannella) meridionalis
-5 -4.5 -4 -3.5 -3 -2.5 -2 -1.5 -1 -0.5 0
Ostracods Abundance
120
100
80
60
40
20
0
16.6 17.3 16.8 16.9 16.7 17.1 17.45 17 17.2
Paracypris bertelsae
Togoina argentinensis
Henryhowella (Wichmannella) meridionalis
Cytherella spp.
Nutrients
0.4
0.35
0.3
0.25
0.2
0.15
0.1
0.05
0
17.45 17.3 16.6 17.2 17.1 16.8 16.7 16.9 17
Ba/Ti
P/Ti

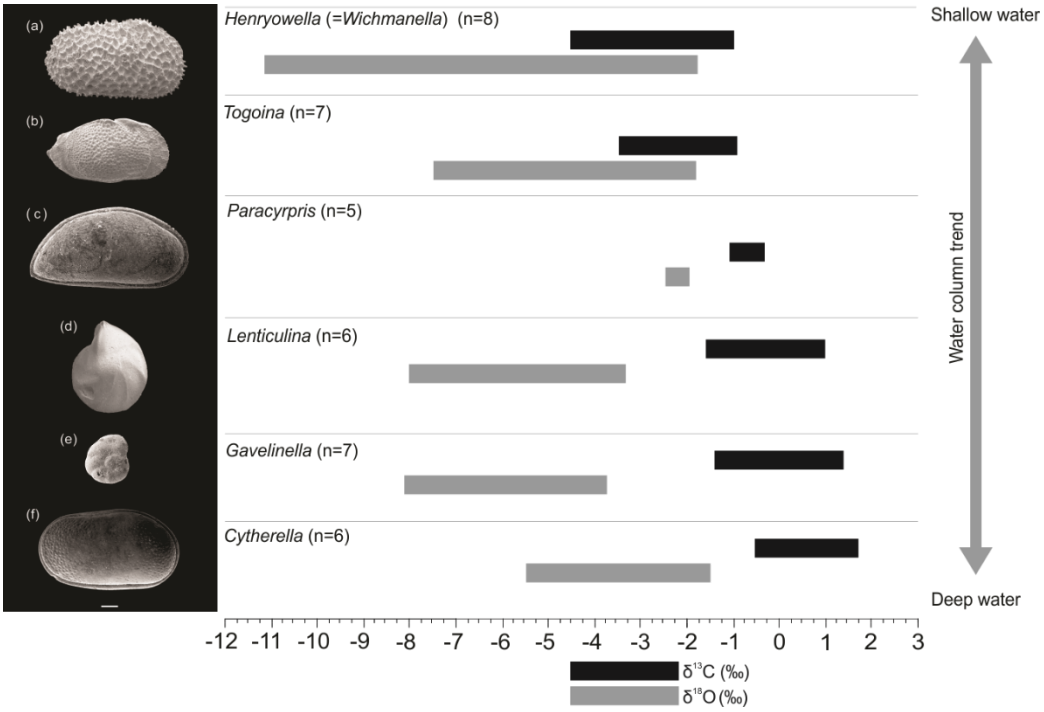
(a)
(b)
(c)
(d)
(e)
(f)
Henryowella (=Wichmanella) (n=8)
Togoina (n=7)
Paracyrpris (n=5)
Lenticulina (n=6)
Gavelinella (n=7)
Cytherella (n=6)
Shallow water
Water column trend
Deep water
-12 -11 -10 -9 -8 -7 -6 -5 -4 -3 -2 -1 0 1 2 3
δ13C (‰)
δ18O (‰)

Supporting Information for:

Paleoecology of selected Danian marine ostracods suggested by stable carbon ($\delta^{13}C$) and oxygen ($\delta^{18}O$) isotopes

Figure S1: Preservation state in different stratigraphic intervals. Note that ostracods *Henryhowella* (*Wichmanella*) *meridionalis* have much better preservation than *Lenticulina* and *Gavelinela* specimens in different depths.

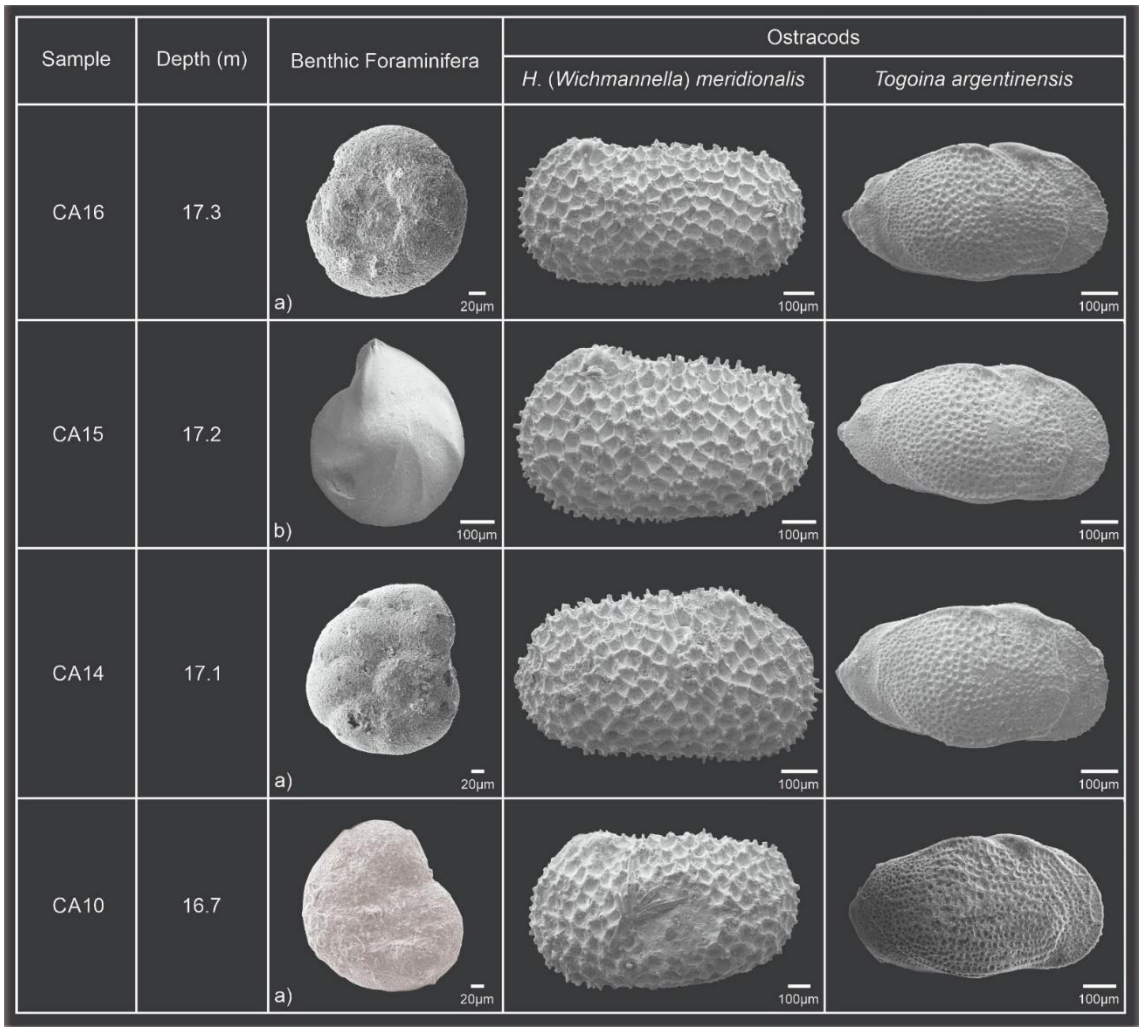

Figure S2: (a) SEM image from *H.* (*Wichmanella*) *meridionalis* valve from CA13 sample (17 m); (b) detail of different structures in valve: calcite (in blue circle); gypsum crystals (in red circle) and clay (green circle)

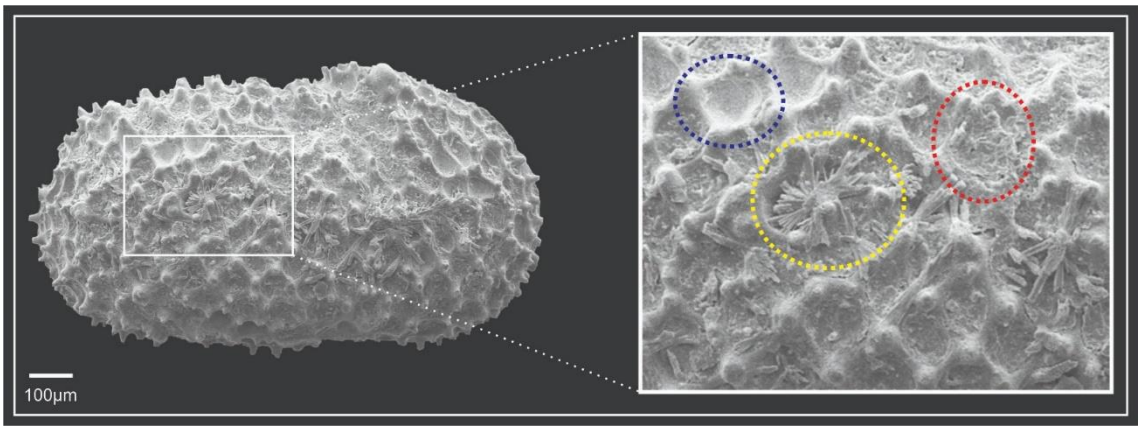

Table S1: Thickness in µm of *Togoina argentinensis* valves

Sample	Depht (m)	Thickness (µm)	Preservation
CA17	17.45	10.09	*glassy*
CA16	17.3	19.57	*glassy*
CA15	17.2	20.54	*glassy*
CA14	17.1	22.46	*glassy*
CA13	17.0	17.19	*pseudo-glassy*
CA12	16.9	23.95	*glassy*
CA11	16.8	18.08	*pseudo-glassy*
CA10	16.7	17.11	*pseudo-glassy*

Table S2: Thickness in µm of *H.* (*Wichmanella*) *meridionalis* valves

Sample	Depht (m)	Thickness (µm)	Preservation
CA17	17.45	38.41	*glassy*
CA16	17.3	32.40	*glassy*
CA15	17.2	14.99	*glassy*
CA14	17.1	11.31	*glassy*
CA13	17.0	21.41	*pseudo-glassy*
CA12	16.9	26.59	*glassy*
CA11	16.8	17.63	*glassy*
CA10	16.7	36.8	*pseudo-glassy*

Figure S3: Micro-Raman -Spectroscopy in *Henryhowella* (*Wichmanella*) *meridionalis* valve CA10-16.6m: Organic matter. Smoothed for D and G band highlight

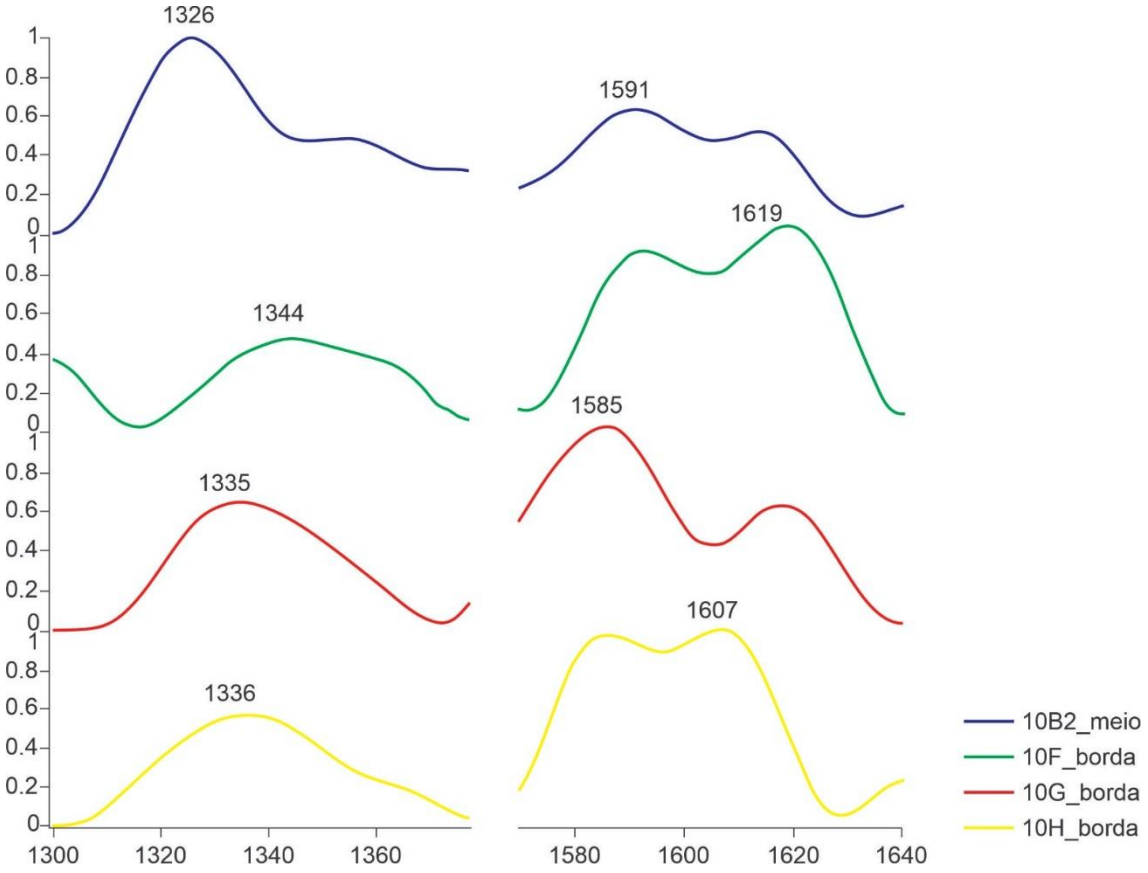

Figure S4: Raman spectra of *Henryhowella* (*Wichmanella*) *meridionalis* valve CA10-16.6 m. The detectable peaks are 1087 cm^{-1}, with a blue shift, confirming the presence of calcium carbonate Mg-enriched.

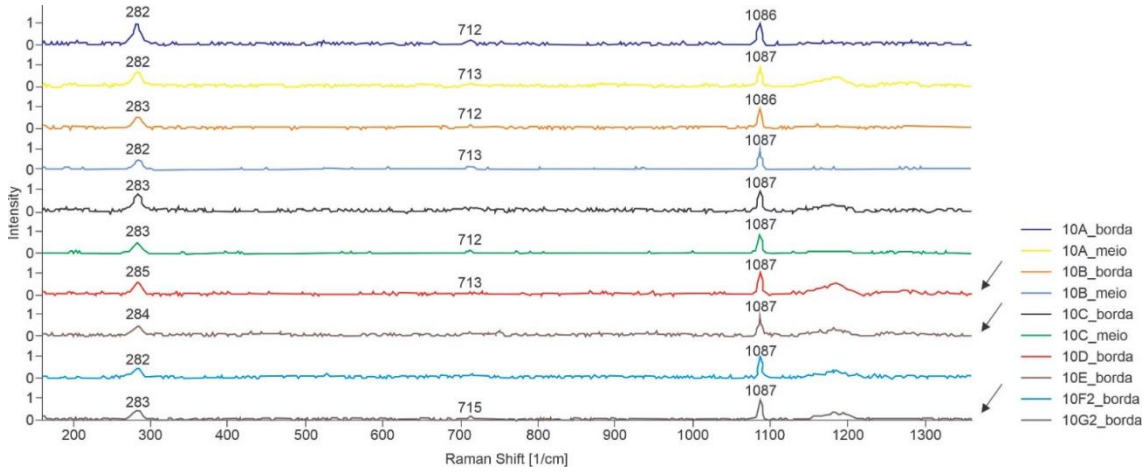

CAPÍTULO 4 – O IMPACTO DAS PERTURBAÇÕES AMBIENTAIS COM BASE EM FORAMINÍFEROS PLANCTÔNICOS DO ODP SITE 1262

Capítulo 4:

Impact of early Danian environmental perturbations on mid-latitude planktic foraminiferal assemblages from the ODP Site 1262 (South Atlantic Ocean)

Guilherme Krahl[1,2], Ignacio Arenillas[3], Vicente Gilabert[3,4], Karlos G.D. Kochhann[1,2], Marlone H.H. Bom[1,2], Gerson Fauth[1,2], José A. Arz[3]

Publicado em: *Newsletter on Stratigraphy* doi.org/10.1127/nos/2023/0744

Impact of early Danian environmental perturbations on mid-latitude planktic foraminiferal assemblages from the ODP Site 1262 (South Atlantic Ocean)

Guilherme Krahl[1,2], Ignacio Arenillas[3], Vicente Gilabert[3,4], Karlos G.D. Kochhann[1,2], Marlone H.H. Bom[1,2], Gerson Fauth[1,2], José A. Arz[3]

[1] Technological Institute for Paleoceanography and Climate Change, itt OCEANEON, UNISINOS University, Av. UNISINOS, 950, 93022-750 São Leopoldo, RS, Brazil

[2] Geology Graduate Program, UNISINOS University, Av. UNISINOS, 950, 93022-000 São Leopoldo, RS, Brazil

[3] Departamento de Ciencias de la Tierra, and Instituto Universitario de Investigación en Ciencias Ambientales de Aragón (IUCA), Universidad de Zaragoza, E-50009 Zaragoza, Spain

[4] Departament de Dinàmica de la Terra i de l'Oceà, Facultat de Ciències de la Terra de la Universitat de Barcelona, 08028, Barcelona, Spain

Corresponding author: Guilherme Krahl (gkrahl@unisinos.br)

Abstract

After the mass extinction at the Cretaceous/Paleogene (K/Pg) boundary (~66 Ma), life forms quickly radiated to occupy ecological niches in the world's oceans. Nevertheless, the aftermath of the Chicxulub impact, the massive volcanism of the Deccan Traps and climatic perturbations endured during the early Danian. The impact of consequent carbon cycle perturbations on nascent plankton communities, such as the Dan-C2 event (~65.80 to ~65.71 Ma), is still poorly known. In this work, we present a detailed study of planktic foraminiferal assemblages from Ocean Drilling Program (ODP) Site 1262 (Walvis Ridge, South Atlantic Ocean), spanning the first ~400 kyr of the Danian.

No relevant perturbations in planktic foraminiferal assemblages and carbonate preservation indices have been identified at Site 1262 during the Dan-C2 event. Approximately 50 kyr before the beginning of the Dan-C2 event, a Hg-rich interval, potentially linked to the emplacement of the Ambenali Formation of the Deccan Traps massive volcanism, is recorded between ~65.95 and 65.82 Ma. It coincides with an increase in aberrant planktic foraminifera (~65.93 to ~65.82 Ma), allowing to establish a cause-effect relationship. Additionally, a bloom of triserial guembelitriids was recognized between ~65.87 and ~65.78 Ma, also preceding the Dan-C2 event but lagging the Hg-rich interval and the bloom of aberrant planktic foraminifera. The lag time between the first volcanic episode and ecosystem response may be due to factors such as an inefficient biological pump and increases in temperature, microbial activity and food supply at the ocean surface. A second Hg-rich interval identified between ~65.70 and ~65.65 Ma has been tentatively tied to the Mahabaleswar Formation of the Deccan Traps. Neither the second volcanic episode nor the Dan-C2 event resulted in relevant environmental perturbations at Site 1262. This suggests that, although

volcanism may have had an impact on early plankton communities in the early Danian through metal contamination, marine ecosystems likely became progressively more stable and resistant to changes in volcanic emissions and the carbon cycle.

Keywords. Early Danian, Planktic foraminifera, Mercury, Dan-C2, Deccan Traps

4.1 INTRODUCTION

The mass extinction at the Cretaceous/Paleogene (K/Pg) boundary was one of the greatest extinction events in the Earth's geological history (see Schulte et al. 2010 and references therein). It was triggered by the impact of the Chicxulub asteroid in the Yucatan Peninsula (Hildebrand et al. 1991). Impact evidence is recorded globally in a fine airfall layer rich in siderophile elements (e.g., iridium, osmium and nickel), impact glasses (microtektites), Ni-spinels, and shocked quartz (Alvarez et al. 1980, Orth et al. 1981, Schulte et al. 2010, Ravizza and Vonderhaar 2012), as well as a thick complex clastic unit, which contains Chicxulub-impact-derived material and whose deposition was linked to impact-induced processes (earthquakes, tsunamis, submarine landslides, and debris flows) that took place within a distance of up to 1000 km from the Chicxulub impact structure (see Arz et al. 2022 for a review). Models based on the size, velocity, and angle of the impactor as well as the nature of the impact site, among other data, predict that the Chicxulub impact would have triggered severe environmental disturbances in the first months and years of the Danian, causing a global mass extinction event (e.g., Kring 2007, Schulte et al. 2010, Morgan et al. 2022) in which the planktic foraminifera underwent an extinction accounting for probably ~95% of the Cretaceous species (see Arenillas et al. 2022, and references therein).

Another large-scale disturbance that occurred across the Cretaceous-Paleogene (K-Pg) transition was the eruption of ~500 000 km^3 of lava over a large area of present-day India known as the Deccan Traps (DT) (see Schoene et al. 2019, Sprain et al. 2019, and references therein). In order to establish the eruptive history of the DT, $^{40}Ar/^{39}Ar$ dating methods have been applied to basalt plagioclases (Sprain et al. 2019), and U–Pb dating methods to zircons collected in red bole horizons between basalt flows (Schoene et al. 2019). High-precision data from the DT show that the main phase of the eruptions started near the C30n/C29r geomagnetic polarity reversal (Maastrichtian) and diminished shortly after the C29r/C29n reversal (Danian) (Schoene et al. 2019, Sprain et al. 2019). The estimated duration of the massive volcanism of the DT is very similar in the two main eruption models proposed to date: ~700-800 kyr according to the model put forward by Schoene et al. (2019, 2021) and ~1 Myr according to that of Sprain et al. (2019). Nonetheless, there are two critical differences between the two models: 1) Schoene et al. (2019) suggest a sequence of mega-pulses, whereas Sprain et al. (2019) suggest a quasi-continuous release of lava flows; 2) according to Sprain et al. (2019), the most voluminous eruptions of the DT (i.e., those corresponding to the Poladpur, Ambenali, and Mahabaleshwar Formations) occurred in the early Danian, whereas according to Schoene et al. (2019), the eruptive pulse that originated the Poladpur Fm. occurred in the latest Maastrichtian, preceding the K/Pg mass extinction event by ~30 kyr (Schoene et al. 2019, 2021). According to Sprain et al. (2019), the emplacement of the Ambelani Fm. occurred between ~65.95 and 65.62 Ma (~50 and 380 kyr after the K/Pg boundary), with a pulse between ~65.95 and 65.85 Ma (50 and 150 kyr after the K/Pg boundary) according to Schoene et al. (2019). The onset of Mahabaleshwar Fm. emplacement occurred ~65.62 Ma (380 kyr after the K/Pg boundary), with a pulse between 65.62 and 65.57 Ma (380 and 430 kyr after the K/Pg boundary) according to Schoene et al. (2019).

Between the K/Pg and C29r/C29n boundaries, the first recorded paleoclimatic event of the Danian is known as Dan-C2 (Quillévéré et al. 2008), which has been attributed to large-scale inputs of greenhouse gases from the DT (Coccioni et al. 2010, Punekar et al. 2014). The Dan-C2 event is typically recorded by a double negative carbon isotope excursion (CIE-1 and CIE-2) and lasted for ~100 kyr (Quillévéré et al. 2008, Gilabert et al. 2022). The onset of this event varies slightly with the astrochronological age model used as a reference, being estimated to occur ~160 kyr after the K/Pg boundary by Barnet et al. (2019) or 200 kyr after the K/Pg boundary by Gilabert et al. (2022). The two age models differ mainly in the astronomical solution used, but they agree in tying Dan-C2 to the first 405-kyr eccentricity maximum ($Pc_{405}1$) of the Paleocene (Barnet et al. 2019; Gilabert et al. 2022). Dan-C2 shows broad similarity to other hyperthermal events, for example negative carbon ($\delta^{13}C$) and oxygen ($\delta^{18}O$) isotope excursions measured in bulk sediments and planktic foraminifera, coupled with drops in $CaCO_3$ content in deep ocean sediments. So far, the record of this event is restricted to the following Atlantic and Tethyan localities: Ocean Drilling Program (ODP) Site 1049C (NW Atlantic; Quillévéré et al. 2008), Deep Sea Drilling Program (DSDP) Sites 527 and 528 (SE Atlantic; Quillévéré et al. 2008), ODP Site 1262 (SE Atlantic; Kroon et al. 2007, Barnet et al. 2019), Gubbio (Italy; Coccioni et al. 2010), DSDP Site 516F (SE Atlantic; Krahl et al. 2020), Caravaca (SE Spain; Gilabert et al. 2021), and Zumaia (N Spain; Gilabert et al. 2022).

In general, hyperthermal events are paced and modulated by astronomical frequencies, specifically by eccentricity (see Westerhold et al. 2020, and references therein). Bottom-water oxygenation (ventilation) decreased in the deep Atlantic Ocean (Coccioni et al. 2010, Krahl et al. 2020), and a ~4°C warming in North Atlantic surface waters occurred during the Dan-C2 event (Quillévéré et al. 2008). However, in contrast to other hyperthermal events, no warming in deep waters

(e.g., $\delta^{18}O_{benthic}$) has yet been recorded for Dan-C2 (Quillévéré et al. 2008, Barnet et al. 2019, Arreguín-Rodríguez et al. 2021), raising the question as to whether it was indeed a hyperthermal event (Barnet et al. 2019).

Planktic foraminifera and calcareous nannofossils were strongly affected by the K/Pg boundary extinction event (e.g., Smit 1982, Molina et al. 1996, Olsson et al. 1999, Arenillas et al. 2000ab, Thibault et al. 2016, Lowery et al. 2018). The high rates of species-level extinction reduced the richness of phyto- and zooplankton communities, affecting several trophic levels in the ocean (Sheehan et al. 1996). The early Danian was a time of ecosystem recovery after the K/Pg boundary extinction (Molina 2015). The earliest Danian assemblages are characterized by low diversity, high single-species dominance, and rapid evolutionary turnovers (Smit 1982, Arenillas et al. 2000a, Aze et al. 2011, Arenillas and Arz 2017, Huber et al. 2020, Lowery et al. 2021), as well as by blooms of smaller generalist and/or opportunist species (Kroon and Nederbragt 1990, Arenillas et al. 2000b, Pardo and Keller 2008, Punekar et al. 2014, Gilabert et al. 2021). During the recovery of species richness in the early Danian (Lowery and Fraass 2019), planktic foraminifera also responded to carbon cycle perturbations (e.g., Jehle et al. 2015, 2019, Bornemann et al. 2021). However, the impact of Dan-C2 and the influence of the DT eruptions on early Danian planktic foraminiferal assemblages is poorly understood (Gilabert et al. 2021, 2022).

Here we present a multiproxy approach to investigate the impact of DT volcanism and the Dan-C2 event on early Danian planktic foraminiferal assemblages in the South Atlantic Ocean. We studied the lower Danian interval at Ocean Drilling Program (ODP) Site 1262, drilled on the Walvis Ridge, which presents an excellent record of the Dan-C2 event (Zachos et al. 2004). Site 1262 has been the basis for several multiproxy studies exploring carbon cycle dynamics (e.g., Birch et al. 2016, 2021, Woelders et al. 2017, Hull et al. 2020), as well as for the characterization

of the Dan-C2 event (e.g., Barnet et al. 2019, Arreguín-Rodríguez et al. 2021). Together with other well-known localities, it has allowed the astronomical calibration of the Danian events (Dinarès-Turell et al. 2014) upon which the Geological Time Scale GTS2020 for the Danian is based (Gradstein et al. 2020).

4.2 MATERIAL AND METHODS

4.2.1 Geographical location and stratigraphy of Site 1262

During ODP Leg 208, Sites 1262 and 1267 cored the K–Pg transition on the Walvis Ridge, eastern South Atlantic Ocean (27°11.15′S, 1°34.62′W; Zachos et al. 2004). We studied Hole 1262B by collecting forty samples across the K–Pg transition of core 208-1262B-22H-3-5 (Figure 1), which was located at a paleolatitude of ~40°S (Van Hinsbergen et al. 2015) and deposited in the upper abyssal zone (~3000 m water depth; Zachos et al. 2004). The depths assigned to each sample correspond with the meters composite depth scale (mcd), spanning the interval between 216.83 and 214.88 mcd. Overall, the sediments recovered at Site 1262 vary from clays to carbonate-rich oozes (Zachos et al. 2004).

The K/Pg boundary (208-1262B-22H-4, 137 cm; 216.52 mcd) is marked by an irregular contact between upper Maastrichtian light gray-brown clayey nannofossil oozes and overlying lower Danian red-brown clays (Figure 2; see Appendix A), the latter of which are moderately bioturbated. Microtektites (impact glasses) related to the Chicxulub impact have been reported within this reddish clay directly above the K/Pg boundary (Zachos et al. 2004). The magnetostratigraphy of Site 1262 is based on shipboard paleomagnetic measurements conducted at 5-cm resolution, supplemented by discrete samples (Bowles 2006, Westerhold et al. 2008). On this basis, the C29r/C29n

reversal was placed at 215.00 mcd (Bowles, 2006; Westerhold et al. 2008; Dinarès-Turell et al. 2014). Complementary to these findings, Site 1262 has been the subject of several studies reporting sedimentological and geochemical data (such as oxygen, carbon, and osmium isotopes) for the studied interval (e.g., Ravizza and Peucker-Ehrenbrink 2003, Robinson et al. 2009, Kroon et al. 2007, Alegret et al. 2012, Birch et al. 2016, Woelders et al. 2017, Barnet et al. 2018, 2019, Hull et al. 2020).

4.2.2 Micropaleontological methods and the planktic foraminiferal dataset

For each sample collected from Site 1262, approximately 10 g of sediments were soaked in de-ionized water for 72 hours, before being washed over 63 μm sieves. The residues were dried in an oven at temperatures below 40 °C. We picked approximately 400 planktic foraminiferal specimens per sample from the ≥63 μm residues. The quantitative planktic foraminiferal distribution and paleoenvironmental indexes at Site 1262 are shown in Appendix B, and the depth habitats of the planktic foraminiferal species in Appendix C. Taxonomic identifications at genus and species levels followed Olsson et al. (1999) and Koutsoukos (2014), whereas biostratigraphic interpretations are based on Berggren and Pearson (2005) and Wade et al. (2011). For comparison, we have also used the most recent biozonation of Arenillas et al. (2021) for the lower Danian, which is based on the taxonomic and biostratigraphic interpretations of Arenillas et al. (2000a,b, 2004, 2018). In light of the known paleoecological preferences of the identified taxa (Boersma and Premoli Silva 1983, D'Hondt and Zachos 1993, Huber and Boersma 1994, Berggren and Norris 1997, Olsson et al. 1999, Coxall et al. 2000, Aze et al. 2011, Koutsoukos 2014, Huber et al. 2020), we grouped them according to their inferred paleodepth habitats into ecogroups (mixed-layer, thermocline and sub-thermocline taxa; see Appendix C). Variations in the relative abundances of

these groups are useful to evaluate changes in water column stratification (e.g., Lowery et al. 2021).

Changes in the relative abundances of planktic and benthic foraminifera (the P/B ratio) may be related to paleobathymetry (e.g., Van der Zwaan et al. 1990), paleoproductivity (e.g., Berger and Diester-Haass 1988), and/or carbonate dissolution at the seafloor (e.g., Hancock and Dickens 2005, Nguyen and Speijer 2014, Luciani et al. 2017). Given that the paleobathymetry at Site 1262 did not change markedly within the studied interval (Zachos et al. 2004), we assume that changes in the P/B ratio were mainly caused by changes in the calcite saturation state of deep waters and, to a lesser extent, by changes in paleoproductivity. We calculated the P/B ratio as follows: P/B ratio (%) = [planktic specimens/ (planktic + benthic specimens) *100].

We also calculated the fragmentation index (FI) quantifying the number of fragmented individuals. We counted as fragments specimens with clearly missing or deteriorated chambers, as well as specimens exhibiting features of fragmentation such as large holes. The fragmentation index was calculated as follows: FI (%) = [(number of fragments)/ (number of fragments + complete individuals) *100].

Finally, we estimated the foraminiferal abnormality index (FAI) in accordance with the morphological criteria used by Arenillas et al. (2018). To identify morphological abnormalities in foraminiferal tests, we compared forms considered aberrant with typical "normal" specimens recognized in the literature (e.g., Olsson et al. 1999, Arenillas et al. 2018, 2021).

4.2.3 Geochemical methods (stable isotopes, carbonate content, Hg and Mn content)

Approximately 1.5 g of bulk sediments from each sample were crushed with an agate mortar and pestle for stable isotope analysis. Sample aliquots (100-150 μg) were reacted with phosphoric

acid, and the resulting CO_2 was analyzed with a Finnigan MAT 253 mass spectrometer coupled to a Carbo-Kiel type IV device at the Leibniz Laboratory for Radiometric Dating and Stable Isotope Research, University of Kiel. The standard external error based on duplicate measurements is better than ±0.05‰ for $\delta^{13}C_{bulk}$ and ±0.08‰ for $\delta^{18}O_{bulk}$. The results were calibrated against the standard NBS-19, and values are reported as deviations (‰) from the Vienna PeeDee Belemnite scale (VPDB).

The carbonate content ($CaCO_3$%) was measured in oven-dried (38-40 ºC for 48 hours) ground sediment samples from Site 1262. For each sample, a ~0.26 g aliquot of homogenized sediments was measured for total carbon (TC) content in a LECO SC-144DR carbon and sulfur analyzer at the Technological Institute for Paleoceanography and Climate Change (itt OCEANEON; UNISINOS University). Total organic carbon (TOC) was also measured in ~0.26 g sample aliquots after the sediments had been treated with HCl 6N and washed with warm water until neutral pH (pH = 7) was reached. We calculated the $CaCO_3$ content according to Stax and Stein (1995) as follows: $CaCO_3$% = [TC(%) – TOC(%)] * 8.33. Since our primary goals were to analyze the planktic foraminiferal assemblages and measure the Hg and Mn content of the samples in order to assess the DT volcanism at Site 1262 (see just below), the sampling resolution for isotopic analysis is markedly lower than that of Woelders et al. (2017), so we have compared and correlated the $\delta^{13}C_{bulk}$ and $\delta^{18}O_{bulk}$ data of these authors in Appendix A. Geochemical data from Site 1262 are shown in Appendix D.

For determination of mercury (Hg) concentrations were measured (~0.5 to 0.7 g of bulk sediment aliquots) by an atomic absorption using a direct mercury analyzer (Milestone- DMA-80 evo Tricell) in the itt Oceaneon (Universidade do Vale do Rio dos Sinos). All 34 samples is initially dried

and thermally decomposed in an oxygen flow, where the Hg vapors are trapped on a gold amalgamator and subsequently desorbed for quantification. Finally, the Hg content is determined using atomic absorption spectrophotometry (253.65 nm). Mn concentrations were measured for the same set of samples after digestion of 150 mg per g of ground sediments in a solution of nitric and hydrochloric acids, using an inductively coupled plasma optical emission spectroscope (ICP-OES) iCAP 7400 (Thermo Fischer Scientific). Both analyses were carried out at itt OCEANEON (UNISINOS University).

Mercury concentrations (Hg) were measured (~0.1 g of bulk sediment aliquots) by atomic absorption using a direct mercury analyzer (DMA-80 evo tricell). All 40 samples were thermally decomposed, and the Hg vapor was captured in a gold amalgamator and subsequently released (temperature 850 °C). The quantification of Hg was performed by atomic absorption spectroscopy and concentrations data are reported in ppb (parts per billion). All 40 samples were thermally decomposed, and the Hg vapor was captured in a gold amalgamator and subsequently released (temperature 850 °C). The quantification was determined by atomic absorption spectroscopy (254 nm). Mn concentrations were measured for the same set of samples after digestion of 150 mg per g of ground sediments in a solution of nitric and hydrochloric acids, using an inductively coupled plasma optical emission spectroscope (ICP-OES) iCAP 7400 (Thermo Fischer Scientific). Both analyses were carried out at itt OCEANEON (UNISINOS University).

4.3 RESULTS

4.3.1 Record of CIEs and carbonate preservation disturbances at Site 1262

The $\delta^{13}C_{bulk}$ record at Hole 1262B (Figure 2a, b) displays the negative isotope excursion usually associated with the K/Pg boundary (~1‰ $\delta^{13}C$) between the samples at 216.55 and 216.50 mcd

and the Dan-C2 double-peaked negative excursion between 215.52 and 215.07 mcd. According to our $\delta^{13}C_{bulk}$ data, the CIE-1 of the Dan-C2 event (lowest $\delta^{13}C$) is placed between 215.47 and 215.37 mcd, and the CIE-2 of Dan-C2 between 215.27 and 215.17 mcd (Figure 2). Our isotope data show a similar behaviour as those from Hole 1262C previously reported by Woelders et al. (2017), albeit of lower resolution. Unlike our isotope data from Hole 1262B, Woelders et al. (2017) identified a negative $\delta^{18}O_{bulk}$ excursion at ~216 mcd in Hole 1262C. According to the stratigraphic correlation in Appendix A, this oxygen isotope excursion should be placed approximately between 215.92 and 215.86 mcd in Hole 1262B. From this horizon onwards, the $\delta^{18}O_{bulk}$ values remain relatively high until the top of the Dan-C2 interval.

The carbonate content appears to oscillate parallel to $\delta^{13}C_{bulk}$ and $\delta^{18}O_{bulk}$, with marked drops at the K/Pg boundary (from 74.41 to 54.47%) and within the Dan-C2 interval (decreasing to approximately 20%; Figure 2c). We recognize a third drop in $CaCO_3$ content (from 56.13 to 23%) and $\delta^{18}O_{bulk}$ centered at 214.80 mcd, although this does not correlate with a CIE at Site 1262 (Figure 2a). A remarkable feature of the geochemical record of Site 1262 is the progressive decline in $\delta^{13}C_{bulk}$ values and carbonate content between the K/Pg boundary and the base of the Dan-C2 interval (Figure 2a, c).

The P/B ratio indicates a predominance of planktic foraminifera, with an average value of 93.4% across the studied interval (Figure 2d), which is a result expected for open marine conditions and abyssal depths. Nevertheless, the P/B ratio drops to 81.0% at the base of the Dan-C2 interval, rapidly recovering before the first CIE. The average value of the fragmentation index (FI) across the studied section is 9.14% (Figure 2e). Although this average FI value is low, it is noteworthy that, between 215.55 and 215.15 mcd, the FI reaches a mean value of 13.4%, the highest in the whole dataset (Appendix B). The FI value rises sporadically at 214.80 mcd, reaching an isolated

maximum of 15.0%. This rise in FI coincides with the decrease in $CaCO_3$ content (33.69 to 23%) and a drop in the $\delta^{18}O_{bulk}$ value (0.127 to -0.116‰) (Figure 2a), as well as a moderate decrease in the P/B ratio (94 to 90.25%) (Figure 2d).

4.3.2 Mercury chemostratigraphy

Hg concentrations in sediment measured at Site 1262 varied between 0.99 and 7.16 ppb, with an average of 3.19 ppb. Two intervals of increased Hg concentration were observed during the lower Danian (Figure 2g). The first interval, between 216.37 and 215.67 mcd, exhibits Hg concentrations ranging from 3.04 to 7.16 ppb (average = 4.72 ppb). In the second interval (215.02 to 214.86 mcd), the Hg concentrations show a mean value of 3.88 ppb (max. = 4.46 ppb). It is noteworthy that the Hg concentrations remain low in the interval assigned to the Dan-C2 event. Within the Dan-C2 interval, the Hg concentrations range between 2.41 and 1.41 ppb (averaging 2.66 ppb) (Figure 2g). The Hg/TOC ratio (Figure 2h) depicts trends similar to the values of the Hg concentrations. Two positive Hg/TOC anomalies can be recognized: (i) between 216.37 and 215.67 mcd (average = 39.58; max. = 63.80; min. = 26.09), and (ii) between 215.02 to 214.86 mcd (average = 31.51; max. = 39.98; min. = 27.66). Within the Dan-C2 interval, the Hg/TOC ratio remains low (Figure 2h), at between 20.11 and 12.02 (average = 16.98). At Site 1262 (Figure 2g, h), the base (215.02 mcd) of the second Hg and Hg/TOC anomaly (ii) is located slightly below the top of the CIE-2 of the Dan-C2 interval (215.17 mcd).

4.3.3 Planktic foraminiferal biostratigraphy

To study the planktic foraminiferal biostratigraphy and assemblages at Site 1262, we used a sampling resolution of between 3 and 5 cm. In the lower Danian of Site 1262, we recognized eighteen

planktic foraminiferal species, which were assigned to seven genera according to the taxonomy of Olsson et al. (1999) and Koutsoukos (2014) (Appendix B). Through the text and figures, moreover, we show the equivalence of this taxonomy to the more splitter-oriented taxonomy of Arenillas et al. (2021, and references therein). Most of the Danian species identified at Site 1262 are illustrated in Figures 3 and 4. Changes in the relative abundance of the Danian planktic foraminiferal species at Site 1262 are illustrated in Figure 5.

The highest occurrences (HOs) of typical Cretaceous species, assigned to the genera *Abathomphalus, Globotruncana, Globotruncanita, Contusotruncana*, *Heterohelix* s.l. (*Planoheterohelix* and *Laeviheterohelix*), *Pseudoguembelina*, *Pseudotextularia*, *Planoglobulina*, *Racemiguembelina*, *Rugoglobigerina*, *Muricohedbergella, Planohedbergella* and *Globigerinelloides*, were identified at 216.55 mcd, characterizing the uppermost part of the *Pseudoguembelina hariaensis* Zone *sensu* Nederbragt (1991). Some Cretaceous planktic foraminiferal specimens were observed in small proportions in the lowermost Danian samples and have been interpreted as reworked.

The lower Danian key-biohorizons recognized at Site 1262 were the lowest occurrence (LO) of *Parasubbotina pseudobulloides* at 216.32 mcd (Figure 5q, Appendix B), the HO of *Parvularugoglobigerina eugubina* s.l. (*Trochoguembelitria*, i.e., trochospiral guembelitriids with a pore-mounded, rugose wall) at 216.17 mcd (Figure 5g, Appendix B), and the LO of *Subbotina triloculinoides* at 215.82 mcd (Figure 5r, Appendix B). This stratigraphic interval corresponds to Subbiozones Dan3b, Dan4c and Dan4b of Arenillas et al. (2021), suggesting a small hiatus that affects the lowermost Danian, probably Biozone P0 (or Dan1) and the lower part of Biozone Pα (Dan2 and Dan3a). Nevertheless, this hiatus could be even smaller if there is condensed sedimentation between the uppermost Maastrichtian sample and the lowermost Danian sample studied here, where Chicxulub-impact-derived microtektites have been identified (see section 4.1).

4.3.4 Planktic foraminiferal assemblages after the K/Pg boundary

The composition and structure of planktic foraminiferal assemblages at Site 1262 were modified significantly during the earliest Danian (Figures 5 and 6). The relative abundance of microperforated species for the whole interval was 47.4%, with relative abundances ranging between 31.0% and 87.5% (Figure 6a). These species belong to the families Guembelitriidae (genera *Guembelitria* s.l. [*Chiloguembelitria*], *Globoconusa* and *Parvularugoglobigerina* s.l. [*Trochoguembelitria*]) and Chiloguembelinidae (genera *Woodringina* and *Chiloguembelina*) (Figure 5a to 5h). The relative abundance of normally perforated taxa for the whole interval was 52.5%, ranging between 12.5 and 69 %. Species with normal perforations belong to the families Eoglobigerinidae (genera *Eoglobigerina*, *Parasubbotina*, and *Subbotina*), Truncorotaloididae (genus *Praemurica*), and Globanomalidae (genus *Globanomalina*) (Figures 5i to 5r).

In the first 25 cm (up to 216.27 mcd) above the K/Pg boundary, an increase in species richness is observed (Figure 5s). The test size of the species identified in this stratigraphic interval (Figure 6 sample B) is considerably smaller than those in the Maastrichtian (Figure 6, sample A). This interval is characterized by increased abundances of microperforated species (Figure 6a), represented mainly by species of *Woodringina* and *Guembelitria* s.l. (*Chiloguembelitria*) (Figures 5a to 5c). The relative abundance of mixed-layer species, which include the microperforate species and those of *Praemurica*, is also very high (75.1%), whereas thermocline and sub-thermocline species are predominant above this interval (Figure 6b).

Guembelitria s.l. [*Chiloguembelitria*] increases in relative abundance between 215.92 and 215.12 mcd, with a bloom between 215.97 and 215.42 mcd. Therefore, at Site 1262, the bloom of triserial guembelitriids is first recorded 40 cm below the base of the Dan-C2 interval at 215.52 mcd (Figure 6), but the relative abundance of *Guembelitria* s.l. remains relatively high until almost the top of

the Dan-C2 interval at 215.17 mcd (Figure 6). There is also a small increase in the FAI between 216.27 and 215.62 mcd (1.37%), with two pronounced peaks at 216.1 (1.75%) and 215.8 mcd (2.6%) (Figure 6d). Although the relative abundances of aberrant specimens are overall low (~2%), they exceed background levels between 216.27 and 215.67 mcd. The specimens with aberrant tests mostly belong to the families Truncorotaloididae (genus *Praemurica*) and Eoglobigerinidae (genera *Subbotina*, *Parasubbotina* and *Eoglobigerina*). The abnormalities identified in these specimens were: (i) protuberant chambers (Figures 7a-b); (ii) additional chambers (Figures 7c-f); (iii) abnormal last chambers (Figures 7g-j); (iv) elongated last chambers (Figures 7k-l); (v) atypical test growth rates (Figures 7m-p). This increase in FAI is located below the double CIE interval that characterizes the Dan-C2 event.

Between the top of the Dan-C2 interval (215.17 mcd) and the C29r/C29n boundary (215 mcd) the average relative abundance of *Subbotina* increases up-core (from 5.97% to 15.35% in average). Similarly, *Chiloguembelina* increases its relative abundance from 6.62% to 10.77% (Figure 6e). This increase in the relative abundance of *Subbotina* and *Chiloguembelina* occurs parallel to an increase in the overall planktic foraminiferal test sizes (Figure 6, sample D). The relative abundance of these genera undergoes a sharp decrease at 214.80 mcd before returning to the overall increasing trend. This shift is possibly related to a drop in the carbonate saturation state and the consequent poorer preservation of the foraminiferal tests (Figure 6).

4.4 DISCUSSIONS

4.4.1 Age model and dating of planktic foraminiferal and isotope events

For the age model, we followed the astrochronological models reported by Dinarès-Turell et al. (2014) and Woelders et al. (2017) and the magnetostratigraphic study carried out by Bowles (2006)

and Westerhold et al. (2008) at Site 1262. We chose the 405-kyr eccentricity-based tuning (Batenburg et al. 2018) because it is the most reliable for ages older than ~52 Ma (Laskar et al. 2011). Based on this astronomical framework, the age of the K/Pg boundary was calibrated at 66 001 Ma and the C29r/C29n boundary at 65 700 Ma (Dinarès-Turell et al. 2014, Gradstein et al. 2020, see Appendix E). Previous astrochronologically calibrated age models for Site 1262 (e.g., Westerhold et al. 2008, Dinarès-Turell et al. 2014, Woelders et al. 2017) used a composite depth scale for Site 1262 following the splice-tie points established by Zachos et al. (2004), which allowed correlation and combination of the Holes A, B and C of Site 1262. As we have only studied Hole B, we show the stratigraphic correlation with Hole C (Appendix A and E). The age of each sample from Hole 1262B was estimated by interpolation between the astronomically calibrated tie-points (Appendix E). Moreover, this age model was revised by taking into account the recent astronomical calibration of LOs of the earliest Danian planktic foraminiferal species (Appendix E) by Gilabert et al. (2022) from the well-known Zumaia section (Spain), which was also part of the astrochronological framework of Dinarès-Turell et al. (2014). According to our new planktic foraminiferal biostratigraphic data from Site 1262 (Figure 5), the LOs of *Eoglobigerina* (base of Subbiozone Dan3b), *Parasubbotina*, *Globanomalina*, and *Praemurica* coincide with the lowermost Danian sample studied here (216.50 mcd), suggesting a small hiatus which possibly affects Biozone P0 (or Dan1) and the lower part of Biozone Pα (Dan2 and Dan3a). In fact, Biozone P0, according to the original definition of Smit (1982) at Caravaca (Spain; see Arenillas et al. 2021), has not been observed in any deep-sea drilling sites, including the most complete ones known to date, such as ODP Site 1049 (Blake Nose Plateau; Norris et al. 1999). Biozone P0 (or Dan1) has only been identified in the most continuous, complete and expanded lower Danian sections worldwide (Molina et al. 2009, Arenillas et al. 2021), such as El Kef and Aïn Settara (Tunisia), and Caravaca and Zumaia

(Spain), which were used to establish the highest-resolution planktic foraminiferal zonations for this interval (Smit 1982, Arenillas et al. 2004, 2021).

The lowermost Danian sample studied here (216.50 mcd), where the LO of *Eoglobigerina* is recognized, has been dated to 65 975 Ma following the astronomically refined timescale of Gilabert et al. (2022), suggesting that the small hiatus could comprise the first 26 kyr of the early Danian. Nonetheless, it should be borne in mind that this sample is 2 cm above the K/Pg boundary (216.52 mcd), and in this 2 cm thick basal Danian interval, Chicxulub-impact-derived microtektites and a remarkable negative $\delta^{13}C_{bulk}$ excursion have been reported (Zachos et al. 2004, Kroon et al. 2007, Woelders et al. 2017). Accordingly, Biozone P0 (Dan1) and/or the lower part of Biozone Pα (Dan2 and Dan3a) could perhaps be condensed and mixed in this basal Danian interval. For this reason, we conservatively suggest that the lowermost Danian hiatus spans roughly one precession cycle (~21 kyr). In addition, the lower Danian at Site 1262 is characterized by clays that are moderately bioturbated (Zachos et al. 2004), so the early Danian planktic foraminiferal assemblages could be mixed in the first lower Danian samples. This hypothesis could also explain why the latter contain a relatively high abundance of triserial guembelitriids, typical precisely of the absent Biozone P0 (or Dan1) and the lowermost part of Biozone Pα (or lower Dan2) (Smit 1982, Arenillas et al. 2000a,b, 2018, Gilabert et al. 2021, 2022). The recognition of this small hiatus at Site 1262 precludes analysis of the evolution of planktic foraminiferal assemblages immediately after the K/Pg boundary extinction event. Furthermore, it makes it necessary to modify slightly the age model proposed by Dinarès-Turell et al. (2014) at Site 1262 (Appendix E). However, the remaining stratigraphic record studied here, i.e., from the upper part of Biozone Pα (Dan3b) to Biozone P1b (Dan4b), seems to be continuous and complete at Site 1262, allowing the Dan-C2 event to be analyzed and its relationship with DT volcanism assessed.

According to the slightly readjusted age model for Site 1262, the key biohorizons, i.e., the LO of *P. pseudobulloides* (base of Dan4), the HO of *Trochoguembelitria* (= HO of *Parvularugoglobigerina eugubina* s.l. *sensu* Olsson et al. 1999; top of Pα), and the LO of *S. triloculinoides* (bases of Biozones P1b and Dan4b), are calibrated respectively at 65.943, 65.916 and 65.854 Ma, i.e., 58, 85 and 147 kyr after the K/Pg boundary (Figure 8). These dating are similar to those astronomically estimated by Gilabert et al. (2022), except for the LO of *S. triloculinoides*. The latter is a problematic datum because it has been placed in different stratigraphic positions: within magnetozone C29n well above Dan-C2 (Berggren and Pearson 2005, Quillévéré et al. 2008, Coccioni et al. 2010, Wade et al. 2011), at the base of C29n (Huber and Quillévéré 2005), and within magnetozone C29r (Arenillas et al. 2004, 2021), either within the Dan-C2 interval (Gilabert et al. 2021, 2022) or below the base of the Dan-C2 interval (Krahl et al. 2020, this study, Figure 5r). These data suggest that it is a diachronous biozone marker, at least in the South Atlantic Ocean. An alternative explanation may be the taxonomic difficulties in distinguishing *S. triloculinoides* and its ancestor *Eoglobigerina microcellulosa* (see Arenillas et al. 2021), whose interspecific boundaries may be very diffuse.

According to the age model explained above the base and top of the Dan-C2 interval are calibrated at 65.798 (215.52 mcd) and 65.714 Ma (215.07 mcd), i.e., 203 and 287 kyr after the K/Pg boundary (Figure 8a, Appendix D), which is compatible with the ages given by other authors (Barnet et al. 2019, Gilabert et al. 2022). The base and top of the CIE-1 of Dan-C2 are calibrated at 65.789 (215.47 mcd) and 65.772 Ma (215.37 mcd), i.e., 212 and 229 kyr after the K/Pg boundary. Finally, the base and top of the CIE-2 of Dan-C2 are calibrated at 65.753 (215.27 mcd) and 65.734 Ma (215.17 mcd), i.e., 248 and 267 kyr after the K/Pg boundary.

4.4.2 Evaluation of the carbonate preservation and Hg concentrations at Site 1262

The decreased carbonate content of the deep ocean sediments deposited during the negative CIEs of the Paleogene are usually attributed to the lysocline and carbonate compensation depth (CCD) shoaling during hyperthermal events (e.g., Leon-Rodriguez and Dickens 2010, Luciani et al. 2010, Coccioni et al. 2012, 2019, Galazzo et al. 2013, D'Onofrio et al. 2016, Deprez et al. 2017, Intxauspe-Zubiaurre et al. 2018). At Site 1262, the P/B ratio dropped, and the FI values increased moderately during the Dan-C2 event (Figure 2), suggesting a change in the carbonate saturation state that could be related to a transient increase in ocean acidification, similar to what was observed at DSDP Site 516F (Rio Grande Rise, South Atlantic; Krahl et al. 2020). According to Kucera et al. (1997), the FI values associated with strong carbonate dissolution for the Maastrichtian of the Walvis Ridge and Rio Grande Rise are usually > 40%. This result was obtained by using more lenient criteria for calculating FI than this study, considering only those specimens that preserve less than half of their test as fragments. Nevertheless, based on stricter criteria (see above), we observe that the FI values at Site 1262 oscillate around 16% during Dan-C2 (Figure 2, Appendix B), similar to the low FI values reported for the Dan-C2 interval at Caravaca (Gilabert et al. 2021). We observed dissolution features in planktic foraminiferal tests, such as abrasion marks, broken and/or isolated chambers, and corroded walls (Figure 6, sample C), although they were not abundant. We thus suggest that carbonate dissolution was low to moderate within the Danian interval at Site 1262. Our interpretation is compatible with those based on Fe enrichments (Barnet et al. 2019) and well-preserved calcareous benthic foraminiferal assemblages, which were not significantly affected by the Dan-C2 event (Arreguín-Rodríguez et al. 2021), suggesting deposition above the CCD.

Mercury concentrations and TOC values at Site 1262 show weak negative correlation (r = -0.194; Figure 9a). The fact that there is no covariation between Hg and TOC suggests that TOC enrichments are not solely responsible for Hg accumulation in the section, supporting a volcanic Hg source. TOC values <0.2%, such as those at Site 1262 (Figure 2, Appendix D), can also generate artificial Hg/TOC peaks (Grasby et al. 2019). However, we consider this possibility unlikely due to the strong resemblance between the records of the Hg concentration and the Hg/TOC ratio (Figure 2). In fact, the Hg concentration can be controlled by redox conditions (Shen et al. 2019). We used the Mn concentrations as a proxy for redox conditions (e.g., Yao et al. 2021). These exhibit a low positive correlation (r = 0.464; Figure 9c) with Hg concentrations at Site 1262, suggesting that seafloor oxygenation had no significant influence on Hg enrichments.

The Hg concentration in sediments can be also affected by diagenesis. We used $\delta^{18}O_{bulk}$ values as indicators of diagenetic intensity, since these can be significantly altered by changes in carbonate precipitation (Watkins et al. 2014) or during extensive carbonate diagenesis (Swart 2015). At Site 1262B, no significant covariation was observed for Hg content and $\delta^{18}O_{bulk}$ (r = 0.435; Figure 9b), suggesting that none of these diagenetic processes was responsible for the Hg enrichments. We thus suggest that the Hg accumulation in the early Danian sediments at Site 1262 was mainly controlled by the global intensity of volcanic emissions.

4.4.3 Stepwise recovery of early Danian planktic foraminiferal assemblages

The lowermost planktic foraminiferal assemblages identified at Site 1262, recorded within the first 25 cm above the K/Pg boundary (upper part of Biozone Pα, or Subbiozone Dan3b), were dominated by microperforated genera such as *Woodringina* (Figures 5a-b), *Guembelitria* s.l. (Figure

5c), and *Parvularugoglobigerina* s.l. (Figures 5g-h), which inhabited the mixed-layer in the surface ocean (D'Hondt and Zachos 1993, Olsson et al., 1999, Lowery et al. 2021). These assemblages suggest that eutrophic conditions occurred in the upper water column during this time interval, in accordance with observations from the Chicxulub impact site (Jones et al. 2019; Lowery et al. 2021). The dominance of mixed-layer planktic foraminiferal taxa after the K/Pg boundary was a consequence of global collapse of the marine biological pump and its subsequent restoration (Birch et al. 2016). In the earliest Danian, less export productivity and thus enhanced remineralization of organic matter in the surface ocean would have favored the proliferation of mixed-layer taxa (Jones et al. 2019).

After this first interval, no significant variations in species richness were observed at Site 1262, implying that the Dan-C2 event and the DT volcanism had a low impact on planktic foraminiferal species richness (Figure 5). A rapid increase in the abundance of deep-dwelling taxa (thermocline dwellers as *Eoglobigerina*, *Chiloguembelina*, *Globanomalina* and sub-thermocline dwellers as *Parasubbotina pseudobulloides*; Aze et al. 2011, Appendix C), occurred ~65.93 Ma (216.25 mcd), i.e., ~70 kyr after the K/Pg boundary (Figure 8f). This suggests increased stratification in the water column from that time on, which was not significantly interrupted by the Dan-C2 event or by the DT volcanic activity. The relative abundance of *Subbotina* and *Chiloguembelina* increased ~272 kyr after the K/Pg boundary (~65.729 Ma; 215.15 mcd), rising from 5.97 to 15.35% in *Subbotina* and from 6.62 to 10.77% in *Chiloguembelina* (Figure 6). Within the deep-dwellers (Figure 8f), *Chiloguembelina* and *Subbotina* (Berggren and Norris 1997, Coxall et al. 2000, Luciani et al. 2020) increased their relative abundance, suggesting a recovery of the pelagic ecosystem towards the end of the Dan-C2 event with increased stratification of the water column (Gilabert et al. 2021, Lowery et al. 2021). According to Birch et al. (2016, 2021), the first phase of partial recovery of

the $\delta^{13}C$ gradient between the surface and deep ocean occurred about ~270 kyr after the K/Pg boundary (~215.15 mcd in Site 1262). This recovery phase is almost coeval with the increases in abundance of *Subbotina* and *Chiloguembelina*, as well as with an increase in the overall test sizes of planktic foraminifera at Site 1262 (Figure 6, sample D).

4.4.4 Links between the Dan-C2 event and Deccan Traps (DT) volcanic activity?

The mercury chemostratigraphy at Site 1262 allows us to identify two intervals during the early Danian with high Hg concentrations that can be linked to the increased DT volcanic activity. The first Hg-rich interval is dated to between 65.952 (216.375 mcd) and 65.825 Ma (215.675 mcd), i.e., between 49 and 176 kyr after the K/Pg boundary (Figure 8c, Appendix D). Both the onset and the end of this Hg-rich interval preceded the onset of the Dan-C2 event (65.798 Ma) by about 154 and 27 kyr respectively. These observations suggest that the stressing paleoenvironmental conditions in the upper water column linked to DT volcanism ended shortly before the onset of the Dan-C2 event. In fact, considering the ages and the uncertainty of the radiometric dating (±64 kyr, U-Pb; ±213 kyr, $^{40}Ar/^{39}Ar$) calculated by Schoene et al. (2021), the first Hg-rich interval at Site 1262 correlates well with the emplacement of the Ambenali Fm. (~65.95 Ma, Figure 8). Since this Hg-rich interval does not coincide with the Dan-C2 interval at Site 1262, we can conclude that there was no direct temporal link between the Dan-C2 event and the emplacement of the Ambenali Fm., as Gilabert et al. (2022) already proposed.

The second Hg-rich interval began almost at the C29r/C29n boundary (215 mcd, 65.700 Ma) (Figures 2 and 8), and specifically occurred between 65.705 Ma (215.02 mcd) and 65.653 Ma (214.86 mcd), i.e., between 296 and 348 kyr after the K/Pg boundary (Figure 8c, Appendix D). This second

Hg-rich interval is notably shorter (52 kyr) than the first one (127 kyr), and its average Hg/TOC value is appreciably lower (31.5) than that of the first one (43). Although it could also be genetically related to higher volcanic activity in the DT, this second Hg-rich interval had a very weak influence on the climate, since no relevant isotopic event is associated with it (Figure 8). Moreover, it did not influence the ocean environments either, since no relevant turnovers in the planktic foraminifera assemblages are observed (Figure 5). The DT volcanic episode closest to the second Hg-rich interval is the one that produced the Mahabaleshwar Fm., whose emplacement began ~65.62 Ma (Schoene et al. 2019, Sprain et al. 2019), i.e., 381 kyr after the K/Pg boundary. The estimated difference of ~30 kyr between the end of the second Hg-rich interval and the onset of the emplacement of the Mahabaleshwar Fm. prevents us from establishing a robust link between the two episodes. Nevertheless, if the hole studied (Hole 1262B) had a small hiatus affecting the lowermost part of the magnetozone C29n, the second Hg-rich interval would consequently be more modern and could be coeval to emplacement of the Mahabaleshwar Fm. Another possible explanation could be terminal reactivation of the Ambenali eruptive episode. The reactivation of a DT volcanic formation is more difficult to explain according to the mega-pulse eruptive model of Schoene et al. (2019). Instead, this feature could be more consistent with the quasi-continuous eruption model of Sprain et al. (2019).

4.4.5 Environmental disruptions linked to the volcanic activity

Recent studies have explored a possible relationship between increased abundances of aberrant planktic foraminiferal specimens (increased FAI) with a proliferation of triserial guembelitriids in the early Danian and intervals of higher volcanic activity, which can tentatively be related to enrichment in toxic heavy metals such as Hg (e.g., Arenillas et al. 2018, Gilabert et al. 2021). Our

multiproxy approach at Site 1262 lends further support to the idea that DT volcanic emissions, recorded as Hg-rich intervals, are one of the main environmental stress factors that potentially caused disturbances in the planktic foraminiferal assemblages during the early Danian.

In accordance with the readjusted age model for Site 1262 proposed here, increased relative abundances of aberrant planktic foraminiferal specimens occurred at Site 1262 between ~65.934 (216.27 mcd) and ~65.817 Ma (215.62 mcd), i.e., between ~67 and ~184 kyr after the K/Pg boundary (Figure 8d), coinciding approximately with the first Hg-rich interval identified. At Site 1262, species with a higher abundance in aberrant tests belong to thermocline and sub-thermocline dwellers including *Eoglobigerina*, *Parasubbotina*, and *Subbotina* (Figure 7), which is unlike other localities at or near continental margins, such as Caravaca and Zumaia (Spain) or El Kef (Tunisia), where the aberrant specimens are more common among mixed-layer dweller *Guembelitria* s.l. and FAI values are much more anomalous, around 10 times larger (Arenillas et al. 2018, Gilabert et al. 2021). Several environmental stressors can potentially cause morphological abnormalities in planktic foraminiferal tests, including increases in temperature, eutrophy and/or acidity of ocean waters (Mancin and Darling 2015, Arenillas et al. 2018). Among recent foraminifera, contamination by heavy metals and trace elements is considered one of the most likely causes for such abnormalities (e.g., Coccioni et al. 2009, Frontalini et al. 2009). Since no relevant changes in temperature, acidity, and nutrient supply are observed across this interval (Figures 6 and 8), we suggest that the main cause of this increase in aberrant specimens was contamination by heavy metals from the DT volcanic emissions. The inefficient biological pump during this interval could contribute to extend over time, on a ~10^4 years scale, the recycling and remineralization of heavy metals and other trace elements at the ocean surface, in a mechanism similar to that proposed by Jiang et al.

(2010) to explain why ejecta metals remained dissolved in the surface ocean for thousands or tens of thousands of years after the Chicxulub impact at the K/Pg boundary.

We have also identified a bloom of triserial guembelitriids (Figure 8e), preceding the Dan-C2 event, between ~65.872 (215.92 mcd) and ~65.781 Ma (215.42 mcd), i.e., between ~129 and 220 kyr after the K/Pg boundary (Figures 6c and 8e). Similar blooms of triserial guembelitriids have been reported before the Dan-C2 event at Contessa Highway (Coccioni et al. 2010), DSDP Site 577 (Pacific Ocean; Smit and Romein 1985), Agost (Spain; Canudo et al. 1991), Caravaca and Zumaia (Gilabert et al. 2021, 2022), ODP Site 528 (South Atlantic Ocean; D'Hondt and Keller 1991), and El Kef (Arenillas et al. 2018). Triserial guembelitriids are considered opportunists that inhabited surface waters and thrived under high-stress environmental conditions, proliferating on continental margins and near volcanic areas where nutrients are abundant, whether they are of upwelling, continental or volcanic origin (Kroon and Nederbragt 1990, Pardo and Keller 2008, Keller and Pardo 2004). Consequently, a remarkable environmental change at the ocean surface of the South Atlantic Ocean is required to explain the proliferation of guembelitriids in an oceanic pelagic environment away from continental margins as Site 1262 (Figure 8). However, at Site 1262, the triserial guembelitriid bloom started (~62 kyr) and ended (~36 kyr) later than the increased FAI interval (Figure 8d), unlike what is recorded in pelagic sections placed at or near the continental margins (e.g. Caravaca, Zumaia and El Kef) where both intervals coincide (Arenillas et al. 2018, Gilabert et al. 2021, 2022). The cause-effect relationship between the DT volcanism, marked by the Hg-rich and increased FAI interval, and the guembelitriid proliferation is therefore difficult to establish at Site 1262, so a different mechanism or a different environmental stressor is required.

Remarkable changes in benthic foraminiferal assemblages at Site 1262 were reported before the Dan-C2 interval (Arreguín-Rodríguez et al. 2021), approximately coinciding with the triserial guembelitriid bloom. The authors reported that the predominant benthic foraminiferal taxa during this interval were indicative of environmental instability and an enhanced food supply to seafloor. Similarly, Bralower et al. (2020) also identified changes in the calcareous nannoplankton assemblages, such as the proliferation of the calcareous dinocyst *Cervisella*, which, as *Guembelitria* s.l., is an opportunistic taxon that preferably inhabited continental margins with high nutrient availability. At Site 1262, the triserial guembelitriid bloom coincides with a high abundance of thermocline and sub-thermocline planktic foraminiferal taxa, such as *Eoglobigerina*, *Parasubbotina*, and *Subbotina* (Figure 6b), and of the nannofossil *Braarudosphaera* (Bralower et al. 2020), indicating that the bloom occurred during a time interval with a well-stratified water column. Consequently, the environmental change that caused the proliferation of guembelitriids at Site 1262 seems to have affected only the ocean surface.

Bralower et al. (2020) reported deposition of microcrystalline calcite structures, at Site 1262 and at many other localities, evidencing a second global acme of microbial phytoplankton (probably cyanobacteria) after the one that occurred immediately after the K/Pg boundary event. At Site 1262, this second microbial bloom is recorded between ~65.93 (216.28 mcd) and ~65.90 Ma (216.08 mcd), i.e., between 71 and 101 kyr after the K/Pg boundary. Kulal et al. (2020), among others, reported that the microbial activity can remove toxic heavy metals from water. We propose consequently that the bloom of microbial activity helped remove Hg and other toxics from the surface ocean, explaining why the malformations primarily affected thermocline and sub-thermocline dwellers at Site 1262. In addition, the maximum in microbial activity occurred towards the end of the first Hg-rich interval and the beginning of the bloom of opportunist planktic taxa, such

as *Cervisella* and *Guembelitria* s.l. This microbial maximum could not only help remove toxic elements but also increase the nutrient availability in the surface ocean, favoring the proliferation of nannoplankton and planktic foraminiferal opportunistic taxa (Bralower et at. 2020; this study).

The nutrient availability in the surface ocean could also be higher due to the inefficient biological pump (Henehan et al. 2019). The very low transfer efficiency (quantity of organic matter that sinks below 1000 m; Henson et al. 2012, Lowery et al. 2021) allowed the recycling and remineralization of the nutrients to continue at the ocean surface. The low transfer efficiency at Site 1262 would explain why the $\Delta^{13}C$ gradient in the water column is locally low, and why the benthic foraminiferal assemblages indicate low food supply to the sea floor before microbial and triserial guembelitriid blooms (Arreguín-Rodríguez et al. 2021).

We suggest, therefore that the emplacement of Ambenali Fm. could be the cause of the increase in Hg and aberrant specimens, whereas the triserial guembelitriid bloom seems to be more closely linked to an increase in microbial activity that provided additional food supply to the ocean surface. If the extra nutrient source that triggered the increased microbial activity was also from the DT volcanism, the weak biological pump during all this interval could be the reason that, in oceanic pelagic environments such as that of Site 1262, there was a lag between the increased FAI interval and the triserial guembelitriid bloom. Unlike what occurs in localities placed at or near the continental margins, the inefficient biological pump at Site 1262 could lead to sustained recycling and remineralization of organic matter in the surface ocean, causing the microbial bloom to occur ~20 kyr later than the beginning of increased DT volcanic activity. The microbial activity increased only when the volcanic nutrient supply was a little higher, and the triserial guembelitriid bloom lasted for 36 kyr after the end of this DT eruptive phase, because the biological pump, although improved, was still inefficient, allowing nutrients to be recycled and to remain in the surface ocean.

Another environmental factor that could have favored the triserial guembelitriid bloom was the increase in ocean surface temperatures at ~65.87 Ma (215.92 mcd), i.e., 131 kyr after the K/Pg boundary and 72 kyr before the beginning of Dan-C2 event, as suggested by the $\delta^{18}O$ record at Site 1262 (Figure 2 and Figure 8b; and Appendix A). In the early Danian, the changes in the ocean surface temperature seem to have been mainly linked to orbital forcing, especially modulated by 405-kyr and 100-kyr eccentricity (Gilabert et al. 2022, and references herein). At Site 1262 (Figure 8), the earliest part of triserial guembelitriid bloom (between ~131 and 176 kyr after the K/Pg boundary) seems to coincide with an interval in which the DT volcanic activity is still high and the ocean surface temperature increased. Subsequently, the relative abundance in triserial guembelitriids decreased (Figure 8e), but remained high until almost the end of the Dan-C2 interval, suggesting that the main environmental stressor in the surface ocean was temperature.

Based on the earliest Danian planktic foraminiferal assemblages from Site 1262, we suggest that unstable conditions in the water column prior to the Dan-C2 event were probably associated with the emplacement of the Ambenali Fm., as Gilabert et al. (2021, 2022) have previously proposed. As mentioned above, the onset of the emplacement of the Ambenali Fm. occurred at ~65.95 Ma (Schoene et al. 2019, Sprain et al. 2019), approximately 50 kyr after the K/Pg boundary, and it lasted for the next ~100 kyr according to Schoene et al. (2019, 2021) or ~330 kyr according to Sprain et al. (2019). Our results show a better correspondence with the mega-pulse model of Schoene et al. (2019) than with the quasi-continuous model of Sprain et al. (2019), since the proxies of increased volcanic activity (Hg and Hg/TOC anomalies) and the greater environmental stress (increased FAI and triserial guembelitriid bloom) seem to be coeval with a shorter emplacement time of the Ambenali Fm. (Figures 6 and 8). Except maybe for the increased microbial activity

and triserial guembelitriid bloom, the paleobiological response to the emplacement of the Ambelani Fm. was apparently quite weak (Figures 6 and 8). It was a response similar to those reported for the Maastrichtian DT volcanic phases, such as the one associated to the emplacement of the Kalsubai subgroup between ~66.30 and 66.10 Ma (Schoene et al. 2019, Sprain et al. 2019) that was one of the triggers of the Late Maastrichtian Warming Event (Barnet et al. 2018, Gilabert et al. 2021b, 2022).

4.5 CONCLUSIONS

Detailed analyses of the planktic foraminiferal assemblages, including the foraminiferal abnormality index (FAI), the fragmentation index (FI), and the P/B ratio, and of several geochemical proxies, including $\delta^{13}C$, $\delta^{18}O$, $CaCO_3$%, Mn, Hg, and the Hg/TOC ratio, were carried out at Site 1262 (South Atlantic) for the first ~400 kyr of the early Danian. This multiproxy study allowed us to recognize the most relevant changes in climate, ocean surface environment, and water column structure at Site 1262 during this interval. On the basis of the $\delta^{13}C$ and $\delta^{18}O$ data (reported here and in previous works), the paleoclimatic Dan-C2 event is recognized between ~65.80 and ~65.71 Ma.

Two intervals with Hg and Hg/TOC anomalies are identified at Site 1262 and interpreted as evidence of higher volcanic activity linked to the Deccan Traps (DT). The first Hg-rich interval, which was the longer and greater Hg anomaly, occurred between ~65.95 and 65.82 Ma, preceding the onset of the Dan-C2 event by ~40 kyr. The second Hg-rich interval, which was shorter and smaller, occurred between ~65.70 and 65.65 Ma, beginning near the end of Dan-C2 and ending notably later. In light of the age model here reported for Site 1262 and the latest radiometric dating of the

DT volcanic formations, we can conclude that there was no direct temporal link between the Dan-C2 event and the massive DT volcanism, whereas the first Hg-rich interval seems strongly linked to the emplacement of the Ambenali Formation of the Deccan Traps. The origin of the second Hg-rich interval is still unclear, but could be related to the emplacement of the Mahabaleshwar Fm.

Higher values in aberrant planktic foraminiferal abundance (FAI) are documented only during the first Hg-rich interval, suggesting an increased contamination by heavy metal poisoning from the DT volcanic emissions, specifically during the emplacement of the Ambenali Fm. In addition, a triserial guembelitriid bloom occurred between ~65.87 and ~65.78 Ma, also preceding the Dan-C2 event but lagging with respect to the interval of high Hg content and increased FAI. The lag at Site 1262 between both intervals can be explain by a combination of several environmental factors, such as the inefficient biological pump, the increase in temperatures, and the increase in the microbial activity and food supply to the ocean surface, the latter perhaps still linked to the terminal volcanic emissions linked to the Ambelani Fm. During the Dan-C2 event, environmental stress seems to have been considerably reduced, although the continuing high abundance of triserial guembelitriids denotes environmental instability, perhaps related to higher ocean surface temperatures. From the Dan-C2 event to the end of the interval studied, no evidence of environmental stress is recognized. Conversely, we observed a progressive increase in the relative abundance of species that inhabited the thermocline from the middle part of Dan-C2, suggesting a progressive stratification and stabilization of the water column. All these evidences suggest that, although volcanism may have had an impact on planktic foraminiferal assemblages in the early Danian through metal contamination, marine ecosystems likely became progressively more stable and resistant to changes in volcanic emissions and the carbon cycle.

Acknowledgements

We thank the editor, Joerg Pross, and the three reviewers, Chris Lowery, Andy Fraass and an anonymous reviewer, for thoughtful and constructive reviews which improved the manuscript. We deeply thank Sietske Batenburg for support. We are grateful to the International Ocean Discovery Program (IODP) for providing the studied samples, and to Capes for providing the postgraduate grant for G. Krahl and M.H.H. Bom. This research is part of the grants PGC2018-093890-B-I00 funded by MCIN/AEI/10.13039/501100011033 and by ERDF A way of making Europe, and DGA group E33_20R funded by the Aragonese Government and by ERDF A way of making Europe. Vicente Gilabert acknowledges support from Ministerio de Universidades (MIU) and European Union (Margarita Salas post-doctoral grant) funded by European Union-NextGeneration EU. We thank R. Glasgow for improving the English text.

4.6 REFERENCES

Alegret, L., Thomas, E., Lohmann, K.C. 2012. End-Cretaceous marine mass extinction not caused by productivity collapse. Proceedings of the National Academy of Sciences 109 (3), 728–732. https://doi.org/10.1073/pnas.1110601109

Alvarez, L.W., Alvarez, W., Asaro, F., Michel, H.V., 1980. Extraterrestrial cause for the Cretaceous-Tertiary extinction. Science 208, 1095–1108. https://doi.org/10.1126/science.208.4448.1095.

Arenillas, I., Arz, J.A., 2017. Benthic origin and earliest evolution of the first planktonic foraminifera after the Cretaceous/Paleogene boundary mass extinction. Historical Biology 29(1), 17–24. https://doi.org/10.1080/08912963.2015.1119133

Arenillas, I., Arz, J.A., Gilabert, V., 2018. Blooms of aberrant planktic foraminifera across the K/Pg boundary in the Western Tethys: causes and evolutionary implications. Paleobiology 44(3), 1–17. https://doi.org/10.1017/pab.2018.16.

Arenillas, I., Arz, J.A., Molina, E., Dupuis, C., 2000a. The Cretaceous/Paleogene (K/P) boundary at Aïn Settara, Tunisia: sudden catastrophic mass extinction in planktic foraminifera. Journal of Foraminiferal Research 30(3), 202–218. https://doi.org/10.2113/0300202

Arenillas, I., Arz, J.A., Molina, E., Dupuis, C., 2000b. An independent test of planktic foraminiferal turnover across the Cretaceous/Paleogene (K/P) boundary at El Kef, Tunisia: Catastrophic mass extinction and possible survivorship. Micropaleontology 46(1), 31–49.

Arenillas, I., Gilabert, V., Arz, J.A., 2021. New biochronological scales of planktic foraminifera for the early Danian based on high-resolution biostratigraphy. Geosciences 11(479), 1–26. https://doi.org/10.3390/geosciences11110479

Arenillas, I., Arz, J.A., Metsana-Oussaid, F., Gilabert, V., Belhai, D., 2022. Hypothesis testing on the planktic foraminiferal survival model after the KPB extinction: evidence from Tunisia and Algeria. Fossil Record 25(1), 43–63. https://doi.org/10.3897/fr.25.79958

Arreguín-Rodriguez, G.J., Barnet, J.S.K., Leng, M.J., Littler, K., Kroon, D., Schmidt, D.N., Thomas, E., Alegret, L., 2021. Benthic foraminiferal turnover across the Dan-C2 event in the eastern South Atlantic Ocean (ODP Site 1262). Palaeogeography, Palaeoclimatology, Palaeoecology (572), 1–15. https://doi.org/10.1016/j.palaeo.2021.110410

Aze, T., Ezard, T.H.G., Purvis, A., Coxall, H.K., Stewart, R.M., Wade, B.S., Pearson, P.N., 2011. A phylogeny of Cenozoic macroperforate planktonic foraminifera from fossil data. Biological Reviews (86), 900 – 927. https://doi.org/10.1111/j.1469185X.2011.00178.x

Arz, J. A., Arenillas, I., Grajales, J. M., Liesa, C. L., Soria, A. R., Rojas, R., Calmus. T., Gilabert, V., 2022. No evidence of multiple impact scenario across the Cretaceous/Paleogene boundary based on planktic foraminiferal biochronology. In: C. Koeberl, P. Claeys & S. Montanari (Eds.), From the Guajira desert to the Apennines, and from Mediterranean microplates to the Mexican killer asteroid: Honoring the Career of Walter Alvarez, GSA Special paper 557, in press. https://doi.org/10.1130/2022.2557(20)

Barnet, J.S.K., Littler, K., Kroon, D., Leng, M. J., Westerhold, T., Rohl, U., Zachos, J.C., 2017. A new high-resolution chronology for the late Maastrichtian warming event: Establishing robust temporal links with the onset of Deccan volcanism. Geology 46(2), 147–150. https://doi.org/10.1130/G39771.1

Barnet, J.S.K., Littler, K., Westerhold, T., Kroon, D., Leng, M.J., Bailey, I., Rohl, U., Zachos, J.C., 2019. A high-fidelity benthic stable isotope record of late Cretaceous early Eocene climate change and carbon-cycling. Paleoceanography and Paleoclimatology 34, 672–691. https://doi.org/10.1029/2019PA003556

Batenburg, S.J., Friedrich, O., Moriya, K., Voigt, S., Cournède, C., Moebius, I., Blum, P., Bornemann, A., Fiebig, J., Hasegawa, T., Hull, P.M., Norris, R.D., Röhl, U., Sexton, P.F., Westerhold, T., Wilson, P.A., IODP Expedition Scientists, 2018. Late Maastrichtian carbon isotope stratigraphy and cyclostratigraphy of the Newfoundland Margin (Site U1403, IODP Leg 342). Newsletters on Stratigraphy 51 (2), 245e260. https://doi.org/10.1127/nos/2017/0398.

Berger, W.H., Diester-Haass, L., 1988. Paleoproductivity: The benthic/planktonic ratio in foraminifera as a productivity index. Marine Geology 81, 15–25. https://doi.org/10.1016/0025-3227(88)90014-X

Berggren, W.A., Norris, R.D., 1997. Biostratigraphy, phylogeny and systematics of Paleocene trochospiral planktic foraminifera. Micropaleontology 43, 1–116. https://doi.org/10.2307/1485988

Berggren, W.A., Pearson, P.N., 2005. A revised tropical and subtropical Paleogene planktonic foraminiferal zonation. Journal of Foraminiferal Research 35, 279–298. https://doi.org/10.2113/35.4.279

Birch, H.S., Coxall, H.K., Pearson, P.N., Kroon, D., Schmidt, D.N., 2016. Partial collapse of the marine carbon pump after the Cretaceous-Paleogene boundary. Geology 44(4), 287–290. https://doi.org/10.1130/G37581.1

Birch, H., Schmidt, D.N., Coxall, H.K., Kroon, D., Ridgwell, A., 2021. Ecosystem function after the K/Pg extinction: decoupling of marine carbon pump and diversity. Proceeding of The Royal Society Bulletin 288. 20210863. https://doi.org/10.1098/rspb.2021.0863

Boersma, A., Premoli Silva, I., 1983. Paleocene planktonic foraminiferal biogeography and the paleooceanography of the Atlantic Ocean. Micropaleontology 29. 355–381.

Bornemann, A., Jehle, S., Lägel, F., Deprez, A., Petrizzo, M.R., Speijer, R.P., 2021. Planktic foraminiferal response to an early Paleocene transient warming event and biostratigraphic implications. International Journal of Earth Sciences 110, 583–594. https://doi:10.1007/s00531-020-01972-z

Bralower, T.J., Cosmidis, J., Heaney, P. J., Kump, L.R., Morgan, J.V., Harper, D.T., Lyons, S.L., Freeman, K.H., Grice, K., Wendler, J.E., Zachos, J.C., Artemieva, N., Chen, S.A., Gulick, S.P.S., House, C.H., Jones, H.L., Lowery, C.M., Nims, C., Schaefer, B., Thomas, E., Vajda, V. 2020.

Origin of a global carbonate layer deposited in the aftermath of the Cretaceous-Paleogene boundary impact. Earth and Planetary Science Letters 548, 116476. https://doi.org/10.1016/j.epsl.2020.116476

Bowles, J., 2006. Data report: revised magnetostratigraphy and magnetic mineralogy of sediments from Walvis Ridge, Leg 208. In: Kroon, D., Zachos, J.C., Richter, C. (Eds.), Proc. ODP, Sci. Results, vol.208. Ocean Drilling Program, College Station, TX, pp.1–24.

Canudo, J.I., Keller, G., Molina, E., 1991. Cretaceous/Tertiary boundary extinction pattern and faunal turnover at Agost and Caravaca, S.E. Spain. Marine Micropeleontology 17, 319–341. https://doi:10.1016/0377-8398(91)90019-3.

Coccioni, R., Frontalini, F., Marsili, A., Mana, D., 2009. Benthic foraminifera and trace element distribution: a case-study from the heavily polluted lagoon of Venice (Italy). Marine Pollution Bulletin 59, 257–267. https://doi.org/10.1016/j.marpolbul.2009.08.009

Coccioni, R., Frontalini, F., Bancalà, G., Fornaciari, E., Jovane, L., Sprovieri, M., 2010. The Dan-C2 hyperthermal event at Gubbio (Italy): Global implications, environmental effects, and cause(s). Earth and Planetary Science Letters 297(1-2), 298–305. https://doi:10.1016/j.epsl.2010.06.031

Coccioni, R., Bancalà, G., Catanzarit, R., Fornaciari, E., Frontalini, F., Giusberti, L., Jovane, L., Luciani, V., Savian, J., Sprovieri, M., 2012. An integrated stratigraphic record of the Palaeocene–lower Eocene at Gubbio (Italy): new insights into the early Palaeogene hyperthermals and carbon isotope excursions. Terra Nova 24, 380–386. https://doi.org/10.1111/j.1365-3121.2012.01076.x.

Coccioni, R., Frontalini, F., Catanzariti, R., Jovane, L., Rodelli, D., Rodrigues, I.M.M., Savian, J.F., Giorgioni, M., Galbrun, B., 2019. Paleoenvironmental signature of the Selandian-Thanetian Transition Event (STTE) and Early Late Paleocene Event (ELPE) in the Contessa Road section

(western Neo-Tethys). Palaeogeography, Palaeoclimatology, Palaeoecology 523(1), 62–77. https://doi.org/10.1016/j.palaeo.2019.03.023

Coxall, H., Pearson, P.N., Shacketon, N.J., Hall, M., 2000. Hantkeninid depth evolution; an evolving life strategy in a changing ocean. Geology 28, 87–90. https://doi.org/10.1130/0091-7613(2000)28<87:HDAAEL>2.0.CO;2

Coxall, H., D'Hondt, S., Zachos, J., 2006. Pelagic evolution and environmental recovery after the Cretaceous-Paleogene mass extinction. Geology 34, 297–300. https://doi:10.1130/G21702.1.

Deprez, A., Jehle, S., Bornemann, A., Speijer, R.P., 2017. Pronounced biotic and environmental change across the latest Danian warming event (LDE) at Shatsky Rise, Pacific Ocean (ODP Site 1210). Marine Micropaleontology 137, 31–45. https://doi.org/10.1016/j.marmicro.2017.10.001

Dinarès-Turell, J., Westerhold, T., Pujalte, V., Röhl, U., Kroon, D. (2014). Astronomical calibration of the Danian stage (early Paleocene) revisited: Settling chronologies of sedimentary records across the Atlantic and Pacific Oceans. Earth and Planetary Science Letters 405, 119–131. https://doi:10.1016/j.epsl.2014.08.027

D'Hondt, J., 2005. Consequences of the Cretaceous/Paleogene Mass Extinction for Marine Ecosystems. Annual Review of Ecology, Evolution, and Systematics 36, 295–317. https://doi.org/10.1146/annurev.ecolsys.35.021103.105715

D'Hondt, S., Keller, G., 1991. Some patterns of planktic foraminiferal assemblage turnover at the Cretaceous-Tertiary boundary. Marine Micropaleontology 17(1-2), 77–118. https://doi.org/10.1016/0377-8398(91)90024-Z

D'Hondt, S., Zachos, J.C., 1993. On Stable Isotopic Variation and Earliest Paleocene Planktonic Foraminifera. Paleoceanography 8, 527–547. https:// doi.org/10.1029/93PA00952

D'Onofrio, R., Luciani, V., Fornaciari, E., Giusberti, L., Galazzo, F.B., Dallanave, E., Westerhold, T., Sprovieri, M., Telch, S., 2016. Environmental perturbation at the early Eocene ETM2, H2, and I1 events as inferred by Tethian calcareous plankton (Terche section, northeastern Italy). Paleoceanography 31, 1225–1247. https://doi:10.1002/2016PA002940

Font, E., Adatte, T., Sial, A.N., Lacerda, L.D., Keller, G., Punekar, J., 2016. Mercury anomaly, Deccan Volcanism and the end-Cretaceous Mass Extinction. Geology 44, 171–174. https://doi.org/10.1130/G37451.1

Frontalini, F., Buosi C., Da Pelo, S., Coccioni, R., Cherchi, A., Bucci, C., 2009. Benthic foraminifera as bio-indicators of trace element pollution in the heavily contaminated Santa Gilla lagoon (Cagliari, Italy). Marine Pollution Bulletin 58, 858–877. https://doi.org/10.1016/j.marpolbul.2009.01.015

Galazzo, F.B., Giusberti, L., Luciani, V. Thomas, E., 2013. Paleoenvironmental changes during the Middle Eocene Climatic Optimum (MECO) and its aftermath: The benthic foraminiferal record from the Alano section (NE Italy). Palaeogeography, Palaeoclimatology, Palaeoecology 378, 22–25. https//:doi.org/10.1016/j.palaeo.2013.03.018

Gilabert, V., Arenillas, I., Arz, J.A., Batenburg, S.J., Robinson, S.A., 2021a. Multiproxy analysis of paleoenvironmental, paleoclimatic and paleoceanographic changes during the early Danian in the Caravaca section (Spain). Palaeogeography, Palaeoclimatology, Palaeoecology 110513, https://doi.org/10.1016/j.palaeo.2021.110513.

Gilabert, V., Arz, J.A., Arenillas, I., Robinson, S.A., and Ferrer, D., 2021b. Influence of the Latest Maastrichtian Warming Event on planktic foraminiferal assemblages and ocean carbonate saturation at Caravaca, Spain: Cretaceous Research, v. 125, 104844, https://doi .org/10.1016/ j.cretres.2021.104844.

Gilabert, V., Batenburg, S.J., Arenillas, I., Arz, J.A., 2022. Contribution of orbital forcing and Deccan volcanism to global climatic and biotic changes across the Cretaceous-Paleogene boundary at Zumaia, Spain. Geology 49, 21–25 https://doi.org/10.1130/G49214.1

Gradstein, F., Ogg, J., Schmitz, M., Ogg, G., 2020. Geological time Scale 2020. Elsevier.

Grasby, S.E., Them II, T.R., Chen, Z., Yin, R., Ardakani, O.H., 2019. Mercury as a proxy for volcanic emissions in the geologic record. Earth-Science Reviews 196, https://doi.org/10.1016/j.earscirev.2019.102880

Hancock, H.J.L., Dickens, G.R., 2005. Carbonate dissolution episodes in Paleocene and Eocene sediment, Shatsky Rise, west-central Pacific. In: Bralower, T.J., Premoli Silva, I., Malone, M.J. (Eds.), Proceedings of the Ocean Drilling Program, Scientific Results 198. Texas A & M Univ., College Station, pp. 1–24. Available at World Wide Web. odp.tamu.edu/publications/198_SR/116/116.htm

Hildebrand, A.R., Penfield, G.T., Kring, D.A., Pilkington, M., Antonio, C.Z., Boynton, W.V., 1991. Chicxulub crater: A possible Cretaceous/Tertiary boundary impact crater on the Yucatan peninsula, Mexico. Geology 19, 867–871. https://doi:10.1130/0091-7613(1991)0192.3.CO;2

Huber, B.T., Boersma, A., 1994. Cretacaeous origin of *Zeauvigerina* and its relationship to Paleocene Biserial planktonic foraminifera. Journal of Foraminiferal Research 41, 268–287. https://doi.org/10.2113/gsjfr.24.4.268

Huber, B.T., Quillévéré, F., 2005. Revised Paleogene planktonic foraminiferal biozonation for the Austral Realm. Journal of Foraminiferal Research 35, 299–314. https://doi.org/10.2113/35.4.299

Huber, B., Petrizzo, M.R., MacLeod, K., 2020. Planktonic Foraminiferal Endemism at Southern High Latitudes Following the Terminal Cretaceous Extinction. The Journal of Foraminiferal Research 50(4), 382–402. https;//doi.org/10.2113/gsjfr.50.4.382

Hull, P.M., Bornemann, A., Penman, D.E., Henehan, M.J., Norris, R.D., Wilson, P.A., Blum, P., Alegret, L., Batenburg, S.J., Bown, P.R., Bralower, T.J., Cournede, C., Deutsch, A., Donner, B., Friedrich, O., Jehle, S., Kim, H., Kroon, D., Lippert, P.C., Loroch, D., Moebius, I., Moriya, K., Peppe, D.J., Ravizza, G.E., Rohl, ¨ U., Schueth, J. D., Sepulveda, J., Sexton, P.F., Sibert, E.C., Sliwinska, K.K., Summons, R.E., Thomas, E., Westerhold, T., Whiteside, J.H., Yamaguchi, T., Zachos, J.C., 2020. On impact and volcanism across the Cretaceous-Paleogene boundary. Science 367, 266–272. https://doi.org/10.1126/science.aay5055

Henson, S.A., Sanders, R., Madsen, E. 2012. Global patterns in efficiency of particulate organic carbon export and transfer to the deep ocean. Global Biogeochemical Cycles, 26, GB1028. https://doi.org/10.1029/2011GB004099

Intxauspe-Zubiaurre, B., Martinez-Braceras, N., Payros, A., Ortiz, S., Dinarès-Turell, J., Flores, J.A., 2018. The last Eocene hyperthermal (Chron C19r event, ~41.5 Ma): Chronological and paleoenvironmental insights from a continental margin (Cape Oyambre, N Spain). Palaeogeography, Palaeoclimatology, Palaeoecology 505, 198–216. https://doi.org/10.1016/j.palaeo.2018.05.044

Jehle, S., Bornemann, A., Deprez, A. Speijer, R.P., 2015. The Impact of the Lasted Danian Event on Planktic Foraminiferal Faunas at ODP Site 1210 (Shatsky Rise, Pacific Ocean). PLoS ONE 10(11), e0141644. https://doi.10.1371/journal.pone.0141644

Jehle, S., Bornemann, A., Friederike, A., Deprez, A., Speijer, R.P., 2019. Paleoceanographic changes across the Latest Danian Event in the South Atlantic Ocean and planktic foraminiferal response. Palaeogeography, Palaeoclimatology, Palaeoecology 525, 1–13. https://doi.org/10.1016/j.palaeo.2019.03.024

Jones, H.L., Lowery C.M., Bralower, T.J., 2019. Delayed calcareous nannoplankton boom-bust successions in the earliest Paleocene Chicxulub (Mexico). Geology 47, 753–756. https://doi.org/10.1130/G46143.1

Keller, G., Pardo, A., 2004. Age and paleoenvironmental of the Cenomanian-Turonian global stratotype section and point at Pueblo, Colorado. Marine Micropaleontology 51, 95–128. https://doi.org/10.1016/j.marmicro.2003.08.004

Keller, G., Mateo, P., Punekar, J., Khozyem, H., Gertsch, B., Spangenberg, J., Bitchong, A. M., Adatte, T., 2018. Environmental changes during the Cretaceous-Paleogene mass extinction and Paleocene-Eocene Thermal Maximum: Implications for the Anthropocene. Gondwana Research 56, 69–89. https://doi.org/10.1016/j.gr.2017.12.002

Keller, G., Mateo, P., Monkenbusch, J., Thibault, N., Punekar, J., Spangenberg, J. E., Abramovich, S., Ashckenazi-Polivoda, S., Schoene, B., Eddy, M. P., Samperton, K. M., Khadri, S. F. R., Adatte, T., 2020. Mercury linked to Deccan Traps volcanism, climate change and the end-Cretaceous mass extinction. Global and Planetary Change 194, 103312. https://doi.org/10.1016/j.gloplacha.2020.103312

Koutsoukos, E.A.M., 1996. The Cretaceous-Tertiary boundary at Poty, NE Brazil-event stratigraphy and palaeoenvironments. Bulletin - Centres de Recherches Exploration-Production Elf- Aquitaine 16, 413–431.

Koutsoukos, E.A.M., 2014. Phenotypic plasticity, speciation, and phylogeny in early Danian planktic foraminifera. Journal of Foraminiferal Research 44(2), 109–142. https://doi.org/10.2113/gsjfr.44.2.109

Krahl, G., Bom, M.H.H., Kochhann, K.G.D., Souza, L. V., Savian, J.F., Fauth, G., 2020. Environmental changes occurred during the early Danian at the Rio Grande Rise, South Atlantic Ocean. Global and Planetary Change 191, 103197. https://doi:10.1016/j.gloplacha.2020.103197

Kring, D.A., 2007. The Chicxulub impact event and its environmental consequences at the Cretaceous/Tertiary boundary. Palaeogeography, Palaeoclimatology, Palaeoecology 255, 4–21. https://doi.org/10.1016/j .palaeo.2007.02.037

Kroon, D., Nederbragt, A.J., 1990. Ecology and paleoecology of triserial planktic foraminifera. Marine Micropaleontology 16(1-2), 25–38. https://doi.org/10.1016/0377-8398(90)90027-j

Kroon, D., Zachos, J.C., et al., 2007. 1. Leg 208 synthesis: Cenozoic climate cycles and excursions. In: Kroon, D., Zachos, J.C., Richter, C. (Eds.), Proceedings of the Ocean Drilling Program, Scientific Results, 208, pp. 1–55.

Kucera, M., Malmgren, B.A. Sturesson, U., 1997. Foraminiferal dissolution at shallow depths of the Walvis Ridge and Rio Grande Rise during the latest Cretaceous: Inferences for deep-water circulation in the South Atlantic. Palaeogeography, Palaeoclimatology, Palaeoecology 129, 195–212. https://doi:10.1016/S0031-0182(96)00133-2.

Kulal, D.K., Loni, P.C., Dcosta, C., Some, S., Kalambate, P.K. 2020. Cyanobacteria: as a promising candidate for heavy-metals removal. Advances in Cyanobacterial Biology, 291–300. https://doi.org/10.1016/B978-0-12-819311-2.00019-X

Laskar, J., Gastineau, M., Delisle, J.-B., Farrés, A., Fienga, A., 2011. Strong chaos induced by close encounters with Ceres and Vesta. Astronomy and Astrophysics 532, L4, https://doi.org/10.1051/0004-6361/201117504.

Leighton, A.D., Hart, M.B., Smart, C.W., Leng, M.J., Hampton, M., 2017. Timing Recovery after the Cretaceous/Paleogene Boundary: evidence from the Brazos River, Texas, USA. Journal Foraminiferal Research 47(3), 229–238. https://doi.org/10.2113/gsjfr.47.3.229

Leon-Rodriguez, L., Dickens, G.R., 2010. Constraints on ocean acidification associated with rapid and massive carbon injections: The early Paleogene record at ocean drilling program site 1215, equatorial Pacific Ocean. Palaeogeography, Palaeoclimatology, Palaeoecology 298(3-4), 409–420. https://doi.org/10.1016/j.palaeo.2010.10.029

Lowery, C.M., Bralower, T.J., Owens, J.D., Rodríguez-Tovar, F.J., Jones, H., Smit, J., Whalen, M.T., Claeys, P., Farley, K., Gulick, S.P.S., Morgan, J.V., Green, S., Chenot, E., Christeson, G.L., Cockell, C.S., Coolen, M.J.L., Ferriere, L., Gebhardt, C., Goto, K., Kring, D.A., Lofi, J., Ocampo-Torres, R., Perez-Cruz, L., Pickersgill, A.E., Poelchau, M.H., Rae, A.S.P., Rasmussen, C., Rebolledo-Vieyra, M., Riller, U., Sato, H., Tikoo, S.M., Tomioka, N., Urrutia-Fucugauchi, J., Vellekoop, J., Wittmann, A., Xiao, L., Yamaguchi, K.E., Zylberman, W., 2018. Rapid recovery of life at ground zero of the end-Cretaceous mass extinction. Nature 558, 288–291. https://doi.org/10.1038/s41586-018-0163-6

Lowery, C.M., Fraass, J.S., 2019. Morphospace expansion paces taxonomic diversification after end Cretaceous mass extinction. Nature Ecology and Evolution 3, 900–904. https://doi.org/10.1038/s41559-019-0835-0

Lowery, C.M., Jones, H.L., Bralower, T., Cruz, L.P., Gebhardt, C., Whalen, M.T., Chenot, E., Smit, J., Phillips, M.P., Choumiline, K., Arenillas, I., Arz, J.A., Garcia, F., Ferrand, M., Lofi J., Gulick, S.P.S., Exp. 364 Science Party, 2021. Early Paleocene Paleoceanography and Export Productivity in the Chicxulub Crater. Paleoceanography Paleoclimatology 36(11). e2020PA004241. https://doi.org/10.1029/2020PA004241

Luciani, V., Giusberti, L., Agnini, C., Fornaciari, E., Rio, D., Spofforth, D.J.A., Pälike, H., 2010. Ecological and evolutionary response of Tethyan planktonic foraminifera to the middle Eocene climatic optimum (MECO) from the Alano section (NE Italy). Palaeogeography, Palaeoclimatology, Palaeoecology 292, 82–95. https://doi.org/10.1016/j.palaeo.2010.03.029

Luciani, V., D'Onofrio, R., Dickens, G.R., Wade, B.S., 2017. Planktic foraminiferal response to early Eocene carbon cycle perturbations in the southeast Atlantic Ocean (ODP Site 1263). Global and Planetary Change 158, 119–133. https://doi.org/10.1016/j.gloplacha.2017.09.007

Luciani, V., D'Onofrio, R., Filippi, G., Moretti, S., 2020. Which was the habitat of early Eocene planktic foraminifer *Chiloguembelina*? Stable isotope paleobiology from th Atlantic Ocean and implication for paleoceanographic reconstructions. Global and Planetary Change 191, 103216. https://doi.org/10.1016/j.gloplacha.2020.103216.

Mancin, N., Darling, K., 2015. Morphological abnormalities of planktonic foraminiferal tests in the SW Pacific Ocean over the last 550ky. Marine Micropaleontology 120, 1–19. https://doi.org/10.1016/j.marmicro.2015.08.003

Molina, E., 2015. Evidence and causes of the main extinction events in the Paleogene based on extinction and survival patterns of foraminifera. Earth-Science Reviews 140, 166–181. https://doi.org/10.1016/j.earscirev.2014.11.008

Molina, E., Arenillas, I., Arz, J.A., 1996. The Cretaceous/Tertiary boundary mass extinction in planktic foraminifera at Agost (Spain). Revue de Micropaléontologie 39(3), 225–243. https://doi.org/10.1016/S0035-1598(96)90075-6

Molina, E., Alegret, L., Arenillas, I., Arz, J.A., Gallala, N., Grajales-Nishimura, M., Murillo-Muñetón, G., Zaghbib-Turki, D., 2009. The Global Boundary Stratotype Section and Point for the base of the Danian Stage (Paleocene, Paleogene, "Tertiary", Cenozoic): auxiliary sections and correlation. Episodes 32(2), 84–95. https://doi.org/10.18814/epiiugs/2009/v32i2/002

Morgan, J.V., Bralower, T.J., Brugger, J., Wünnemann, K., 2022. The Chicxulub impact and its environmental consequences. Nature Review Earth Environment 3, 338–354. https://doi.org/10.1038/s43017-022-00283-y

Nederbragt, A.J., 1991. Late Cretaceous biostratigraphy and development of Heterohelicidae (planktic foraminifera). Micropaleontology 37, 329–372. https://doi.org/10.2307/1485910

Nguyen, T.M.P., Speijer, R.P., 2014. A new procedure to assess dissolution based on experiments on Pliocene–Quaternary foraminifera (ODP Leg 160, Eratosthenes Seamount, Eastern Mediterranean). Marine Micropaleontology 106, 22–39. https://doi.org/10.1016/j.marmicro.2013.11.004

Norris, R.D., Huber, B.T., Self-Trail, J., 1999. Synchroneity of the K-T oceanic mass extinction and meteorite impact: Blake Nose, western North Atlantic. Geology 27, 419– 422. https://doi:10.1130/0091-7613(1999)027<0419:SOTKTO>2.3.CO;2

Olsson, R.K., Berggren, W.A., Hemleben, C., Huber, B.T., 1999. Atlas of Paleocene Planktonic Foraminifera. Smithsonian Contributions to Paleobiology, 1–252. https://doi.org/10.5479/si.00810266.85.1

Orth, C.J., J.S. Gilmore, J.D. Knight, C.L. Pillmore, R.H. Tschudy, J., Fassett, E., 1981. An iridium abundance anomaly at the palynological Cretaceous-Tertiary boundary in northern New Mexico. Science 214(4527), 1341–1343. https://doi.org/ 10.1126/science.214.4527.1341

Pardo, A., Keller, G., 2008. Biotic effects of environmental catastrophes at the end of the Cretaceous and early Tertiary: *Guembelitria* and *Heterohelix* blooms. Cretaceous Research 29(5-6), 1058–1073. https://doi.org/10.1016/j.cretres.2008.05.031

Punekar, J., Mateo, P., Keller, G., 2014. Effects of Deccan volcanism on paleoenvironment and planktic foraminifera: A global survey. The Geological Society of America Special Paper (505). https://doi:10.1130/2014.2505(04)

Quillévéré, F., Norris, R.D., Kroon, D., Wilson, P.A., 2008. Transient ocean warming and shifts in carbon reservoirs during the early Danian. Earth Planetary Science Letters 265, 600−615. https://doi:10.1016/j.epsl.2007.10.040

Ravizza, G., Peucker-Ehrenbrink, B., 2003. Chemostratigraphic evidence of Deccan volcanism from the marine Os isotope record. Science 302, 1392–1395. https://doi:10.1126/science.1089209

Ravizza, G, Vonderhaar, D., 2012. A geochemical clock in earliest Paleogene pelagic carbonates based on the impact induced Os isotope excursion at the Cretaceous-Paleogene boundary. Paleoceanography 27, PA3219. https://doi:10.1029/2012PA002301

Robinson, N., Ravizza, G., Coccioni, R., Peucker-Ehrenbrink, B., Norris, R., 2009. A high-resolution marine osmium isotope record for the late Maastrichtian Distinguishing the chemical fingerprints of the Deccan and KT impactor. Earth Planetary Science Letters 281, 159–168. https://doi:10.1016/j.epsl.2009.02.019.

Schoene, B., Eddy, M.P., Samperton, K.M., Keller, C.B., Keller, G., Adatte, T., Khadri, S.F.R., 2019. U-Pb constraints on pulsed eruption of the Deccan Traps across the end-Cretaceous mass extinction. Science 363, 862–866. https://doi:10.1126/science.aau2422.

Schoene, B., Eddy, M.P., Keller, C.B., Samperton, K.M., 2021. An evaluation of deccan traps eruption rates using geochronologic data. Geochronology 3, 181–198. https://doi.org/10.5194/gchron-3-181-2021

Schulte, P., Alegret, L., Arenillas, I., Arz, J.A., Barton, P.J., Bown, P.R., Bralower, T.J., Christeson, G.L., Claeys, P., Cockell, C.S., Collins, G.S., Deutsch, A., Goldin, T.J., Goto, K., Grajales-Nishimura, J.M., Grieve, R.A.F., Gulick, S.P.S., Johnson, K.R., Kiessling, W., Koeberl, C., Kring, D.A., MacLeod, K.G., Matsui, T., Melosh, J., Montanari, A., Morgan, J. V., Neal, C.R., Nichols, D.J., Norris, R.D., Pierazzo, E., Ravizza, G., Rebolledo-Vieyra, M., Reimold, W.U., Robin, E., Salge, T., Speijer, R.P., Sweet, A.R., Urrutia-Fucugauchi, J., Vajda, V., Whalen, M.T., Willumsen, P.S., 2010. The Chicxulub asteroid impact and mass extinction at the Cretaceous-Paleogene boundary. Science 327, 1214–1218. https://doi:10.1126/science.1177265.

Sheehan, P.M., Coorough, P.J., Fastovsky, D.E., 1996. Biotic selectivityduring the K/T and Late Ordovician extinction events, in The Cretaceous-Tertiary Event and Other Catastrophes in Earth History, edited by G. Ryder, D. Fastovsky, and S. Gartner, Geological Society of America Special Papers 307, 477–489.

Shen, J., Algeo, T. J., Planaysky, N. J., Yu, J., Feng, Q., Song, H., Rowe, H., Zhou, L., Chen, J., 2019. Mercury enrichments provide evidence of Early Triassic volcanism following the End-Permian mass extinction. Earth-Science Reviews 195, 191–212. https://doi.org/10.1016/j.earscirev.2019.05.010

Smit, J., 1982. Extinction and evolution of planktonic foraminifera after a major impact at the Cretaceous/Tertiary boundary. Geological Society of America Special Papers 190, 329–352. https://doi.org/10.1130/SPE190-p329,1982

Smit, J., Romein, A.J.T., 1985. A sequence of events across the Cretaceous-Tertiary boundary. Earth Planetary Science Letters 74, 155-170. https://doi:10.1016/0012-821X(85)90019-6

Sial, A.N., Lacerda, L.D., Ferreira, V.P., Frei, R., Marquillas, R.A., Barbosa, J.A., Gaucher, C., Windmöller, C.C., Pereira, N.S., 2013. Mercury as a proxy for volcanic activity during extreme environmental turnover: the Cretaceous–Paleogene transition. Palaeogeography, Palaeoclimatology, Palaeoecology 387, 153–164. https://doi.org/10.1016/j.palaeo.2013.07.019

Sial, A.N., Chen, J., Lacerda, L.D., Frei, R., Tewari, V.C., Pandit, M.K., Gaucher, C., Ferreira, V.P., Cirilli, S., Peralta, S., Korte, C., Barbosa, J.A., Pereira, N.S., 2016. Mercury enrichment and mercury isotopes in Cretaceous–Paleogene boundary successions: links to volcanism and palaeoenvironmental impacts. Cretaceous Research 66, 60–81. https://doi.org/10.1016/j.cretres.2016.05.006

Sprain, C.J., Renne, P.R., Vanderkluysen, L., Pande, K., Self, S., Mittal, T., 2019. The eruptive tempo of Deccan volcanism in relation to the Cretaceous-Paleogene boundary. Science 363, 866–870. https://doi:10.1126/science.aav1446

Swart, P.K., 2015. The geochemistry of carbonate diagenesis: The past, present and future. Sedimentology 62(5), 1233–1304. https://doi.org/10.1111/sed.12205

Stax, R., Stein, R., 1993. Long-term changes in the accumulation of organic carbon in Neogene sediments, Ontong Java Plateau. Proceedings of the Ocean Drilling Program 130, 573–579. https://doi.10.2973/odp.proc.sr.130.039.1993

Thibault, N., Galbrun, B., Gardin, S., Minoletti, F., Le Callonnec, L.L., 2016. The end- Cretaceous in the southwestern Tethys (Elles, Tunisia): orbital calibration of paleoenvironmental events before the mass extinction. International Journal of Earth Sciences 105, 771–795. https://doi.org/10.1007/ s00531-015-1192-0

Van der Zwaan, G.J., Jorissen, F.J., De Stigter, H.C., 1990. The depth dependency of planktonic/benthic foraminiferal ratios: constraints and applications. Marine Geology, 95(1), 1–16. https://doi.org/10.1016/0025-3227(90)90016-D

Van Hinsbergen, D.J.J., Groot, L.V., Van Schaik, J.S., Spakman, W., Bijl, P.K., Sluijs, A., Langereis, C.G., Brinkhuis, H., 2015. A Paleolatitude Calculator for Paleoclimate Studies. PLoS ONE 10(6), e0126946. https://doi:10.1371/journal.pone.0126946

Wade, B.S., Pearson, P.N., Berggren, W.A., Pälike, H., 2011. Review and revision of Cenozoic tropical planktonic foraminiferal biostratigraphy and calibration to the geomagnetic polarity and astronomical time scale. Earth Science Reviews 104, 111– 142. https://doi.org/10.1016/j.earscirev.2010.09.003

Watkins, J.M., Hunt, J.D., Ryerson, F.J., DePaolo, D.J., 2014. The influence of temperature, pH, and growth rate on the $\delta^{18}O$ composition of inorganically precipitated calcite. Earth and Planetary Science Letters 404, 332–343. https://doi.org/10.1016/j.epsl.2014.07.036

Westerhold, T., Röhl, U., Raffi, I., Fornaciari, E., Monechi, S., Reale, V., Bowles, J., Evans, H.F., 2008. Astronomical calibration of the Paleocene time. Palaeogeography Palaeoclimatololy Palaeoecology 257, 377–403. https://doi.org/10.1016/j.palaeo.2007.09.016

Westerhold, T., Rohl, U., Donner, B., McCarren, H.K., Zachos, J.C., 2011. A complete high-resolution Paleocene benthic stable isotope record for the Central Pacific (ODP site 1209). Paleoceanography 26, PA2216. https://doi.org/10.1029/2010PA002092

Westerhold, T., Marwan, N., Drury, A.J., Liebrand, D., Agnini, C., Anagnostou, E., Barnet, J.S.K., Bohaty, S.M., De Vleeschouwer, D., Florindo, F., Frederichs, T., Hodell, D.A., Holbourn, A.E., Kroon, D., Lauretano, V., Littler, K., Lourens, L.J., Lyle, M., Palike, H., Rohl, U., Tian, J., Wilkens, R.H., Wilson, P.A., Zachos, J.C., 2020. An astronomically dated record of Earth's climate and its predictability over the last 66 million years. Science 369, 1383–1387. https://doi.org/10.1126/science

Woelders, L., Vellekoop, J., Smit, J., Kroon, D., Casadío, S., Prámparo, M., Dinarès-Turell, J., Peterse, F., Sluijs, A., Speijer, R.P., 2017. Latest Cretaceous climatic and environmental change in the South Atlantic region. Paleoceanography 32, 466–483. https://doi:10.1002/2016PA003007

Yao, H., Chen, X., Yin, R., Grasby, S.E., Weissert, H., Gu, X., Wang, C., 2021. Mercury evidence of intense volcanism preceded oceanic anoxic event 1d. Geophysical Research Letters 48, e2020GL091508. https://doi.org/10.1029/2020GL091508

Zachos, J.C., Kroon, D., Blum, P., et al. 2004. Leg 208 Summary, Proceedings of the Ocean Drilling Program Initial Reports (208), 77845–9547. https://doi:10.2973/odp.proc.ir.208.2004

Figure captions

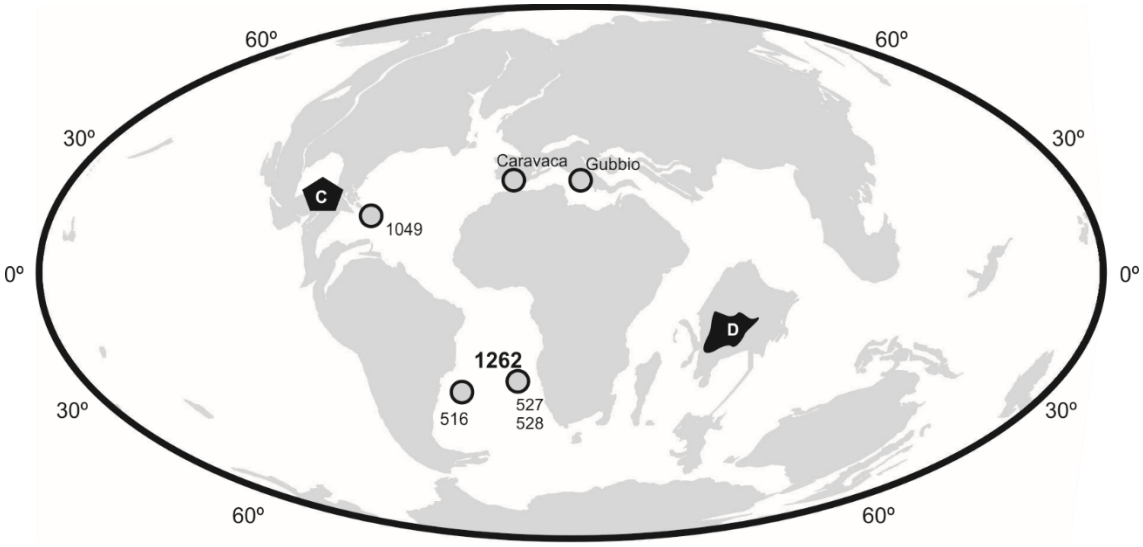

Figure 1. Paleogeographic reconstruction for the K/Pg boundary (66 Ma) after ODSN plate reconstruction (ODSN system: http://www.odsn.de/odsn/services/paleomap/paleomap.html), showing the location of ODP Site 1262 and other localities discussed in the text. Abbreviations: C = Chicxulub crater; D = Deccan Traps.

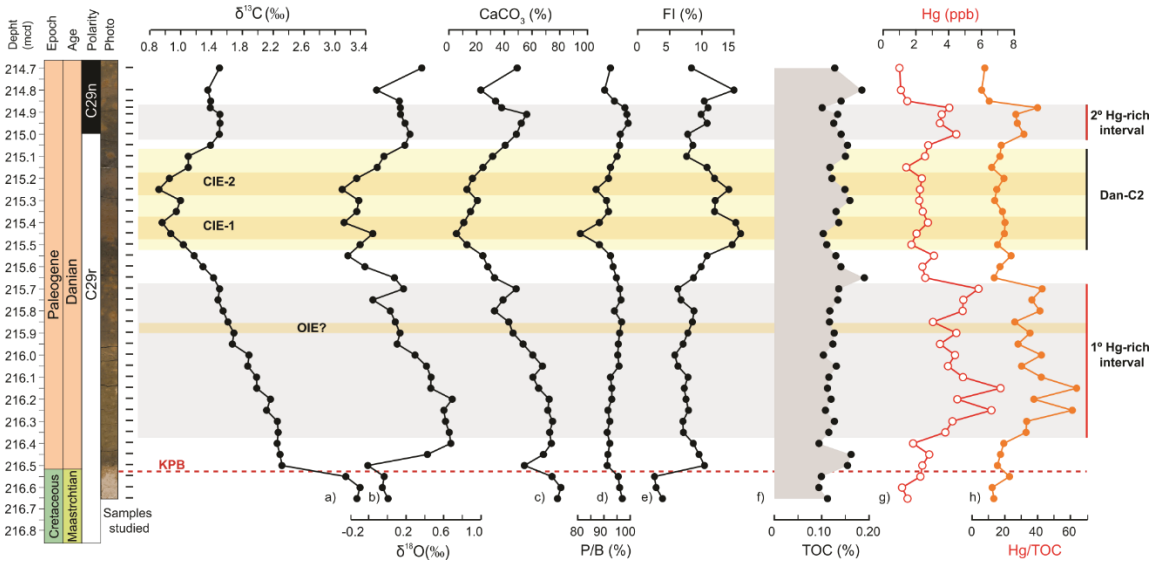

Figure 2. Geochemical record at Site 1262. a) bulk sediment carbon ($\delta^{13}C$, ‰); b) oxygen stable isotopes ($\delta^{18}O$, ‰); c) calcium carbonate content ($CaCO_3$ %); d) planktic/benthic foraminiferal ratio: P/B ratio (%); e) foraminiferal fragmentation index: FI (%); f) total organic carbon (TOC) content; g) Hg concentration (ppb) and Hg/TOC ratio. Stratigraphic position of the C29r/C29r reversal at Hole B according to Bowles (2006) and Westerhold et al. (2008). Stratigraphic position of CIE-1 and CIE-2 od Dan-C2 based on this study. Estimated stratigraphic position of oxygen isotope excursion (OIE) based on the correlation with Hole C (see Appendix A). KPB = Cretaceous/Paleogene boundary.

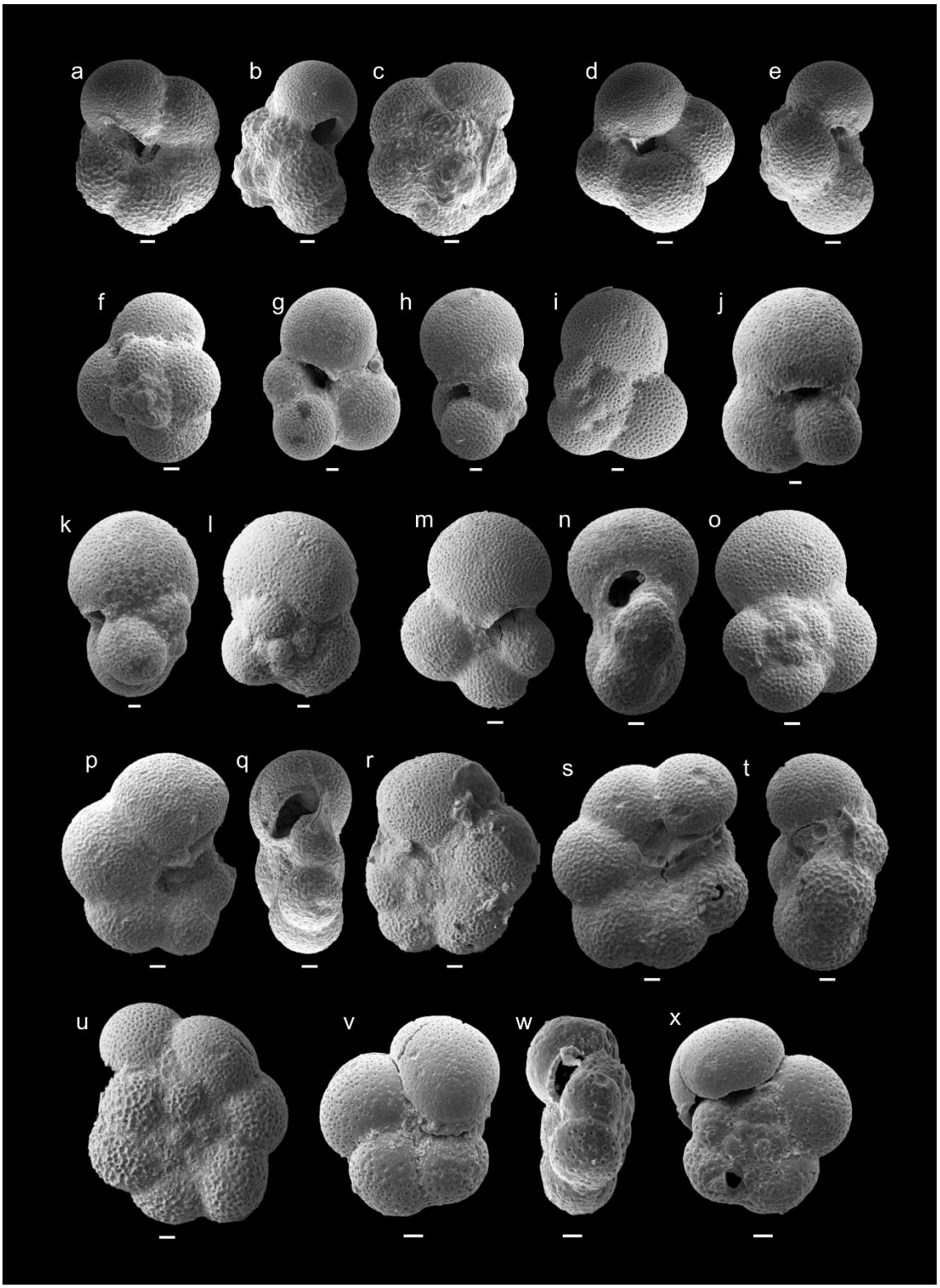

Figure 3. Scanning electron microscope (SEM) micrographs of Danian planktic foraminifera from Site 1262 (scale bars = 10 μm). a-c. *Eoglobigerina edita* (*E. polycamera* according to A21) (215.78

mcd). d-f. *Eoglobigerina eobulloides* (*E.* cf. *trivialis* according to A21) (215.43 mcd). g-i. *Subbotina trivialis* (*E.* cf. *trivialis* according to A21) (215.29 mcd). j-l. *Subbotina triloculinoides* (214.88 mcd). m-o. *Parasubbotina varianta* (214.88 mcd). p-r. *Praemurica pseudoinconstans* (215.10 mcd). s-u. *Praemurica taurica* (215.89 mcd). v-x. *Globanomalina planocompressa* (*G. imitata* according to A21) (215.58 mcd). A21 = Taxonomy in Arenillas et al. (2021, and references herein).

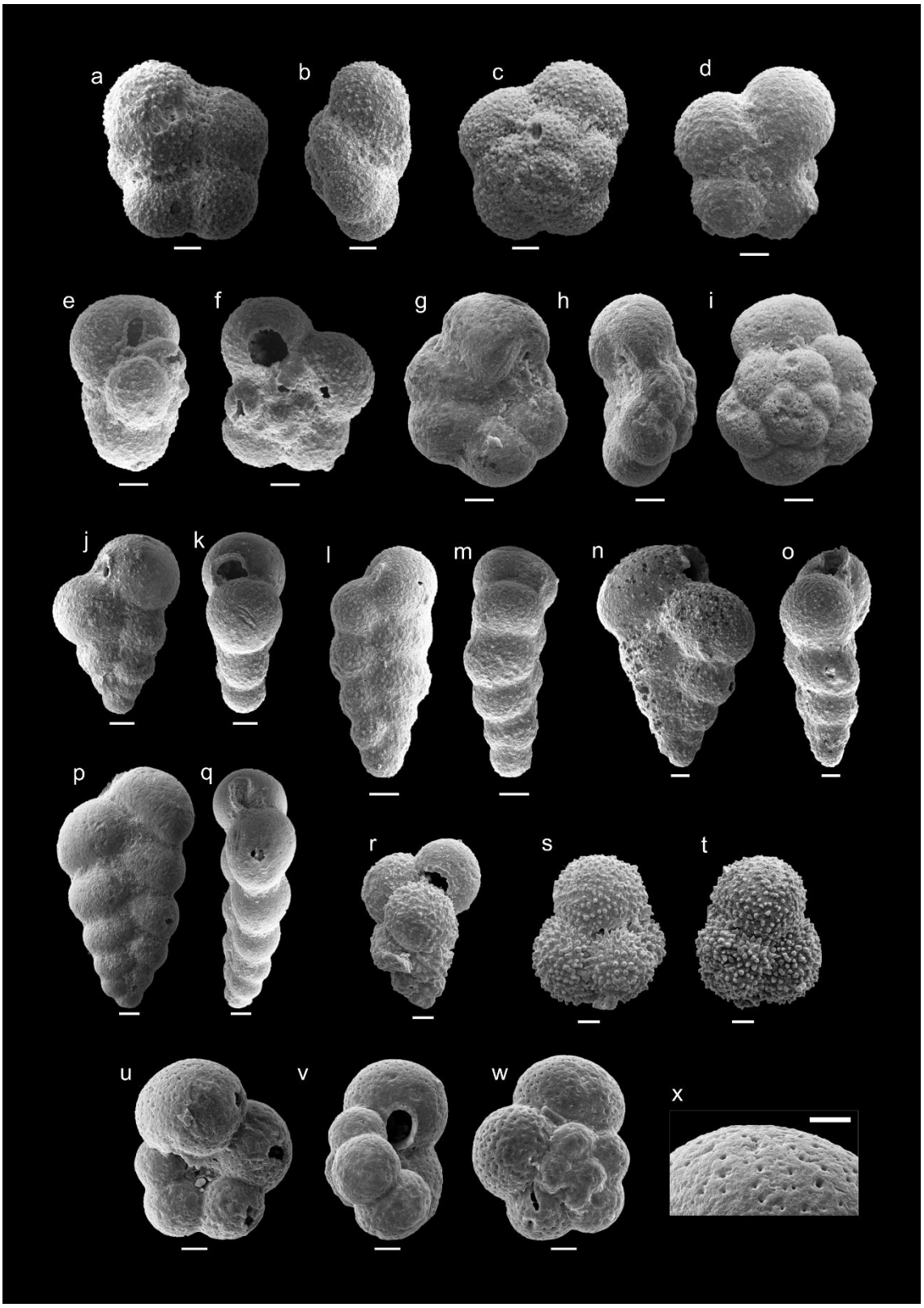
a
b
c
d
e
f
g
h
i
j
k
l
m
n
o
p
q
r
s
t
u
v
w
x

Figure 4. SEM micrographs of Danian planktic foraminifera from Site 1262 (scale bars = 10 μm). a-c. *Praemurica nikolasi* (*Globanomalina imitata* according to A21) (215.03 mcd). d-f. *Parvularugoglobigerina eugubina* s.l. (*Trochoguembelitria liuae* according to A21) (216.03 mcd). g-i. Transitional specimen between *Parvularugoglobigerina eugubina* s.s. and *Globanomalina archaeocompressa* (large *Pv. eugubina sensu* Smit 1982) (216.63 mcd). j-k. *Woodringina claytonensis* (215.43 mcd). l-m. *Woodringina hornerstownensis* (215.07 mcd). n-o. *Chiloguembelina midwayensis* (214.88 mcd). p-q. *Chiloguembelina morsei* (*Ch. taurica* according to A21) (215.03 mcd). r. *Guembelitria cretacea* s.l. (*Chiloguembelitria danica* according to A21) (216.03 mcd). s-t. *Globoconusa daubjgersensis* (214.88 mcd). u-w. *Parasubbotina* aff. *pseudobulloides* (*Eoglobigerina praeedita* according to A21) (215.73 mcd). x. Texture detail of the latter. A21 = Taxonomy in Arenillas et al. (2021, and references herein).

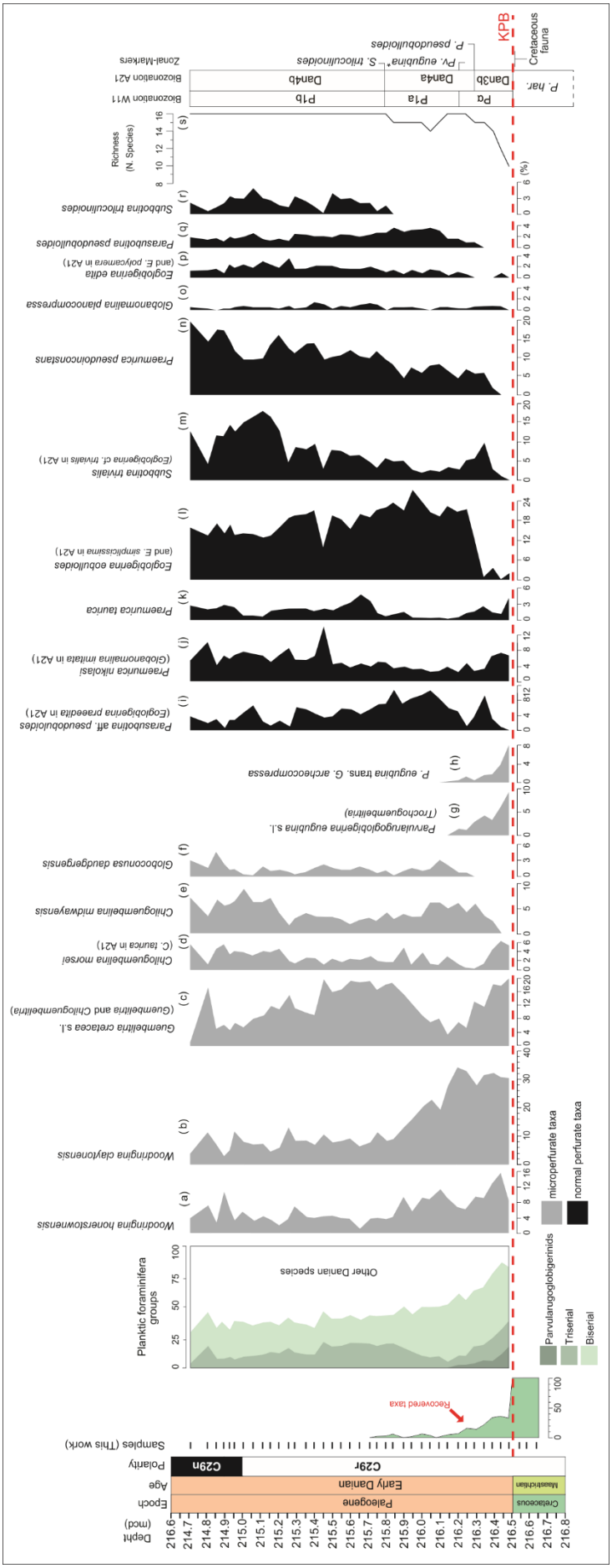
Depth (mcd)
Epoch
Age
Polarity
Cretaceous
Paleogene
Maastrichtian
Early Danian
C29r
C29n
Samples (This work)
Recovered taxa
Planktic foraminifera groups
Other Danian species
Parvulangoglobigerinids
Triserial
Biserial
microperforate taxa
normal perforate taxa
Woodringina hornerstownensis
Woodringina claytonensis
Guembelitria cretacea s.l. (Guembelitria and Chiloguembelitria)
Chiloguembelina morsei (C. taurica in A21)
Chiloguembelina midwayensis
Globoconusa daubjergensis
Parvulangoglobigerina eugubina s.l. (Trochoguembelitria)
P. eugubina trans. G. archaeocompressa
Parasubbotina aff. pseudobulloides (Eoglobigerina praeedita in A21)
Praemurica nikolaei (Globanomalina imitata in A21)
Praemurica taurica
Eoglobigerina eobulloides (and E. simplicissima in A21)
Subbotina triloculinoides (Eoglobigerina cf. trivialis in A21)
Praemurica pseudoinconstans
Globanomalina planocompressa
Eoglobigerina edita (and E. polycamera in A21)
Parasubbotina pseudobulloides
Subbotina triloculinoides
Richness (N. Species)
Biozonation W11
Biozonation A21
Zonal-Markers
P. hariP. eugubina*S. triloculinoidesP. pseudobulloides
Pa
P1a
P1b
Dan3b
Dan4a
Dan4b
KPB
Cretaceous fauna

Figure 5. Relative abundances (%) at Site 1262B of the Danian planktic foraminiferal species and groups: parvularugoglobigerinids s.l. (*Parvularugoglobigerina* s.s. and *Trochoguembelitria*), biserial (*Woodringina* and *Chiloguembelina*), triserial (*Guembelitria* s.s. and *Chiloguembelitria*) and other genera (*Globoconusa*, *Eoglobigerina*, *Subbotina*, *Parasubbotina*, *Praemurica*, and *Globanomalina*). All relative abundances of planktic foraminifera are arranged from 5a to 5r. Danian planktic foraminiferal zones of W11 (Wade et al. 2011) and A21 (Arenillas et al. 2021). P. har. = *Pseudoguembelina hariaensis* Zone *sensu* Nederbragt (1991).

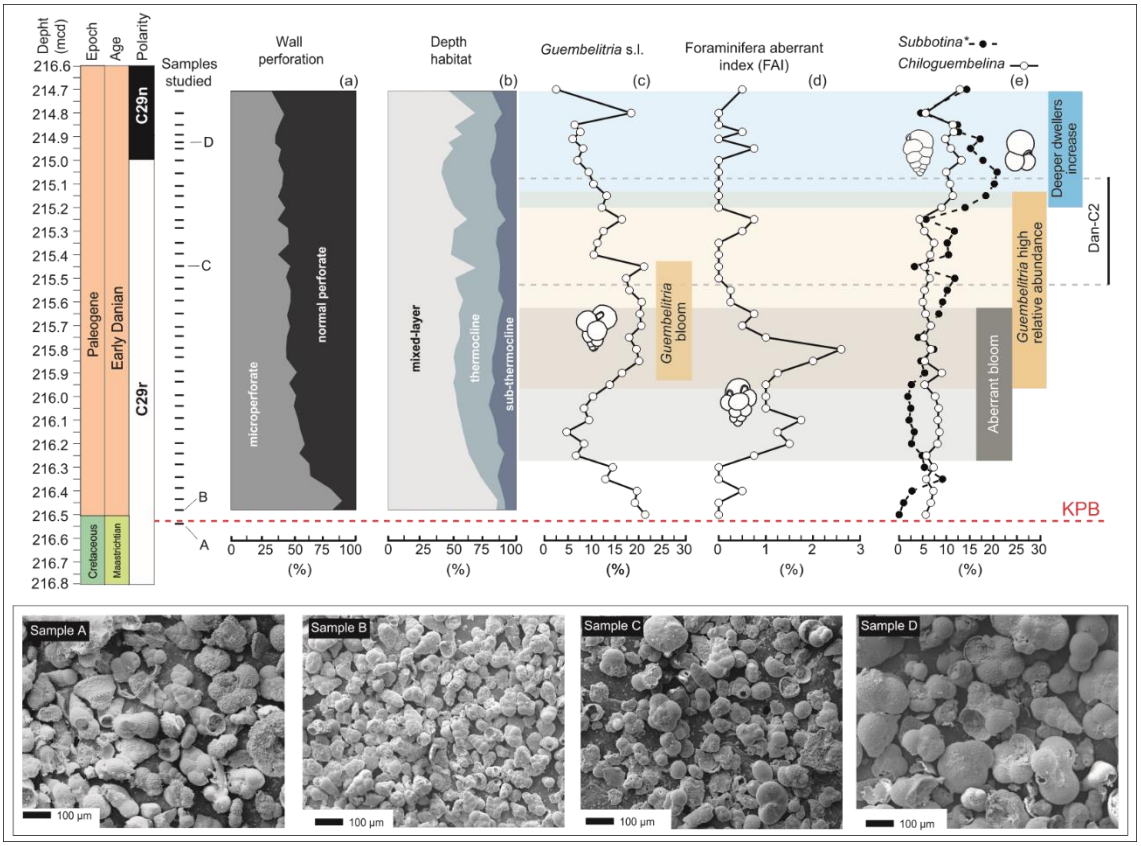

Figure 6. Main changes in the planktic foraminiferal assemblages occurring at Site 1262 during the early Danian. a) Relative abundance (%) of planktic foraminiferal taxa according to their wall

perforation (microperforate *vs.* macroperforate); b) Abundance of planktic foraminiferal taxa according to their depth habitat, which is related to the stratification of the upper water column; c) Relative abundance (%) in triserial guembelitriids (*Guembelitria* s.s. and *Chiloguembelitria*); d) Foraminiferal abnormality index (FAI): relative abundance (%) in aberrant planktic foraminiferal specimens; e) Relative abundances (%) in *Subbotina* and *Chiloguembelina*; *Subbotina**: species *trivialis* has been included in *Subbotina* according to the W11 taxonomy, but the A21 taxonomy assigned it to the genus *Eoglobigerina* (*E.* cf. *trivialis*). Scanning electron microscope (SEM) detail of samples A to D (identified in the time axis) showing the overall trend of planktic foraminiferal test sizes and the main biogenic components in the studied interval at Site 1262. Sample A = large-sized planktic foraminiferal assemblage of the Maastrichtian; Sample B = reduced sizes of planktic foraminifera just after the K/Pg boundary; Sample C = biogenic constituents with presence of calcispheres within the Dan-C2 interval; Sample D = increased sizes of planktic foraminiferal tests after the Dan-C2 event.

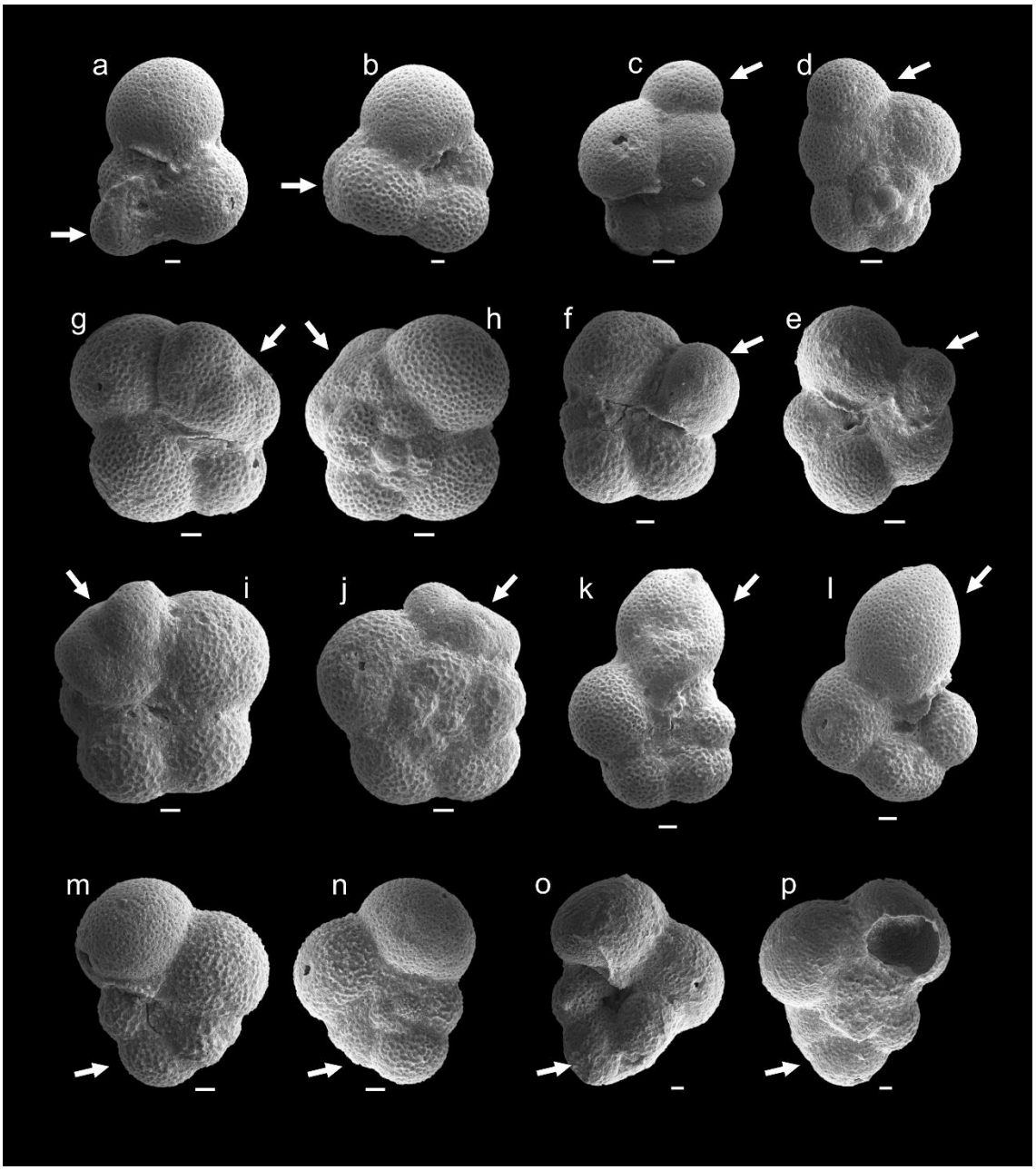

Figure 7. SEM micrographs of planktic foraminifera with test abnormalities from Site 1262 (scale bars = 10 μm). a. *Subbotina* spp. (215.68 mcd). b. *Subbotina* spp. (216.03 mcd). c-d. *Parasubbotina* spp. (215.93 mcd). e. *Parasubbotina* or *Eoglobigerina* spp. (216.58 mcd). f. *Eoglobigerina* spp. (215.98 mcd). g-h. *Parasubbotina* spp. (216.03 mcd). i-j. *Parasubbotina pseudobulloides*

(215.13 mcd). k. *Parasubbotina* spp. (215.93 mcd). l. *Praemurica* spp. (216.03 mcd). m-n. *Eoglobigerina* spp. (215.68 mcd). o-p. *Praemurica pseudoinconstans* (216.03 mcd). Arrows indicate morphological abnormalities.

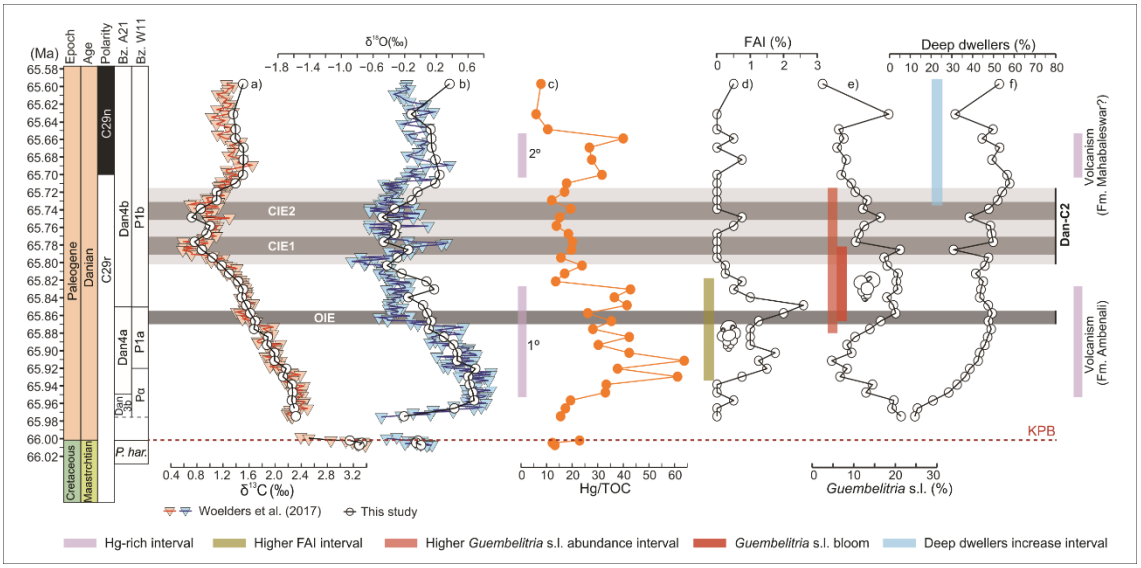

Figure 8. Main changes in planktic foraminiferal assemblages and geochemical proxies during the early Danian at Site 1262, according to the age model here proposed. a - b) bulk sediment carbon and oxygen stable isotopes from this work and Woelders et al. (2017); c) Hg/TOC ratio; d) Foraminiferal abnormality index (FAI); e) Relative abundances (%) in *Guembelitria* s.l. [*Chiloguembelitria*]; f) Relative abundances (%) in deep-dwelling taxa (thermocline + sub-thermocline dwellers; see Appendix C for further details).

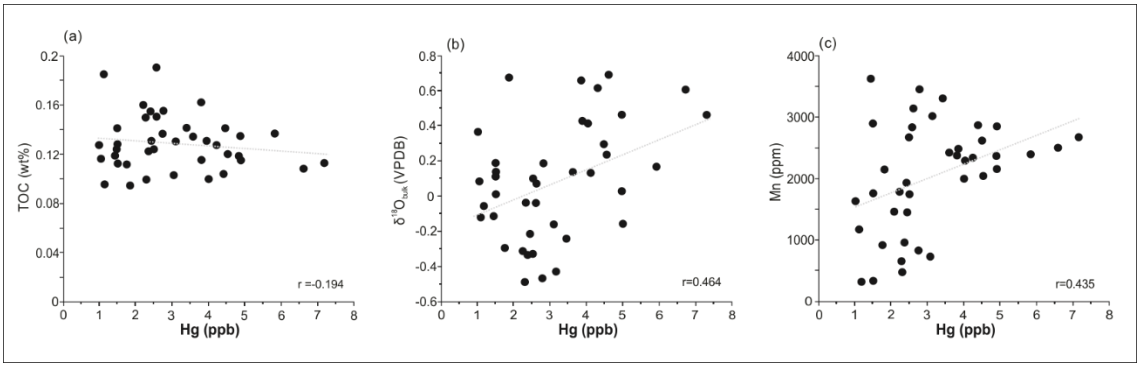

Figure 9. Crossplots of Hg concentrations versus TOC (a), $\delta^{18}O_{bulk}$ (b), and Mn concentrations (c). Pearson correlations (r) are also shown.

Table of contents – Electronic Supplementary Material (ESM)

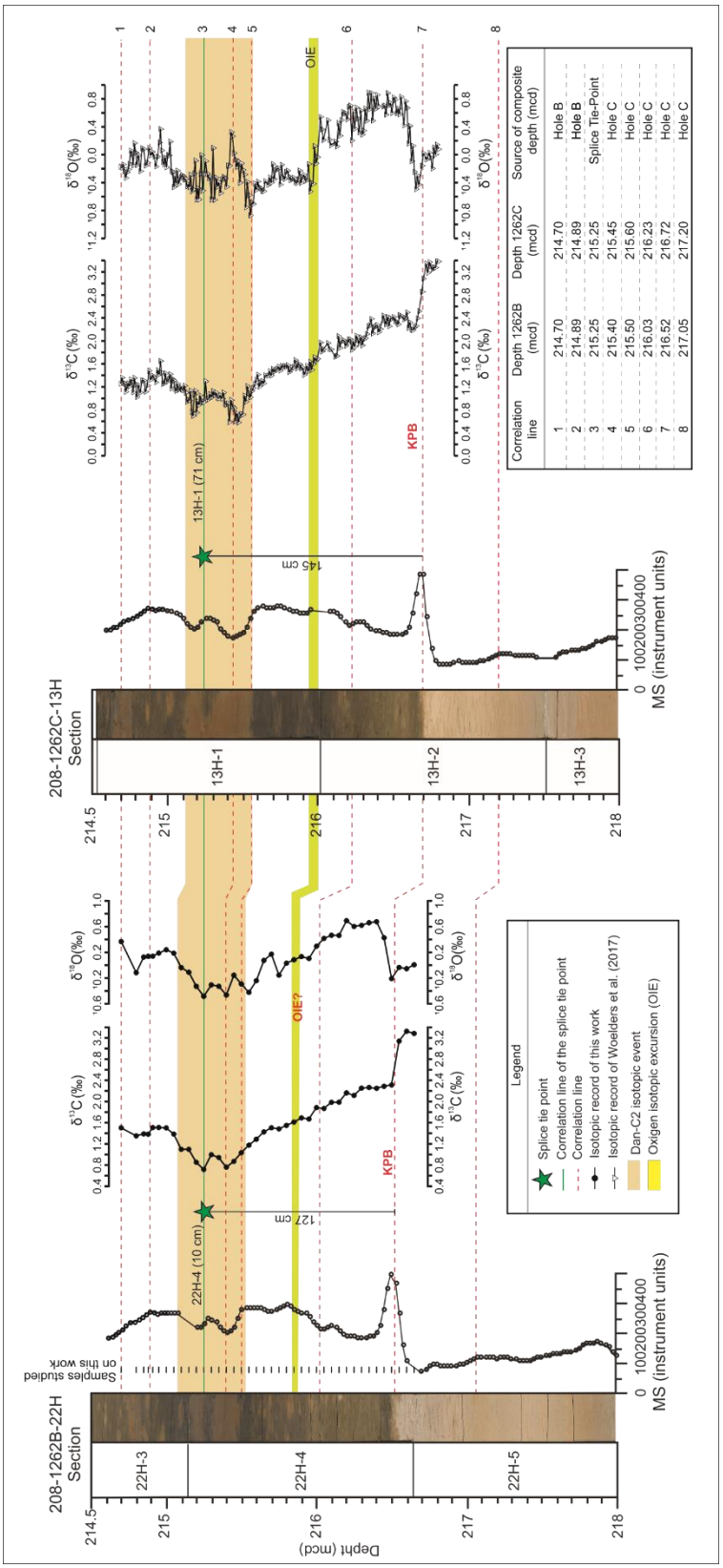
208-1262B-22H Section
208-1262C-13H Section
Depth (mcd)
MS (instrument units)
Samples studied on this work
22H-4 (10 cm)
127 cm
13H-1 (71 cm)
145 cm
KPB
OIE?
OIE
Legend
Splice tie point
Correlation line of the splice tie point
Correlation line
Isotopic record of this work
Isotopic record of Woelders et al. (2017)
Dan-C2 isotopic event
Oxygen isotopic excursion (OIE)
Correlation line
Depth 1262B (mcd)
Depth 1262C (mcd)
Source of composite depth (mcd)
Hole B
Splice Tie-Point
Hole C

Appendix A: Comparison and correlation of Holes 1262B (this work) and 1262C. Bulk $\delta^{13}C$ and $\delta^{18}O$ data in this study compared and correlated with those of Woelders et al. (2017), which are based on composite depths from several holes of Site 1262 (in the studied interval, from Holes B and C). Interval shaded in orange corresponds to the Dan-C2 interval (CIE-1 and CIE-2). Green star marks the splice tie point defined by Zachos et al. (2004). Other tie points (correlation lines) based on Dinarés-Turell et al. (2014).

Appendix B. Planktic foraminiferal distribution and indexes at Site 1262: magnetostratigraphy (Bowles 2006, Westerhold et al. 2008); planktic/benthic ratio (%); fragmentation index (FI %); relative abundance (%) of the species (index species in red); relative abundance (%) in aberrant specimens (FAI %; gray shading = increase in aberrant specimens); species richness; planktic foraminiferal zones of W11 (Wade et al., 2011) and A21 (Arenillas et al., 2021); relative abundance (%) of the genera; micro- and macroperforated taxa (%); relative abundance (%) in Cretaceous taxa; relative abundance (%) in planktic foraminiferal groups according to their depth habitat (mixed layer, thermocline and sub-thermocline dwellers); planktic foraminiferal groups: parvularugoglobigerinids s.l., biserial (*Woodringina* and *Chiloguembelina*), triserial (*Guembelitria* s.s. and *Chiloguembelitria*) and other genera (orange shading = bloom in triserial guembelitriids). Age calibration for each sample is showed, which is based on the magnetostratigraphic framework reported by Bowles (2006) and Westerhold et al. (2008) at Site 1262 (Appendix E).

Appendix C. Paleoecological preferences (depth habitats) of the planktic foraminiferal species recovered at Site 1262. References: a - Olsson et al. (1999); b - D'Hondt and Zachos (1993); c -

Huber and Boersma (1994); d - Boersma and Premoli Silva (1983); e - Koutsoukos (2014); f - Huber et al. (2020); g - Berggren and Norris (1997), h - Aze et al. (2011); i - Coxall et al. (2000). See equivalence with the taxonomy of Arenillas et al. (2021) in main text and in Appendix B.

Appendix D. Geochemical data for Site 1262: bulk sediment carbon and oxygen stable isotope measurements ($\delta^{13}C_{bulk}$ and $\delta^{18}O_{bulk}$); $CaCO_3$ content (%); Hg content (ppb); Total Organic Content (TOC, %); Mn content (ppm); stratigraphic position of Hg-rich intervals (gray shading), and Dan-C2 interval (yellow shading) and its CIEs (orange shading). Age calibration for each sample is showed, which is based on the magnetostratigraphic framework reported by Bowles (2006) and Westerhold et al. (2008) at Site 1262 (Appendix E).

Appendix E. Depth-age model for Hole 1262B, based tie points calibrated on 405 kyr eccentricity tunning (Dinarès-Turell et al. 2014; Woelders et al. 2017) but considering the lowermost Danian hiatus (see main text). The main micropaleontological and geochemical events recognized at Site 1262 are shown in depth scale (mcd), time-scale (Ma), and in kyr from the KPB. Remarks: Paleomagnetism framework for each sample follow Bowles (2006) and Westerhold et al. (2008).

CAPÍTULO 5 – REGISTROS DE MICROFÓSSEIS CALCÁRIOS E PALEOAMBIENTAIS NA BACIA DE NEUQUÉN AO LONGO DA TRANSIÇÃO CRETÁCEO-PALEOGENO (K-Pg)

Capítulo 5:

Calcareous microfossils and paleoenvironmental changes across the Cretaceous-Paleogene (K-Pg) boundary at the Cerro Azul Section, Neuquén Basin, Argentina”

R. M. Guerra, Andrea Concheyro, K. G. D. Kochhann, M. H.H. Bom, D. Ceolin, T. Musso, J. F. Savian, G. Fauth, foi publicado no periódico Palaeogeography, Palaeoclimatology, Palaeoecology.

Calcareous microfossils and paleoenvironmental changes across the Cretaceous-Paleogene (K-Pg) boundary at the Cerro Azul Section, Neuquén Basin, Argentina

Rodrigo M. Guerra[a,*], Andrea Concheyro[b,c], Karlos G. D. Kochhann[a], Marlone H. H. Bom[a], Daiane Ceolin[a], Telma Musso[d], Jairo F. Savian[e], Gerson Fauth[a]

[a]*Instituto Tecnológico de Paleoceanografia e Mudanças Climáticas (itt Oceaneon), UNISINOS, Av. UNISINOS, 950, 93022-750 - São Leopoldo, RS, Brazil*

[b]*Instituto Antártico Argentino (IAA), Buenos Aires, Argentina*

[c]*IDEAN-CONICET, Departamento de Ciencias Geológicas, Universidad de Buenos Aires, Pabellón II, Ciudad Universitaria, 1428 - Buenos Aires, Argentina*

[d]*CONICET, Instituto de Investigación y Desarrollo en Ingeniería de Procesos, Biotecnología y Energías Alternativas y Facultad de Ingeniería and Universidad Nacional del Comahue, Buenos Aires, 1400, 8300 - Neuquén, Argentina.*

[e]*Departamento de Geologia, Instituto de Geociências, Universidade Federal do Rio Grande do Sul, Av. Bento Gonçalves, 9500, 91501-970 Porto Alegre, Brazil*

[*]Corresponding author.

E-mail addresses: rmguerra@unisinos.br (R.M. Guerra), andrea@gl.fcen.uba.ar (A. Concheyro), kkochhann@unisinos.br (K.G.D. Kochhann), marloneb@unisinos.br (M.H.H. Bom), daiaceolin@unisinos.br (D. Ceolin), telma.musso@probien.gob.ar (T. Musso), gersonf@unisinos.br (G. Fauth).

Abstract

We investigate changes in calcareous nannofossil and ostracod communities, which reflect surface and bottom water conditions, respectively, across the Cretaceous-Paleogene transition (K-Pg) at the Cerro Azul Section, Jagüel Formation, Neuquén Basin, Argentina. The K-Pg transition at the Cerro Azul Section is characterized by calcareous nannofossil and ostracod turnovers, from assemblages dominated by Cretaceous forms to assemblages composed by incoming Danian taxa and several survivor species. These assemblage changes were associated with a collapse in carbonate production at the K-Pg boundary, probably related to a drop of surface water productivity, and a subsequent recovery in the early Danian, as suggested by carbonate content, log(Ba/Fe) and log(Ba/Ti) trends. During the Late Maastrichtian, peak relative abundances of *Eiffellithus* spp., just before the K-Pg transition, were probably related to enhanced surface water productivity. High abundances of *Cervisiella operculata* suggest decreased surface productivity during the earliest Danian. This surface productivity collapse may have reduced food availability in the benthic habitat, which probably led to the stablishment of Citherudiae-dominated ostracod assemblages. Upward in the section, increased relative abundances of *Braarudosphaera bigelowii*, are probably related to overall intensified weathering conditions and, consequently, increased continental runoff and fresh water input.

Keywords: Mass extinction, Maastrichtian, Danian, calcareous nannofossils, ostracods, South Atlantic

5.1 INTRODUCTION

The end of the Cretaceous is marked by a severe loss of diversity in marine and terrestrial environments during the K-Pg mass extinction event, one of the “big five” mass extinctions (e.g.,

Raup and Sepkoski, 1982; Sepkoski 1996). Its causes are usually associated to an asteroid impact (e.g., Alvarez et al., 1980; Kent, 1981; Bonté et al., 1984; Alvarez, 1987; Smit, 1990; Canudo et al., 1991; Olsoon et al., 1997; Schulte et al., 2010), volcanism (e.g., Keller et al., 2008; 2011; Font et al., 2011; 2018; Punekar et al., 2014; 2015; Abrajevitch et al., 2015) or multiple causal agents (Ward et al., 1995; Hallam, 2005; Alegret et al., 2012; Mateo et al., 2015; Renne et al., 2015). Therefore, the K-Pg boundary can be identified based on a combination of different observations, such as biostratigraphy, geochemical enrichments of platinum group elements (PGE) and of others elements, mainly iridium, of presumably extraterrestrial origin (e.g., Elliot et al.,1994, Goderis et al., 2013; Açikalin et al., 2015; Oca et al., 2015; 2017; Ibáñez-Insa et al., 2017).

In the marine pelagic ecosystem, planktic organisms were severely affected by the K-Pg event (e.g., Smit, 1982; Huber et al., 2002; Schulte et al., 2010, and references therein). For instance, calcareous nannofossil assemblages recorded a 93% species loss (Bown, 2005) and planktic foraminifera were also severely impacted, with only few species being unambiguously considered survivor taxa (e.g., Koutsoukos, 2014). In contrast, benthic foraminifera seem to have crossed the K-Pg transition with no major extinction (D'Hondt, 2005). How ostracod occurrences were affected by the K-Pg extinction event, however, remains unclear, since this group likely exhibited regional heterogeneities (Ceolin et al., 2016a; Yamaguchi et al., 2017).

The different responses of these microfossil groups to the K-Pg extinction event were likely related to the fact that they inhabited different environments in the water column. While benthic foraminifera and ostracods are affected by bottom water conditions, calcareous nannofossils and planktic foraminifera respond to changes in highly dynamic parameters of surface waters. Therefore, the impact of the K-Pg extinction event on microfossils assemblages can be assessed by correlating micropaleontological data to environmental reconstructions based on sedimentological

and geochemical analyses. Such reconstructions usually provide valuable information on changes in primary productivity (e.g., Faul et al., 2003; Hull and Norris, 2011; Lowery et al., 2018), sedimentary input, dissolved oxygen content of seawater (e.g., Shrivastava, et al., 2013; Oca et al., 2014; 2017; Rostami et al., 2018), paleotemperature (e.g., Woelders et al., 2017), among other parameters.

In order to recognize the effects of the K-Pg event in calcareous microfossils communities, each new section documented is a valuable contribution. The Cerro Azul Section (Neuquén Basin - Argentina) is one of the most complete records of the K-Pg boundary interval known from South America. Micropaleontological studies of the K-Pg section at the Cerro Azul Section are so far limited to initial observations on calcareous nannofossils assemblages (Musso et al., 2012) and ostracods taxonomy (Ceolin et al., 2015; 2016b). Besides, Sial et al. (2014) traced Hg anomalies, a proxy for volcanic activity, across the K-Pg boundary at the Cerro Azul Section.

Here, we present a detailed record of changes in calcareous nannofossil and ostracod assemblages across the K-Pg boundary at the Cerro Azul Section, and correlate them with geochemical and magnetic susceptibility data in order to constrain possible environmental drivers. This comprehensive characterization of the K-Pg transition at the Cerro Azul Section has the potential to advance our understanding of paleoenvironmental conditions that prevailed in the Southern Hemisphere, which has been limited by the low number of known K-Pg successions.

5.2 MATERIALS AND METHODS

5.2.1 Geological setting and sampling strategy

The Cerro Azul Section (38° 50’48” S, 67° 52’20” W) is located in the Neuquén Basin, where the Jagüel Formation crops out (Fig. 1). The Neuquén Basin is a sedimentary basin in western Argentina with deposits ranging in age from Upper Triassic to Paleogene. Three major sedimentary supercycles are represented in the filling of the basin: Jurásico (Late Triassic-Late Jurassic), Ándico (Late Jurassic-Early Cretaceous) and Riográndico (Late Cretaceous-Paleogene) (Groeber, 1929; 1946; 1953). The upper part of the Riográndico cycle comprises the Malargue Group, which is represented by the Jagüel, Roca and Carrizo (Pircala) Formations (late Maastrichtian-Paleocene). The Malargue Group represents the first Atlantic transgression into the basin (Wichmann, 1927; Bertels, 1979; Uliana and Dellape, 1981), during a time of relative tectonic quiescence and epeiric floodings that resulted from a sea level rise (Ramos and Ramos, 1979; Uliana and Biddle, 1988). During the time of deposition of the Malargue Group (Upper Cretaceous-lower Paleogene), the Neuquén Basin was a foreland basin closed off to the north and west, creating an embayment, and was dominated by tidal currents under an overall arid climate (Barrio, 1990).

The Jagüel Formation (Andreis et al., 1974) is characterized by a homogeneous fine-grained sedimentary succession, with fossils that indicate a late Maastrichtian to Danian age (Uliana and Dellape, 1981). An outer shelf depositional setting was assigned to the Jagüel Formation by Bertels (1969a), Andreis et al. (1974) and by Uliana and Dellape (1981). No evidence of currents is present, indicating that the Jagüel Formation sediments were deposited below the level of influence of normal-weather waves, largely from suspended material.

Within the Jagüel Formation, two fine-grained lithofacies were recognized (Musso et al., 2012): yellowish grey Maastrichtian calcareous mudstones and light olive grey Danian calcareous mudstones. X-ray diffraction analyses of whole rock samples show very similar composition for both lithofacies: clay minerals>>calcite>quartz>>feldspars>zeolites>cristobalite (Musso et al., 2012). The main clay minerals are interstratified illite/smectite (R0 type) and variable proportions of illite and kaolinite (Musso et al., 2012).

A total of 18 samples were collected from the Cerro Azul Section, spanning the yellow greyish calcareous mudstone in the uppermost Maastrichtian, overlaid by an olive grey calcareous mudstone at the base of the Paleocene (Fig. 1). We collected samples during two field campaigns. First, samples were collected with a 0.5-1.0 m spacing (Fig. 1). Following preliminary calcareous nannofossil biostratigraphy, the K/Pg boundary was located between 16.40 m (sample CA7) and 17.45 m sample CA17) in the section. Therefore, a second sampling campaign was performed to sample the stratigraphic interval between 16.40 and 17.45 m at 10 cm resolution (samples CA8 to CA16; Fig. 1). Our sampling strategy enables high-resolution paleoenvironmental reconstructions for the earliest Danian interval at the Neuquén Basin.

Figure 1 about here format portrait two columns.

5.2.2 Calcareous nannofossils

Samples were prepared following the smear-slide technique described in Bown and Young (1998), and analyzed using a petrographic microscope Zeiss Axio Imager A2, at 1000x magnification. In order to achieve a quantitative analysis of the assemblages, at least 400 specimens were counted per slide, followed by the scanning of three additional longitudinal traverses (~300 fields

of view), looking for rare taxa missing in the initial counts that were marked in the distribution table with "X". The counting of some species (e.g., *Cervisiella operculata* and *Braarudosphaera bigelowii*) was difficult since specimens were usually broken. For *C. operculata*, we followed the criteria of Gardin and Monechi (1998), counting as single specimens all fragments larger than 4 µm. For *B. bigelowii*, every pentalith constructed by more than three elements was considered a single specimen (Jiang and Gartner, 1986).

Preservation of calcareous nannofossils was evaluated under light microscope using qualitative criteria to assess the degree of etching and/or overgrowth, where: "Good" indicates specimens with little or no etching and/or overgrowth; "moderate" suggests that specimens exhibit moderate etching and/or overgrowth, but are still easily recognizable; and "poor" implies that specimens display extreme etching and/or overgrowth (Roth and Thierstein, 1972; Roth, 1983).

5.2.3 Ostracods

Each sample consisted of 20 g of sediments prepared according to the standard method to recover ostracods (Sohn et al., 1965, detailed in Slipper, 1997). Samples were washed through 63 and 180 µm sieves and then dried at 60°C. All ostracods were handpicked under a Zeiss V8 stereomicroscope from each grain size fraction (63-180 and >180 µm).

5.2.4 Carbonate content and total organic carbon and sulfur measurements

Approximately 10 g of each sample were ground in an agate mortar and dried at 40°C. Total carbon (TC) was measurement on ~0.26 g sediment aliquots, using a LECO SC 144 DR analyser at the Instituto Tecnológico de Paleoceanografia e Mudanças Climáticas (itt Oceaneon -

UNISINOS). For sulphur determination, the same amount (~0.26 g) of the catalyst vanadium pent-oxide was added to the sample. Total organic carbon (TOC) was determined in carbonate-free aliquots (~0.26 g) previously treated with hydrochloric acid (6 N). For calculation of carbonate content, we used the stoichiometric equation ($CaCO_3$ = (TC-TOC) x 8.333) (Stax and Stein, 1995). Four duplicate measurements give a standard error of 0.02% for TOC and 0.20% for $CaCO_3$.

5.2.5 XRF measurements

X-ray fluorescence (XRF) measurements were performed on ground sediments, using an Epsilon 1 PanAlytical XRF analyser at the itt Oceaneon – UNISINOS. Results were reported in raw counts per second (cps) and, subsequently, interpreted and discussed as logarithmic elemental ratios. Samples were measured at 10 kV (150 µA, no filter) for Al, Mg, Si; 12 kV (400 µA , Al-50 filter) for Ca, K, Ti and V; 20 kV (250 µA, Al-200 filter) for Co, Cr, Fe and Mn; 50 kV (100 µA, Ti filter) for Ba, Cu, Ni, Rb, Sr and Zr. Using these settings, measurement time was about six minutes per sample.

5.2.6 Magnetic susceptibility

Between 18 and 12 m at the Cerro Azul Section, 16 discrete samples of 8 cm^3 were collected in plastic cubic boxes for magnetic susceptibility (χ) measurements. These measurements were carried out at the Paleomagnetism Laboratory of the University of São Paulo (USPMag), Brazil. Magnetic susceptibility (χ) measurements were made with a MFK1-FA Multi-Function Kappabridge at two operating frequencies (976 and 15616 Hz; χ_{lf} and χ_{hf}, respectively), in a field of 200 A/m, and results are reported as mass-normalized values (m^3/kg). Frequency dependence (χ_{fd}) of magnetic susceptibility was measured in all samples in order to check for the occurrence

of superparamagnetic (SP) to stable single domain (SSD) particles (Dearing et al., 1996; Hrouda and Pokorný, 2012). The frequency dependence (%) was calculated from the difference between measurements at high and low frequencies [$\chi_{fd} = (\chi_{lf} - \chi_{hf}) / \chi_{lf}$].

5.3 RESULTS

5.3.1 Calcareous nannofossil biostratigraphy

The standard biozonations of Perch-Nielsen (1985) and Martini (1971) were applied for the Upper Cretaceous and Danian sections, respectively. When necessary, biozones were compared with the high latitude biozonation of Watkins et al. (1996). It was possible to identify two biostratigraphic zones/subzones at the Cerro Azul Section (Fig. 2), which are described below.

5.3.1.1 Latest Maastrichtian (Samples CA1 - CA8)

CC26b Subzone: The Cretaceous section was defined based on the occurrences of *Micula prinsii*, *Nephrolithus frequens* and *Prediscosphaera stoveri*. According to Perch-Nielsen (1985), the first occurrence (FO) of *M. prinsii* defines the base of the CC26b Subzone, latest Maastrichtian. *Micula prinsii* was only identified at the lowermost sample at our section, and its scarcity could be related to its mid to low-latitude paleobiogeographic preference (Perch-Nielsen et al., 1982). On the other hand, *N. frequens*, considered a high-latitude Late Maastrichtian species, shows low abundance at the Cerro Azul Section but it is present in most of the Cretaceous interval. The interval between samples CA2 to CA8 (Figs. 1 and 2), shows the higher abundances of *Prediscosphaera stoveri*, and probably can be assigned to the uppermost Maastrichtian *Prediscosphaera*

stoveri Acme Subzone of Watkins et al. (1996), between the onset of *P. stoveri* high abundances and the FO of *Biantholithus sparsus*.

5.3.1.2 Cretaceous-Paleogene boundary and Danian (Samples CA9 - CA18)

NP1 Zone: The definition of the base of the Danian Stage has changed over time. Martini (1971) suggested that the K-Pg transition was defined by the last occurrence (LO) of *Arkhangelskiella cymbiformis* and other Cretaceous species. Considering possible reworking of Cretaceous taxa in Danian samples, Perch-Nielsen (1971) and Romein (1979) suggested the FO of *Biantholithus sparsus* and the beginning of the *Cervisiella operculata* and/or *Braarudosphaera bigelowii* acme to mark the K-Pg transition. At the Cerro Azul Section, we defined the K-Pg boundary between samples CA8 and CA9 (Figs. 1 and 2), based on the FO of *B. sparsus* at 16.60 m (sample CA9). Furthermore, the FO of *Cruciplacolithus primus* at 18.45 m in the section suggests deposition within the mid/end of the NP1 Zone (Romein, 1979).

The placement of the K-Pg boundary at 16.65 m at the Cerro Azul Section is further supported by a peak in the log(Cr+Co)/Rb ratio, 5 cm above the boundary level (Fig. 2). Rb is assumed to mainly replace K in the structure of clay minerals (Calvert and Pedersen, 2007) and, therefore, is used to normalize Cr and Co counts for terrigenous influx. Meanwhile, Cr and Co are moderate siderophile elements (Goderis et al., 2013) with reported increased abundances in K-Pg ejecta layers related to the end-Cretaceous asteroid impact (Goderis et al., 2013; Açikalin et al., 2015; Oca et al., 2015).

Figure 2 about here format portrait two columns.

5.3.2 Calcareous microfossil assemblages

The Cerro Azul Section records diverse and well-preserved calcareous microfossil assemblages. We identified 99 species of calcareous nannofossils and 65 ostracod taxa (taxonomic study previously published in Ceolin et al., 2015; 2016b) with overall moderate to good preservation. Range charts with the complete stratigraphic distribution of calcareous nannofossils and ostracods at the Cerro Azul Section can be found as Online Supplementary data (Tables S1 and S2, respectively) and the most representative calcareous nannofossil and ostracod species mentioned in the text are illustrated in Figs. 3 and 4.

Maximum richness (taxa per sample) of calcareous nannofossils is 57 species in the lower part of the upper Maastrichtian section (13.65 m; sample CA3), while ostracods present a maximum of 25 species in the uppermost Maastrichtian section (16.40 m; sample CA7). Conversely, minimum calcareous nannofossils richness is 33 species in the middle of the Danian section (17.10 m; sample CA14), whereas the first Danian sample (16.60 m; CA9) is barren for ostracods.

Figures 3 and 4 about here format portrait two columns.

For further analysis, we added relative abundances of calcareous nannofossil and ostracod species into three distinctive species groups, according to their known stratigraphic occurrence (Fig. 2): Cretaceous taxa; survivor taxa; and incoming taxa. Similar species groups have been distinguished in most of the calcareous nannofossils studies over the K-Pg transition since Percival and Fischer (1977).

5.3.2.1 Cretaceous taxa

This group of species is considered to have become extinct before or at the end of the Maastrichtian. In fact, some species of the group show sporadic occurrences through the base of the Danian (see Online Supplementary Data Tables S1 and S2), probably due to reworking of Cretaceous sediments.

For calcareous nannofossils, the Cretaceous section is dominated by three groups of species: ***Micula* spp.** (66-90%), composed of *M. concava, M. cubiformis, M. murus, M. murus*/*prinsii, M. staurophora, M. swastica*, *M. premolisilvae* and *M. prinsii*; ***Prediscosphaera* spp.** (1-16%), including *P. cretacea, P. desiderograndis, P. grandis, P. majungae, P. microrhabdulina, P. spinosa* and *P. stoveri*; and ***Eiffellithus* spp.** (1-15%), comprising *E. gorkae, E. paralellus* and *E. turriseiffelii*. Other common species in the Late Maastrichtian assemblages are *Ahmuellerella octoradiata, Arkhangelskiella cymbiformis, Cribrosphaerella ehrenbergii* and *Kamptnerius magnificus* (see Online Supplementary Data Table S1).

Micula staurophora is the most abundant species at the Cerro Azul Section (49-79%). Although most of the Cretaceous taxa abruptly decline after the K-Pg boundary, *M. staurophora* is common above the boundary, with a trend of decreasing abundances toward the top of the section (Fig. 5). The Late Maastrichtian species *M. murus* and *M. prinsii* are overall rare and show discontinuous occurrences in the basal part of the section (12.50 to 15.15 m).

Prediscosphaera cretacea and *P. stoveri* prevail among the *Prediscosphaera* spp. group. Both species showed increased abundances, representing 10-16% of the assemblage, in the interval between 12.90 and 15.15 m. Upward in section, they decrease in abundance toward the uppermost Maastrichtian (Fig. 5).

The uppermost 1.35 m of the Cretaceous (samples CA5 to CA8) show the highest relative abundances of *Eiffellithus* species, ranging from 4 to 15% (Fig. 5). The most abundant species of the group is *E. gorkae*, usually smaller than 8 µm in size. *Eiffellithus paralellus* occurs only sporadically throughout the section. *Watznaueria barnesiae*, usually one of the most abundant Cretaceous species, is rare at the Cerro Azul Section, reaching only 1.6% of the assemblage at 13.65 m (see Online Supplementary Data Table S1).

The Cretaceous ostracod fauna is composed of 48 species and 28 genera. The most abundant family is Trachyleberididae, represented by the species *Apatoleberis noviprinceps, Cythereis rionegrensis, Keijia flexuosa, Nigeria punctata, Hystherocythereis attenuata, Mimicocythereis attilai, Paramunseyella epaphroditus, Actinocythereis tuberculata* and *Petalocythereis venusta.* The most abundant and richest interval in the Maastrichtian occurs at 16.40 m (sample CA7), recording the highest counts of *P. venusta, N. punctata, Sthenarocythereis erymnos, P. epaphroditus* and *M. attilai* (see Online Supplementary Data Table S2).

Figure 5 about here format portrait two columns.

5.3.2.2 Survivor taxa

Cretaceous species that survived into the Paleogene, with continuous occurrences and in some cases even displaying higher abundance in the Danian, are included in the group of survivor taxa.

Cervisiella spp. and *Braarudosphaera bigelowii* are the dominant calcareous nannofossil taxa in this group of species. The *Cervisiella* spp. group, representing calcareous dinoflagellate

cysts, is composed mainly of *Cervisiella operculata*. This taxon was rare during the Late Maastrichtian and increases in abundance just after the K-Pg boundary (Fig. 6), ranging from 19 to 70% of the total assemblage in the Danian. *Braarudosphaera bigelowii* was also rare during the Cretaceous, but reached higher relative abundances, up to 50%, during the Danian.

The relative abundances of *C. operculata* and *B. bigelowii* show opposite trends during the Danian. Where *C. operculata* exhibits high abundances, *B. bigelowii* decreases in content, and vice-versa (Fig. 6). *Cyclagelosphaera reinhardtii* is rare in the upper Maastrichtian interval but increases in abundance in the interval between 16.70 to 16.90 m, reaching 4-6% of the total assemblage. Other survivor species are *Biscutum castrorum, Cervisiella saxea, Goniolithus fluckigeri, Markalius apertus* and *Markalius inversus* (see Online Supplementary Data Table S1).

The ostracod fauna collapsed at the K-Pg boundary, as evidenced by the barren sample at 16.50 m. At 16.60 m (sample CA9), some of the Late Cretaceous species reappeared, displaying even higher relative abundances through the Danian, and are herein considered survivor taxa. These species are *Eucytherura stibaros, Argilloecia abnormalis, Henryhowella* (*Wichmannella) meridionalis, Cythereis trajectiones* and *Cytherella* spp. *Cytherella* was left in a multi specific category because most of specimens are juveniles, which are difficult to identify at species level. A single record of *Petalocythereis venusta* and *Actinocythereis tuberculata* just after the boundary, is probably related to reworking processes (see Online Supplementary Data Table S2).

Figure 6 about here format portrait two columns.

5.3.2.3 Incoming taxa

The Incoming taxa group consists of those species with first occurrences after the K-Pg boundary. For calcareous nannofossils, a total of 17 incoming taxa were identified, including *Biantolithus sparsus*, *Biscutum harrisonii*, *Braarudosphaera sequela*, *Cruciplacolithus primus*, *Lanternithus duocavus*, *Micrantholithus* spp., *Neochiastozygus* spp., *Neocrepidolithus* spp. and *Prinsius dimorphosus*. The ostracod incoming fauna is also characterized by 17 species in which the most abundant taxa are *Togoina argentinensis*, *Hemingwayella verrucosus* and *Paracypris bertelsae* (see Online Supplementary Data Table S1 and S2)

5.3.3 Geochemistry

The logarithmic ratio between XRF-derived Ca and terrigenous elements counts (Al, K, Ti, Si and Fe) precisely tracks variations in $CaCO_3$ content at the Cerro Azul Section (Fig. 5; Online Supplementary Data Table S3). $CaCO_3$ content shows an average value of 27% within Subzone CC26b, and drops markedly to 8.5% in the 5 cm above the K-Pg transition. Within Zone NP1, $CaCO_3$ content depicts a recovery trend to values of ~26% between 35 and 55 cm above the K-Pg boundary. TOC values are low at the studied section, with a maximum value of 0.4% within Zone NP1, 55 cm above the K-Pg transition (Fig. 5).

Elemental ratios of log(Ba/Fe) and log(Ba/Ti) show their highest values in the upper part of Subzone CC26b, at 15.15 m, and dropped after the K-Pg transition (lower part of Zone NP1; Figs. 5 and 6). Following the K-Pg transition, log(Ba/Fe) and log(Ba/Ti) depicted increased values between 17.00 and 17.10 m, before a second drop (Figs. 5 and 6). Log(K/Rb), log(K/Ti) and log(K/Fe) show overall lower mean values within Zone NP1 (Fig. 6), when compared to mean values within Zone CC26b.

5.3.4 Magnetic susceptibility

Magnetic susceptibility (χ) data from the Cerro Azul Section are provided in Online Supplementary Data Table S3 and illustrated in Fig. 5. Low frequency (χ_{lf}) values of Maastrichtian and Danian samples from the Cerro Azul Section vary between 7.25 x 10^{-8} m^3/kg and 1.50 x $10^{-7}m^3$/kg, with mean value of 1.02 x $10^{-7}m^3$/kg. High frequency (χ_{hf}) values for the same interval vary between 6.96 x 10^{-8} m^3/kg and 1.44 x 10^{-7} m^3/kg, with mean of 9.91 x 10^{-8} m^3/kg. Values of χ_{fd} are below 5% (Fig. 5), which suggest that SP grains do not control the assemblages of magnetic grains (Dearing et al., 1996). However, our results indicate a change in concentration of magnetic mineral along the Cerro Azul Section. The K-Pg boundary is marked by a positive shift in χ for both operating frequencies followed by a gradual increase in χ though the Danian (Fig. 5).

5.4 DISCUSSION

5.4.1 Calcareous nannofossil biostratigraphic relevance

Micula prinsii is rare at the Cerro Azul Section, with a few specimens identified at 12.5 m. Despite its low abundance, it is a remarkable finding because it confirms the presence of the Late Cretaceous CC26b Subzone in Argentina. The finding of *M. prinsii* is important to improve previous results in the area (e.g., Keller et al., 2007), since it confirms the occurrence of the K-Pg boundary interval in Argentina.

Furthermore, it was possible to report for the Cerro Azul Section the presence of two distinctive holococoliths described by Lees (2007) in Tanzania: *Calculites juliae* (Early Maastrichtian) and *Bilapillus wadeae* (Cenomanian-Santonian). Therefore, we can extend their biostratigraphic and paleobiogeographic ranges to the Late Maastrichtian of the South Atlantic Ocean.

5.4.2 Calcareous nannofossil paleoecology and paleoceanographic significance

Calcareous nannofossil assemblages at the Cerro Azul Section are characterized by a mix of high and mid latitude species. According to Perch-Nielsen et al. (1982), during the latest Maastrichtian, there was a mixing zone at ~40ºS in the South Atlantic Ocean (close to the Cerro Azul Section area) where cold surface currents coming from the south and the relatively warm waters from the north mixed. Assemblages compositions described at the Cerro Azul Section likely resulted from the mixing of different surface currents at this paleoceanographic front.

Figure 7 displays some important studies of calcareous nannofossils over the K-Pg transition worldwide. Most of the discussion is centered around these sections and all references are provided at the figure caption, so that we can refer solely to the locations in the text.

For the Late Maastrichtian interval, most of the species expected to be found at high latitudes occurred at the Cerro Azul Section (e.g. *Nephrolithus frequens*, *Cribrosphaerella daniae*, *Kamptnerius magnificus* and abundant *Prediscosphaera stoveri*). Few species with confirmed mid to low latitude preferences, such as *Micula murus, Micula prinsii* and some species of *Lithraphidites*, also occurred. The high abundance of *Micula staurophora* (~70%), in comparison with *Watznaueria barnesiae* (<1% in most of the samples) is noteworthy. Both species are well known to dominate Late Cretaceous assemblages worldwide. Usually *M. staurophora* was the dominant taxon at high latitudes, whereas *W. barnesiae* dominated at low latitudes, but both were scarce or absent at high southern latitudes (Wind, 1979).

Figure 7 about here format portrait two columns.

The paleobiogeographic distributions of *M. staurophora* and *W. barnesiae* could suggest that surface water temperature acted as a controlling factor. However, at the Cerro Azul Section, low abundances of *W. barnesiae* in comparison with *M. staurophora* were also likely influenced by the depositional environment. According to Watkins and Self-Trail (2005), *M. staurophora* was clearly more abundant in relatively proximal environments, while *W. barnesiae* preferred offshore settings. This interpretation is in accordance with an outer shelf depositional setting for the Jagüel Formation (Bertels, 1969a; Andreis et al., 1974; Uliana and Dellape, 1981). Comparable patterns of *M. staurophora*-dominated assemblages in the latest Maastrichtinan were described for a few onshore K-Pg sections, such as Hor Hahar (Israel), Braggs Section (Alabama), Bajada de Jagüel (Argentina), and Brazos River (Texas).

Increased abundances of *M. staurophora* have been also related to poor preservation and diagenetic biases due to its high resistance to dissolution (Hill, 1975; Thierstein, 1976; 1980; 1981; Eshet and Almogi-Labin, 1996). At the studied section, preservation does not seem to be an issue, since most species are well-preserved, including small, delicate and dissolution-prone forms (e.g. *Ahmuellerella octoradiata*, *Cribrosphaerella ehrenbergii*, *Eiffellithus turriseiffelii*, *Nephrolithus frequens*, *Prediscosphaera cretacea* and *P. stoveri*). Likewise, species richnesses in the uppermost Maastrichtian of the Cerro Azul Section (35-57 species) are similar to the ones described at El Kef (Tunisia) (45-65 species), one of the K-Pg sections with exceptionally well-preserved calcareous nannofossils (Pospichal, 1996a; Gardin and Monechi, 1998).

Therefore, the increased abundances of *M. staurophora* must reflect environmental conditions. Lees (2002) described changes in abundances of *M. staurophora* in both Austral and Tropical locations, and related its dominance to a probable r-selected ecological strategy. High *M. staurophora* relative abundances at the Cerro Azul Section are correlated with drops in the Shannon

diversity index (Fig. 5), suggesting that this species could indeed live in environments not suitable for other taxa.

Peak abundance of *Eiffellithus* spp. just before the K-Pg boundary at the Cerro Azul Section, correlates with relatively high log(Ba/Fe) and log(Ba/Ti) ratios, suggesting that it could be related to enhanced surface water productivity (Eshet and Almogi-Labin, 1996; Friedrich et al., 2005; Bernaola and Monechi, 2007; Thibault and Gardin, 2007) (Fig. 5; see Section 4.3). We used terrigenous elements, such as Fe and Ti, to normalize Ba counts and account for detrital Ba input. Therefore, we assume that changes in the log(Ba/Ti) and log(Ba/Fe) ratios reflect changes in the accumulation of biogenic Ba and, consequently, paleoproductivity (e.g., Calvert and Pedersen, 2007; Hull and Norris, 2011).

Within the Danian, assemblages at the Cerro Azul Section resemble high latitude ones, due to the consistent presence of *Neocrepidolithus* spp. and reduced abundances of mid to low latitude species, such as *Futyania petalosa* and *Neobiscutum* species. Nevertheless, we did not recover the high latitude species *Hornibrookina edwardsii*.

The succession just above the K-Pg boundary is characterized by a sequence of *Cervisiella operculata* and *Braarudosphaera bigelowii* high abundance intervals (Fig. 2), previously referred to as “blooms” or “acmes”. *Cervisiella* spp. (=*Thoracosphaera* of some authors) high abundance intervals in the earliest Danian were described for most of the Tethyan K-Pg sections (Agost; Biarritz; Bulgarian sections; Caravaca; Egyptian sections; Elles; El Kef; Hor Hahar; Italian sections; Lattengebirge), North Atlantic (DSDP Site 384; Beloc; Brazos River; El Mulato), South Atlantic (DSDP Sites 356 and 527; ODP Site 1262; Bajada de Jagüel), Pacific (DSDP Sites 465; 577) and Indian Ocean (ODP Sites 750; 752) sites. However, Southern Ocean ODP Sites 690 and 738, as

well as the Danish sections, do not present such pattern. *B. bigelowii* high abundances were probably restricted to epicontinental seas, such as the Bajada de Jagüel and Brazos River sections, as well as a few Tethyan sections (Agost; Biarritz; Bulgarian sections; Caravaca; Egyptian sections; El Kef and Italian sections), and a single open ocean location at DSDP Site 384.

The highest abundances of these species just after the K-Pg boundary seems to be a powerful tool for biostratigraphic and/or paleoceanographic interpretations. For instance, Tantawy (2003) suggested a subdivision of the Danian NP1 Zone based on the *Cervisiella* spp. (NP1a) and *Braarudosphaera bigelowii* (NP1b) increased abundances. Nevertheless, more high-resolution studies, ideally coupled to magnetostratigraphic analyses, are needed in order to test these propositions.

Cervisiella operculata is a dinoflagellate whose changes in abundances were probably driven by unusual environmental conditions, such as major changes in primary productivity and salinity fluctuations (Eshet et al., 1992; Gardin, 2002). During periods of environmental stress, this species had the ability to encyst and even proliferate in the absence of other competitors. A similar encystment refuge may be assumed for the calcareous nannofossil species *B. bigelowii* (Lamolda et al., 2016), however there may be other possible triggers for its increased abundances, such as shallow depositional environments, low salinity, increase in fresh-water influx or eutrophication (Bukry, 1974; Thierstein and Berger, 1979; Müller, 1985; Barrera and Keller, 1994; Cunha and Shimabukuro, 1997).

At the Cerro Azul Section, the onset of *C. operculata* high abundance was correlated to the collapse in primary productivity evidenced by the drops in log(Ba/Fe), log(Ba/Ti) and $CaCO_3$ (Fig. 6; see Section 4.3). This pattern suggests that *C. operculata* could colonize a “new” environment with reduced competition with other taxa. The post-K-Pg recovery in log(Ba/Ti) and log(Ba/Fe),

between 17.00 and 17.10 m, correlates to the interval of *B. bigelowii* increased abundances at the Cerro Azul Section, suggesting this species thrived under relatively higher primary productivity. Additionally, decreased mean log(K/Rb), log(K/Ti) and log(K/Fe) during the Danian suggest that intensified weathering conditions occurred at areas surrounding the Neuquén Basin and, consequently, increased continental runoff. In marine fine-grained siliciclastic sediments, K is mainly delivered as illite, which is a clay mineral formed at source regions under relatively dry climate conditions (e.g., Calvert and Pedersen, 2007; Croudace and Rothwell, 2015). Therefore, we interpreted drops in logarithmic ratios between K and typical terrigenous elements (Ti, Fe and Rb) as indicative of wetter climates. Furthermore, higher magnetic susceptibility (χ) values during the Danian, relative to the Maastrichtian values, suggest an increased contribution of terrigenous material, and whole-rock mineralogical analyses confirm the occurrence of illite at the Cerro Azul Section (Musso et al., 2012).

5.4.3 Ostracod paleoecology and paleoenvironmental significance

High abundances of the sthenohaline family Trachyleberididae during the Late Maastrichtian (Fig. 5) at the Cerro Azul Section, represented mainly by *Petalocythereis venusta*, *Apatoleberis noviprinceps*, *Hystherocythereis attenuata* and *Nigeria punctata*, suggest deposition in a shallow shelf setting (Bertels, 1975; Neale, 1975). These taxa present ornamented and robust carapaces, with ocular tubercles, indicating deposition within the photic zone (Morkhoven, 1962; Benson, 1974; Whatley 1983a; b; Fauth, 2000). According to Bertels (1975), during the Late Maastrichtian a deepening trend occurred in some parts of the Neuquén Basin, with significant occurrences of ostracods and foraminifera. Furthermore, increased abundances of Trachyleberididae correlate

with intervals characterized by high log(Ba/Ti) and log(Ba/Fe), which suggest enhanced primary productivity (Fig. 5).

Cytheruridae is the second most abundant family at the Cerro Azul Section. Taxa assigned to this family are characterized by small and thin carapaces, and inhabited mostly epineritic and eurihaline environment (Morkhoven, 1963). According to Ballent and Whatley (2009), in the Neuquén Basin, Cytheruridae were diverse in shelf settings during the Mesozoic, mainly in the Jurassic and early Cretaceous. Besides, this family thrived under warm-temperate water conditions, with normal salinity levels and a low energy regime (Ballent and Whatley, 2009).

The K-Pg boundary at the Cerro Azul Section is marked by the extinction of 22 ostracod species, suggesting that, at least in shallow marine environments, these organisms were severely affected by the event (Fig. 2; Online Supplementary Data Table S2). Previous studies in the Neuquén Basin (Bertels, 1969b) recognized the extinction of virtually all ostracod species at the K-Pg boundary level, which were replaced by an incoming Danian fauna. At the Cerro Azul Section, the succession after the boundary depicts a recovery phase, expressed as increasing abundances of Trachyleberididae, Cytheruridae and Cytherellidae taxa (Figs. 5 and 6).

Within the Danian interval of the Cerro Azul Section, the highest abundance of the Cytheruridae, just above the K-Pg boundary, can be correlated with the *Cervisiella operculata* high abundance interval and a decrease of the log(Ba/Ti) and log(Ba/Fe) ratios, suggesting a link to low surface primary productivity and decreased food supply to the seafloor (Figs. 5 and 6). According to Dingle (1984), increased abundances of Cytheruridae could also indicate stressing environmental conditions which were common during the recovery phase after the K-Pg boundary.

Despite the lower abundance and richness of ostracod species in the Danian, in comparison with the Maastrichtian, the dominance of the family Trachyleberididae at the Cerro Azul Section

agrees with patterns described for other K-Pg sections in South America (e.g., Poty quarry - Fauth et al., 2005; Paraíba Basin - Lima Barros et al., 2018) and could indicate the establishment of more stable environmental conditions during the post-extinction recovery phase. Increased abundances of cytherellids (Fig. 6) in the recovery phase could indicate enhanced primary productivity, as suggested by Santos Filho et al. (2017) for the Turonian-Coniacian, which is herein supported by increased $CaCO_3$ content and high log(Ba/Fe) and log(Ba/Ti) ratios at the Cerro Azul Section. This family occurs associated with the highest abundances of *Paracypris bertelsae* and *Argilloecia abnormalis*, which are smooth marine species characteristic of mid to outer neritic environments and outer carbonate plataforms (Babinot and Colin, 1983; Piovesan et al., 2009; Santos Filho et al., 2017).

5.4.4 Primary productivity and carbonate production during the K-Pg transition

Geochemical and paleontological data presented herein point to a collapse of primary productivity and, consequently, carbonate production at the K-Pg boundary at the Cerro Azul Section. This interpretation is supported by marked drops in $CaCO_3$ content, log(Ba/Fe) and log(Ba/Ti) that followed the K-Pg boundary (5 cm above the transition). This interval is also marked by relatively high magnetic susceptibility values (Fig. 5) that, in deeper marine settings, generally mark clay intervals just above the K-Pg boundary (e.g., Font et al., 2018 and references therein). The drops in log(Ba/Fe), log(Ba/Ti) and carbonate content at the K-Pg boundary were followed by a recovery phase between 45 and 55 cm above the boundary level, which is also reflected in enhanced TOC concentrations of the sediments. Similar paleoproductivity recovery patterns, which followed the K-Pg boundary, were described in other oceanic regions (Hull and

Norris, 2011; Lowery et al., 2018); however, its timing relative to the boundary level at the Cerro Azul Section remains unclear from our data.

As reported by Hull and Norris (2011), paleoproductivity reconstructions across the K-Pg boundary in the South Atlantic Ocean point to an asymmetric pattern, with a drop in paleoproductivity occurring in the western South Atlantic (São Paulo Plateau) and no changes recorded in the central South Atlantic (Walvis Ridge). Our results support the drop in primary and/or export productivity at the K-Pg boundary in the western South Atlantic Ocean reported by Hull and Norris (2011). However, our record depicts an early Danian paleoproductivity recovery phase that is not seen at the São Paulo Plateau record.

5.5 CONCLUSIONS

The Cerro Azul Section provides a continuous record of the K-Pg transition in a shallow marine setting of the Atlantic marine incursion into the Neuquén Basin. The occurrence of *Micula prinsii* in the section, reported herein for the first time in the Neuquén Basin, confirms the occurrence of the K-Pg transition at the Cerro Azul Section, based on calcareous nannofossils biostratigraphy. Calcareous nannofossil species that were previously reported only for Tanzanian and Danish Late Cretaceous sections, such as *Calculites juliae* and *Bilapillus wadeae*, have their paleobiogeographic ranges herein expanded to the western South Atlantic Ocean. Ostracod assemblages were severely affected by the K-Pg boundary event, suggesting that at least in shallow marine environments these organisms were impacted by changes in environmental parameters.

The paleoenvironmental effects of the K-Pg boundary event are evidenced by both micropaleontological and geochemical data at the Cerro Azul Section. Geochemical data depict a

drop of surface productivity and, consequently, carbonate production at the K-Pg transition, followed by a recovery phase in the early Danian. Calcareous nannofossil taxa included in *Eiffellithus* spp. display increased relative abundances in the latest Maastrichtian, when surface water productivity was probably high. Conversely, high abundances of *Cervisiella operculata* and the ostracod family Cytheruridaein the earliest Danian were coupled with drops in surface water productivity. This interval was followed by increased relative abundances of *Braarudosphaera bigelowii*, which correlate with periods of enhanced weathering intensity and, consequently, continental runoff/freshwater input. An environmental recovery phase after the K-Pg boundary can also be inferred from increased abundances of the ostracod families Trachyleberididae and Cytherellidae.

Acknowledgements

This study was partly financed by the Coordenação de Aperfeiçoamento de Pessoal de Nível Superior - Brasil (CAPES) - finance codes 88.887.111026/2015-00 and IODP/CAPES 8888.091703/2014-01. The authors would like to thank David K. Watkins and one anonymous reviewer for constructive comments on the manuscript, as well as, the Paleomagnetism Laboratory of the University of São Paulo (USPMag), Brazil, for magnetic susceptibility analyses and the Instituto Tecnológico de Paleoceanografia e Mudanças Climáticas (itt Oceaneon - UNISINOS), for geochemical analyses. JFS thanks the National Council for Scientific and Technological Development (CNPq) grants #304022/2018-7; #427280/2018-4, and Fundação de Amparo à Pesquisa do Estado do Rio Grande do Sul (FAPERGS) grant #16/2551-0000213-4. This is contribution R-360 of the Instituto de Estudios Andinos “Don Pablo Groeber” (UBA- CONICET). GF is greatfull for collaboration in the project CNPq (309918/2015-4).

5.6 REFERENCES

Abrajevitch, A., Font, E., Florindo, F., Roberts, A.P., 2015. Asteroid impact vs. Deccan eruptions: the origin of low magnetic susceptibility beds below the Cretaceous-Paleogene boundary revisited. Earth and Planetary Science Letters. 430, 209-223.

Açikalin, S., Vellekoop, J., Ocakoglu, F., Yilmaz, I.O., Smit, J., Altiner, S.Ö., Goderis, S., Vonhof, H., Speijer, R.P., Woelders, L., Fornaciari, E., Brinkhuis, H., 2015. Geochemical and paleontological characterization of a new K-Pg boundary locality from the Northern branch of the Neo-Tethys: Mudurnu - Göynük Basin, NW Turkey. Cretaceous Research. 52, 251-267.

Aguado, R., Lamolda, M.A., Maurrasse, J-M.R., 2005. Nanofósiles del límite Cretácico/Terciario cerca Beloc (Haití): bioestratigrafia, composición de las asociaciones e implicaciones paleoclimáticas. Journal of Iberian Geology. 31(1), 9-24.

Alegret, L., Thomas, E., Lohmann, K.C., 2012. End-Cretaceous marine mass extinction not caused by productivity collapse. Proceedings of the National Academy of Sciences. 109, 728-732.

Alvarez, L.W., 1987. Mass extinctions caused by large bolide impacts. Physics Today. 87, 25-33.

Alvarez, L.W., Alvarez, W., Asaro, F., Michel, H.V., 1980. Extraterrestrial cause for the Cretaceous-Tertiary extinction. Science. 208, 1095-1108.

Andrade, G.C.C., 2010. Nanofósseis Calcários do Maastrichtiano Superior ao Daniano do Poço Poty, Bacia Paraíba, Nordeste do Brasil. Master dissertation, Universidade Federal de Pernambuco. 102 p.

Andreis, R., Iñíguez Rodríguez, A., Lluch, J., Sabio, D., 1974. Estudio sedimentológico de las formaciones del Cretácico superior del área del Lago Pellegrini (provincia de Río Negro, República Argentina). Revista de la Asociación Geológica Argentina. 29(1), 85-104.

Babinot, J.F., Colin, J.P., 1983. Marine late cretaceous ostracode faunas from southwestern Europe: a paleoecological synthesis, in: Maddocks, R.F. (Ed.), Applications of Ostracoda. University of Houston Geosciences, pp. 394-399.

Ballent, S.C., Whatley, R.C., 2009. Taxonomy and zoogeography of the Mesozoic Cytherurid ostracoda from west-central Argentina. Palaeontology. 52(1), 193-218.

Barrera, E., Keller, G., 1994. Productivity across the K/T boundary in high latitudes. Geological Society of America Bulletin. 106, 1254-1266.

Barrio, C.A., 1990. Late Cretaceous-Early Tertiary sedimentation in a semi-arid foreland basin (Neuquén basin, western Argentina). Sedimentary Geology. 66, 255-275.

Benson, R.H., 1974. The role of ornamentation in the design and function of the ostracoda carapace. Geoscience and Man. 6, 47-57.

Bernaola, G., Monechi, S., 2007. Calcareous nannofossil extinction and survivorship across the Cretaceous-Paleogene boundary at Walvis Ridge (ODP Hole 1262C, South Atlantic Ocean). Palaeogeography, Palaeoclimatology, Palaeoecology. 255(1-2), 132-156

Bertels, A., 1969a. Estratigrafía del límite Cretácico-Terciario en la Patagonia septentrional. Revista de la Asociación Geológica Argentina. 24, 41-54.

Bertels, A., 1969b. Micropaleontologia y Estratigrafia Del Limite Cretacico-Terciario em Huantrai-co (Provincia del Neuquén). Ostracoda. Parte II. Ameghiniana. 6(4), 253-290.

Bertels, A., 1975. Ostracode ecology during the Upper Cretaceous and Cenozoic in Argentina. Bulletins of American Paleontology. 65 (282), 317-351.

Bertels, M., 1979. Paleobiogeografia de los foraminiferos del Cretácico superior y Cenozoico de América del Sur. Ameghiniana. 16(3/4), 273-356

Bonté, P., Delacotte, O., Renard, M., Laj, C., Boclet, D., Jehanno, C., Rocchia, R., 1984. An iridium rich layer at the Cretaceous/Tertiary boundary in the Bidart section (southern France). Geophysics Research Letters. 11, 473-476.

Bown, P.R., 2005. Calcareous nannoplankton evolution: a tale of two oceans. Micropaleontology. 51, 299-308.

Bown, P.R., Young, J.R., 1998. Techniques, in: Bown, P.R. (Ed.), Calcareous Nannofossil Biostratigraphy. British Micropalaeontological Society Series. Chapman and Hall/Kluwer Academic Publishers, London, pp. 16-28.

Bukry, D., 1973. Coccolith and silicoflagellate stratigraphy, Tasman Sea and southwestern Pacific Ocean, Deep Sea Drilling Project, Leg 21. Initial Reports of the DSDP. 21, 885-893.

Bukry, D., 1974. Coccoliths as paleosalinity indicators: evidence from Black Sea. AAPG Memoir. 20, 353-363.

Calvert, S.E., Pedersen, T.F., 2007. Elemental proxies for palaeoclimatic and palaeoceanographic variability in marine sediments: interpretation and application, in: Hillaire-Marcel, C., De Vernal, A. (Eds.), Proxies in Late Cenozoic Paleoceanography. Developments in Marine Geology, Vol 1, Elsevier, pp. 567-644.

Canudo, J.I., Keller, G., Molina, E., 1991. Cretaceous/Tertiary boundary extinction pattern and faunal turn over at Agost and Caravaca, S.E. Spain. Marine Micropaleontology. 17, 319-341.

Ceolin, D., Whatley, R.C., Fauth, G., Concheyro, A., 2015. New genera and species of Ostracoda from the Maastrichtian and Danian of the Neuquén Basin, Argentina. Papers in Palaeontology. 1(4), 425-495.

Ceolin, D., Bergue, C.T., Fauth, G., 2016a. Stratigraphic resolution and the K-Pg ostracode record, in: Khosla, A., Lucas, S.G. (Eds.), Cretaceous Period: biotic diversity and biogeography. New Mexico Museum of Natural History and Science Bulletin, pp. 75-83.

Ceolin, D., Whatley, R.C., Fauth, G., Concheyro, A., 2016b. The Nodoconchiinae, a new subfamily of Cytheridae (Crustacea, Ostracoda). Journal of Micropalaeontology. 35, 90-101.

Claeys, A., Kiessling, W., Alvarez, W., 2002. Distribution of Chicxulub ejecta at the Cretaceous-Tertiary boundary, in: Koeberl, C., MacLeod, K.G. (Eds.), Catastrophic Events and Mass Extinctions: Impacts and Beyond. Geological Society of America, Special Papers. 356, 55-68.

Croudace, I.W., Rothwell, R.G., 2015. Future developments and innovations in high-resolution core scanning, in: Croudace, I.W., Rothwell, R.G. (Eds.), Micro-XRF studies of sediment cores: applications of a non-destructive tool for the environmental sciences. Developments in Paleoenvironmental Research. 17, 627-647.

Cunha, A.S., Shimabukuro, S., 1997. *Braarudosphaera* blooms and anomalous enrichments of *Nannoconus*: evidence from the Turonian South Atlantic, Santos Basin, Brazil. Journal of Nannoplankton Research. 19, 51-55.

D'Hondt, S., 2005. Consequences of the Cretaceous/Paleogene mass extinction for marine ecosystems. Annual Review of Ecology, Evolution, and Systematics. 36, 295-317.

Dearing, J.A., Dann, R.J.L., Hay, K., Lees, J.A., Loveland, P.J., Maher, B.A., O'Grady, K., 1996. Frequency-dependent susceptibility measurements of environmental materials. Geophysical Journal International. 124(1), 228-240.

Del Río, C.J., Concheyro, A., Martínez, S.A., 2011. The Maastrichtian-Danian at General Roca (Patagonia, Argentina): a reappraisal of the chronostratigraphy and biostratigraphy of a type locality. Neues Jahrbuch für Geologie und Paläontologie, Abhandlungen. 259, 129-156.

Dingle, R.V., 1984. Mid-Cretaceous ostracoda from southern Africa and the Falkland Plateau. Annals of the South American Museum. 93(3), 98-211.

Ehrendorfer, T., Aubry, M-P., 1992. Calcareous nannoplankton changes across the Cretaceous/Paleocene boundary in the Southern Indian Ocean (ODP Site 750A). Proceedings of the ODP, Scientific Results. 120, 451-470.

Elliot, D.H., Askin, R.A., Kyte, F.T., Zinsmeister, W.J., 1994. Iridium and dinocysts at the Cretaceous-Tertiary boundary on Seymour Island, Antarctica: Implications for the K-T event. Geology. 22, 675-678.

Eshet, Y., Almogi-Labin, A., 1996. Calcareous nannofossil as paleoproductivity indicators in Upper Cretaceous organic rich sequences in Israel. Marine Micropaleontology. 29, 37-61.

Eshet, Y., Moshkovitz, S., Habid, D., Benjamii, C., Magatitz, M., 1992. Calcareous nannofossil and dinoflagellate stratigraphy across the Cretaceous/Tertiary boundary at HorHahar, Israel. Marine Micropaleontology. 18, 199-228.

Faris, M., Ghandour, I.M., Maejima, W., 2007. Calcareous nannofossils and mineralogical changes across the Cretaceous/Paleogene boundary at Wadi Nukhul, Southwestern Sinal, Egypt. Journal of Geosciences. 50, 15-34.

Faul, K. L., L. D. Anderson, and M. L. Delaney., 2003. Late Cretaceous and early Paleogene nutrient and paleoproductivity records from Blake Nose, western North Atlantic Ocean, Paleoceanography, 18(2), 1042.

Fauth, G., 2000. The Cretaceous-Tertiary boundary ostracods from Poty Quarry, Pernambuco-Paraíba Basin, northeastern Brazil: systematics, biostratigraphy, paleoecology and palaeobiogeography. Ph.D. thesis, University of Heidelberg. 170p.

Fauth, G., Colin, J.-P., Koutsoukos, E.A.M., Bengtson, P., 2005. Cretaceous-Tertiary boundary ostracods from Poty quarry, Pernambuco, northeastern Brazil. Journal of South American Earth Sciences. 19, 285-305.

Font, E., Nedelec, A., Ellwood, B.B., Mirao, J., Silva, P.F., 2011. A new sedimentary benchmark for the Deccan Traps volcanism? Geophysical Research Letters. 38, L24309.

Font, E., Adatte, T., Andrade, M., Keller, G., Bitchong, A.M., Carvalho, C., Ferreira, J., Diogo, Z., Mirão, J., 2018. Deccan volcanism induced high-stress environment during the Cretaceous-Paleogene transition at Zumaia, Spain: Evidence from magnetic, mineralogical and biostratigraphic records. Earth and Planetary Science Letters. 484, 53-66.

Fornaciari, E., Giusberti, L., Luciani, V., Tateo, F., Agnini, C., Backman, J., Oddone, M., Rio, D., 2007. An expanded Cretaceous-Tertiary transition in a pelagic setting of the Southern Alps (central-western Tethys). Palaeogeography, Palaeoclimatology, Palaeoecology. 255, 98-131.

Friedrich, O., Herrle, J.O., Hemleben, C., 2005. Climatic changes in the Late Campanian-Early Maastrichtian: micropaleontological and stable isotopic evidence from an epicontinental sea. Journal of Foraminiferal Research. 35(3), 228-247.

Gardin, S., 2002. Late Maastrichtian to early Danian calcareous nannofossils at Elles (Northwest Tunisia). A tale of one million years across the K-T boundary. Palaeogeography, Palaeoclimatology, Palaeoecology. 178, 211-231.

Gardin, S., Monechi, S., 1998. Paleoecological change in middle to low latitude calcareous nannoplankton at the Cretaceous-Tertiary boundary. Bulletin de la Societe Geologique de France. 169, 709-723.

Goderis, S., Tagle, R., Belza, J., Smit, J., Montanari, A., Vanhaecke, F., Erzinger, J., Claeys, Ph., 2013. Reevaluation of siderophile element abundances and ratios across the Cretceous-Paleogene

(K-Pg) boundary: implications for the nature of the projectile. Geochimica et Cosmochimica Acta. 120,417-446.

Groeber, P., 1929. Líneas fundamentales de la Geología del Neuquén, sur de Mendoza, y regiones adyacentes. Publicación de la Dirección de Minas, Geología e Hidrología. 58, 1-10.

Groeber, P., 1946. Observaciones geológicas a lo largo del meridiano 70°. Hoja Chos Malal. Revista de la Asociación Geológica Argentina. 1, 177-208.

Groeber, P., 1953. Mesozoico. En: Geografía de la República Argentina. Sociedad Argentina de Estudios Geográficos GAEA. 2(1), 1-141.

Hallam, T., 2005. Catastrophes and lesser calamities: the Causes of mass extinctions. Oxford University Press, New York, 226 p.

Henriksson, A.S., 1996. Calcareous nannoplankton productivity and succession across the Cretaceous-Tertiary boundary in the Pacific (DSDP Site 465) and Atlantic (DSDP Site 527) Oceans. Cretaceous Research. 17, 451-477.

Herm, Von D., Hillebrandy, A.V., Perch-Nielsen, K., 1981. Die Kreide/Tertiär-Grenze im Lattengebirge (Nördliche Kalkalpen) in mikropaläontologischer Sicht. Geologica Bavarica. 82, 319-344.

Hill, M.E., 1975. Selective dissolution of Mid-Cretaceous (Cenomanian) calcareous nannofossils. Micropaleontology. 21(2), 227-235.

Hrouda, F., Pokorný, J., 2012. Modelling accuracy limits for frequency dependent anisotropy of magnetic susceptibility of rocks and soils. Studia Geophysica et Geodaetica. 56, 789-802.

Huber, B.T., Watkins, D.K., 1992. Biogeography of Campanian-Maastrichtian calcareous plankton in the region of the Southern Ocean: paleogeographic and paleoclimatic implications, in: The Antarctic paleoenvironment: a perspective on global change. Antarctic Research Series. 56, 31-60.

Huber, B.T., MacLeod, K.G., Norris, R.D., 2002, Abrupt extinction and subsequent reworking of Cretaceous planktonic foraminifera across the Cretaceous-Tertiary boundary: Evidence from the subtropical North Atlantic, in: Koeberl, C., MacLeod, K.G. (Eds.), Catastrophic Events and Mass Extinctions: Impacts and Beyond. Geological Society of America, Special Papers. 356, 277-289.

Hull, P.M., Norris, R.D., 2011. Diverse patterns of the ocean export productivity change across the Cretaceous-Paleogene boundary: new insights from biogenic barium. Paleoceanography. 26, PA3205.

Ibáñez-Insa, J., Pérez-Cano, J., Fondevilla, V., Oms, O., Rejas, M., Fernández-Turiel, J.L., Anadón, P., 2017. Portable X-ray fluorescence identification of the Cretaceous-Paleogene boundary: Application to the Agost and Caravaca sections, SE Spain. Cretaceous Research. 78, 139-148.

Jiang, M.J., Gartner, J., 1986. Calcareous nannofossil succession across the Cretaceous/Tertiary boundary in east-central Texas. Micropaleontology. 32(3), 232-255.

Keller, G., Adatte, T., Tantawy, A.A., Berner, Z., Stueben, D., 2007. High stress Late Cretaceous to early Danian paleoenvironment in the Neuquén Basin, Argentina. Cretaceous Research. 28, 939-960.

Keller, G., Adatte, T., Gardin, S., Bartolini, A., Bajpai, S., 2008. Main Deccan volcanism phase ends near the K-T boundary: evidence from the Krishna-Godavari Basin, SE India. Earth and Planetary Science Letters. 268, 293-311.

Keller, G., Rhowmick, P.K., Upadhyay, H., Dave, A., Reddy, A.N., Jaiprakash, B.C., Adatte, T., 2011. Deccan volcanism linked to the Cretaceous-Tertiary boundary mass extinction: new evidence from ONGC Wells in the Krishna-Godavari Basin. Journal Geological Society of India. 78, 399-428.

Kent, D.V., 1981. Asteroid extinction hypothesis. Science, 650, 211.

Lamolda, M.A., Melinde-Dobrinescu, M., Kaiho, K., 2016.Calcareous nannoplankton assemblage changes linked to paleoenvironmental deterioration and recovery across the Cretaceous-Paleogene boundary in the Betic Cordillera (Agost, Spain). Palaeogeography, Palaeoclimatology, Palaeoecology. 411(3), 438-452.

Koutsoukos, E.A.M., 2014. Phenotypic plasticity, speciation, and phylogeny in early Danian planktic foraminifera. Journal of Foraminiferal Research. 44, 109-142.

Lees, J.A., 2002. Calcareous nannofossil biogeography illustrates palaeoclimate change in the Late Cretaceous Indian Ocean. Cretaceous Research. 23, 537-634.

Lees, J.A., 2007. New and rarely reported calcareous nannofossils from the Late Cretaceous of coastal Tanzania: outcrop samples and Tanzania Drilling Project Sites 5, 9 and 15. Journal of Nannoplankton Research. 29(1), 39-65.

Lees, J.A., Bown, P.R., Young, J.R., Riding, J.B., 2004. Evidence for annual records of phytoplankton productivity in the Kimmeridge Clay Formation coccolith stone bands (Upper Jurassic, Dorset, UK). Marine Micropaleontology. 52, 29-49.

Lima Barros, C., Piovesan, E.K., Agostinho, S.M.O., 2018. Cretaceous-Paleogene ostracods from the Paraíba Basin, northeastern Brazil. Journal of South American Earth Sciences. 83, 117-136.

Lowery, C.M., Bralower, T.J., Owens, J.D., Rodríguez-Tovar, F.J., Jones, H., Smit, J., Whalen, M.T., Claeys, Ph., Farley, K., Gulick, S.P.S., Morgan, J.V., Green, S., Chenot, E., Christeson, G.L., Cockell, C.S., Coolen, M.J.L, Ferrière, L., Gebhardt, C., Goto, K., Kring, D.A., Lofi, J., Ocampo-Torres, R., Perez-Cruz, L., Pickersgill, A.E., Poelchau, M.H., Rae, A.S.P., Rasmussen, C., Rebolledo-Vieyra, M., Riller, U., Sato,H., Tikoo, S.M., Tomioka, N., Urrutia-Fucugauchi, J., Vellekoop, J., Wittmann, A., Xiao, L., Yamaguchi, K.E., Zylberman, W., 2018. Rapid recovery of life at ground zero of the end-Cretaceous mass extinction. Nature. 558, 288-291.

Martini, E., 1971. Standard Tertiary and Quaternary calcareous nannoplankton zonation. Proceedings of the 2nd Planktonic Conference, Roma, 739-785.

Mateo, P., Keller, G., Adatte, T., Spangenberg, J.E., 2015. Mass wasting and hiatuses during the Cretaceous-Tertiary transition in the North Atlantic: relationship to the Chicxulub impact? Palaeogeography, Palaeoclimatology, Palaeoecology. 441(1), 96-115.

Monechi, S., 1977. Upper Cretaceous and Early Tertiary nannoplankton from the Scaglia Umbra Formation (Gubbio, Italy). Revista Italiana di Paleontologia. 83, 759-802.

Monechi, S., 1985. Campanian to Pleistocene calcareous nannofossils stratigraphy from the northwest Pacific Ocean, Deep Sea Drilling Project Leg 86. Initial Reports of the DSDP. 86, 301-336.

Morkhoven, F.P.C.M. van., 1962. Post-Palaeozoic Ostracoda: their morphology, taxonomy and economic use. Elsevier Publishing Company, Amsterdam-London-New York, 1, 204 p.

Morkhoven, F.P.C.M. van., 1963. Post-Palaeozoic Ostracoda: their morphology, taxonomy and economic use. Elsevier Publishing Company, Amsterdam-London-New York, 2, 478 p.

Moshkovitz, S., Habib, D., 1993. Calcareous nannofossil and dinoflagellate stratigraphy of the Cretaceous-Tertiary boundary, Alabama and Georgia. Micropaleontology. 39(2), 167-191.

Müller, C., 1985. Biostratigraphic and paleoenvironmental interpretation of the Goban Spur region based on a study of calcareous nannoplankton. Initial Reports of the DSDP. 80, 573-599.

Musso, T., Concheyro, A., Pettinari, G., 2012. Mineralogía de arcillas y nanofósiles calcáreos de las formaciones Jagüel y Roca em el sector oriental del lago Pellegrini, Cuenca Neuquina, República Argentina. Andean Geology. 39(3), 511-540.

Neale, J., 1975. The ostracod fauna from the Santonian chalk (Upper Cretaceous) of Gingin, Western Australia. Special Papers in Palaeontology. 16, 1-111.

Oca, C.S-M., Rodríguez-Tovar, F.J., Martínez-Ruiz, F., 2014. Distribución de metals traza en sedimentos del límite Cretácico-Paleógeno: implicaciones paleoambientales. Macla. 19, aa-zz.

Oca, C.S-M., Rodríguez-Tovar, F.J., Martínez-Ruiz, F., 2015. Geochemical and isotopic characterization of trace fossil infillings: New insights on trace marker activity after the K-Pg impact event. Cretaceous Research. 57, 391-401.

Oca, C.S-M., Rodríguez-Tovar, F.J., Martínez-Ruiz, F., Monaco, P., 2017. Paleoenvironmental conditions across the Cretaceous-Paleogene transition at the Apennines sections (Italy): An integrated geochemical and ichnological approach. Cretaceous Research. 71, 1-13.

Olsoon, R.K., Miler, K.G., Browning, J.V., Habib, D., Sugarman, P.J., 1997. Ejecta layer at the Cretaceous-Tertiary boundary, Bass River, New Jersey (Ocean Drilling Program Leg 174AX). Geology. 25(8), 759-762.

Perch-Nielsen, K., 1971. Neue Coccolithenaus dem Paleozän von Dänemark, der Bucht von Biskaya und dem Eozän der Labrador See. Bulletin of the Geological Society of Denmark. 21, 51-66.

Perch-Nielsen, K., 1977. Albian to Pleistocene calcareous nannofossils from the Western South Atlantic, DSDP Leg 39. Initial Reports of the DSDP. 39, 699-823.

Perch-Nielsen, K., 1979a. Calcareous nannofossils at the Cretaceous/Tertiary boundary near Biarritz, France, in: Christensen, W.K., Birkelund, T. (Eds.), Cretaceous-Tertiary boundary events, Volume II, Copenhagen (University of Copenhagen), pp. 151-155.

Perch-Nielsen, K., 1979b. Calcareous nannofossils in Cretaceous/Tertiary boundary sections in Denmark, in: Christensen, W.K., Birkelund, T. (Eds.), Cretaceous-Tertiary boundary events, Volume II, Copenhagen (University of Copenhagen), pp. 120-126.

Perch-Nielsen, K., 1985. Mesozoic calcareous nannofossils, in: Bolli, H.M., Saunders, J.B., Perch-Nielsen, K. (Eds), Plankton Stratigraphy. Cambridge University Press, Cambridge 1, 329-426.

Perch-Nielsen, K., McKenzie, J., He, Q., 1982. Biostratigraphy and isotope stratigraphy and the "catastrophic" extinction of calcareous nannoplankton at the Cretaceous/Tertiary boundary, in: Silver, L.T., Schultz, P.H. (Eds.), Geological Implications of Impacts of Large Asteroids and Comets on the Earth. Geological Society of America, Special Papers. 190, 353-371.

Percival, S.F., Fischer, A.G., 1977. Changes in calcareous nannoplankton in the Cretaceous-Tertiary biotic crisis at Zumaya, Spain. Evolutionary Theory. 2, 1-35.

Piovesan, E.K., Bergue, C.T., Fauth, G., 2009. Cretaceous ostracodes from Pará-Maranhão Basin, Brazil: taxonomy and preliminary paleoecological and paleobiogeographical inferences. Revue de Paléobiologie. 28(2), 437-456.

Pospichal, J.J., 1991. Calcareous nannofossils across Cretaceous/Tertiary boundary at Site 752, eastern Indian Ocean. Proceedings of the ODP, Scientific Results. 121, 395-413.

Pospichal, J.J., 1996a. Calcareous nannoplankton mass extinction at the Cretaceous/Tertiary boundary: an update, in: Ryder, G., Fastovsky, D., Gartner, S. (Eds.), The Cretaceous-Tertiary boundary event and other catastrophes in Earth history. Geological Society of America, Special Papers. 307, 335-360.

Pospichal, J.J., 1996b. Calcareous nannofossils and clastic sediments at the Cretaceous-Tertiary boundary, northeastern Mexico. Geology. 24(3), 255-258.

Pospichal, J.J., Bralower, T.J., 1992. Calcareous nannofossils across the Cretaceous/Tertiary boundary, Site 761, northwest Australian margin. Proceedings of the ODP, Scientific Results. 122, 735-751.

Pospichal, J.J., Wise, S.W., 1990. Calcareous nannofossils across the K/T boundary, ODP hole 690C, Maud Rise, Weddell Sea. Proceedings of the ODP, Scientific Results. 113, 515-532.

Punekar, J., Mateo, P., Keller, G., 2014. Effects of Deccan volcanism on paleoenvironment and planktic foraminifera: a global survey. Geological Society of America, Special Papers. 505, 91-116.

Punekar, J., Keller, G., Khozyem, H.M., Adatte, T., Font, E., Spangenberg, J., 2015. A multi-proxy approach tode code the end-Cretaceous mass extinction. Palaeogeography, Palaeoclimatology, Palaeoecology. 441(1), 116-136.Ramos, E.D., Ramos, E.D., Ramos, V.A., 1979. Los ciclos magmáticos de la República Argentina. Actas VII Congreso Geológico Argentino. 1, 771-796.

Raup, D.M., Sepkoski, J.J.Jr., 1982. Mass extinction in the marine fossil record. Science. 215, 1501-1503.

Renee, P.R., Sprain, C.J., Richards, M.A., Self, S., Vanderkluysen, L., Pande, K., 2015. State shift in Deccan volcanism at the Cretaceous-Paleogene boundary, possibly induced by impact. Science. 350, 76-78.

Romein, A.J.T., 1977. Calcareous nannofossils from the Cretaceous/Tertiary boundary interval in the Barranco del Gredero (Caravaca, Prov. Murcia, SE Spain). Proceedings of the Koninklijke Nederlandse Akademie ven Wetenschappen Amsterdam. Serie B, 80(4), 256-279.

Romein, A.J.T., 1979. Lineages in Early Paleocene nannoplankton. Utrecht Micropaleontological Bulletins. 22, 18-22.

Rostami, M.A., Leckie, R.M., Font, E., Frontalini, F., Finkelstein, D., Koeberl, C., 2018. The Cretaceous-Paleogene transition at Galanderud (northern Alborz, Iran): a multidisciplinary approach. Palaeogeography, Palaeoclimatology, Palaeoecology. 493, 82-101.

Roth, P.H., 1983. Jurassic and Lower Cretaceous calcareous nannofossils in the Western North Atlantic (Site 534): biostratigraphy, preservation, and some observations on biogeography and paleoceanography. Initial Reports of the DSDP. 76, 587-621.

Roth, P.H., Thierstein, H., 1972. Calcareous nannoplankton: Leg 14 of the Deep Sea Drilling Project. Initial Reports of the DSDP. 14, 421-485.

Santos Filho, M.A.B., Fauth, G., Piovesan, E.K., 2017. Cretaceous ostracods of the Barreirinhas Basin: taxonomy, biostratigraphic considerations and paleoenvironmental inferences. Journal of South American Earth Sciences. 73, 130-152.

Schulte, P., Alegret, L., Arenillas, I., Arz, J.A., Barton, P.J., Bown, P.R., Bralower, T.J.,Christeson, G.L., Claeys, P., Cockell, C.S., Collins, G.S., Deutsch, A., Goldin, T.J., Goto, K., Grajales-Nishimura, J.M., Grieve, R.A.F., Gulick, S.P.S., Johnson, K.R., Kiessling, W., Koeberl, C., Kring, D.A., MacLeod, K.G., Matsui, T., Melosh, J., Mon-tanari, A., Morgan, J.V., Neal, C.R., Nichols, D.J., Norris, R.D., Pierazzo, E., Ravizza, G., Rebolledo-Vieyra, M., Reimold, W.U., Robin, E., Salge, T., Speijer, R.P., Sweet, A.R., Urrutia-Fucugauchi, J., Vajda, V., Whalen, M.T., Willumsen, P.S., 2010. The Chicxulub asteroid impact and mass extinction at the Cretaceous-Paleogene boundary. Science. 327, 1214-1218.

Sepkoski, J.J.Jr., 1996. Patterns of Phanerozoic extinctions: a perspective from global data bases, in: Walliser, O.H. (Ed.), Global Events and Event Stratigraphy. Springer, Berlin, pp. 35-52.

Shrivastava, J.P., Mukhopadhyay, S.K., Pal, S., 2013. Chemico-mineralogical attributes of clays from the late Cretaceous-early Paleogene succession of the Um Sohryngkew river section of Meghalaya, Índia: palaeoenvironmental inferences and the K-Pg boundary. Cretaceous Research. 45, 247-257.

Sial, A.N., Chen, J., Lacerda, L.D., Peralta, S., Gaucher, C., Frei, R., Cirilli, S., Ferreira, V.P., Marquillas, R.A., Barbosa, J.A., Pereira, N.S., Belmino, I.K.C., 2014. High-resolution Hg chemostratigraphy: A contribution to the distinction of chemical fingerprints of the Deccan volcanism and Cretaceous-Paleogene Boundary impact event. Palaeogeography, Palaeoclimatology, Palaeoecology. 414, 98-115.

Slipper, I.J., 1997. Turonian (Late Cretaceous) ostracoda from Dover, south-east England (BL). Ph.D. thesis, University of Greenwich. 433 p.

Smit, J., 1982. Extinction and evolution of planktonic foraminifera after a major impact at the Cretaceous/Tertiary boundary, in: Silver, L.T., Schultz, P.H. (Eds.), Geological Implications of Impacts of Large Asteroids and Comets on the Earth. Geological Society of America, Special Papers. 190, 329-352.

Smit, J., 1990. Meteorite impact, extinctions and the Cretaceous-Tertiary Boundary. Geologie en Mijnbouw. 69, 187-204.

Sohn, I.G., Berclan, J.M., Peck, R.E., 1965. Ostracods, in: Kummel, B., Raup. D. (Eds.), Handbook of paleontological techniques. W.H. Freeman and Company, San Francisco, pp. 77-89.

Stax, R., Stein, R., 1995. Data report: organic carbon and carbonate records from Detroit seamount and Patton-Murray seamount: results from sites 882 and 887 (north Pacific Transect). Proceedings of the ODP, Scientific Results. 145, 645-655.

Stoykova, K., Ivanov, M., 2004. Calcareous nannofossils and sequence stratigraphy of the Cretaceous/Tertiary transition in Bulgaria. Journal of Nannoplankton Research. 26(1), 47-61.

Tantawy, A.A.A.M., 2003. Calcareous nannofossil biostratigraphy and paleoecology of the Cretaceous-Tertiary transition in the central eastern desert of Egypt. Marine Micropaleontology. 47, 323-356.

Tantawy, A.A., 2011. Calcareous nannofossils across the Cretaceous-Tertiary boundary at Brazos, Texas, U.S.A.: extinction and survivorship, biostratigraphy, and paleoecology, in: Keller, G., Adatte, T. (Eds.), The End-Cretaceous Mass Extinctions and the Chixculub Impact in Texas, SEPM Special Publications. Volume 10, 157-178.

Thibault, N., Gardin, S., 2006. Maastrichtian calcareous nannofossil biostratigraphy and paleoecology in the Equatorial Atlantic (Demerara Rise, ODP Leg 207 Hole 1258A). Revue de Micropaleontology. 49, 199-214.

Thibault, N., Gardin, S., 2007. The Late Maastrichtian nannofossil record of climate change in the South Atlantic DSDP Hole 525A. Marine Micropaleontology. 65, 163-184.

Thierstein, H.R., 1976. Mesozoic calcareous nannoplankton biostratigraphy of marine sediments. Marine Micropaleontology. 1, 325-362.

Thierstein, H.R., 1980. Selective dissolution of Late Cretaceous and Earliest Tertiary calcareous nannofossils: experimental evidence. Cretaceous Research. 2,165-176.

Thierstein, H.R., 1981. Late Cretaceous Nannoplankton and the change at the Cretaceous-Tertiary boundary. SEPM Special Publication. 32, 355-394.

Thierstein, H.R., Berger, W., 1979. On phanerozoic mass extinctions. Naturwissenschaften. 66, S46.

Thierstein, H.R., Okada, H., 1979. The Cretaceous/Tertiary boundary event in the North Atlantic. Initial reports of the DSDP. 43, 601-616.

Uliana, M.A., Biddle, K.T., 1988. Mesozoic-Cenozoic paleogeographic and geodynamic evolution of southern South America. Revista Brasileira de Geociências. 18(2), 172-190.

Uliana, M., Dellapé, D., 1981. Estratigrafía y evolución paleoambiental de la sucesión Maastrichtiano- Eoterciaria del engolfamiento neuquino (Patagonia Septentrional). Actas VIII Congreso Geológico Argentino. 3, 673-711.

Ward, W.C., Keller, G., Stinnesbeck, W., Adatte, T., 1995, Yucatán subsurface stratigraphy: implications and constraints for the Chicxulub impact. Geology. 23, 876-877.

Watkins, D.K., Self-Trail, J.M., 2005. Calcareous nannofossil evidence for the existence of the Gulf Stream during the Maastrichtian. Paleoceanography 20, PA3006, doi:10.1029/2004PA001121.

Watkins, D.K., Wise, S.W., Pospichal, J.J., Crux, J., 1996. Upper Cretaceous calcareous nannofossil biostratigraphy and paleoceanography of the Southern Ocean, in: Moguilevsky, A., Whatley, R. (Eds.), Microfossils and Oceanic Environments. University of Wales, Aberystwyth Press, pp. 355-381.

Whatley, R., 1983a. The application of ostracoda to palaeoenvironmental analysis, in: Maddocks, R.F. (Ed.), Applications of Ostracoda. University of Houston Geosciences, pp. 51-77.

Whatley. R., 1983b. Some simple procedures for enhancing the use of ostracoda in palaeoenvironmental analysys. Norwegian petroleum Directorate Bulletin. 2, 129-145.

Wichmann, R., 1927. Los estratos con Dinosaurios y su techo en el Este del Territorio del Neuquén. Dirección General de Minería, Geología e Hidrología. 32, 3-25.

Wind, F.H., 1979. Maestrichtian-Campanian nannofloral provinces of the southern Atlantic and Indian oceans, in: Talwani, M., Hay, W., Ryan, W.B.F. (Eds.), Deep Sea Drilling Results in the Atlantic Ocean: continental margins and paleoenvironment, pp. 123-137.

Woelders, L., Vellekoop, J., Kroon, D., Smit, J., Casadío, S., Pràmparo, M.B., Dináres-Turell, J., Peterse, F., Sleijs, A., Lenaertz, J.T.M., Speijer, R.P., 2017. Latest Cretaceous climatic and environmental change in the South Atlantic region. Paleoceanography, 32, 466–483.

Yamaguchi, T., Bornemann, A., Matsui, H., Nishi, H., 2017. Latest Cretaceous-Paleocene deep-sea ostracode fauna at IODP Site U1407 (western North Atlantic) with special reference to the Cretaceous/Paleogene boundary and the Latest Danian Event. Marine Micropaleontology. 135, 32-44

Figure 1: A: Location of the Cerro Azul Section in Argentina; B: studied stratigraphic section with the position of samples (empty circles) used for micropaleontological, geochemical and paleomagnetic analyses. Stratigraphic intervals marked with “X” denote levels covered by soil. Map modified from Del Río et al. (2011) and section modified from Musso et al. (2012).

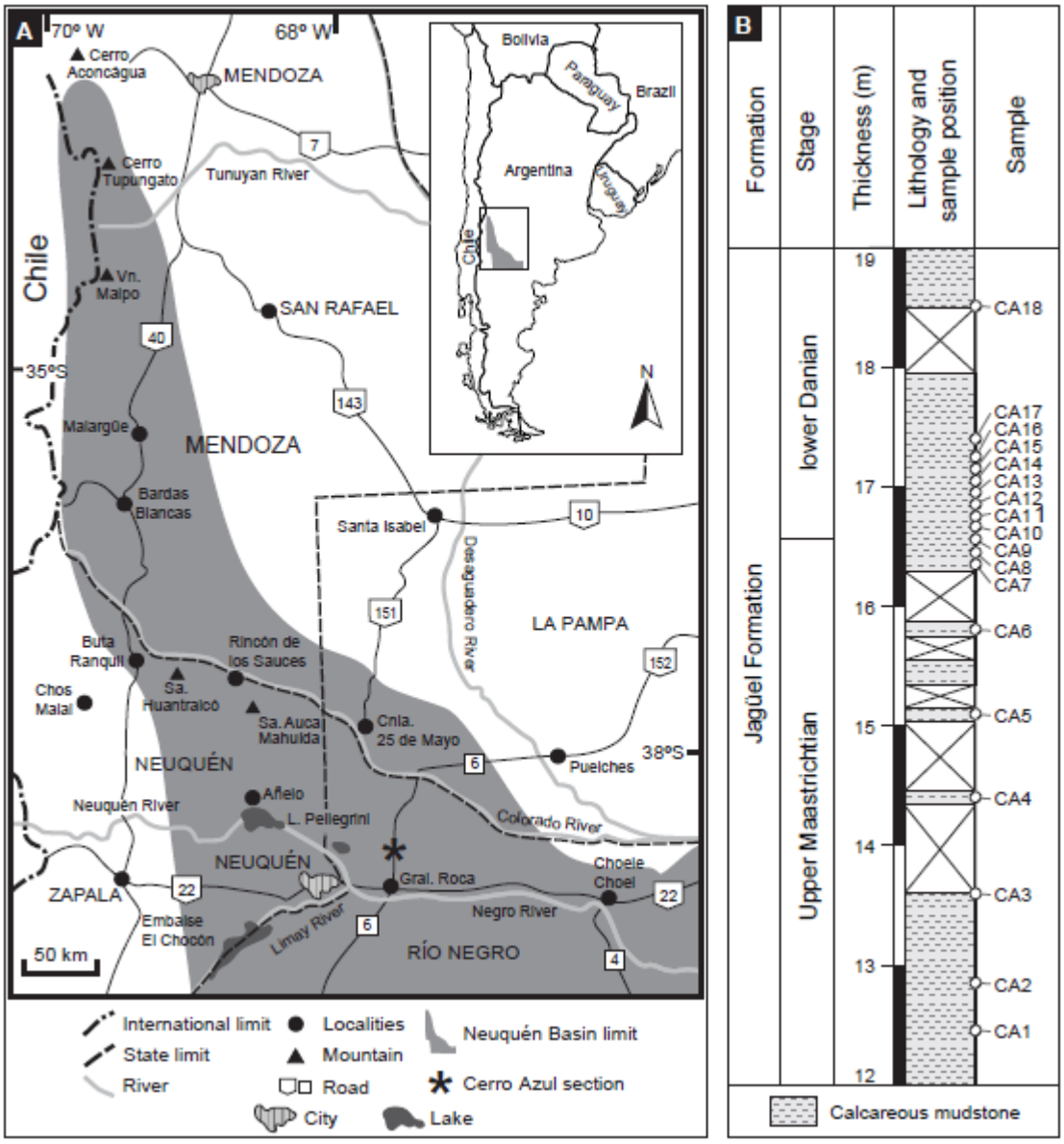

Figure 2: Stratigraphic succession at the Cerro Azul Section with stratigraphic ranges of selected calcareous nannofossil species, relative abundances of cretaceous, survival and incoming calcareous nannofossil and ostracod taxa, calcium carbonate content ($CaCO_3$) of sediments and the log(Cr+Co)/Rb ratio (a tracer for siderophile elements content in the sediments). Empty circles denote the position of samples within the section.

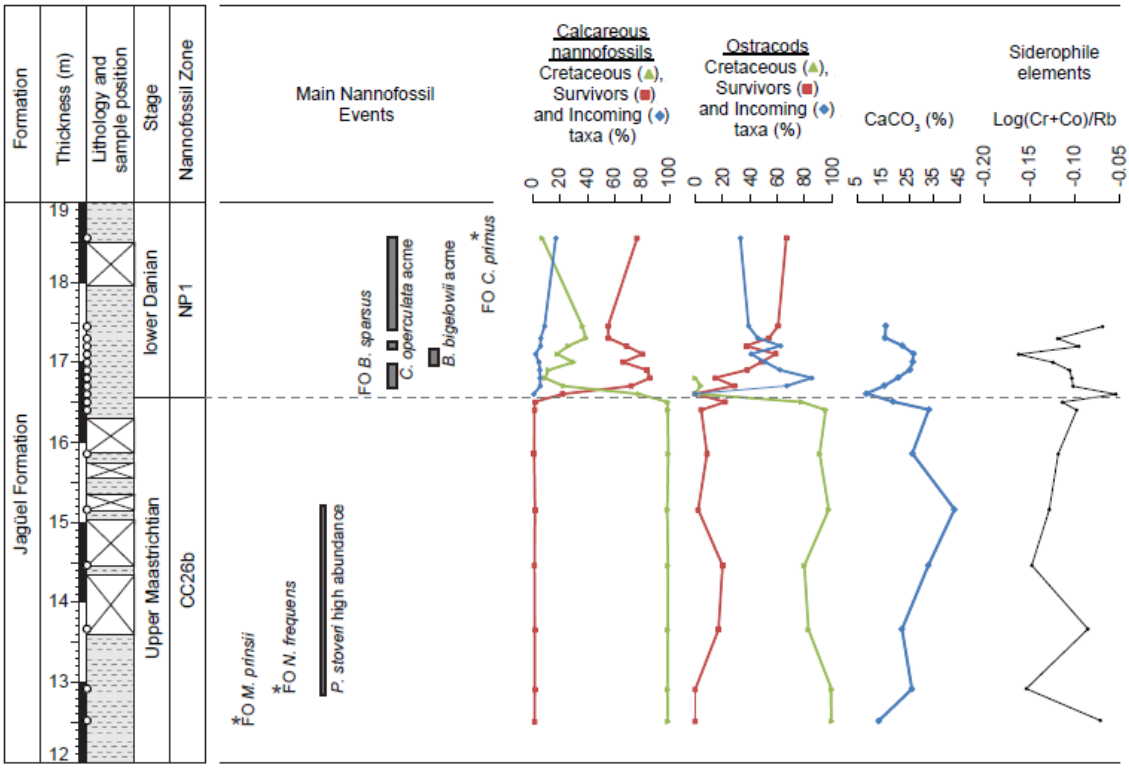

Figure 3: Representative calcareous nannofossils species from the Cerro Azul Section. 1, *Micula staurophora* (sample CA4); 2, *Watznaueria barnesiae* (sample CA3); 3/4, *Calculites juliae* (sample CA3); 5/6, *Bilapillus wadeae* (sample CA4); 7/8, *Nephrolithus frequens* (sample CA7); 9/10, *Micula prinsii* (sample CA1); 11/12, *Prediscosphaera stoveri* (sample CA2); 13, *Braarudosphaera bigelowii* (sample CA14); 14, *Cervisiella operculata* (sample CA11); 15, *Cyclagelosphaera reinhardtii* (sample CA11); 16, *Zeugrhabdotus sigmoides* (sample CA18); 17/18, *Biantholithus sparsus* (sample CA9); 19/20, *Cruciplacolithus primus* (sample CA18). Scale bars represent 5 µm

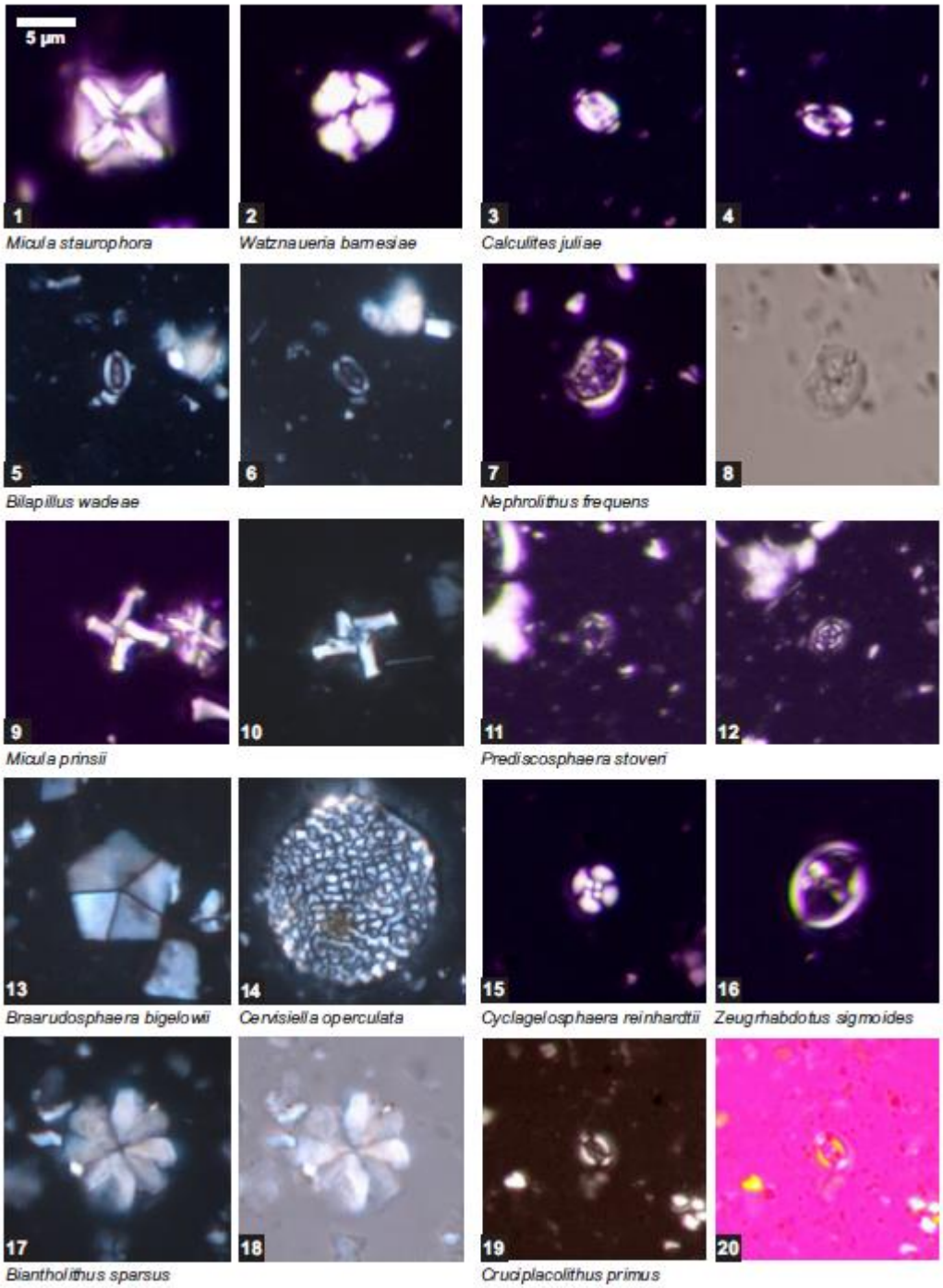
5 µm
1
Micula staurophora
2
Watznaueria barnesiae
3
Calculites juliae
4
5
Bilapillus wadeae
6
7
Nephrolithus frequens
8
9
Micula prinsii
10
11
Prediscosphaera stoveri
12
13
Braarudosphaera bigelowii
14
Cervisiella operculata
15
Cyclagelosphaera reinhardtii
16
Zeugrhabdotus sigmoides
17
Biantholithus sparsus
18
19
Cruciplacolithus primus
20

Figure 4: Representative ostracod species from the Cerro Azul Section. Cretaceous taxa: 1, *Actinocythereis tuberculata*; 2, *Petalocythereis venusta*; 3, *Mimicocythereis atillai*; 4, *Nigeria punctata*; 5, *Paramunseyella epaphroditus*; 6, *Apatoleberis noviprinceps*; 7, *Cytheropteron translimitares*; 8, *Hystherocythereis attenuata*. Survivor taxa: 9, *Henryhowella* (*Wichmannella*) *meridionalis*; 10, *Eucytherura stibaros*; 11, *Argilloecia abnormalis*; 12, *Cythereis trajectiones*. Incomming taxa: 13, *Togoina argentinensis*; 14, *Heinia prostratopleuricos*; 15, *Hemingwayella verrucosus*; 16, *Nodoconcha polytorosa*; 17, *Nodoconcha upsilon*; 18, *Paracypris bertelsae*; 19, *Paracypris imaguncula*; 20, *Cythereis stratios*. All scale bars represent 100 µm, except those in B, D and E that represent 20 µm.

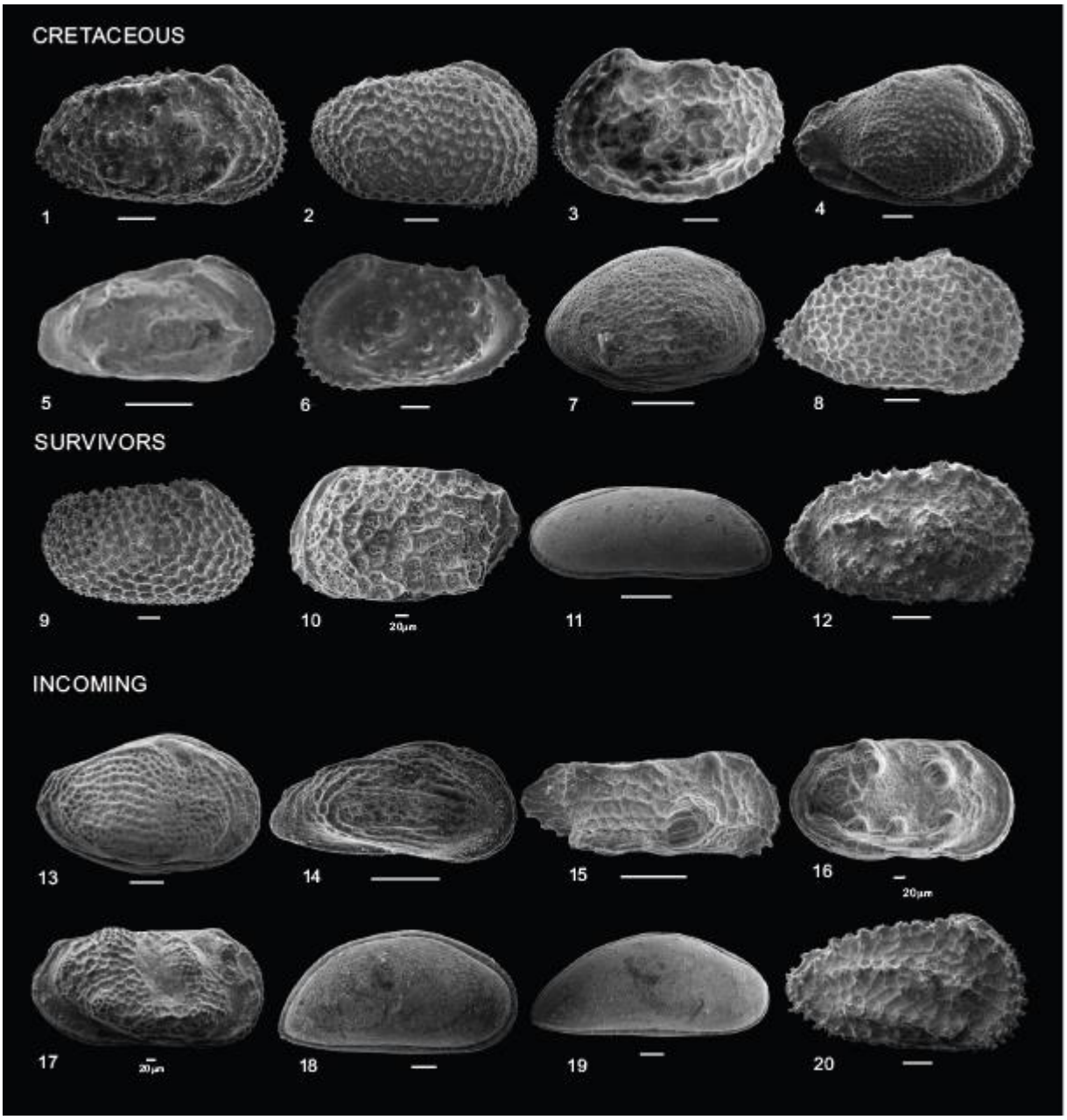
CRETACEOUS
1
2
3
4
5
6
7
8
SURVIVORS
9
10
20µm
11
12
INCOMING
13
14
15
16
20µm
17
20µm
18
19
20

Figure 5: Micropaleontological, geochemical and magnetic data throughout the K-Pg transition at the Cerro Azul Section. Geochemical data are: A: Total organic carbon (TOC) content; B: calcium carbonate content ($CaCO_3$ - light green curve) and log(Ca/Al+K+Ti+Si+Fe) ratio (log(Ca/Terr.) - dark green curve); C: Log(Ba/Ti) (red curve) and log(Ba/Fe) (orange curve) ratios; D: Magnetic susceptibility (χ_{hf} - light blue; χ_{lf} - dark blue); E: Log(K/Ti) (light magenta), log(K/Rb) (dark magenta) and log(K/Fe) (blue-magenta) ratios; Micropaleontological data are: F: Calcareous nannofossil Shannon diversity; G: Relative abundance of *Micula staurophora*; H: relative abundances of *Cervisiella operculata* (blue curve) and *Braarudosphaera bigelowii* (red curve); I: relative abundances of *Eiffellithus* spp. (blue curve) and *Prediscosphaera* spp. (red curve); J: Absolute abundances of Cytheruridae (blue curve), Trachyleberididae (black curve) and Cytherellidae (red curve). Empty circles denote the position of samples within the section. Terr.: terrigenous.

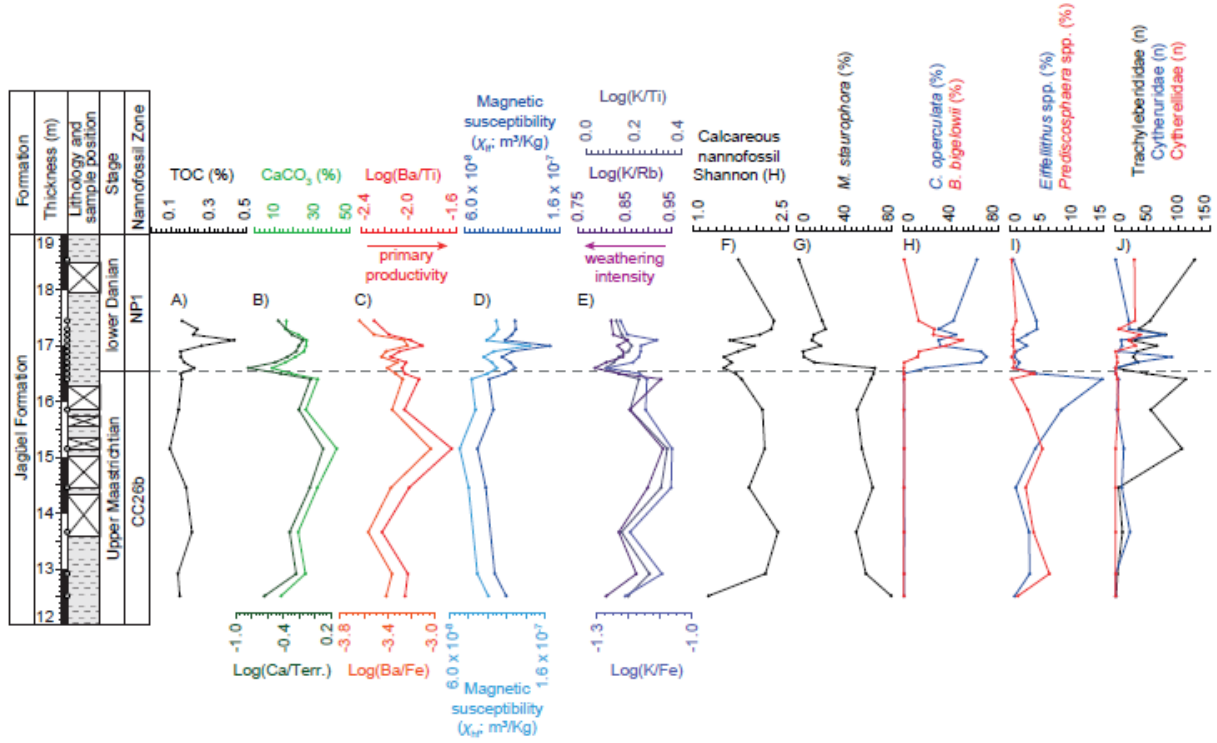

Figure 6: Expanded view of selected micropaleontological and geochemical data over the K-Pg transition and Danian recovery phase at the Cerro Azul Section. A: relative abundances of *Cervisiella operculata* and *Braarudosphaera bigelowii*; B: Absolute abundances of Cytheruridae, Trachyleberididae and Cytherellidae; C: calcium carbonate content ($CaCO_3$) and log(Ca/Al+K+Ti+Si+Fe) ratio (log(Ca/Terr.)); D: Log(Ba/Ti) and log(Ba/Fe) ratios; Curves colors as in Fig. 5. Empty circles denote the position of samples within the section. Terr.: terrigenous.

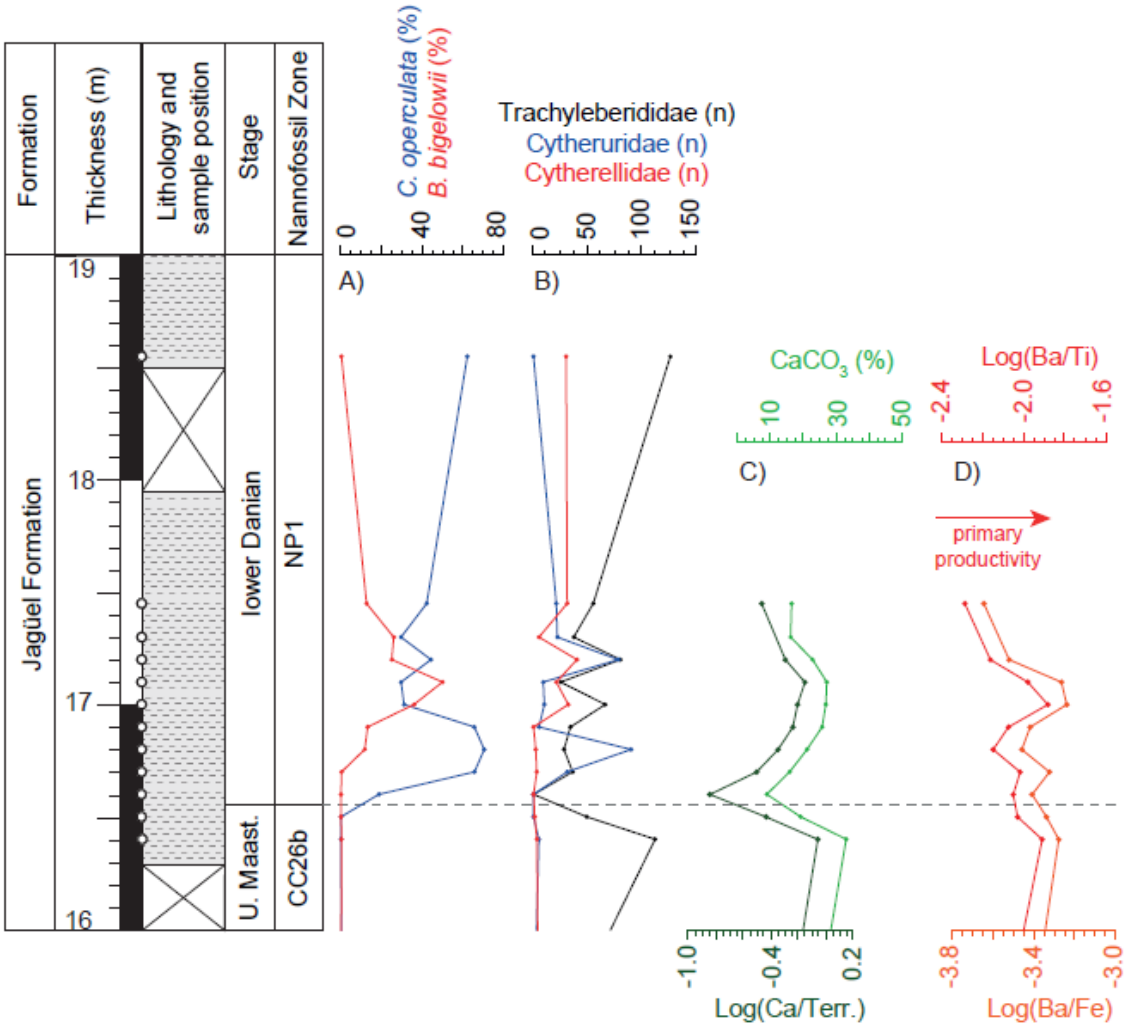

Figure 7: Paleogeographic map of the Late Cretaceous (modified from Claeys et al., 2002) showing the location of the Cerro Azul Section and other K-Pg sections and sites considered in the discussion. References: DSDP Site 356 (Perch-Nielsen, 1977); DSDP Site 384 (Thierstein and Okada, 1979); DSDP Site 465 (Henriksson, 1996); DSDP Site 527 (Henriksson, 1996); DSDP Site 577 (Monechi, 1985; Gardin and Monechi, 1998); ODP Site 690 (Pospichal and Wise, 1990); ODP Site 738 (Pospichal, 1996a); ODP Site 750 (Ehrendorfer and Aubry, 1992); ODP Site 752 (Pospichal, 1991); ODP Site 761 (Pospichal and Bralower, 1992); ODP Site 1262 (Bernaola and Monechi, 2007); Agost Section (Lamolda et al., 2016); Bajada de Jagüel Section (Keller el al., 2007); Beloc Section (Aguado et al., 2005); Biarritz Section (Perch Nielsen, 1979a); Braggs Sections (Moshkovitz and Habib, 1993); Brazos River Section (Jiang and Gartner, 1986; Tantawy, 2011); Bulgarian Sections (Stoykova and Ivanov, 2004); Caravaca Section (Romein, 1977; Gardin and Monechi, 1998); Denmark Sections (Perch Nielsen, 1979b); Egyptian Sections (Tantawy, 2003; Faris et al., 2007); El Kef Section (Gardin and Monechi, 1998); El Mulato Section (Pospichal, 1996b); Elles Section (Gardin, 2002); Hor Hahar Section (Eshet et al., 1992); Italian Sections (Monechi, 1977; Gardin and Monechi, 1998; Fornaciari et al., 2007); Lattengebirge Section (Herm et al., 1981); Poty Quarry Section (Andrade, 2010).

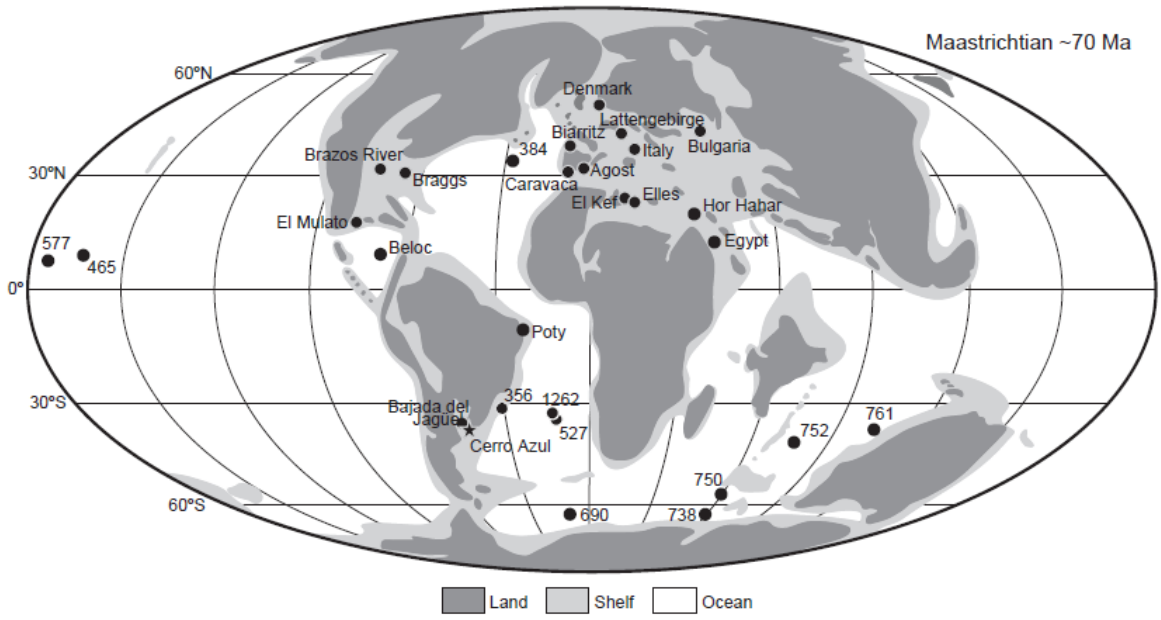

Supplementary Material

Table S1: Total calcareous nannofossil counts at the Cerro Azul Section across the K-Pg transition.

Table S2: Total ostracod counts at the Cerro Azul Section across the K-Pg transition.

Table S3: Geochemical and magnetic susceptibility data at the Cerro Azul Section across the K-Pg transition.

Capítulo 6: Síntese Intergadora

Capítulo 6

Síntese Integradora

CONSIDERAÇÕES FINAIS

O clima do início do Paleógeno é marcado por uma série de eventos de curto prazo e possui registros de algumas das temperaturas mais quentes do Cenozoico. De fato, o ciclo do carbono e o sistema climático passaram por mudanças críticas neste período. No entanto, os registros paleoclimáticos e paleoambientais para o Daniano, em particular no hemisfério sul são pouco documentados. A diagênese é um fator que pode influenciar na robustez dessas reconstruções de paleoclimáticas. Logo, a identificação e a quantificação da alteração diagenética e seu impacto sobre a composição química da calcita do microfóssil a ser analisado continua sendo um grande desafio para estudos paleoceanográficos e paleoclimáticos. Logo, partindo da hipótese de que estimativas de paleotemperatura mais assertivas seriam possíveis por meio de uma caracterização geoquímica microestrutural prévia, a presente tese dissertou sobre resultados obtidos neste tema em dois distintos locais do Daniano para o Oceano Atlântico Sul: o Site ODP 1262 Walvis Ridge, que compreende um contexto marinho profundo e a Seção Cerro Azul, localizado na Bacia de Neuquén, Argentina, que compreende um ambiente marinho raso. Alguns questionamentos foram levantados ao longo da pesquisa, e puderam ser respondidos ao longo dos capítulos.

No capítulo 2, foram identificados em testas de foraminíferos bentônicos da espécie *Nuttalides truempy*, a presença de fases carbonáticas autigênicas, tais como girvasita, siderita e Kutnoherita. Estes espécimes representavam intervalos estratigráficos que correspondem aos eventos de aquecimento rápido, como o Dan –C2. Tais evidências, identificadas por diferentes técnicas levantam dúvidas sobre "a resposta silenciosa de temperatura do fundo oceânico", com base em foraminíferos bentônicos. Isso porque o fracionamento isotópico ocorrido parece não ter sido oriundo da calcita e sim de sua respectiva fase carbonática autigênica, ou seja, a cristalização destas fases afetou os sinais ambientais de $\delta^{18}O$. A ocorrência abundante de dinocistos calcários

nestes momentos críticos do início do Paleógeno, tornou-se possível os registros de $\delta^{18}O$, demonstrando que os sinais ambientais dos sedimentos (*bulk*) estão dominados por estes micritos/dinocistos.

O capítulo 3 apresentou os registros de $\delta^{13}C$ e $\delta^{18}O$ em quatro espécies de ostracodes oriundos da Seção Cerro Azul, na bacia de Neuquén. Com base nos sinais isotópicos em dispersão, as diferenças interespecíficas ficaram bem claras entre registros oriundos de carapaças lisas e registros de valvas ornamentadas. As valvas analisadas de *Cytherella* spp. obtiveram sinais isotópicos muito próximos aos dos espécimes bentônicos *Lenticulina* e *Gavelinella*. Paleonutrientes como P e Ba foram associados aos registros de $\delta^{13}C$ e constatamos mudanças na espessura das valvas das espécies ornamentadas *Togoina argentinensis* e *Henryhowella* (*Wichmannela*) *meridionalis*.

Um estudo detalhado sobre a assembleia de foraminíferos planctônicos no ODP site 1262, foi realizado e ilustrado no capítulo 4. Nesta pesquisa, foi observado formas aberrantes no mesmo intervalo rico em mercúrio, que está relacionado ao vulcanismo Deccan registrado no mesmo intervalo de tempo (~65,95 e 65,82 Ma). Os impactos de eventos hipertermais na superfície oceânica observada neste trabalho, levantou os questionamentos aplicados e relatados no Capítulo 2, sobre a aparente boa preservação dos microfósseis e a possível aplicação dos dinocistos calcários como ferramenta paleoceanográfica.

Por fim, o estudo apresentado no Capítulo 5, referente as mudanças nas comunidades de nanofósseis calcários e ostracodes ao longo da transição Cretáceo-Paleógeno, permitiu verificar que as mudanças observadas nessas assembleias apresentavam uma relação com a queda da produtividade da água superficial. A subsequente recuperação ao Daniano é sugerida por tendências de log(Ba/Fe) que foram investigados com base em ostracodes no Capítulo 3. Assim

como observado no Site 1262, a grande abundância de dinocistos calcários (*Cervisiella operculata*) também foi observada na Seção Cerro Azul.

Esta pesquisa foi realizada durante o período da pandemia de COVID-19 e alguns experimentos previstos foram executados apenas em 2023. As análises relacionadas a aplicação de paleotemperatura com base em ostracodes e também por TEX_{86}, além do mapeamento em escala submicron, realizados na nova linha CARNAÚBA do Sírius, contemplarão um manuscrito em construção como atividade de encerramento desta etapa.